CHEMICAL IONISATION MASS SPECTROMETRY

BY

R.E. MATHER B.Sc., Grad.R.I.C.

A thesis submitted for the degree of

Doctor of Philosophy

at the

University of Kent at Canterbury

May 1979

To my parents

KENT UNIVERSITY LIBRARY

D29289/80

F 84739

ACKNOWLEDGEMENTS

I am extremely grateful to my supervisor, Dr. J.F.J. Todd, for his guidance, encouragement and constructive criticisms throughout the course of this work.

I would also like to thank Dr. J.M.B. Bakker and Dr. R. Mallaby of Shell Research Ltd. for their help and advice during the time I spent at Shell Research, Sittingbourne, Kent.

In addition thanks are due to: my colleagues Dr. G. Lawson, Mr. R.B. Turner and Mr. R.M. Waldren for helpful discussions during the course of this work, Messrs. D.A. Pugh, G.S. Jackson, P.R.J. Smith, W.T. Povey and R.J. Oliver for constructing some of the apparatus and for their continuing assistance with mechanical and electronic problems and Messrs. P.C.B. Perry, P.D. Wyeth and A.J.W. Hewett of Shell Research Ltd. for their skill in constructing the two ion sources and for assisting with instru--mental modifications.

I am also very grateful to Miss D. Paine for typing this thesis and to my wife for proof-reading the original manuscript.

Finally, I would like to thank the Science Research Council for their sponsorship which was in the form of a CASE studentship and also Shell Research Ltd. for other financial assistance.

ABSTRACT

Almost all of the work on chemical ionisation (CI) mass spectrometry, reported to date, has been performed using the high pressure mass spectrometric technique in which the ion source is operated at a pressure of *ca.* 1 Torr. This work involves the development of an ion source, based on the three-dimensional quadrupole ion trap (QUISTOR), with which it is possible to perform CI studies at pressures of *ca.* 10^{-5} Torr.

The characteristic features of the chemical ionisation process are first described in general terms and this is followed by a literature review of the instrumental aspects of chemical ionisation mass spectrometry. After a brief theoretical description of the Quistor an account is given of the physical characterisation of the device, which includes a study of the limits of stability and also ion loss and ejection processes. This is followed by a description of the design, construction and characterisation of a Quistor-type ion source for a magnetic sector mass spectrometer and the use of this instrument to produce low pressure CI mass spectra. The modification of the same type of mass spectrometer to operate in the high pressure CI mode is then described, this includes the design and construction of a high pressure ion source and the sample and reagent gas introduction systems. Finally, the performance of the Quistor as a low pressure CI ion source is compared with that of the high pressure CI ion source.

TABLE OF CONTENTS

LIST OF FIGURES

Chapter 6

CHAPTER 1

INTRODUCTION

1.1 Mass Spectrometry

Mass spectrometry is one of the most powerful and versatile of all instrumental methods of analysis. Molecules of the sample are ionised and the ions formed are sorted according to their mass-to-charge ratios by utilising electric or a combination of electric and magnetic fields. A mass spectrum of the sample is obtained by determining the relative abundance of each ionic species present. From this it is possible to derive information on the molecular structure of the sample.

The most commonly used method of sample ionisation in mass spectrometry is electron impact (EI) ionisation where sample molecules are bombarded with electrons, usually emitted from a heated tungsten filament, having a nominal energy of 70 eV. Sample molecular ions formed in this way may be in highly excited electronic states and may subsequently fragment by a number of different pathways to produce the ions which make up the mass spectrum of the sample. One of the most useful aspects of mass spectrometry is that it is possible to deduce the molecular weight of the sample directly from the value of the mass to charge ratio (m/e) of its molecular ion. However, for certain samples electron impact ionisation produces such extensive fragmentation that the molecular ion may be completely absent from the mass spectrum or in extremely low relative abundance, making positive assignment of a molecular weight to the sample impossible.

In order to reduce the extent of fragmentation for such samples in an effort to enhance the relative abundance of the molecular ion it is possible to employ an alternative ionisation process such as field ionisation (FI), field desorption (FD) or chemical ionisation (CI). These are

known as "gentle" ionisation techniques because considerably less energy is imparted to the sample molecule than is the case for electron impact. Both field ionisation and field desorption involve subjecting the sample molecules to a high intensity electric field, which has the effect of stripping an electron from the molecules. The latter technique is especially useful for the analysis of involatile and highly polar samples.

Chemical ionisation is the most widely used of all the "gentle" ionisation techniques. Sample molecules undergo ion-molecule reactions with reagent ions, produced by ionising a reagent gas, and a charged entity, usually a proton, is transferred to the sample molecule thus effecting its ionisation.

1.2 Chemical Ionisation

The technique of chemical ionisation was invented by Munson and Field[5,6]. A mixture of the sample under investigation and a large excess of a reagent gas is introduced into an ion source and ionised, usually by electron impact. Almost all of the initial ionisation occurs in the reagent gas, because it is in large excess, to produce the reagent gas primary ions. These subsequently react with reagent gas molecules to produce a set of reagent ions. The sample is then ionised by ion-molecule reactions which occur between these reagent ions and the sample molecules. For the general case this process may be represented by the following set of equations:

$$P + e^- \rightarrow P_1^+ , P_2^+ , P_3^+ \ldots\ldots\ldots P_i^+$$

$$P_i^+ + P \rightarrow R_1^+ , R_2^+ , R_3^+ \ldots\ldots\ldots R_i^+$$

$$R_i^+ + S \rightarrow S_1^+ + F_1$$

$$S_1^+ \rightarrow S_2^+ + F_2$$

$$\vdots$$

$$\rightarrow S_i^+ + F_i$$

where P represents a reagent gas molecule, P_i^+ the primary ions, R_i^+ the

reagent ions, S a sample molecule, S_i^+ are the ions which make up the chemical ionisation mass spectrum of the sample and F_i are the respective neutral fragments. S_1^+ is usually the ion formed by addition of a proton to the sample molecule, but depending on the chemical nature of the sample and the reagent gas it may be the ion produced as a result of the abstraction of a hydride ion from the sample molecule. These ions termed $(M+1)^+$ and $(M-1)^+$ respectively have become known as quasi-parent or quasi-molecular ions.

One of the most commonly used reagent gases in chemical ionisation mass spectrometry (CIMS) is methane. Figure 1.1 shows the variation in the relative abundances of ions in the methane plasma as a function of pressure.

Figure 1.1 Plot showing the Variation in the Relative Abundances of Ions in the Methane Plasma as a Function of Pressure*

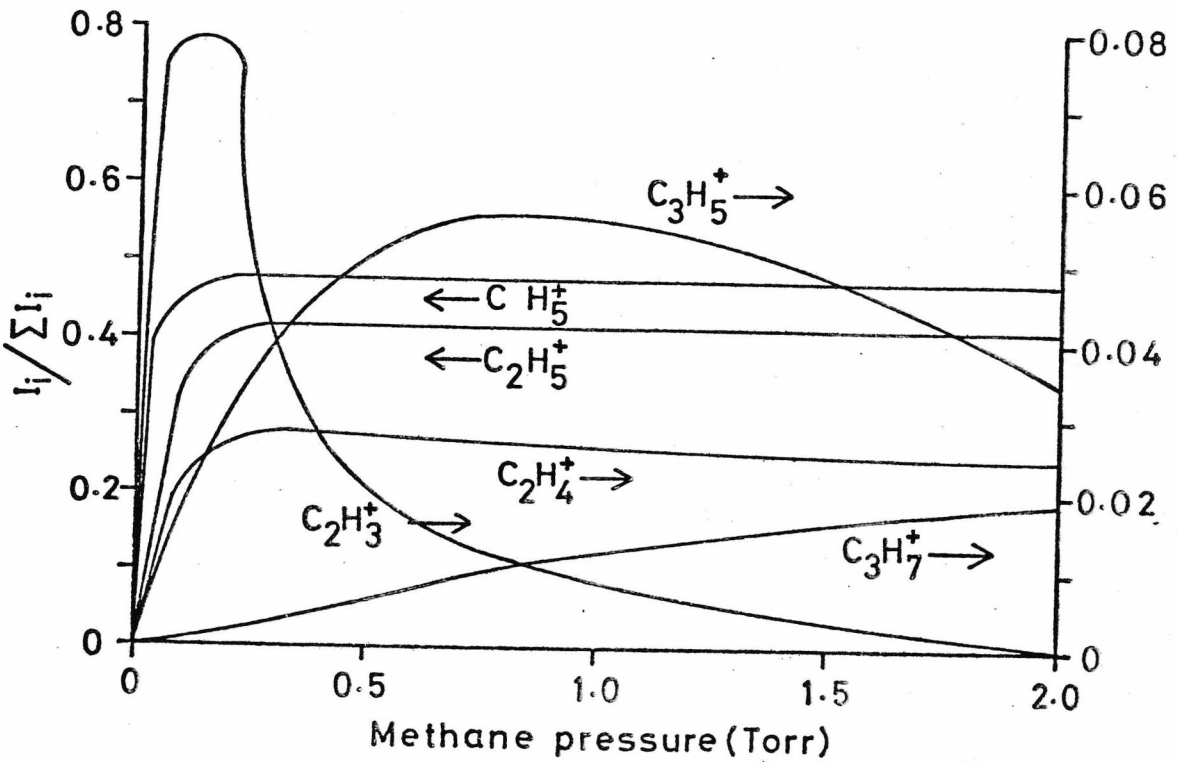

* *Taken from Reference 6.*

All of the methane primary ions react rapidly with methane molecules to give product ions by the following well-established series of reactions[3]:

$$CH_4^+ + CH_4 \longrightarrow CH_5^+ + CH_3$$

$$CH_3^+ + CH_4 \longrightarrow C_2H_5^+ + H_2$$

$$CH_2^+ + CH_4 \longrightarrow C_2H_4^+ + H_2$$

$$CH_2^+ + CH_4 \longrightarrow C_2H_3^+ + H_2 + H$$

$$C_2H_3^+ + CH_4 \longrightarrow C_3H_5^+ + H_2$$

Small relative concentrations of $C_3H_7^+$, $C_2H_2^+$, $C_3H_3^+$, $C_3H_4^+$ and $C_4H_9^+$ are formed but these ions do not make an appreciable contribution to the total ionisation. As can be seen from Figure 1.1, above an ion source pressure of *ca.* 0.5 Torr. the relative abundances of the major project ions (CH_5^+ and $C_2H_5^+$) are largely independent of pressure, indicating that these ions react either extremely slowly or not at all with methane molecules. Since CI ion sources are normally operated at a pressure of 1 Torr the two major reagent ions in methane are CH_5^+ and $C_2H_5^+$ which comprise *ca.* 90% of the total ionisation. These reagent ions react mostly by proton or hydride transfer reactions:

$$CH_5^+ + BH \longrightarrow BH_2^+ + CH_4$$

$$CH_5^+ + BH \longrightarrow B^+ + CH_4 + H_2$$

$$C_2H_5^+ + BH \longrightarrow BH_2^+ + C_2H_4$$

$$C_2H_5^+ + BH \longrightarrow B^+ + C_2H_6$$

where B represents any organic (or possibly inorganic) group.

The characteristic feature of the chemical ionisation concept may be looked upon as the utilisation of a specific set of reagent ions to effect a specific type of ion-molecule reaction with the sample molecules. The ions produced as a result of these reactions constitute the chemical ionisation mass spectrum of the sample. Since the same reagent ions react with a wide range of different samples, the chemical ionisation mass spectra produced are comparable with each other and reflect differences in structure, chemical reactivities and quantitative differences in their concentrations.

A list of some of the reagent gases used in CIMS is given in Table 1.1.

Table 1.1 Chemical Ionisation Reagent Gases

	Reagent Gas	Major Reagent Ions
Group 1	CH_4	CH_5^+ , $C_2H_5^+$
	C_3H_8	$i\text{-}C_3H_7^+$
	$i\text{-}C_4H_{10}$	$t\text{-}C_4H_9^+$
	H_2	H_3^+
	H_2O	H_3O^+ , $H_5O_2^+$ ...
	NH_3	NH_4^+ , $N_2H_7^+$ ...
Group 2	He,Ne,Ar	He^+,Ne^+,Ar^+
	N_2	N_2^+
	NO	NO^+
Group 3	O_2	O^-, O_2^-
	~~CH_3NO_2~~ CH_3ONO	CH_3O^-
	CH_2Cl_2	Cl^-,HCl_2^-,$CH_2Cl_3^-$

Reagent ions from the group 1 gases undergo even-electron acid-base type

reactions with sample molecules such as proton transfer. The degree of fragmentation of the quasi-molecular ions ($(M+1)^+$ or $(M-1)^+$) formed in this way may be varied by employing reagent ions with different acid strengths. Reagent ions from group 2 undergo charge transfer reactions with sample molecules, effectively acting as one electron oxidising agents. The sample molecular ion is in this case M^+ and the extent to which this ion fragements may be controlled by employing reagent ions with different recombination energies. The group 3 reagent gases are employed in negative ion chemical ionisation mass spectrometry. The negative reagent ions react with sample molecules predominantly by either proton abstraction or negative ion addition reactions.

The CI mass spectrum of a sample produced using a group 2 reagent gas often resembles the EI mass spectrum of the same sample recorded at low electron energy (*ca.* 20 eV). However, the most commonly used reagent gases, those of group 1, produce mass spectra which are, with few exceptions, very different to the mass spectra produced using any other ionisation technique. The analytical and scientific utility of the method stems from the unique character of the CI mass spectra. This uniqueness results in turn from the operation of a number of special factors in the CI system. Firstly, with reagent gases such as methane and isobutane, ionisation is effected by transfer of massive entities such as protons, hydride ions or alkyl carbonium ions. This type of reaction is not governed by Frank-Condon considerations which are so important in electron impact ionisation. Secondly, the reagent ions from the methane and isobutane plasmas and the sample ions produced when these ions react with the sample molecules are all even-electron ions. Molecular ions produced by electron impact ionisation are odd electron ions and their decomposition chemistry is dominated by the presence of this odd electron. Clearly these two types of ion will fragment by two entirely different mechanisms, that for odd electron ions being the more extensive. A third important factor is that in the CI process considerably less energy is imparted to the sample

molecule compared to that in electron impact ionisation. Consequently the CI mass spectrum of a particular sample will in general contain fewer fragment ions than its EI mass spectrum. A final factor which could contribute to the difference between CI and EI mass spectra is that, according to Field, Munson and Becker[10], in the CI process the ionisation and subsequent fragmentation, if any, is of a localised nature. A CI mass spectrum results from a random attack of the reagent ion at different points on the sample molecule and any fragmentation which occurs is confined to the immediate vicinity of the point of attack. The random attack, localised reaction concept was proposed by Field *et al*[10] to rationalise the methane CI mass spectra of paraffin hydrocarbons. This argument can easily be extended to cover the CI mass spectra of molecules containing polar functional groups. In this case the attack is no longer random but is directed, by the ion-dipole forces existing between the reagent ion and the sample molecule. Any fragmentation reactions which occur as a result of this interaction will be those appropriate to the functional group present. If the sample molecule is polyfunctional then the CI mass spectrum will be made up of fragment ions produced as a result of reactions between the reagent ions and the different functional groups.

As an example of the difference between electron impact and chemical ionisation Figures 1.2(a) and 1.2(b) show, respectively, the EI and CI mass spectra of n-octadecane. The most striking features of the CI mass spectrum are the intense quasi-molecular ion ($(M-1)^+$) which constitutes 43% of the total ionisation, and the low relative intensity of the fragment ions.

To summarise, the salient points about chemical ionisation mass spectrometry are: (i) the amount of fragmentation occurring is small compared to EIMS, (ii) the quasi-molecular ions have large relative intensities, (iii) the ions comprising the CI mass spectrum occur mainly in the high mass region, (iv) the fragmentation processes which do occur are significantly different from those observed in EIMS. Chemical ionisation is especially useful in the determination of molecular weight since with few

Figure 1.2 EI and CI Mass Spectra of n-octadecane *(Taken from Reference 10)*

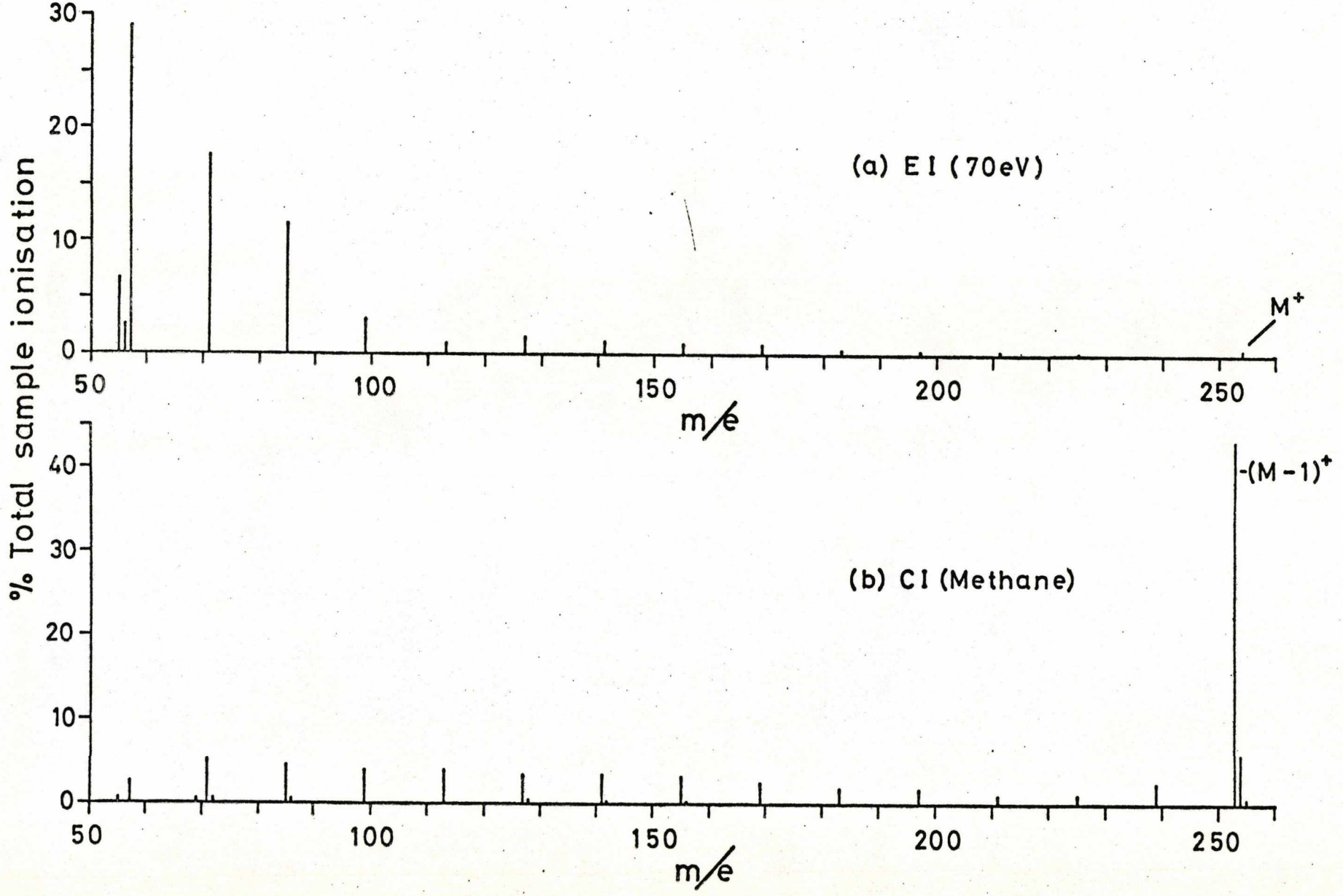

exceptions the quasi-molecular ions are of high relative intensity, whereas, for certain samples the molecular ions in EI mass spectra may be of very low relative intensities or non-existent.

1.3 Experimental Aspects of Chemical Ionisation

The chemical ionisation technique depends upon the occurrence of a series of ion-molecule reactions. In order for this reaction sequence to occur, the experimental conditions must be arranged such that the primary ions undergo a large number of collisions with the reagent gas molecules. Under the low pressure conditions prevailing in a conventional EI ion source the probability of an ion undergoing a collision with a molecule before drifting out of the ion source is very small. The number of collisions may be increased by either: (i) increasing the ion source pressure or (ii) increasing the ion residence time.

Chemical ionisations studies employing the first of these methods involves the use of a high pressure mass spectrometric technique. The reagent gas/sample mixture if introduced into a virtually gas-tight ion source and the total pressure therein is maintained at *ca.* 1 Torr. Such high pressures in the source region of the mass spectrometer necessitate the installation of differential pumping to ensure that the pressure in the analyser region is still maintained at below 10^{-6} Torr. Ionisation of the gas mixture in the ion source, usually by electron impact, produces the primary ions which initiate the CI reaction sequence.

The ion residence time of a conventional EI ion source operated at 10^{-5} Torr is of the order of 10^{-6} to 10^{-5} sec. In order to produce sufficient quantities of CI reagent ions at this pressure it is necessary to employ an ion source which is capable of storing ions for at least 10^{-3} sec. There are many ion storage devices which could in principle be used to produce CI mass spectra but only three of these have actually been employed for CI studies. By far the simplest of these devices is the space charge ion trap[61] which is basically a conventional EI ion source in

which the electron gun and the repeller are operated in a pulsed mode. Another ion storage device which is especially useful for the study of CI reaction mechanisms[77] is the ion cyclotron resonance (ICR) mass spectrometer. Bonner, Lawson and Todd[69], of this Laboratory, have shown that the three dimensional quadrupole ion trap (QUISTOR) may be employed as a CI ion source for a quadrupole mass filter. The Quistor consists of three rotationally-symmetric electrodes with hyperbolic inner surfaces. Ions are created inside the device by an electron beam and are stored by the application of a suitable combination of d.c. and r.f. electric potentials to the Quistor electrodes. After sufficient time has elapsed to allow the CI reactions to take place the ions are pulsed out of the Quistor into the quadrupole mass filter for mass analysis. Chemical ionisation studies which utilise ion storage techniques have become known as low pressure chemical ionisation.

1.4 Aims of This Work and the Organisation of This Thesis

Almost all of the early CI mass spectrometers were modified versions of existing EI instruments. These, and also the commercial instruments which became available later, utilised the high pressure mass spectrometric technique described in Section 1.3. There have been relatively few CI studies performed using any of the ion storage devices, which is somewhat surprising since they apparently have a number of advantages over the high pressure technique: firstly, they do not require either a differential pumping system or a special reagent gas inlet and secondly, since the source operating pressure is relatively low they may be more suitable for the analysis of samples and the use of reagents with very low vapour pressures. However, these apparent advantages may be offset by the fact that, with the possible exception of the space charge trap, the use of ion storage devices for low pressure CI studies requires a specially constructed ion source and a more complex electronic control system.

For this study it was decided to evaluate the use of the Quistor as a low pressure CI ion source and compare its performance with that of a

conventional high pressure CI ion source. In order to make the most meaningful comparison, two separate ion sources were constructed for an AEI Scientific Apparatus Ltd MS9 magnetic sector mass spectrometer. One was based on the Quistor and the other on the 'closed' Nier-type geometry.

The principal aims of this work were:

(i) To continue the work initiated by Bonner[127] of this Laboratory on the physical characteristics of the Quistor with special regard to those directly related to its operation as a low pressure CI ion source.

(ii) To design and construct a Quistor ion source for a magnetic mass spectrometer and investigate the use of this instrument for low pressure CI studies.

(iii) To design and construct a conventional high pressure CI ion source for the same type of magnetic mass spectrometer.

(iv) To compare the performance of the Quistor as a low pressure CI ion source, with that of the high pressure CI ion source, and from this derive information about the relative merits of high and low pressure CI mass spectrometry.

The work on the physical characterisation of the Quistor along with a brief theoretical treatment of the device is described in Chapter 3. This study was performed using the same Quistor/quadrupole mass filter combination as was employed by Bonner[69] in the original work on the use of the Quistor as a low pressure CI ion source. The development of the new Quistor ion source for the MS9 mass spectrometer is described in Chapter 4. This work was performed using the MS9 instrument at the University of Kent but the development of the high pressure ion source, described in Chapter 5, was carried out using the MS9 mass spectrometer at Shell Research Ltd., Sittingbourne, Kent. However, almost all of the work on the comparison of the two ion sources, discussed in Chapter 6, was performed on the instrument at the University of Kent.

In an effort to place the main contents of this thesis in perspective the description of the work performed during this project is preceded by a literature review on the instrumental and experimental techniques employed in chemical ionisation mass spectrometry. The review is intended to show the place of the Quistor in this field.

CHAPTER 2

REVIEW OF THE INSTRUMENTATION AND EXPERIMENTAL TECHNIQUES EMPLOYED IN CHEMICAL IONISATION MASS SPECTROMETRY

2.1 Scope of the Review

The purpose of this review is to describe the various different instruments and experimental techniques which have been employed to produce chemical ionisation (CI) mass spectra, in order to show the place of the three-dimensional quadrupole ion trap in this field, and to discuss the improvements and innovations which have been made in both instrumentation and methodology in the past ten years.

2.2 The Historical Development of Chemical Ionisation

In the early 1950's experimental work started on the kinetics and mechanisms of ion-molecule reactions using mass spectrometers which had been originally designed for analytical purposes. Simply by increasing the ion source pressure, a small number of primary ions, produced by electron impact, underwent reactive collisions with neutral molecules present in the source region. The method was greatly improved by the introduction of efficient differential pumping techniques[1-4] which permitted source pressures of *ca.* 1 Torr whilst the analyser was kept under high vacuum.

The CI process was invented in 1965 by Munson and Field[5,6,7] while using such an instrument to study the high pressure reactions of methane[8,9]. During the course of this work they noticed that the presence of small amounts of certain substances produced very marked changes in the relative concentrations of the ions formed from the methane. It was this observation which developed into the now well established technique of chemical ionisation mass spectrometry (CIMS)[10]. Soon after the invention

many mass spectrometers designed originally for electron impact ionisation (EI) were modified to permit the use of the instrument alternatively in the chemical or electron impact modes of ionisation. Since it is relatively easy to convert a mass spectrometer to operate in the CI mode, many of the early CI instruments were home-made conversions of existing instruments. Very soon, however, a commerical instrument was on the market and since then nearly all analytical mass spectrometers have CI either fitted as standard or offered as an accessory.

2.3 The Experimental Requirements for the Production of a Chemical Ionisation Mass Spectrum

The experimental problem in CIMS is firstly, to produce a set of reagent ions and allow these ions to come into contact with molecules of the sample under such conditions that ion-molecule reactions occur between them, and secondly, to mass analyse and collect the product ions of these reactions and also any other ions arising from the fragmentation of these product ions, this constituting the CI mass spectrum of the sample. Since the production of the reagent ions is also usually dependant on the occurrence of ion-molecule reactions, the choice of ion source and operating conditions for this application must be such that there is a high probability of ion-molecule collisions occurring during the lifetime of the ions in the ion source. In a conventional electron impact ion source, the ion residence time is *ca.* 10^{-5} seconds and under normal operating conditions the ion source pressure is less than 10^{-5} Torr. Clearly under these conditions a primary ion has almost no chance of undergoing a collision with a gas molecule during its brief lifetime in the ion source. Obviously, in order to operate this type of ion source under conditions that permit CI, a method of increasing the number of ion-molecule collisions must be found.

The approximate number of ion molecule collisions an ion will undergo before leaving a particular ion source may be calculated from the

following equation:

$$z_c = k_c \cdot N \cdot \tau$$

where z_c is the number of collisions, k_c is the rate constant for ion-molecule collisions, N is the number density of gas molecules and τ is the ion residence time. It is clear from this equation that there are two ways of increasing the number of ion-molecule collisions in a particular ion source: increase either the ion residence time or the ion source pressure. In terms of instrumentation, increasing the ion source pressure involves using a high pressure mass spectrometric technique in which the ion source is operated at pressures of *ca.* 1 Torr. The number of ion-molecule collisions an ion will experience in an ion source at this pressure is *ca.* 200. This may be calculated from the above equation, where k_c is of the order of 10^{-9} cm^3 $mol^{-1}s^{-1}$, N at 1 Torr and 100°C ≃ 2×10^{16} $mol.cm^3$ and $\tau = 10^{-5}$ seconds (although the actual value of the residence time will depend on the repeller potential). The second method of increasing the number of ion-molecule collisions, increasing the ion residence time, may be achieved by employing any one of a number of ion storage devices. These operate typically at pressures of *ca.* 10^{-5} Torr with storage times of up to *ca.* 1 second. In fact, operated under these conditions, an ion would be expected to undergo the same number of ion-molecule collisions as calculated for the high pressure ion source since the pressure is a factor of 10^5 lower and the residence time a factor of 10^5 higher. The two means of increasing the number of ion-molecule collisions for CI purposes lead to the techniques of high pressure CIMS and low pressure (or ion storage) CIMS.

The methods of mass analysis and ion detection used to produce CI mass spectra are identical to those employed for electron impact mass spectra.

2.4 High Pressure Chemical Ionisation Mass Spectrometry

2.4.1 Introduction

The high pressure technique has been employed to produce the vast majority of CI mass spectra reported to date. Experimentally, a mixture of the sample and the reagent gas is introduced into an ion source and ionised, usually by electron bombardment, under conditions which satisfy the following: (i) almost all the ionisation effected by the electrons occurs in the reagent gas and not in the sample; (ii) the primary ions formed react completely with reagent gas molecules; (iii) the reagent ions should be formed near enough to the electron beam such that they have ample opportunity to react with sample molecules before drifting out of the ion source. In practice, the conditions necessary to satisfy these requirements are a reagent gas to sample ratio of greater than 10^3:1 and a total source pressure in the region of 0.5 to 2.0 Torr. The reagent ions produced react with the sample molecules to form the sample ions which then drift out of the ion source, along with any ions formed from the fragmentation of these sample ions, into the analyser for mass analysis and detection.

2.4.2 Instrumentation

The requirements for operating a mass spectrometer in the high pressure CI mode are conceptually very simple: in order to maintain a pressure of *ca.* 1 Torr inside the ion source the total area of the necessary apertures must be reduced to a minimum, the pumping system of the instrument must be arranged such that the pumping speed in the source region is sufficient to cope with the increased flow of gas from the ion source and also that the pressure in the analyser region is kept below its normal operating maximum pressure, depending upon the type of analyser. Most mass spectrometers, especially those fitted with electron impact ion source, are readily converted to operate in the CI mode. The actual

modifications necessary will depend on the particular instrument but the general requirements may be summarised as follows:-

1. A differential pumping system.
2. A virtually gas-tight ion source which will operate efficiently, at an internal pressure of *ca.* 1 Torr.
3. An inlet system capable of delivering both the reagent gas and the sample directly into the ion source.
4. Modifications to the ion source electronic supplies.
5. A means of determining the pressure inside of the ion source.

Usually no modification of the analyser section of the mass spectrometer is necessary.

2.4.2.1 The Vacuum System

A schematic block diagram of the different vacuum regions in a mass spectrometer when operated in the CI mode is shown in Figure 2.1. For a magnetic deflection mass spectrometer, where the source potential may be as high as 10 kV, the source envelope must be maintained at a pressure below 10^{-4} Torr otherwise arcing may occur. To avoid collisional broadening of mass spectral peaks and loss of sensitivity, the pressure in the analyser region should be kept below 10^{-6} Torr. For a quadrupole mass spectrometer the source envelope may be operated at up to 10^{-3} Torr and the analyser at 10^{-4} Torr without serious degradation of performance. Since the outflow of gas from an ion source maintained at 1 Torr may be anything from 2-20 atmos.mls min^{-1} depending on the total area of the source apertures, differential pumping must be introduced between the source and analyser regions. If the aperture between the source envelope and analyser region is small, then differential pumping may be achieved simply by increasing the pumping capacity of the source region pumping

Figure 2.1 Schematic Block Diagram of the Vacuum Regions in a CI Mass Spectrometer

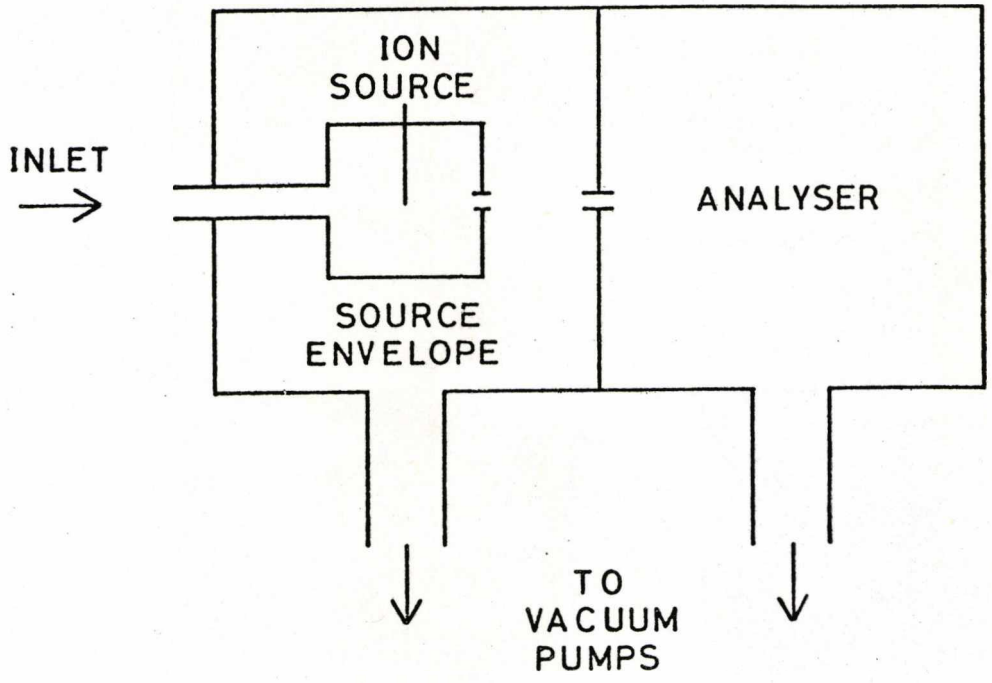

Figure 2.2 Schematic Representation of a Nier-Type Electron Impact Ion Source

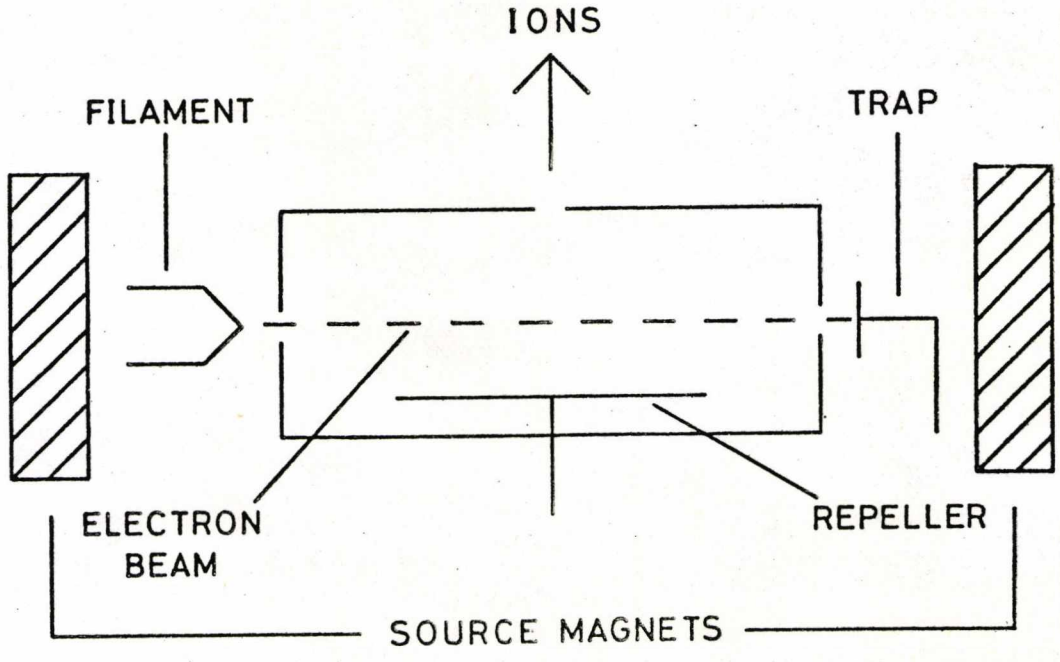

system. However, Yinon and Boettger[18] found it necessary to uprate the analyser pumping system of an A.E.I. Scientific Apparatus Ltd. MS9 such that its performance was not impaired when operated at high resolution. The actual capacity of the source pumping system required will depend on the total area of the source apertures and the conductance of the necessary connections between source envelope and pump. The majority of mass spectrometers modified to operate in the CI mode are fitted with an oil-vapour diffusion pump rated at between 600 and 1400 l s^{-1} which is backed by a rotary pump. The diffusion pump is usually surmounted by a cold trap and an isolation valve which reduces the overall pumping speed at the source to *ca.* 125 to 600 l s^{-1} respectively. Vestal *et al*[11] were able to operate a Varian Associates Ltd. MAT CH7 mass spectrometer in the CI mode at ion source pressures of up to 20 Torr by installing a source region diffusion pump of 2400 l s^{-1} capacity. Michnowicz and Munson[13], in an early modification of a C.E.C. 21-110 B, operated at ion source pressures of *ca.* 0.5 Torr without increasing the capacity of the source region diffusion pump. They achieved this by connecting an additional rotary pump to the outlet of the existing source region diffusion pump and although this provided the necessary throughput the pressure in the source envelope was typically 10^{-3} Torr which resulted in high pressures in the analyser causing a decrease in sensitivity and loss of resolution. Uprating the source pumping capacity normally involves the complete replacement of the original pumping stack. However, Garland, Weinkham and Trager[20] in modifying an A.E.I. Scientific Apparatus Ltd. MS902 mass spectrometer installed a high capacity pumping system in addition to the existing pumping system, the former being isolated when the instrument was operated in the electron impact ionisation mode.

2.4.2.2 The Ion Source

The majority of electron impact ion sources employed in modern analytical mass spectrometers are of the Nier-type illustrated schematically

in Figure 2.2. In order to operate this type of ion source in the CI mode, it is necessary to reduce the size of the ion exit and electron entrance apertures, and to ensure that electrical feedthroughs and sample entrance ports are made gas tight. The problem of opposing requirements is encountered in choosing the dimensions of the necessary ion source apertures: they should be made as large as possible in order to permit efficient ion extraction and entry of the maximum flux of electrons, yet in order to limit the outflow of gas from the ion source and consequently the capacity of the necessary pumping system, these apertures should be as small as possible. For ion sources attached to magnetic mass spectrometers the most common compromise dimensions are a diameter equal to 3×10^{-4} m for the electron entrance hole and 5×10^{-3} m by 5×10^{-5} m for the ion exit slit. Ion sources for quadrupole mass filters are normally fitted with a circular ion exit aperture of between 3×10^{-4} m and 5×10^{-4} m in diameter. A simple calculation (see Chapter 5) shows that for apertures of these dimensions a pumping speed of *ca.* 125 l s^{-1} at the source is required in order to maintain a pressure differential of 10^4 between the source and source envelope. It is not essential to use a slit for the ion exit aperture on magnetic mass spectrometers, Garland *et al*[20] have successfully operated an A.E.I. Scientific Apparatus Ltd. MS902 in the CI mode with an ion source which has a circular ion exit aperture. Bhattacharya and co-workers[14] replaced the electron entrance slit of a Du Pont 21-490 magnetic mass spectrometer with an aperture consisting of three small tunnels which simultaneously allows electrons to enter the ion source and presents a high impedance to gas flow out of the ion source.

The number of electrons that enter a CI ion source is limited by the very small electron entrance aperture and in addition to this an electron beam with a nominal energy of 70 eV will experience total attenuation long before it has traversed an ion source at a pressure of 1 Torr. Consequently, the production of significant numbers of collectable

ions in an ion source operated in the CI mode requires that the length of the electron beam be short compared to that in a conventional electron impact ion source and the energy of the ionising electrons be higher than is the case in electron impact mass spectrometry. Current practice is to operate at electron energies of between 200 and 1000 eV although the optimum value will depend on the design of the ion source and the reagent gas used. In an effort to increase the efficiency of ionising the gaseous medium while at the same time decreasing the outflow of gas from the ion source, Markey *et al*[19] designed a filament assembly which was mounted in the high pressure region of the ion source. This gave an ion beam intensity 10 to 100 times greater than that observed with the filament mounted outside of the high pressure region. However, it is possible that such an arrangement will give rise to thermal predecomposition of the sample and also severely shorten the filament lifetime.

The filament emission current in an electron impact ion source is stabilised with reference to the electron current collected on the trap electrode. Even though high electron energies are employed in CI ion sources the number of electrons traversing the ion source is insufficient to give stable trap currents and so the filament is controlled with reference to the total emission current collected on an electrode placed between the filament and the ion source block. Consequently, trap electrodes are not required on chemical ionisation ion sources unless the source is also to be used in the electron impact mode. However, Garland *et al*[20] found that although it was necessary to use total emission stabilisation the complete disconnection of the trap electrode resulted in a substantial loss of ion current and so the trap was left connected.

It has been found by a number of workers[13,15] that for optimum performance of a CI ion source, the repeller must be operated at the same potential as the walls of the ion chamber. This behaviour was rationalised by Chang *et al*[27] who showed that a repeller potential was in fact defocussing with respect to ion extraction whereas the electrostatic field

generated by an extractor electrode actually focussed the ions towards the ion exit aperture. However, Story *et al*[29], constructed an ion source with both repeller and extractor electrodes and found that optimum CI sensitivity was obtained when both of these electrodes were at the same potential as the ion chamber.

When a mass spectrometer is operated in the CI mode the source envelope is at a relatively high pressure. For magnetic instruments this means an increased probability of electrical breakdowns occurring between the ion source, which is at the accelerating potential, and the nearest ground point, which is usually the electron beam collimating magnets. Yinon and Boettger[18] reported that this was the origin of frequent breakdowns and solved the problem by replacing the original source magnets with smaller ones which were actually mounted on the ion source. Beggs *et al*[15] and also Garland and co-workers[20] found that the removal of the electron beam collimation magnets largely eliminated electrical breakdowns and did not affect the performance of the ion source when operated in the CI configuration.

The methods of sample introduction employed in CIMS are essentially the same as for EIMS with the exception that, for the former, some method of introducing the reagent gas must be provided and all connections between sample re-entrants and the ion source must be gas-tight. The reagent gas has been introduced into CI ion sources from behind the repeller electrode[15,16,18]; however, Markey *et al*[19] found that when using this method samples introduced on the probe were difficult to analyse, apparently because viscous flow conditions forced the vapourised sample away from the region of ionisation. For this reason and also to reduce the probability of leaks from the ion source, the reagent gas and sample are often introduced through the same re-entrant[17,20,22]. The special problems associated with sample introduction on magnetic mass spectrometers are discussed in Section 2.4.2.3.

Since the information obtained from a CI mass spectrum

often complements that obtained from an EI mass spectrum, it is advantageous to modify the mass spectrometer to permit its operation in either ionisation mode, preferably without degrading the instruments performance in the EI mode. There are a number of possible methods of implementing the dual facility of EI and CI on the same instrument. Ampulski[16] and also Garland *et al*[20] constructed ion sources which were specifically designed for CI. These were exchanged with the standard EI ion sources every time a CI mass spectrum was required. This is rather time-consuming since it involves breaking the source vacuum, and although the uprated source pumping capacity of instruments modified for CI studies lead to considerably shorter 'pumpdown' times, the CI technique is so sensitive to interference from water vapour that it is nearly always necessary to bake the source region for several hours after exchanging ion sources. Using two separate ion sources to obtain EI and CI mass spectra has the advantage that the performance of the mass spectrometer in the EI mode is unaffected by its modification for CI studies. Beggs *et al*[15], Hogg[17], and Yinon and Boettger[18] were able to obtain EI and CI mass spectra from a single CI type ion source. Operation in the EI mode was achieved by disconnecting the reagent gas supply and reducing the electron energy to 70 eV. This method has the advantage that both EI and CI mass spectra may be obtained without breaking the source vacuum. However, due to the relatively small source apertures, such an ion source is seldom as sensitive in the EI mode as a conventional 'open' EI ion source. One type of ion source which may be optimised for both EI and CI operation is the tandem EI-CI ion source developed by Arsenault *et al*[21] and also Hogg[22], the principal of which is illustrated in Figure 2.3. The sample/reagent gas mixture is introduced directly into the CI chamber and slowly diffuses out into the vacuum envelope surrounding it in which the EI chamber is located. The pressure in the CI chamber is *ca.* 1 Torr while the pressure outside of this region is $<1\times10^{-4}$ Torr. CI or EI mass spectra may be obtained by activating the respective filament and it is also

Figure 2.3 Schematic Representation of a Tandem EI-CI Ion Source

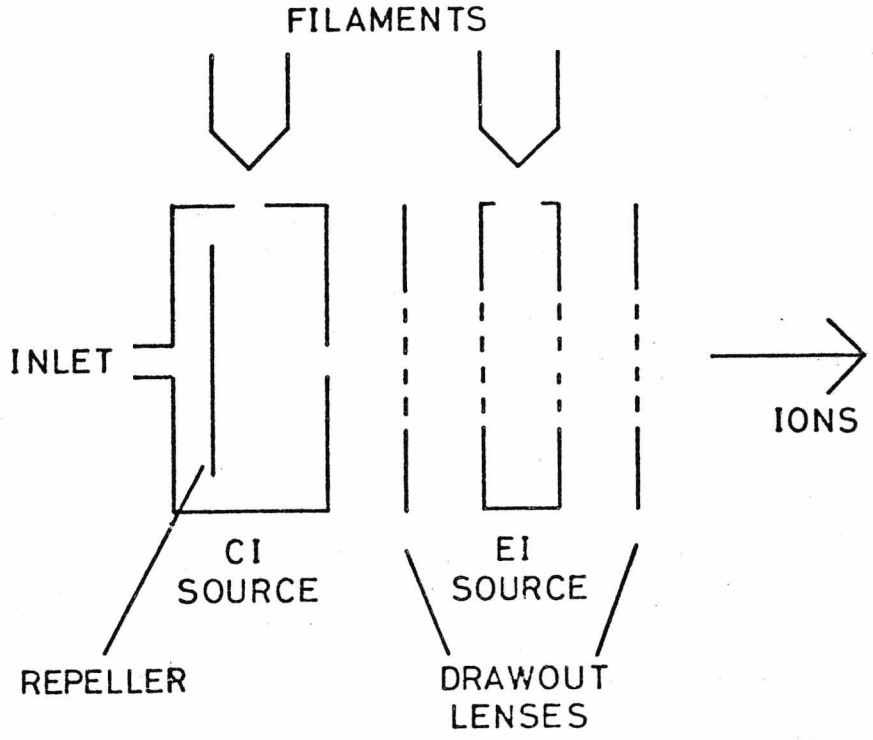

Figure 2.4 Section Through a Hewlett-Packard Dual Configuration Ion Source

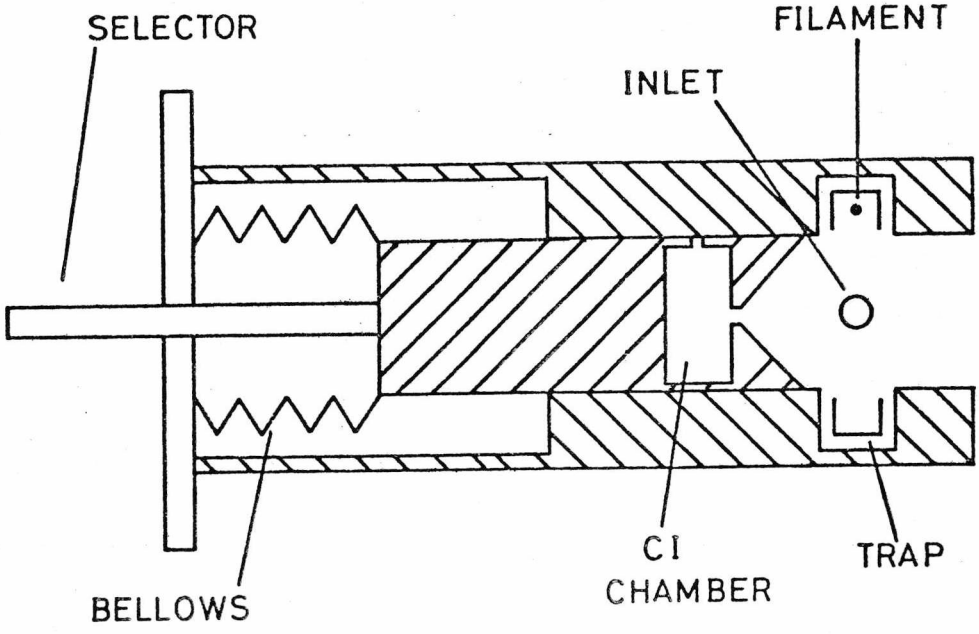

possible to obtain simultaneous EI-CI mass spectra by having both filaments on. The tandem ion source concept and its associated methodology has been patented by Arsenault[30,31] and also by Scientific Research Instruments Inc.[32]. Since the main difference between an EI and a CI ion source is the size of the electron entrance and ion exit apertures, it is possible to obtain both EI and CI mass spectra from a single ion source, optimised for either mode of operation, by arranging to vary the size of these apertures, preferably from outside of the vacuum region. A number of mechanisms have been developed for this purpose ranging from adjustable slits, the size of which is set by a micrometer screw gauge mounted on the outside of the source housing, to the more sophisticated dual configuration ion source developed by Hewlett-Packard Ltd.[33], which is illustrated schematically in Figure 2.4. The diagram shows the ion source in the EI configuration; to change to the CI configuration the CI chamber mounted on the sliding bellows assembly is pushed forward with the selector lever, until the CI electron entrance aperture is exactly aligned with the filament. The CI chamber acts as the repeller when the source is in the EI configuration. It is possible with this system to change from CI to EI operation in less than 1 minute without breaking the source vacuum. Another novel type of combined EI/CI ion source developed by LKB Instruments Ltd. is shown in Figure 2.5. All of the necessary apertures for both modes of operation are included on a movable, gold plated, stainless steel band. Changing from one mode to the other is achieved simply by rotating the band until the correct sized apertures are aligned with the filament and the trap, an operation which takes less than 5 seconds. This ion source and its operation are described in detail by Ryhage[34].

Two other ionisation techniques which are commonly employed in mass spectrometry are field ionisation (FI) and field desorption (FD). The latter technique is especially useful for the ionisation of strongly polar and involatile substances which are prone to thermal decomposition under EI and CI conditions. The fact that mass spectra obtained either

Figure 2.5 LKB Combined EI-CI Ion Source

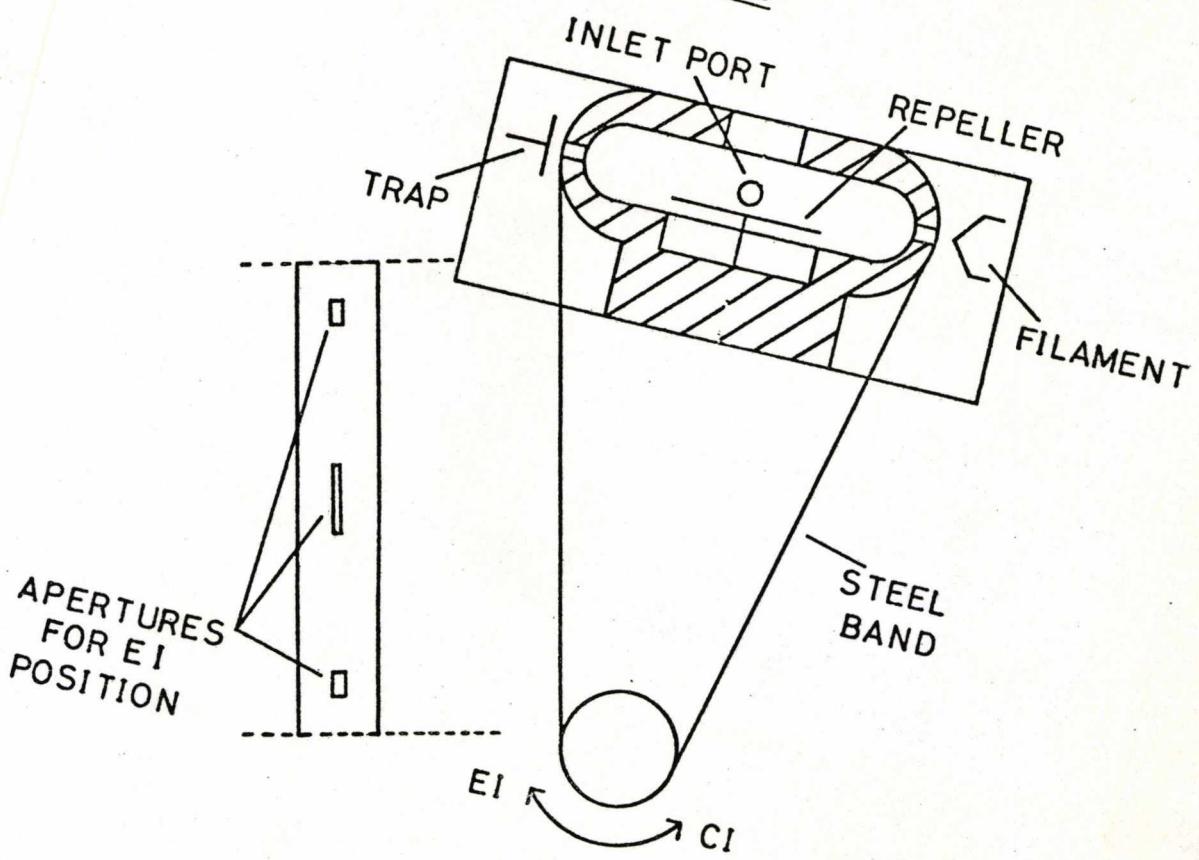

Figure 2.6 Direct Insertion Probe for Introduction of both Reagent Gas and Sample

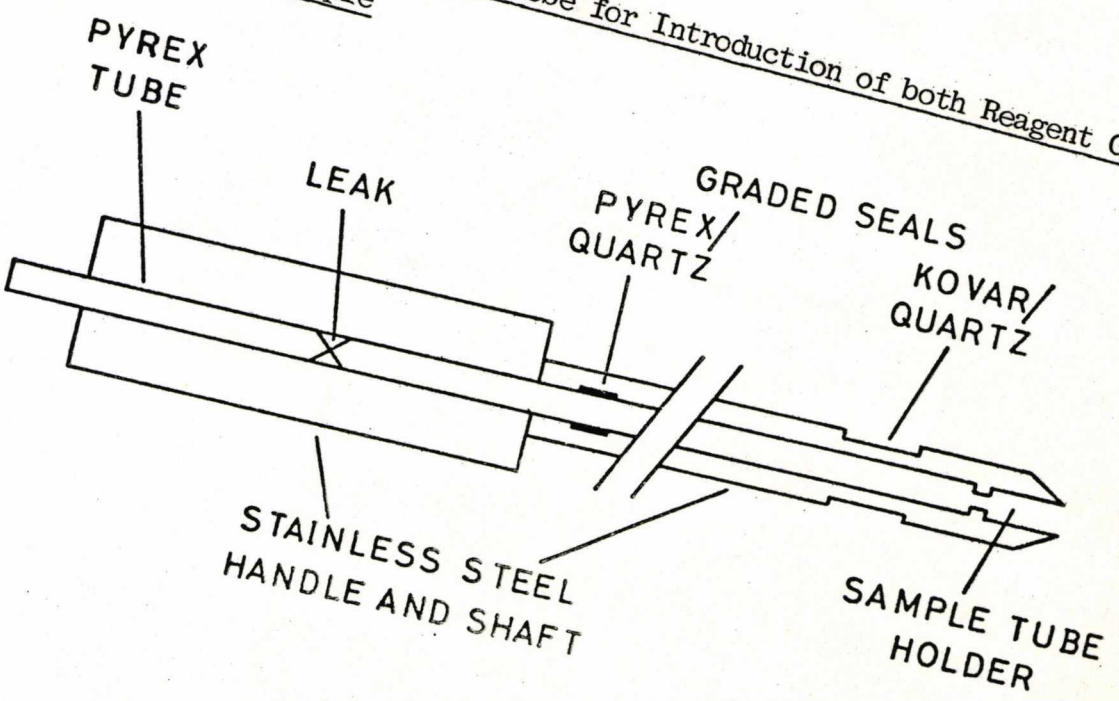

by EI, CI, FI or FD very often complement each other, led Gierlich *et al*[35] to develop a multiple ion source which could be operated in any of these ionisation modes. Another type of multiple ionisation facility is available with the A.E.I. Scientific Apparatus Ltd. MS30 double beam mass spectrometer[36,37]. The double ion beams are produced by two independent ion sources. One of these may be an EI or combined EI/CI ion source while the other may be an EI or a single purpose FD ion source. It is possible to record simultaneously CI and EI, or CI and FD, or EI and FD mass spectra of a sample without breaking the source vacuum.

The type of CI ion source described in this section is the 'standard' CI ion source, various versions of which will be found on most commercially available CI mass spectrometers whether they be magnetic sector or quadrupole instruments. Other types of high pressure CI ion sources are described in Section 2.4.4.

2.4.2.3 Sample and Reagent Gas Introduction Systems

The sample introduction systems used for CIMS are similar to those commonly employed in EIMS. In addition to these, a method of introducing the reagent gas is required and a means of controlling its flow rate. A special problem arises when CI inlet systems are connected to magnetic sector mass spectrometers, where the ion source potential may be as high as 10 kV. At normal CI operating pressures, gases are excellent conductors of electricity and discharges may occur between the ion source and the nearest ground point on the inlet system, presenting a serious risk of high voltage shock to the operator. Futrell and Wojcik[12] performed an elaborate analysis of these phenomena and solved the problem by placing a discharge suppressor in the inlet lines of their mass spectrometer. This consisted of a chain of glass encapsulated resistors each one being interspaced by a porous plug of stainless steel turnings. One end of the resistor chain was connected to the ion source while the other was attached to a ground point. In this way the potential

gradient was limited to a value below that required to accelerate charge carriers to a point where avalanche processes occur, which initiate electric discharges. An alternative solution to this problem, employed in one form or another in the majority of CI mass spectrometers, consists of introducing a capillary leak into the inlet line as close as possible to the ion source. If the pressure on the high side of the leak is maintained at above *ca.* 50 Torr then no electric discharge will occur beyond this point because gases are poor electrical conductors at these pressures.

The reagent gas may be introduced either directly into the ion source through a special inlet port or by way of one of the sample introduction systems. Hogg[17,22] employed a special direct insertion probe for this purpose which is illustrated in Figure 2.6. The sample is placed in the probe tip, which may be heated, in a melting point tube. The reagent gas passes through the length of the probe around the sample tube and into the ion source. Quartz rather than pyrex glass is used at the probe tip because of the poor electrical insulation properties of the latter at temperatures above 150°C. In order to make a gas tight seal, the end of the probe is tapered to fit into a probe guide mounted on the ion source. A similar probe was developed by Garland *et al*[20]. The reagent gas was introduced through a heated glass re-entrant by Yinon and Boettger[18], which push-fitted into a recess in the ion source. This also served as an inlet line for gases and volatile samples, solid samples were introduced on a probe through a separate inlet port. A similar system, developed by Beggs *et al*[15], permitted both volatile and solid samples to be introduced through the same port as the reagent gas.

For CI purposes it is essential that the pressure of the reagent gas in the ion source is kept constant over a long period of time. Several simple methods of achieving this have been devised[17,18,20], based mainly on diaphragm-type gas regulators and large reservoirs. A more sophisticated system, a block diagram of which is shown in Figure 2.7,

has been described by Futrell and Wojcik[12]. In this system the flow of reagent gas into the ion source is controlled by an automatic leak valve which is actuated by a MKS 'Baratron' capacitance manometer. The required pressure is set on the 'Baratron' control unit, this produces an error signal which is proportional to the difference between the set pressure, and that sensed by the pressure transducer connected directly to the ion source. This error signal is sensed by the automatic leak valve control unit which adjusts the leak valve as required, to minimise the error signal.

In CIMS it is often advantageous to be able to obtain mass spectra of a particular sample using two or three different reagent gases. For this purpose many CI mass spectrometers are equipped with double or triple reagent gas inlet lines and facilities to switch rapidly between them. For example, with one such system described by Ryhage[34], it is possible to obtain two mass spectra of a particular sample each with different reagent gases, within five seconds.

As with EIMS special sample introduction/evaporation techniques are required in order to obtain the CI mass spectra of relatively involatile or thermally unstable compounds. Baldwin and McLafferty[23] have described a method of obtaining the CI mass spectra of underivatised peptides, in which the sample is deposited on the extended tip of a solid sample probe which is then introduced directly into the ion plasma of the ion source. In this way, they obtained CI mass spectra with abundant $(M+H)^+$ peaks for samples which when introduced using conventional methods produced mass spectra which showed evidence of extensive thermal decomposition. A similar technique was employed by Knight and Matin[24] for the quantification of a compound which was unstable under gas chromatographic conditions. Hunt *et al*[25] have used field desorption emitters as solid sample probes to obtain the CI mass spectra of salts and thermally labile organic compounds. One very promising method of sample introduction for involatile compounds has been reported by Buttrill and Findeis[26]. In order to obtain the water

Figure 2.7 Block Diagram of a Reagent Gas Pressure Control System

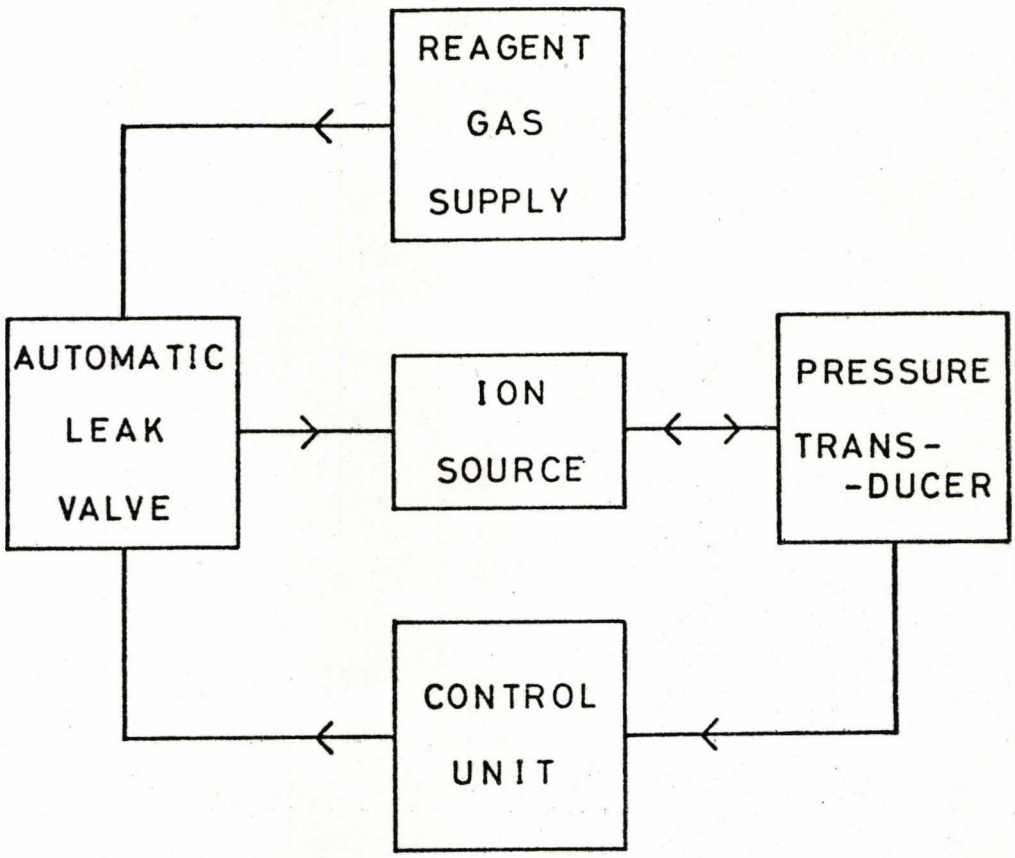

Figure 2.8 Schematic Representation of a Drift Tube Ion Source

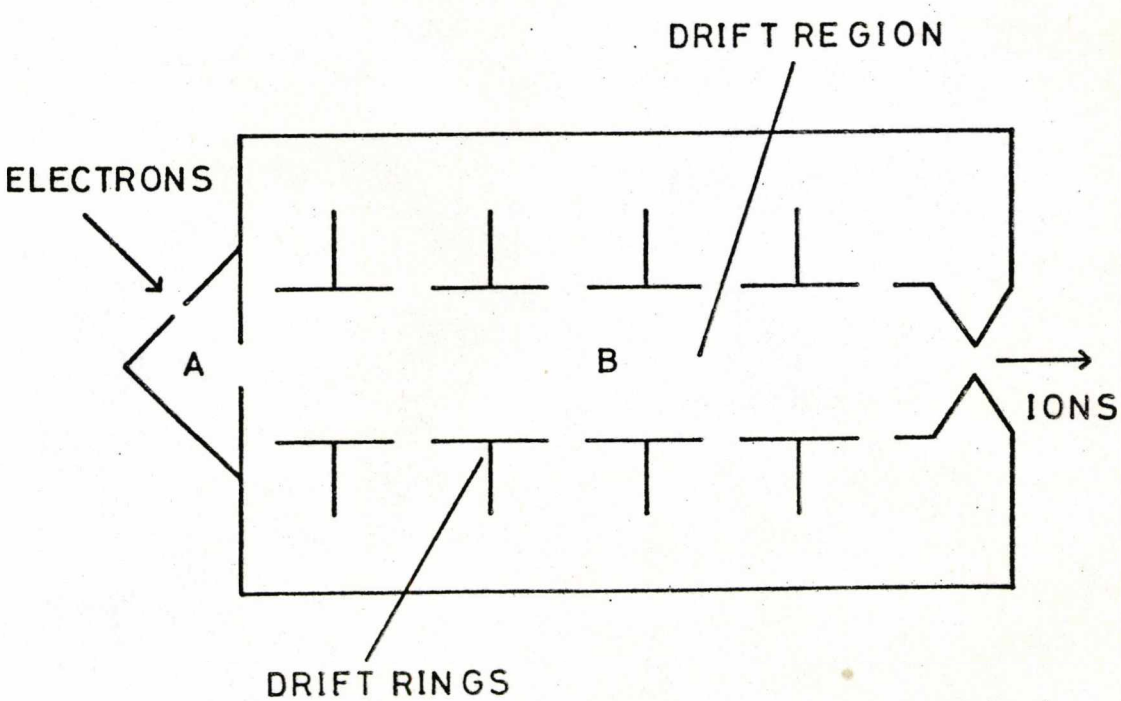

CI mass spectrum of an underivatised tripeptide they placed the sample in a capillary tube above a specially prepared hydrated salt mixture. The capillary was placed in the heated tip of a solid sample probe so that the water vapour released from the salt mixture passed over the sample as it flowed into the ion source. The method was extended to include other reagent gases which were released from molecular sieve pellets held in the probe tip.

2.4.2.4 Electronic Modifications

Only two simple electronic modifications are usually required to convert a mass spectrometer to operate in the CI mode: the electron energy supply must be uprated to between 200 and 1000 eV, and the filament control circuit must be referenced to the total emission current and not the trap current. The optimum value of the electron energy will depend on the design of the ion source and on the operating conditions. Beggs *et al*[15] simply connected a 510V battery in series with the existing electron energy supply on their mass spectrometer in order to increase its maximum value to 600V. Changing from trap to total emission stabilisation of the filament current may usually be achieved by changing certain components in the existing feedback circuit.

Circuit diagrams and descriptions of these modifications for various mass spectrometers have been given by Futrell and Wojcik[12], Beggs *et al*[15] and Hogg[17].

2.4.2.5 Pressure Measurement

The pressure inside an 'open' EI-type ion source may be determined approximately, by means of a pressure gauge mounted somewhere in the vacuum envelope surrounding the ion source, but for a 'closed' CI-type ion source this method is not directly applicable since the pressure inside the CI ion source is expected to be *ca.* 10^4 times greater than in the surrounding vacuum envelope. It is essential to know the pressure

inside a CI ion source for two reasons: (a) for analytical purposes it is necessary to operate in the pressure range where the relative proportions of reagent ions in the reagent gas are constant, and also to have a knowledge of the partial pressure of the sample in the source since CI mass spectra are sometimes dependent on this parameter[40,81,113] (accuracy of pressure measurement is not important in this case); (b) for quantitative CIMS and for kinetic studies of CI-type reactions. Accurate pressure measurement is essential for this purpose.

The pressure inside a CI ion source may be monitored indirectly by pre-calibrating the source envelope ionisation gauge against a known pressure of reagent gas as measured by a McLeod gauge connected directly to the ion source. This method, which was employed by Beggs *et al*[15] and by Hogg[17], together with another indirect method described by Garland *et al*[20] has the disadvantages that the calibration must be repeated for each reagent gas used, and it is not very accurate.

Alternatively, the reagent gas pressure may be measured by connecting a pressure gauge directly to the ion source. A thermocouple gauge was used for this purpose by Ampulski[16]. This too has the disadvantage that it must be calibrated for each reagent gas used. The connection of any type of pressure measurement device directly to a magnetic sector mass spectrometer is subject to the same electrical discharge problems as have already been discussed with respect to CI inlet systems. Futrell and Wojcik[12] employed a MKS 'Baratron' capacitance manometer for pressure measurement which was protected from electrical discharge by their discharge suppressor described in Section 2.4.2.3. The problem was avoided by Yinon and Boettger[18,28] by using a Texas Instruments Quartz Bourdon Tube for pressure measurement. The pressure transducer of this system may be connected directly to a CI ion source even though it will float to accelerating potential, because it is optically coupled to its electronic measurement system which is operated at earth potential. Both this system and the MKS Baratron are very accurate and their calibration is independent of the reagent gas used.

2.4.3 Operational Technique and Instrument Performance

The operation of a mass spectrometer in the CI mode is essentially the same as for the EI mode. In changing from one mode to the other, it is often necessary, depending upon the actual ion source design, to re-optimise the source parameters, particularly the repeller potential, and the ion beam focussing potentials. Special attention must be paid to keeping the source pressure and temperature constant since CI mass spectra are generally more dependent on these two parameters than EI mass spectra.

Since CI mass spectra contain ions of relatively few different values of m/e with gaps of as much as 100 mass units between peaks, assignment of the correct m/e value to a particular peak is extremely difficult without some means of calibrating the mass scale. Reference standards are used for this purpose in EIMS, which may be introduced along with the sample and the mass determined directly or they may be employed to precalibrate the mass scale with the aid of a data system. Dzidic *et al*[38] have shown that perfluorokerosene (PFK), one of the most commonly used mass standards in mass spectrometry may also be employed as a mass standard for CI mass spectra, since the major peaks of its methane CI mass spectrum have the same elemental composition and exact masses as those in its EI mass spectrum. The principal difference is the substantially greater abundance of high mass ions most notably from m/e 643 to 881, a region where PFK produces ions of very low abundance by EI. PFK may be used for either low resolution mass marking or high resolution mass determination of methane - CI mass spectra but is unsuitable for isobutane - CI mass spectra since according to Dzidic *et al*[38] no mass spectrum of PFK is produced with this reagent gas. Bowen and Field[39] employed a series of perfluoro - substituted triazines for mass marking of both methane - and isobutane - CI mass spectra.

The maximum resolving power of a mass spectrometer will not be degraded by its operation in the CI mode, provided that the differential pumping system is adequate enough to maintain the pressure in the analyser

below the point, where collisional broadening of the mass spectral peaks occurs. In an early report by Futrell and Wojcik[12] a resolution of over 50,000 was obtained with a mass spectrometer modified for CI operation for which a resolution of 30,000 was considered nominal high performance. The very narrow ion exit slit employed in CI ion sources often gives rise to an increase in the minimum resolution of the mass spectrometer. Yinon and Boettger[18] for example reported that this parameter increased from 2000 to 7500 for an A.E.I. Scientific Apparatus Ltd. MS902.

The sensitivity of a mass spectrometer operated in the CI mode may be considered either by comparison with its sensitivity in the EI mode under similar operating conditions, or by determining the absolute sensitivity for a standard sample under standard experimental conditions. The former is the only meaningful measure of CI sensitivity at present available, since as yet, there are no agreed standards for CI sensitivity determinations and consequently published values are for various different samples, obtained under diverse experimental conditions, making comparison impossible. Field[40] and also Futrell and Wojcik[12] showed independently that from theoretical considerations the sensitivity, defined as the total sample ion current produced from a certain pressure of sample in the ion source, of CI and EI should be approximately equal. This was first confirmed experimentally by Beggs *et al*[15] who made measurements with two compounds, di-(2-ethylhexyl) phthalate and strychnine, and found that the total ion current in the CI mode was 1.43 and 4.58 times greater, respectively, than in the EI mode. However, the definition of sensitivity used in these studies is not entirely satisfactory since the sample flow rate required to maintain a certain pressure inside a 'closed' CI-type ion source would be considerably lower than that required for an 'open' EI-type ion source. It would be more meaningful to compare the two methods by determining the total charge produced from a known quantity of sample introduced into the ion source. Although very few comparisons of this nature have been performed the evidence accumulating indicates that in

these terms CI sensitivity is at least equal to EI sensitivity and for certain samples it may be much greater. Since the amount of fragmentation in CI is generally smaller than in EI, the charge produced from a given quantity of sample will be concentrated into a smaller number of ions which may lead to a lower absolute detection limit for CI. The sensitivity of CI has been considered in detail by Munson[41].

2.4.4 Other Types of High Pressure Chemical Ionisation Ion Sources and Mass Spectrometers

The ion sources described in Section 2.4.2.2 all employ electrons emitted from a heated filament to effect the initial ionisation of the reagent gas/sample mixture. Hoegger and Bommer[42] developed an ion source in which the initial ionisation was effected by an electrodeless discharge. A plasma was produced by passing argon at a pressure of *ca.* 1 Torr through a microwave discharge tube. This plasma was used to ionise the reagent gas/sample mixture and the ions were mass analysed by a quadrupole mass filter. The only apparent disadvantage of this system was that due to its prototype nature the ion source could not be heated and so only samples with a high vapour pressure could be analysed. A CI ion source employing a negative corona discharge as a means of ionisation has been reported by Kambara and Kanomata[43]. This consisted of a 'closed' ion chamber into which an ordinary sewing needle was inserted. A discharge was maintained at a reagent gas pressure of *ca.* 1 Torr, with a potential of 500V between the needle tip and a repeller electrode. This ion source produced CI mass spectra which were identical to those obtained with a conventional CI ion source. Hunt *et al*[44] have described a CI ion source in which the reagent gas is ionised by a Townsend discharge produced by a discharge tube mounted outside the ion source. This is described in detail in Section 2.7.1. It is preferable to use a discharge type ion source for CI purposes when oxygen or water are employed as reagent gases since these gases tend to severely shorten the lifetime of heated filaments.

The extent of fragmentation of the quasi-molecular ions in CIMS may be controlled by varying the ion source temperature[45], employing a different reagent gas[46] or changing the electric field inside the ion source[13] (i.e. the repeller potential). In the latter method the increase in fragmentation observed when operating at high repeller potentials have been attributed to unimolecular fragmentation of the quasi-molecular ions activated by energetic collisions with neutral reagent gas molecules in the ion source. Price *et al*[47] have described a drift tube CI ion source, shown in Figure 2.8 which uses this effect to provide a variable degree of fragmentation of the quasi-molecular ions in the CI mass spectrum. Ions are formed in region A by electron impact and then drift through the drift tube region B into the mass spectrometer analyser. The ion source is operated at a pressure of *ca.* 0.1 Torr. The energy imparted to a particular ion in the drift region may be varied by changing the value of the voltage gradient down the tube, set by potentials applied to the drift rings. In this way it is possible to increase the 'effective ion temperature' to above 1000^{o}K at the highest drift fields.

A technique has been described by Hodges and Beauchamp[48] for obtaining mass spectra consisting solely of quasi-molecular ions formed by the addition of an alkali ion to the sample molecule. Alkali ions, generated by a thermionic emitter mounted outside of a closed ion source, are injected into a reagent gas containing a trace amount of sample. These ions initially bind to the reagent molecules and are then transferred to the sample.

The ion sources described so far in this survey all operate at pressures in the range *ca.* 0.1 to *ca.* 1 Torr; however, CI processes occur readily at higher pressures. One type of ion source in which CI reactions occur at atmospheric pressure is the atmospheric pressure ionisation (API) source developed by Horning *et al*[49,50]. Such an ion source is shown in Figure 2.9. Samples are introduced, in a suitable solvent, directly into a flowing carrier gas stream which transports the sample into the ionisation region, where it is ionised by a complex series of ion-molecule reactions.

Figure 2.9 Schematic Diagram of an Atmospheric Pressure Ion Source

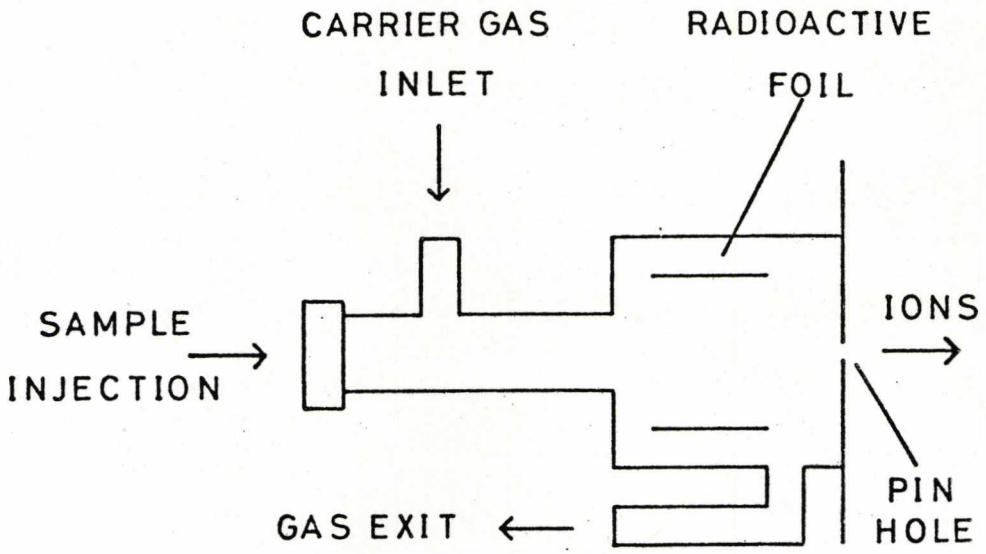

Figure 2.10 Schematic Representation and Pulse Sequence of the Space Charge Trap

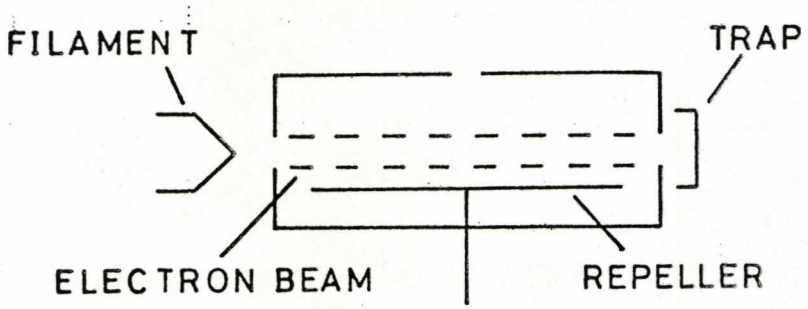

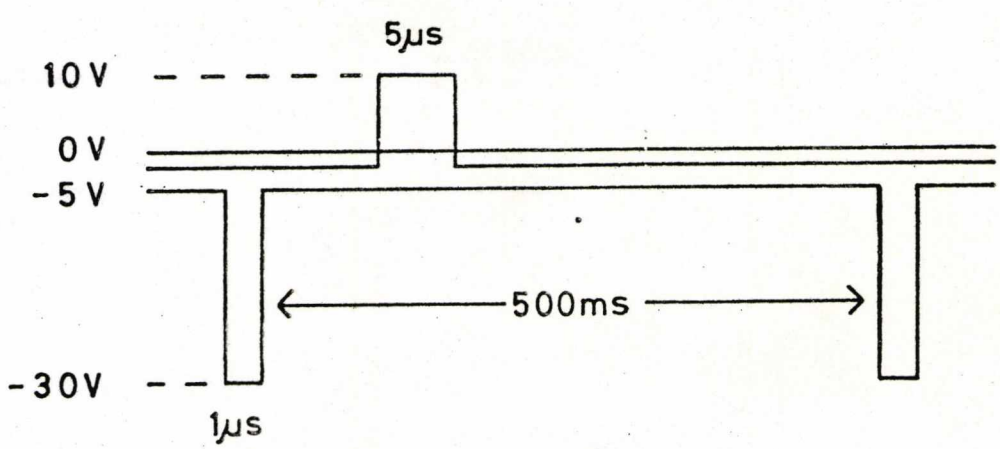

The ionisation is initiated by a radioactive source, usually ^{63}Ni. The ions then drift through a pin hole into a mass spectrometer for analysis. This system is extremely sensitive but has the disadvantage that it is prone to severe interference from trace quantities of impurities in the sample or carrier gas. Another device in which CI reactions occur at atmospheric pressure is the Plasma Chromatograph developed by Karasek[51]. Although this device produces ion-mobility spectra rather than mass spectra, the CI mass spectra of certain samples are very similar to their ion-mobility spectra obtained with the plasma chromatograph[52,53].

High pressure CI ion sources have been fitted to many other types of mass spectrometer besides the conventional quadrupole and magnetic sector instruments[28]. Schoengold and Munson[54] have reported the modification of a time-of-flight mass spectrometer to operate in the high pressure CI mode. A reverse geometry double focusing mass spectrometer has been operated with a high pressure CI ion source by Kruger *et al*[55], in order to explore the capabilities of Mass-Analysed Ion Kinetic Energy Spectrometry (MIKES) in mixture analysis using CI as well as EI to generate the ions. CI studies have also been performed on tandem mass spectrometers[56,57]. These instruments are particularly useful for the study of the mechanisms of CI processes.

2.5 Low Pressure Chemical Ionisation Mass Spectrometry

2.5.1 Introduction

In order for CI studies to be made at low pressures, i.e. less than 10^{-3} Torr, the residence time of an ion in an ion source must be increased such that sufficient ion-molecule reactions occur to effect the chemical ionisation of the sample molecules. In principle, at least, any one of a number of ion storage devices which are currently employed in the study of ion-molecule reactions, may be used as low pressure CI ion sources. Of these devices, only three have been employed to any extent for low pressure CI studies. They are the Space Charge Trap, the Three-Dimensional

Ion Storage Trap (Quistor) and the Ion Cyclotron Resonance Mass Spectrometer.

2.5.2 The Space Charge Trap

This device, in which positive ions are trapped in the negative space charge of an electron beam, was developed by Baker and Hasted[58] for studying the production of multiply charged ions by successive collisions of ions with electrons, in the technique known as Sequential Mass Spectrometry. This ion trapping technique was modified by Bourne and Danby[59] to enable studies of unimolecular ion decomposition and these modifications were adopted by Herod and Harrison[60] and also Ryan and Graham[61] for the study of bimolecular ion-molecule reactions. The space charge trapping of positive ions is one of the simplest methods of studying ion-molecule reactions since it involves the pulsed operation of a conventional electron bombardment ion source as shown in Figure 2.10. Ions produced during a short pulse of electrons of *ca.* 30 eV energy are trapped in the space charge created by a continuous electron beam of 5 eV energy which is insufficient to cause ionisation. A certain time after the ionising pulse a positive pulse applied to the repeller electrode ejects the ions for mass analysis. The entire cycle is repeated at a rate of 2 Hz. Herod and Harrison[60] reported ion trapping times of up to 2.5 ms with such a device and the fact that this may be varied in a controllable manner makes it suitable for the determination of absolute rates of ion-molecule reactions at low pressures.

The space charge trapping technique has been employed by Blair and Harrison[62] to determine the rate coefficients of the reations of the methane reactant ions CH_5^+ and $C_2H_5^+$ with certain polar molecules. There have been very few other reports of the use of this technique in CI related studies, which is somewhat surprising considering its simplicity and the relative ease of modifying a mass spectrometer with a conventional electron impact ion source, to operate in the space charge trapping mode.

2.5.3 The Three-Dimensional Quadrupole Ion Storage Trap (Quistor)

This ion storage device is a three-electrode structure comprising of two end caps and a ring electrode with complementary hyperbolic surfaces and may be considered as a solid of revolution generated by rotating a section through the electrode array of an ideal two-dimensional quadrupole mass filter about an axis perpendicular to the axis of the filter. The employment of precisely formed three-dimensional quadrupolar radio frequency fields for the containment of ions was first described by Paul, Osberghaus and Fischer[63] and by Fischer[64]. Ions are trapped in the device by a combination of r.f and d.c potentials applied to the electrodes. Under appropriate conditions the trajectories of the ions within the device are stable and long trapping times are possible.

The Quistor may be operated in several different modes depending upon the particular application. Fischer[64] and Rettinghaus[65] employed a resonance absorption technique for mass selective detection of stored ions. In this configuration the device is functioning as an ion source, mass filter and detector combined. Dawson *et al*[66] have described a simple and cheap mass spectrometer based upon the quadrupole ion trap fabricated from wire mesh. This device is operated in the mass selective ion storage mode where only ions of one particular mass are stable at any one time. Alternatively, the Quistor may be operated in the so-called total pressure mode where it is possible to store ions possessing a wide range of m/e values simultaneously.

Todd and colleagues[67,68,69] have operated the Quistor in the total pressure mode in conjunction with a quadrupole mass filter for the study of ion-molecule reactions and as a low pressure chemical ionisation source. Their system consists of a Quistor mounted in place of the normal electron impact ion source of a quadrupole mass filter as shown in Figure 2.11. Ions are created inside of the device by a pulse of electrons from an

Section Through the Quistor as Mounted on a Quadrupole Mass Filter

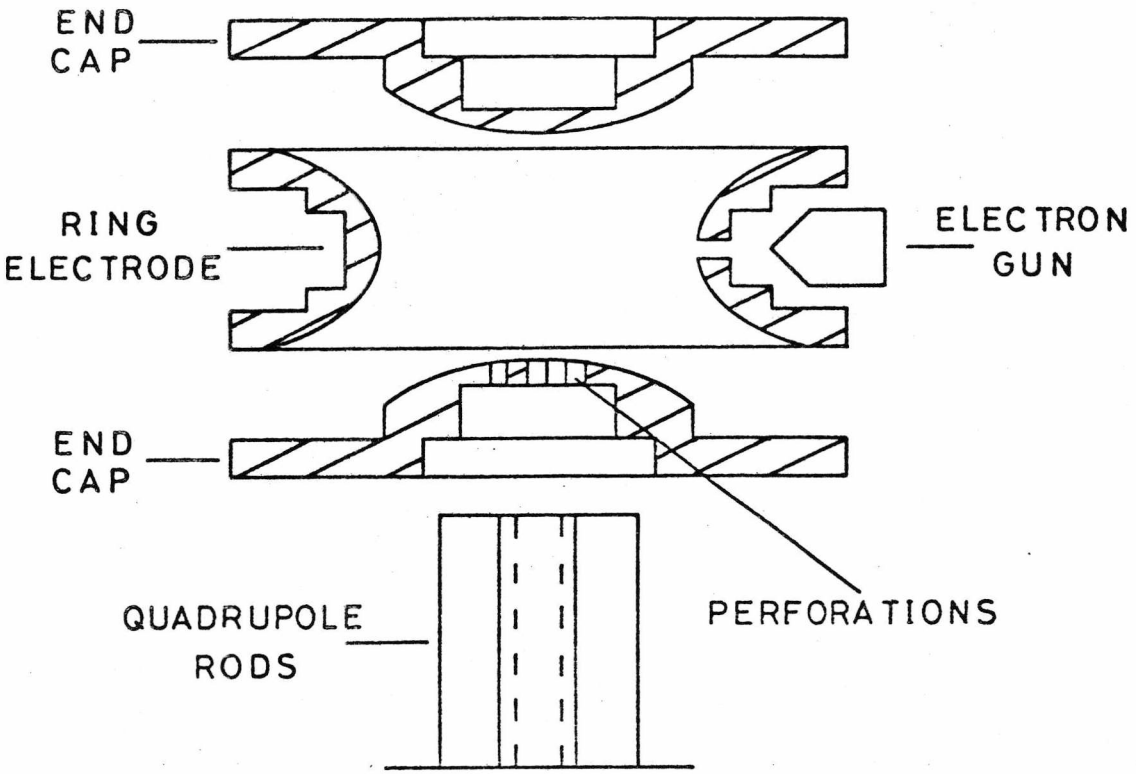

Figure 2.11

electron gun mounted outside the ring electrode. The ions are stored in this case by application of a r.f potential to the ring electrode. After a predetermined time, the storage time, the ions are ejected from the Quistor by application of a suitable pulse to one of the end cap electrodes. The ions pass through perforations in the end-cap and into the mass filter for analysis. For low pressure CI studies the device is operated at a pressure of *ca.* 1×10^{-5} Torr and under these conditions ions may be stored for up to 20 ms. As with the space charge trap the storage time may vary in a controllable manner and so the Quistor may also be employed to determine rate coefficients for ion-molecule reactions[68].

2.5.4 The Ion Cyclotron Resonance (ICR) Mass Spectrometer

This device which is a direct development of the 'Omegatron' described by Hipple *et al*[70,71] differs from the Quistor (as operated in

the 'total pressure' mode) or the Space Charge Trap in that it is a complete mass spectrometer rather than just an ion source. A typical ICR spectrometer is shown in Figure 2.12. Ions are produced in the source region by electron impact. A uniform magnetic field B is orientated along the z axis and a d.c electric field E_s, produced by a potential V_s between plates 1 and 3, is present in the y direction. An ion in crossed d.c electric and magnetic fields will drift in the x direction following a cycloidal trajectory with a characteristic frequency of revolution ω_c. The ion then drifts out of the source region and into the analyser, where, in the presence of the same magnetic field and a d.c electric field E_a, produced by a potential V_a between plates 5 and 6, it will continue to drift in the x direction. In addition to V_a an r.f electric field E_{rf} is introduced in the analyser region normal to the magnetic field. If ω_{rf} is equal to ω_c, an ion will absorb energy from the r.f electric field and be accelerated. Hence the radial component of its cycloidal trajectory will increase. Since ω_c for any ion depends only on its m/e value and the magnetic field strength, a mass spectrum can be obtained by measuring power absorption from the r.f electric field while sweeping this, or the magnetic field. Ions passing through the analyser region are collected on the total ion collector. A small d.c trapping potential is applied to plates 2 and 4 to prevent ions from drifting in the z direction. Although an ICR cell is typically only 9 cm in length, the cycloidal trajectories followed by the ions results in very long ion path lengths (2-50 m) and residence times of between 1 and 25 ms at pressures of *ca.* 10^{-5} Torr.

The ICR spectrometer may be employed to investigate ion-molecule reaction pathways when operated in either the double resonance[72] or source ejection[73] modes. If, for example, the reaction product C^+ could have been produced by reaction of either A^+ or B^+ with a neutral molecule, the correct pathway may be established, using the double resonance technique, in the following manner. The observing oscillator in the analyser region is set to observe the ion C^+ and an additional oscillator

Figure 2.12 Diagram of a Conventional ICR Mass Spectrometer

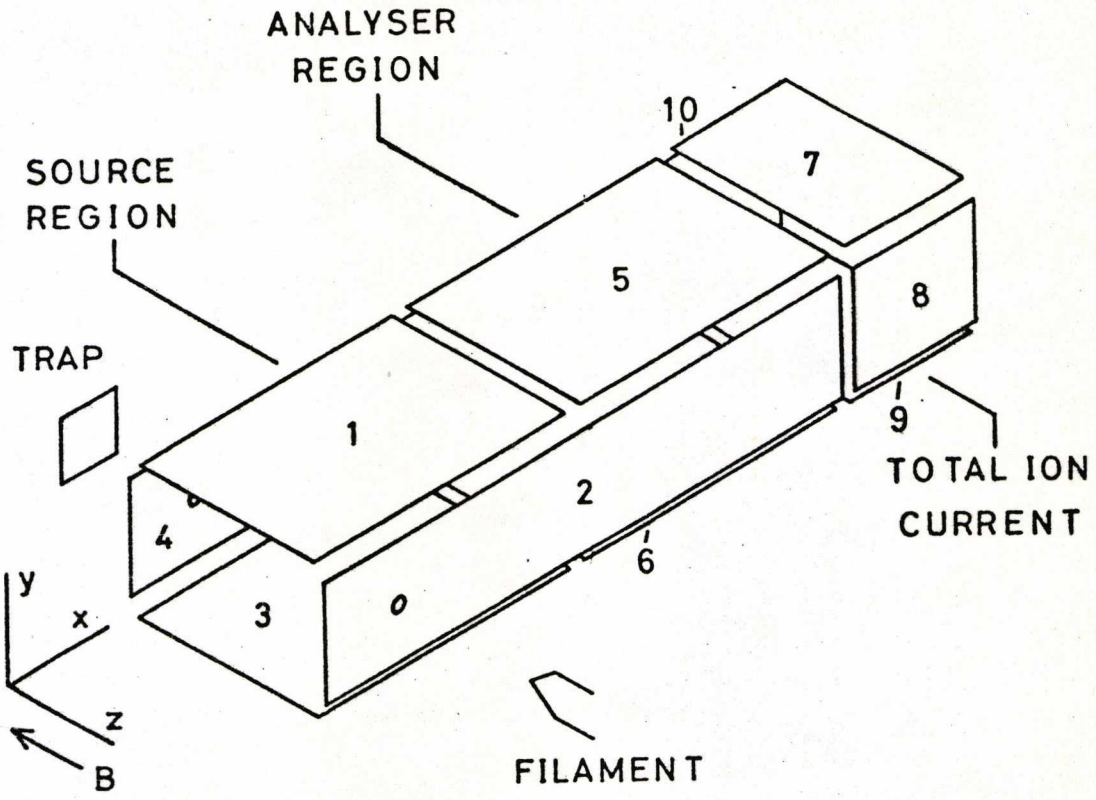

Figure 2.13 Diagram of a Trapped ICR Mass Spectrometer

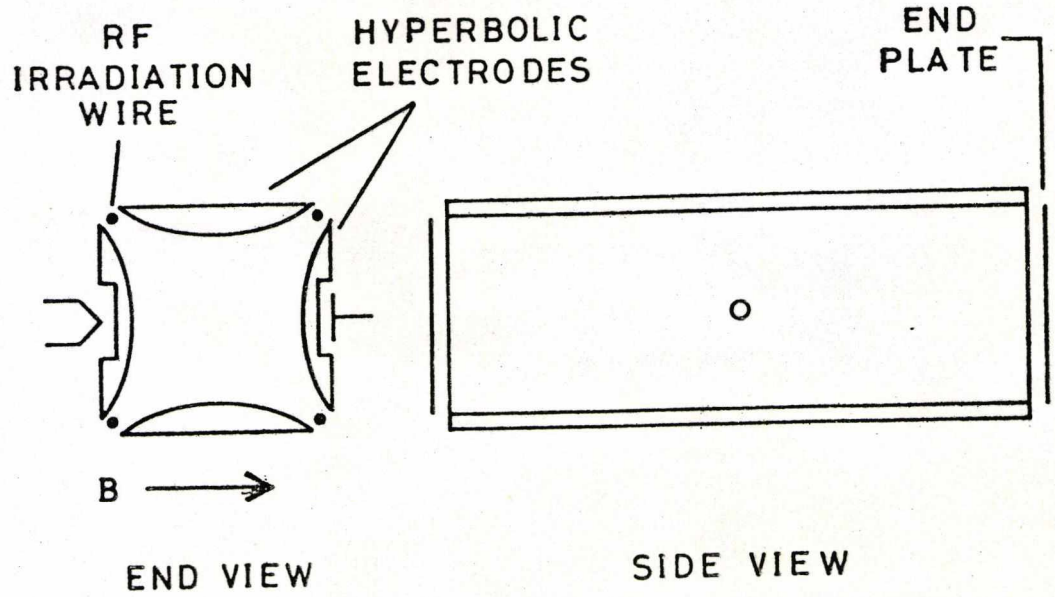

connected to plate 3 (Figure 2.12) of the source region is tuned to the cyclotron frequency of A^+ and B^+ in turn. The peak shape of the C^+ ion will change only when the second oscillator is tuned to the cyclotron frequency of its precursor ion. The source ejection technique is similar except that the additional oscillator is connected between the trapping plates (2 and 4 in Figure 2.12). In this case the oscillator is tuned to the frequency of the ions oscillatory motion in the z direction which arises from the combination of the magnetic field and the electron field produced by the trapping potential.

Another technique known as trapped ion cyclotron resonance has been developed by McIver[74,75]. One of the most recent versions of the trapped ion cyclotron resonance mass spectrometer[76] is shown in Figure 2.13 with which it is claimed, at a pressure of 4.7×10^{-7} Torr, 80% trapping efficiency of ions is observed after 3 seconds. This device differs from conventional ICR spectrometers in that: resonant ions are collected on the upper and lower electrodes the resulting current being amplified by an electrometer, the r.f potential is applied to two pairs of wires running parallel to the long axis of the cell, the device has four hyperbolic electrodes and two end plates which improve the trapping efficiency. The fact that the trapped ICR spectrometer is operated in a pulsed mode makes interpretation of kinetic studies of ion-molecule reactions less complex than for the conventional ICR spectrometer. Double resonance studies are possible with this device using the source ejection technique described previously.

Conventional ICR spectrometers have been employed by Pesheck and Buttrill[77] to study the mechanisms of formation of the principal fragment ions in the methane CI of esters and by Bursey *et al*[78] to investigate acetylation as a CI technique. A four section ICR spectrometer with an extra reaction zone between the source and analyser regions was employed by Clow and Futrell[79] to investigate the mechanisms of formation of various fragment ions from the methane CI of some C_6 hydrocarbons. McIver *et al*[76]

have demonstrated the suitability of the trapped ion cyclotron resonance spectrometer for low pressure CI studies by obtaining both positive and negative CI mass spectra of morphine and acetyl salicyclic acid with various reagent gases.

2.6 Comparison of High and Low Pressure Chemical Ionisation Techniques

2.6.1 Instrumental Considerations

During the early development of conventional high pressure CIMS the two principal difficulties encountered in modifying a mass spectrometer to operate in the CI mode were the installation of a high capacity pumping system and the problems associated with high voltage discharge on magnetic sector instruments. Since neither of these problems arise in low pressure CIMS they may be considered as two possible instrumental advantages of the latter technique. However, the development of modern analytical mass spectrometers and the demands for CI facilities have reached the stage that CI, and therefore high capacity pumping systems, are standard features on many commercial instruments and high voltage discharge is no longer a serious problem. In addition to this, low pressure CI studies using either the Quistor or the ICR spectrometer require specially constructed ion sources which are also in general more difficult to operate than high pressure CI ion sources. Regarding these two devices the conclusion is that they have no great advantage over the high pressure technique for CI studies. By far the simplest method of performing CI studies is with the space charge trapping technique which requires only a conventional mass spectrometer with an electron impact ion source operated in a pulsed mode.

2.6.2 Operational Characteristics

The typical operating conditions for both high and low pressure CI ion sources are shown in Table 2.1. Since there have been relatively few reports of CI studies performed using any of the low pressure CI techniques

Table 2.1 Typical Operating Conditions for High and Low Pressure CI Ion Sources

	Reagent Gas Pressure (Torr)	Sample Pressure (Torr)	Ion Residence Time (Seconds)
Conventional High Pressure CI	1.0	10^{-3}	10^{-4}
Space Charge Trap	10^{-4}	10^{-5}	5×10^{-3}
Quistor	10^{-4}	10^{-6}	5×10^{-3}
Conventional ICR	10^{-4}	10^{-6}	2×10^{-2}
Trapped ICR	10^{-6}	10^{-8}	10

it is impossible to make a general comparison between these, and CI studies performed using the high pressure CI technique. Pesheck and Buttrill[77] compared the low pressure CI mass spectra of some esters obtained with an ICR spectrometer, with a high pressure CI study performed by Munson and Field[45], and concluded that despite the difference in operating conditions the mass spectra were remarkably similar. One fundamental difference between high and low pressure CI mass spectra is that in the latter no collision-stabilised ions arising from either the association of sample molecules with reactant ions, such as $(M+ C_2H_5)^+$ or the clustering of polar reagent gas molecules around reactant ions are generally observed. This is because the lifetimes of association complexes such as $(M+ C_2H_5)^{+*}$ are considerably shorter than the mean ion-molecule collision times in low pressure CI systems, and also the mean kinetic energy of reactant ions and thus the energy content of the $(M+ C_2H_5)^{+*}$ species, is in general higher than the thermal ion energies characteristic of high pressure CI.

In order to determine reaction rate constants for CI processes, it is necessary to know the residence time of ions in the CI ion source. For conventional high pressure ion sources this must be calculated from idealised ion drift considerations. It is well known that such calculations are often substantially in error[80] even under ideal conditions and it is not surprising therefore that early results were not always in agreement with each other[81,82]. In general it is difficult to determine rate constants accurately with this type of ion source unless it has been coverted for pulsed operation as described by Sroka, Chang and Meisels[83]. In contrast to this ion residence time is very well defined in both the Quistor and the space charge trap and so they are more suitable for rate constant determinations than the conventional high pressure ion source. This advantage may, however, be offset by uncertainties in the internal and translational energies of the reagent ions and the difficulty of achieving accurate pressure measurements in low pressure systems. The ICR spectrometer may also be employed for CI rate studies and, when operated in

either the double resonance or source ejection mode the ICR spectrometer may be used to investigate the mechanisms of CI reactions as may the tandem mass spectrometer. Mechanistic studies have been performed using high pressure CI mass spectrometers but the method employed is not as versatile as that used with the former two instruments and usually involves the use of deuterium labelled reagent gases and samples[118,119].

One of the great potential advantages of low pressure CIMS over the high pressure technique is in the analysis of ultra-low vapour pressure compounds. This was demonstrated by McIver *et al*[76] using the trapped ICR spectrometer. They showed that it was possible to obtain CI mass spectra with sample partial pressures of *ca.* 10^{-7} Torr. Calculations indicate that sample vapour pressures as low as 10^{-10} Torr can be detected by this method.

Recently, Lawson and Todd[120] have shown that the Quistor may be employed to enhance the intensity of weak mass spectral peaks and that it may be potentially useful when samples are present in only trace amounts.

2.7 Other Techniques Combined with Chemical Ionisation Mass Spectrometry

2.7.1 Negative Ion Chemical Ionisation Mass Spectrometry (NICIMS)

Historically, negative ion electron impact mass spectrometry has been limited by ion currents which are two or three orders of magnitude lower than the corresponding positive ion currents. The situation improved considerably with the introduction of non-reactive gas enhancement of negative ion mass spectra[84] and the production of negative ions under CI conditions is an obvious extension to this technique.

The formation of negative ions by interaction of electrons with sample molecules can occur by three different mechanisms[85]:

$AB + e^- \rightarrow AB^-$	resonance capture
$AB + e^- \rightarrow A + B^-$	dissociative resonance capture
$AB + e^- \rightarrow A^+ + B^- + e^-$	ion pair production

Each of these processes shows a strong dependence on electron energy.

Resonance capture, which produces molecular anions, involves electrons with near zero energy. Dissociative electron capture is observed with electrons in the energy range 0-15 eV, while ion pair production usually requires electron energies above 10 eV. Under the conditions prevailing in a conventional electron impact ion source, formation of negative ions occurs predominately by the ion pair mechanism and to a lesser extent by resonance capture of electrons, thermalised by interaction with either the walls of the ion chamber or with molecules (i.e. from the positive ion production process $A + e^- \rightarrow A^+ + 2e^-$). The large increase in negative ion currents observed when the ion source pressure is increased to above 10^{-5} Torr for gas enhancement and further to CI conditions of 1 Torr, has been attributed to the large population of thermal electrons generated under these conditions.

The ionisation of sample molecules by attachment of thermal electrons is not 'chemical ionisation' in the strict sense of the term but produces mass spectra which possess the characteristic features of a CI mass spectrum, i.e. ions of high intensity in the molecular weight region and few fragment ions. Electron attachment mass spectrometry, as it is called, was used by von Ardenne[86,87] and colleagues for the determination of the molecular weights of complex organic molecules including steroids, condensed aromatic compounds and natural products. They also reported[88] the observation of true negative CI processes such as attachment of O^- and Cl^- to certain compounds three years before the invention of positive CI. The method employed by von Ardenne[89,90] was to generate a plasma using a low pressure (10^{-1} Torr) argon discharge, containing positive argon ions and a large population of low energy electrons. This plasma was constrained by a strong magnetic field and allowed to pass into a chamber containing the gaseous sample. Although this method was very successful it has not been widely used due to the cost of the Duoplasmatron-type ion source and the extensive modifications required to facilitate its attachment to commercially available mass spectrometers.

The discovery that negative ion beams as intense as positive ion beams, could be produced using a high pressure CI ion source has revived interest in negative ion mass spectrometry in general. Much of the early work on NICIMS was performed by Dougherty and colleagues[91,92,93] who employed a standard high pressure ion source to obtain the negative CI mass spectra of insecticides and pesticides using methane, isobutane and methylene chloride as reagent gases. More recently Hunt *et al*[102] have been exploring the utility of employing strong oxidising agents such as nitric oxide and oxygen as CI reagent gases for both positive and negative CIMS. Since the use of such reagents severely shortens the lifetime of the heated filaments which are normally used to generate the electron beam, Hunt and colleagues[44] have modified a CI ion source to accommodate a Townsend discharge tube. This discharge tube, an exploded diagram of which is shown in Figure 2.14, produces electrons and/or ions, depending on the mode of operation which are carried along with the reagent gas into the ionisation chamber. It consists of two 85% transmission grids interspaced by a hollow lava spacer and encased in another lava spacer. One grid is in electrical contact with the ion source which has a 0.3 cm hole drilled in the wall. A stainless steel tube, which is connected to the reagent gas supply, is in electrical contact with the second grid. To operate the device in the negative ion mode, a potential difference of *ca.* 600V is maintained between the second grid and the ion source which is at accelerating potential. This produces a discharge at reagent gas pressures of *ca.* 1 Torr resulting in 10-30 μA of electrons entering the ion source. The operation of the Townsend discharge source is unaffected by the nature of the reagent gas and it gives rise to mass spectra which are essentially identical to those obtained with a filament as the electron source.

Negative ion CI processes have also been observed at atmospheric pressure by atmospheric pressure ionisation (API) mass spectrometry[49] and by negative ion plasma chromatography-mass spectrometry[94].

The relative sensitivity of positive and negative CIMS is discussed in the next section.

Figure 2.14 Exploded Diagram of a Townsend Discharge Ion Source

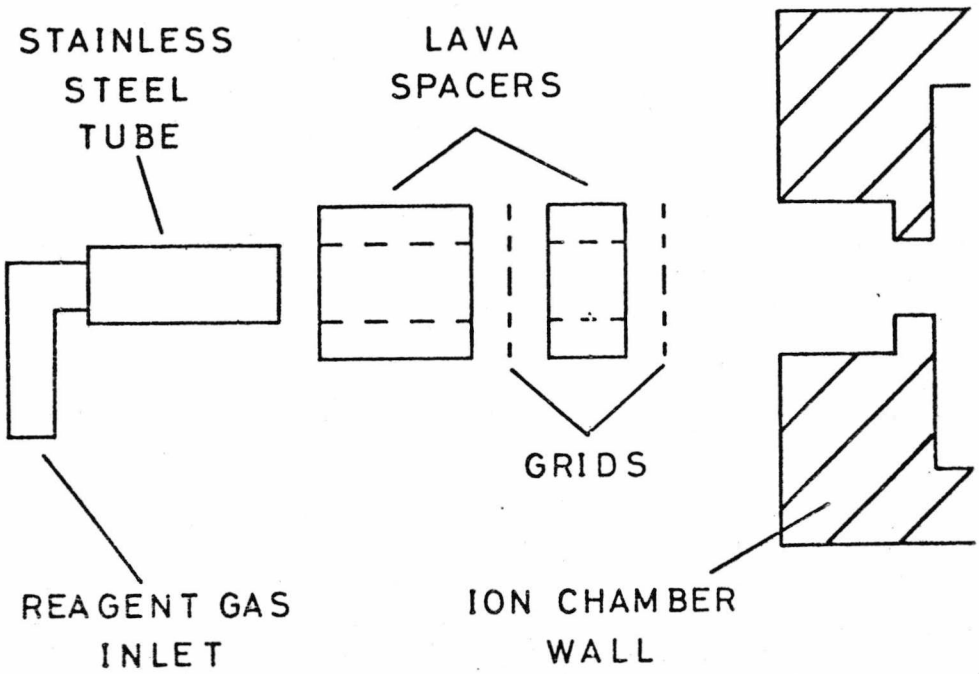

Figure 2.15 Schematic Block Diagram of the Pulsed Positive and Negative Ion CI Mass Spectrometer

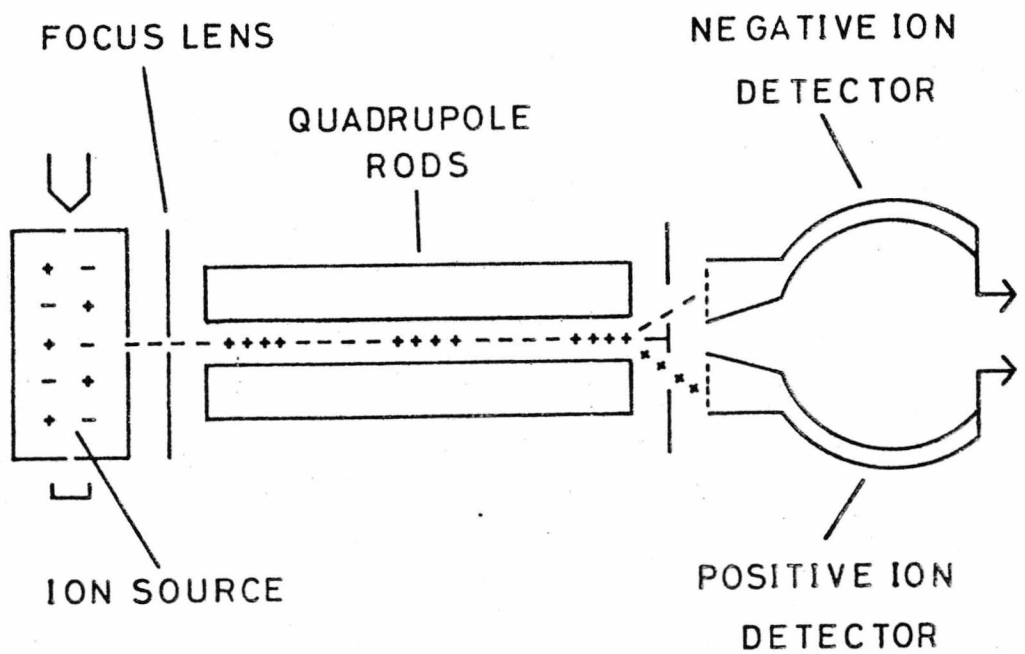

2.7.2 Pulsed Positive and Negative Ion Chemical Ionisation Mass Spectrometry (PPNICI)

This very promising technique developed by Hunt and colleagues[95] depends on the fact that ions of identical m/e but of opposite polarity will traverse a quadrupole mass filter with equal facility. The experimental arrangement is shown in Figure 2.15. Quasi-simultaneous recording of positive and negative CI mass spectra using a conventional quadrupole mass filter is accomplished by switching the polarity of the ion source potential (±1-10V) and focussing lens potential (±10-30V) at a rate of 10 KHz. The alternate 'packets' of positive and negative ions ejected from the ion source traverse the mass filter and are detected by either of two continuous dynode electron multipliers placed side by side. The operating potentials applied to the multipliers are arranged such that positive ions are attracted to one and negative ions to the other. After suitable amplification the outputs from the multipliers are displayed on a light beam oscillograph.

This system may be operated in several distinct CI modes by introducing various different reagent gases into the ion source at a pressure of *ca.* 1 Torr. Using this method it is possible to record simultaneously: electron capture and electron impact type CI mass spectra using argon or nitrogen as the reagent gas, electron capture and Brønstead acid CI mass spectra with methane as the reagent gas, Brønstead base and Brønstead acid CI mass spectra with a mixture of methane and methyl nitrite as the reagent gas, and, by careful control of the amount of methyl nitrite, one can obtain combined electron capture - Brønstead base and Brønstead acid CI mass spectra. More recently, Hunt and colleagues[96], have demonstrated how this system may be used for mass measurement with an accuracy of 5-10 mmu. Since the negative ion methane CI mass spectrum of perfluorokerozene (PFK) is *ca.* 600 times more sensitive than the positive ion spectrum, ions due to the internal standard appear only on the negative trace and so it is possible to use the negative PFK peaks to calibrate sample mass spectra

acquired simultaneously in the positive ion mode.

The PPNICI technique is ideal for comparison of the sensitivity of positive and negative CI for a particular sample since both are recorded under identical conditions. Hunt and colleagues[96] have reported that for certain samples, ion currents obtained under electron capture conditions in the negative ion mode may exceed ion currents in the positive ion mode by two or three orders of magnitude. However, they point out that enhanced sensitivity in the electron capture negative ion mode will only be realised for sample molecules which possess a positive electron affinity and a large cross section for electron capture.

2.7.3 Gas Chromatography Chemical Ionisation Mass Spectrometry (GC-CIMS)

One of the major problems encountered when interfacing a gas chromatograph to a mass spectrometer is how to reduce the quantity of GC effluent to a level whereby a workable pressure is obtained in the mass spectrometer ion source. Many elegant interfaces have been developed for this purpose including: the molecular separator with which the carrier gas is largely removed from the GC effluent, and the use a capillary restrictor at the exit of the GC column to allow a small aliquot of the effluent to enter the mass spectrometer ion source. These methods and their relative advantages have been described in detail by McFadden[97]. An alternative approach to the problem which has the advantage of 100% sample utilisation is to introduce the total GC effluent directly into mass spectrometer ion source. Since the GC is normally operated at atmospheric pressure and the carrier gas flow rates are well above that which can be handled by standard mass spectrometer source pumping systems, 'total effluent' GCMS can only be implemented on mass spectrometers with high capacity source pumping systems. One such system described by Henderson and Steel[98] was able to handle effluent flow rates of up to 20 ml min^{-1}. The implications of this with respect to CIMS are obvious; CI mass spectro-

meters necessarily require high capacity pumping systems and it is therefore possible to connect the exit of a GC column directly to a 'closed' CI ion source to obtain CI mass spectra of the components in the GC effluent.

The early GC-CIMS combination instruments were based on either quadrupole[21,99,100,101] or time-of-flight[54] mass spectrometers because of possible electric discharges in magnetic instruments, from the ion source, which is at high potential, to the grounded gas chromatograph, at high source pressures. This problem has recently been solved[102,103] by placing some form of flow restrictor between the exit of the column and the ion source. The technique employed in the first reports on GC-CIMS was to use the CI reagent gas also as the carrier gas for the GC. Arsenault *et al*[21] employed methane as a combined carrier/reagent gas and reported chromatographic resolution identical to that obtained with helium as the carrier gas. Although this method was very convenient it was not directly applicable to the use of other reagent gases such as isobutane, ammonia and water. Blum and Richter[104] reported that when high efficiency open tubular columns were employed, the use of carrier gases other than hydrogen or helium had adverse effects on the gas chromatographic resolution. Consequently, they operated their GC under standard conditions and mixed the GC effluent with the CI reagent gas just prior to admission into the ion source. This allowed flexibility in the choice of optimal parameters in both GC and mass spectrometer.

The many available methods of monitoring the course of a GCMS run are equally applicable to GC-CIMS, these have been reviewed elsewhere[97]. One method which is specifically applicable to directly coupled GC-CIMS called reactant ion monitoring has recently been reported by Hatch and Munson[105]. Since there is no separator between the GC and the mass spectrometer, a fixed fraction of each component of the gas chromatographic mixture is eluted into the ion source. As this happens there is a decrease in the ion current from the reactant ions due to the reactions of these ions with the added sample. By tuning the mass spectrometer to monitor

one particular reactant ion an ion current vs. time trace may be obtained which strongly resembles the conventional gas chromatography trace. This technique may be extended by careful choice of the reagent gas, to permit selective detection of certain classes of compounds.

2.7.4 Liquid Chromatography - Chemical Ionisation Mass Spectrometry

Liquid chromatography (LC) is rapidly becoming recognised as a powerful new separation technique, being especially valuable for those samples which are not amenable to gas chromatography. The use of LC for many potential applications has been restricted by problems of limited detector versatility, sensitivity, and selectivity. The coupling of a mass spectrometer to a liquid chromatograph largely overcomes these problems and considerably broadens its range of applications. The difficulties associated with LC-MS coupling are even greater than for GCMS since under normal operating conditions liquid flows from the exit of the LC column at the rate of *ca.* 1 ml min^{-1}.

Direct sampling of pure organic liquids into a conventional EI mass spectrometer has been reported by Tal'rose *et al*[106], but the very low source pressures required limits the liquid flow rates to less than 10^{-6} ml min^{-1} which would not give practical sensitivities for solutes. Since the CI mass spectrometer is purpose-built to operate with high flow rates of gas through the ion source, it would seem the ideal instrument to use in conjunction with a LC. To investigate the direct introduction of liquid solutions into a CI mass spectrometer Baldwin and McLafferty[107] took approximately 10 µl of the LC solution and sealed it in a 2 mm capillary, with the end of the tube drawn out into a fine filament. This tube was introduced into the CI ion source on the end of a solid sample probe, the pressure of a bubble of air left in the tube being sufficient to make the liquid spray out of the tube. The flow rate could be increased by either cutting the tip shorter or heating the probe. In this way it was possible to maintain relatively constant source pressures for periods of

several minutes with flow rates that gave the required CI conditions, the solvent acting as the reagent gas. This technique was extended by McLafferty and colleagues[108,109] so that the LC effluent could be monitored directly by the mass spectrometer. The solution is introduced into the ion source through a glass capillary which passes through the centre of a teflon rod. This is introduced into the vacuum system via the direct insertion probe vacuum lock and makes a gas-tight seal with the ion source. Approximately 1% of the total LC effluent, corresponding to a flow rate of 0.01 ml min^{-1}, may be introduced in this way. Combined solvent/reagent liquids such as hexane, pentane, benzene and methanol have been employed to give characteristic CI mass spectra of many solutes. It is also possible to introduce reagent gases concurrently through another re-entrant.

2.8 Types of Reagent Gases Employed in Chemical Ionisation Mass Spectrometry

The two most commonly employed reagent gases in CIMS are methane and isobutane. These effect ionisation of the sample by either proton transfer, hydride abstraction or alkyl ion addition depending on the nature of the sample. The characteristic features of the CI mass spectra of a variety of different compounds using these reagent gases have been described in detail by Field[40]. Hunt[110] has explored the utility of water, ammonia and deuterium oxide as CI reagent gases and has found the latter to be particularly useful for the determination of active hydrogens in organic molecules. In the early work on CIMS ion-molecule reactions between the sample and the reagent ion always involved the transfer of a 'heavy' particle such as a proton, but in the past few years the definition of the term chemical ionisation has been expanded to include charge exchange reactions which involve electron transfer. Einolf and Munson[111] have investigated the use of charge exchange reagent gases such as the rare gases, nitrogen, carbon monoxide and nitric oxide and reported that for certain reagent gases and samples the charge exchange CI mass spectra

were very similar to the EI mass spectra. Mixtures of charge exchange and proton transfer type reagent gases such as argon and water have been employed by Hunt[112] to produce mass spectra which exhibit all the features that are characteristic of both conventional EI and methane CI mass spectra.

The reagent gases mentioned in this section represent only a small fraction of those which have been employed in CIMS and reported in the literature. Any discussion of the characteristic features and particular applications of the various reagent gases and also the applications of CIMS in general is beyond the scope of this review. These subjects have been described in detail elsewhere[40,102,113-117].

2.9 Commercial Instruments

Most mass spectrometer companies who manufacture instruments for organic applications, now offer a chemical ionisation facility either as standard equipment or as an accessory on at least one of their range of instruments. This may be either in the form of a single purpose CI ion source or a dual purpose CI/EI ion source. The various instruments will not be listed here but a few are worthy of special note. For very high resolution studies the MS50 produced by A.E.I. Scientific Apparatus Ltd. may be supplied with a CI ion source. This company also manufactures the dual beam MS30 mass spectrometer which may be converted to operate in the CI mode. Varian Associates Ltd. manufacture a CI mass spectrometer with the facility of photoplate detection. Two reverse-geometry double focussing instruments are available for MIKES-CI studies, one produced by Varian and the other by Vacuum Generators Ltd. Scientific Research Instruments of Baltimore manufacture CI conversion kits for many commercially available mass spectrometers.

Of the low pressure CI techniques, only the conventional ICR mass spectrometer is commercially available. However, it is relatively simple to modify a conventional electron impact ion source to operate in the space charge trapping mode with universally available components.

2.10 Conclusions and Future Developments

This review has shown how a subject which started essentially as an aspect of academic physical chemistry (ion-molecule reaction rate studies) has led to the emergence of an important analytical technique, providing almost infinite scope for gas phase organic chemistry. The inventiveness which characterises mass spectroscopists has resulted in developments and improvements in instrumentation and experimental technique, particularly in the increased sensitivity towards trace material, by more efficient ionisation.

Some of the most encouraging recent developments which show great promise for the future of CIMS include: the selective detection of certain classes of compounds using reagent ion monitoring in GC-CIMS[105], improved methods of introducing relatively involatile samples such as the use of F.D. emitters as solid probes[25] and the generation of the reagent gas within the solid probe in which the sample is deposited[26], and in particular the rapidly expanding field of negative ion CIMS[117].

Modern CI mass spectrometers are becoming more and more sophisticated with rapid changeover between the CI and EI modes of operation and fast switching between different reagent gases. The development of an instrument based on the trapped ICR spectrometer capable of detecting vapour pressures of 10^{-10} Torr[76] may lead to a greater interest in the low pressure CI technique.

CHAPTER 3

THE CHARACTERISATION OF THE THREE DIMENSIONAL QUADRUPOLE ION TRAP (QUISTOR) AS AN ION SOURCE FOR A MASS SPECTROMETER

3.1 Introduction

The Quistor is an ion storage device in which gaseous ions may be constrained within an electro-dynamic quadrupole field produced by a combination of r.f. and d.c. electric potentials applied to an array of hyperbolic electrodes. It is a member of a large family of devices which utilise the strong focussing properties of alternating potential gradient quadrupole fields, the better known members of which include the quadrupole and monopole mass spectrometers. These devices and their various applications have been described in detail by Lawson *et al*[121], Todd[122], Todd *et al*[123], Dawson[124] and Todd and Lawson[125].

In this chapter, the operation and characterisation of the Quistor when employed as an ion source for a quadrupole mass filter is described in detail. The Quistor/mass filter combination was originally developed in this Laboratory and the work on its physical characterisation described in Section 3.4 is in part a continuation of the studies initiated by G. Lawson[126] and R.F. Bonner[127]. However, the majority of the research is directly related to the development of the Quistor as a low pressure CI ion source, in that, from a greater understanding of the physical processes occurring in the Quistor and its ion containment parameters, the optimum conditions for its operation in the CI mode can be established.

3.2 Basic Theoretical Description of Ion Containment in the Quistor

In an ideal quadrupole electric field the potential $\phi_{x,y,z}$ in a rectilinear coordinate system is given by

$$\phi_{x,y,z} = \phi_o(\lambda x^2 + \sigma y^2 + \alpha z^2) \tag{3.1}$$

where λ, σ and α are constants and ϕ_o is the potential difference between oppositely charged electrodes. In the absence of any additional potential arising from the presence of ions within the field, the Laplace condition $\nabla^2\phi = 0$ applies, such that equation (3.1) becomes

$$(\lambda + \sigma + \alpha) = 0 \tag{3.2}$$

Clearly, a number of combinations of λ, σ and α are possible giving rise to a variety of different electrode structures. For the Quistor we have

$$\lambda = \sigma = \pm\, 1/2r_o^2 \; ; \; \alpha = \mp\, 1/2z_o^2 \tag{3.3}$$

where r_o and z_o are the two critical internal dimensions shown in Figure 3.1. Thus in order to satisfy the Laplace condition the geometry of the Quistor must conform to the requirement

$$r_o^2 = 2z_o^2 \tag{3.4}$$

One form of equation (3.1) then becomes

$$\phi_{x,y,z} = \frac{\phi_o}{2}\left(\frac{x^2 + y^2}{r_o^2} - \frac{z^2}{z_o^2}\right) \tag{3.5}$$

Because of the circular symmetry of the device about the z-axis, we can write $x^2 + y^2 = r^2$, and hence equation (3.5) may be written as

$$\phi_{r,z} = \frac{\phi_o}{2r_o^2}\,(r^2 - 2z^2) \tag{3.6}$$

As is illustrated in Figures 3.1 and 3.2, the Quistor is a three electrode

Figure 3.1 Section Through the Quistor Electrode Structure

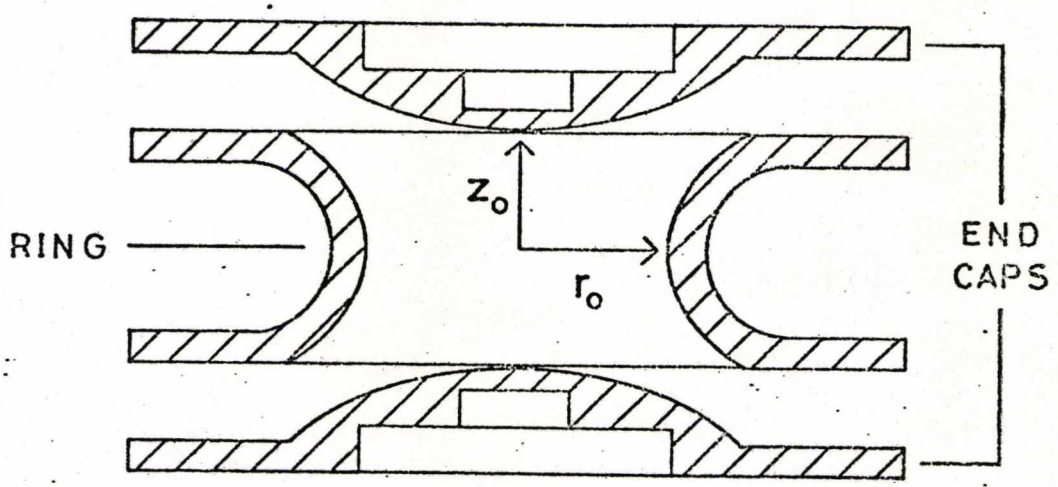

Figure 3.2 Three-Dimensional Representation of the Quistor Electrode Structure

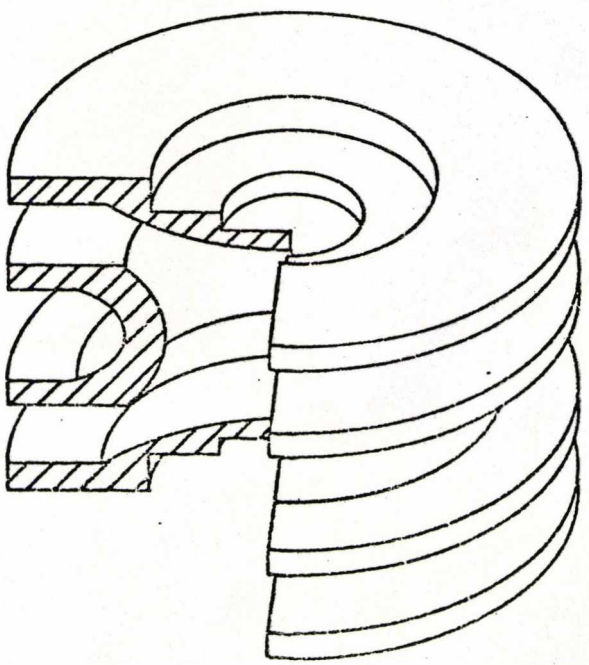

structure, consisting of two 'end-caps' and a ring electrode having cross-sections in the rz plane which are complementary hyperbolae with a ratio of $\sqrt{2}$ in the same semi-axes (r_o/z_o). The three electrodes are rotationally symmetric about the z axis.

The actual form of the potential ϕ_o may be a combination of a d.c. component U and a sinusoidally varying component V_o such that

$$\phi_o = U - V_o \cos \Omega t \tag{3.7}$$

where Ω is the angular frequency and V_o is the amplitude of the alternating potential developed between oppositely charged electrodes. Thus from equation (3.6)

$$\phi_{r,z} = (U-V_o \cos \Omega t)(r^2-2z^2)/2r_o^2 \tag{3.8}$$

Having derived an expression for the potential at any point inside the Quistor it is now possible to develop the equations of ion motion by considering the r and z motion separately. For the z direction, the potential gradient E_z is given by

$$E_z = - \frac{\partial \phi_{r,z}}{\partial z} = (U-V_o \cos \Omega t)2z/r_o^2 \tag{3.9}$$

the force on the ion is then

$$F_z = eE_z = m \frac{d^2z}{dt^2} \tag{3.10}$$

combining equations (3.9) and (3.10) we have

$$\frac{d^2z}{dt^2} - \frac{2e}{mr_o^2} (U-V_o \cos \Omega t)z = 0 \tag{3.11}$$

An analogous treatment for motion in the r direction yields

$$\frac{d^2r}{dt^2} + \frac{e}{mr_o^2}(U-V_o \cos \Omega t)r = 0 \qquad (3.12)$$

The expressions (3.11) and (3.12) are in fact equations of the Mathieu type for which the general form is

$$\frac{d^2u}{d\gamma^2} + (a_u - 2q_u \cos 2\gamma)u = 0 \qquad (3.13)$$

with the transformations

$$u = z \text{ or } r \qquad (3.14)$$

$$a_z = -2a_r = -\frac{8\ eU}{mr_o^2\Omega^2} \qquad (3.15)$$

$$q_z = -2q_r = -\frac{4\ eV_o}{mr_o^2\Omega^2} \qquad (3.16)$$

$$\gamma = \tfrac{1}{2}\Omega t \qquad (3.17)$$

The Mathieu equation for ion motion in the Quistor may be expressed more exactly as

$$\frac{d^2u}{d\gamma^2} + (a_u - 2q_u \cos 2(\gamma-\gamma_o)u = 0 \qquad (3.18)$$

The parameter γ_o takes account of the phase of the alternating field when the ion first experiences its influence. It is generally called the initial phase. Since ions are usually created inside of the Quistor, the initial phase corresponds to the phase at the time of ion creation.

In order to calculate the trajectories of ions within the Quistor, it is necessary to solve the equations of ion motion, (3.11) and (3.12). There are a number of methods of solving equations of the Mathieu type[128], the principal ones being: numerical point-by-point integration[121,128], and

the use of matrix methods with analyses based on phase-space dynamics[128,129]. The detailed solution and properties of the Mathieu equation will not be described here, but the form of the solution will be considered in order to derive the conditions under which ions may be stored in the Quistor.

Solutions to the Mathieu equation may be expressed by

$$u(\gamma) = A' e^{\mu\gamma} \sum_{n=-\infty}^{\infty} C_{2n} \exp(2n\gamma i) + B' e^{-\mu\gamma} \sum_{n=-\infty}^{\infty} C_{2n} \exp(-2n\gamma i) \tag{3.19}$$

where A' and B' are integration constants depending on the initial conditions; that is, u_o, $\dot{u}_o$ and γ_o. The constants C_{2n} and μ depend on the values of a_u and q_u and not on the initial conditions. For an ion to be confined within the Quistor u must remain finite as $\gamma \to \infty$. This is only the case when $\mu = i\beta$ and β is not a whole number. These solutions are the periodic, stable ones. By substituting $\mu = i\beta$ and applying the relationship

$$\exp(i\theta) = \cos\theta + i \sin\theta \tag{3.20}$$

equation (3.19) becomes

$$u(\gamma) = A \sum_{n=-\infty}^{\infty} C_{2n} \cos(2n+\beta)\gamma + B \sum_{n=-\infty}^{\infty} C_{2n} \sin(2n+\beta)\gamma \tag{3.21}$$

where

$$A = (A' + B') \quad \text{and} \quad B = i(A' - B')$$

Equation (3.21) is essentially an expression of the frequency spectrum of ionic motion $u(\gamma)$; each term corresponds to an oscillation with an amplitude given by the relevant C_{2n} coefficient and a radial frequency, ω_n, which may be obtained by transforming to real-time

$$\cos(2n+\beta)\gamma \equiv \cos\ \omega_n t$$

Figure 3.3 Stability Diagram for the Mathieu Equation Considering a Single Co-ordinate Direction

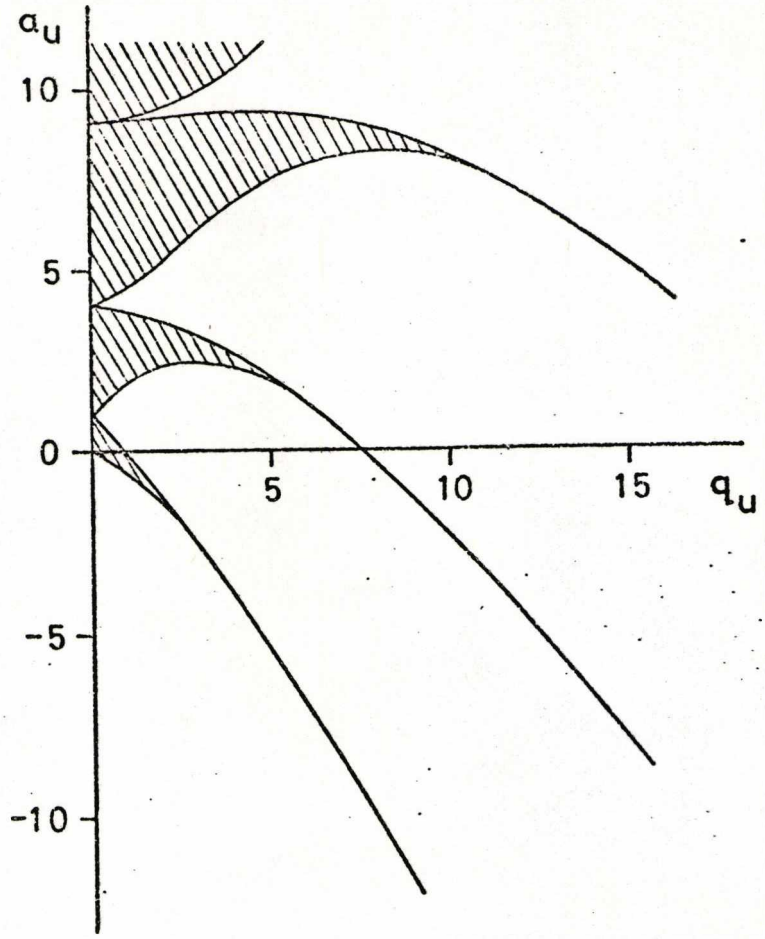

Figure 3.4 Overall Stability Diagram for the Quistor

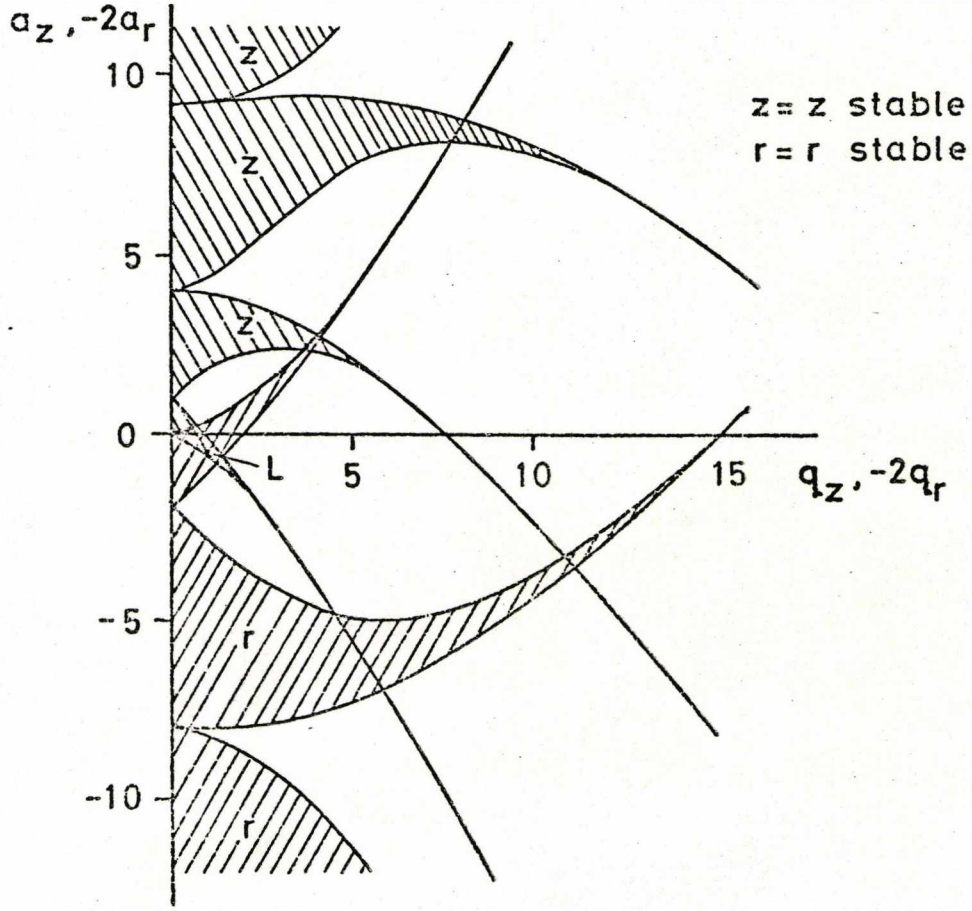

$$\therefore \quad (2n+\beta)\gamma = \omega_n t = (2n+\beta)\frac{\Omega t}{2}$$

$$\therefore \quad \omega_n = (n + \beta/2)\Omega \qquad (3.22)$$

for $n = -\infty \ldots\ldots -1, 0, 1 \ldots\ldots \infty$

From this it can be shown that β determines the frequency of the oscillation and that the complete solution comprises a term with a fundamental frequency $\omega_o (= \beta\Omega/2)$ plus an infinite number of sidebands occurring in pairs.

The methods of calculating the values of A and B for a particular set of initial conditions, and the values of the C_{2n} coefficients and β for a particular a_u and q_u have been described elsewhere[121,128]. For practical purposes it is possible to evaluate the coordinates a, q for lines of constant β ('iso-β lines') which are plotted in a-q space. Figure 3.3 shows such a plot where the shaded areas correspond to regions where non-integral values of β give stable solutions. The boundaries of the shaded regions correspond to integral values of β. However, this a-q stability diagram only represents a single coordinate direction; for an ion to be confined within the Quistor its trajectory must be simultaneously stable in both the r and z directions. Since the a and q values for these two directions differ by a factor of -2 (equations (3.15) and (3.16)), the overall stability diagram for the Quistor may be obtained by superimposing two stability diagrams which differ by a factor of -2 and represent the r and z directions as shown in Figure 3.4. The lower stability region, marked L in Figure 3.4, the one usually employed for ion trapping, is shown in detail in Figure 3.5. (The lines crossing the stability region are the iso-β lines). Thus, if for a particular ion the a, q coordinates as given by equations (3.15) and (3.16), for a particular set of operating conditions, fall within the stability boundaries shown in Figure 3.5, it might be expected to have a stable trajectory and remain trapped in the device indefinitely. However, this represents 'mathematical' stability: in the real case the

Figure 3.5 Lower Stability Region for the Quistor Showing some Iso-β Lines

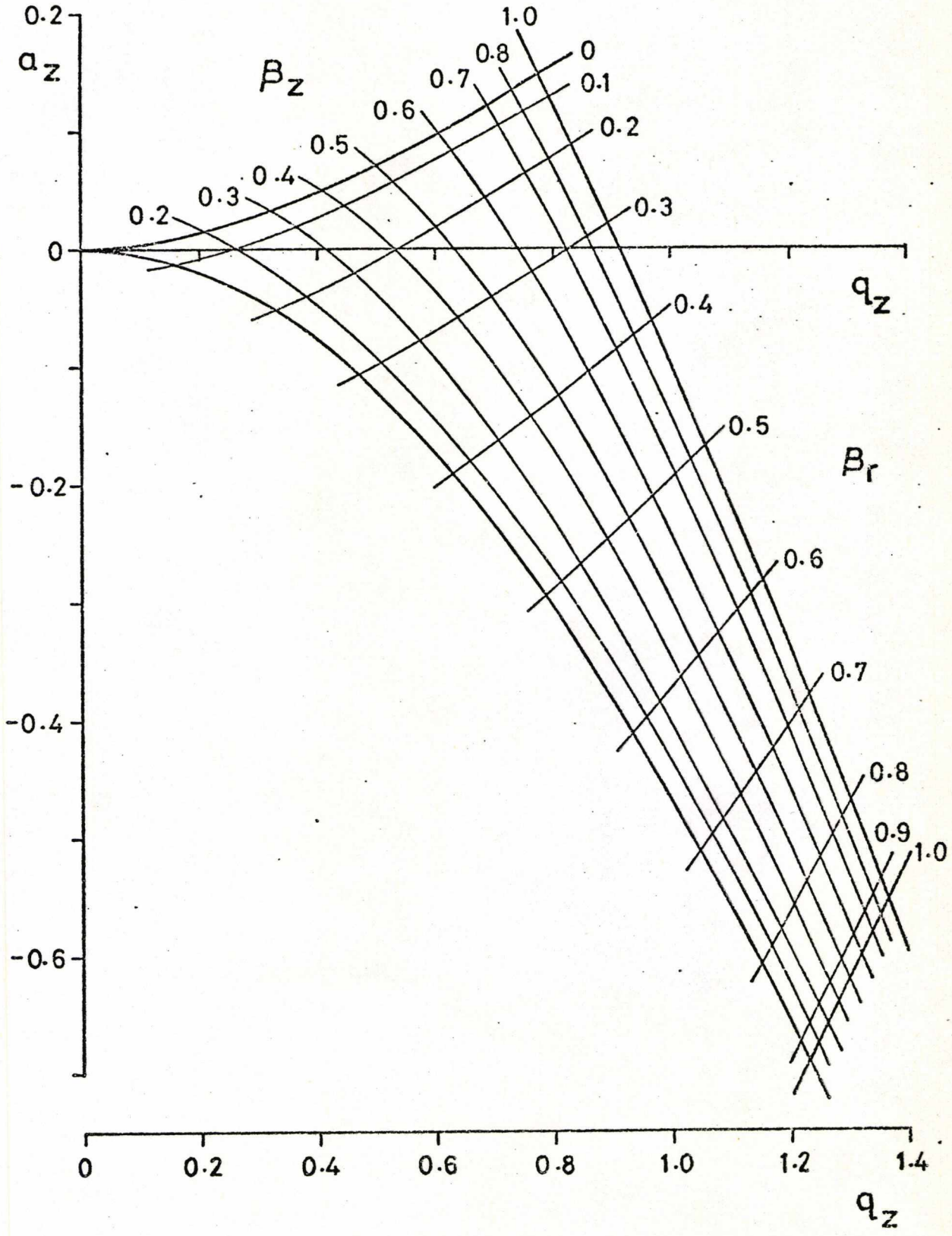

maximum amplitude of oscillation must remain less than the geometrical boundaries of the device. This and other factors which affect ion stability in the Quistor are discussed in Section 3.4.

The two principal modes of operation for the Quistor are: the 'total pressure' mode, and the mass selective ion storage mode. In the latter mode, which is described in Chapter 7, the Quistor functions as a combined ion source and mass analyser. When the Quistor is employed as an ion source for a mass filter or as a low pressure CI ion source, it is operated in the total pressure mode. In this mode the d.c. component U of the applied potential ϕ_o is set to zero, which corresponds to operation along the q_z axis of the stability diagram shown in Figure 3.5. Inspection of equation (3.16) reveals that for a fixed value of the amplitude of the applied r.f. potential V_o, a range of values of m/e should be stable simultaneously for $0 < q_z < \sim 0.91$. In practice the Quistor is operated with the two end caps earthed and the r.f. potential applied to the ring electrode only. Although this necessarily requires that an extra term of $\phi_o/2$ be included in equation (3.6), in order to represent the potential $\phi_{r,z}$ correctly, it does not affect the equations of ion motion and is thus immaterial to the functioning of the device. The practical aspects of Quistor operation are described in Section 3.3.

3.2.1 The Potential Well Model of Ion Trapping

This theoretical model was originally developed by Wuerker *et al*[130] and also by Dehmelt[131]. It is based on the fact that ion motion in the Quistor may be represented as a high frequency 'ripple' superimposed upon a large amplitude low frequency 'secular' oscillation. A slightly more rigorous treatment of this approach has recently been given by Todd *et al*[123]. This is reproduced in part here because it provides the basis for a model with which it is possible to estimate the space charge limited number of ions that can be contained within the Quistor as well as the mean kinetic energy of the secular motion of the ions (Section 3.4.1.3 and Chapter 6).

For motion along the z axis of the trap equation (3.13) may be re-written as

$$\frac{d^2z}{d\gamma^2} = -(a_z - 2q_z \cos 2\gamma)z \tag{3.23}$$

Motion in the z direction may be considered as being made up of two components, a displacement δ, due to the micromotion resulting from the high frequency field and a larger displacement Z, which describes the extent of the motion averaged over a period of the r.f. drive potential.

Then,

$$z = Z + \delta \tag{3.24}$$

If we assume that the driving force, which is related to the value of q, is small, then $\delta << Z$ but $d\delta/dt >> dZ/dt$. Using these approximations and substituting equation (3.24) into equation (3.23) and then integrating assuming $a << q$ and Z to be constant, yields

$$\delta = -\frac{q_z Z}{2} \cos 2\gamma \tag{3.25}$$

This approximate value for δ may be substituted into equation (3.24) and this in turn substituted into equation (3.23) whence the original Mathieu equation becomes

$$\frac{d^2Z}{d\gamma^2} = -a_z Z + \frac{a_z q_z Z}{2} \cos 2\gamma + 2q_z Z \cos 2\gamma - q_z^2 Z \cos^2 2\gamma \tag{3.26}$$

Since the accleration due to the r.f. drive, $d^2\delta/d\gamma^2$, averaged over a period of the r.f. drive is equal to zero, then the acceleration of the secular motion averaged over the same period is given by

$$\left[\frac{d^2Z}{d\gamma^2}\right]_{av} = \frac{1}{\pi}\int_0^{\pi} \frac{d^2z}{d\gamma^2}\, d\gamma \tag{3.27}$$

so that the integral of equation (3.26) taken between these limits is

$$\frac{d^2Z}{d\gamma^2} = -\left(a_z + \frac{q_z^2}{2}\right)Z \tag{3.28}$$

which, written in terms of time becomes

$$\frac{d^2Z}{dt^2} = -\left(a_z + \frac{q_z^2}{2}\right)\frac{\Omega^2}{4}Z \tag{3.29}$$

Equation (3.29) corresponds to simple harmonic motion of the secular motion of the secular component Z and is equivalent to

$$\frac{d^2Z}{dt^2} = -\omega_{oz}^2 Z \tag{3.30}$$

in which ω_{oz} is the secular oscillation frequency and is equivalent to that given by equation (3.22) if

$$\beta_z = \left(a_z + \frac{q_z^2}{2}\right)^{\frac{1}{2}} \tag{3.31}$$

Considering the case of $a_z = 0$ and substituting for q_z into equation (3.29)

$$\frac{d^2Z}{dt^2} = -\left(\frac{e^2 V_o^2}{2m^2 z_o^4 \Omega^2}\right)Z \tag{3.32}$$

The force on an ion of mass m and charge e is therefore given by

$$-m\frac{d^2Z}{dt^2} = e\frac{d\bar{D}_z}{dZ} \tag{3.33}$$

where

$$\frac{d\bar{D}_z}{dZ} = \left(\frac{e V_o^2}{2m z_o^4 \Omega^2}\right)Z \tag{3.34}$$

Integrating equation (3.34) between the limits Z = 0 and Z = z_o gives

$$\overline{D}_z = \frac{e\ V_o^2}{4m\ z_o^2\ \Omega^2} \tag{3.35}$$

Thus when q_z is small an ion can be regarded as oscillating in a parabolic potential well of depth $\overline{D}_z$ in the z direction with a frequency equal to that of the fundamental secular frequency ω_{oz}.

For motion in the r direction equation (3.35) becomes

$$\overline{D}_r = \frac{e\ V_o^2}{4m\ r_o^2\ \Omega^2} \tag{3.36}$$

and since $r_o^2 = 2\ z_o^2$

$$\overline{D}_z = 2\ \overline{D}_r \tag{3.37}$$

This derivation is based on the assumption that $\delta << Z$ but as can be seen from equation (3.25) as q_z increases for constant Z and γ the fraction δ/Z becomes progressively larger so that the assumption ultimately breaks down typically at a value of q_z equal to *ca.* 0.4.

3.3 Experimental Aspects of the Operation of the Quistor

3.3.1 The Experimental System

The experimental system employed for the studies described in this chapter was originally developed by G. Lawson[126] who investigated the use of a Quistor fabricated from wire mesh as an ion source for a quadrupole mass filter. The wire mesh Quistor was subsequently replaced by one accurately machined from stainless steel. The use of this device in the study of the kinetics of ion-molecule reactions was investigated by R.F. Bonner[127] who also made several minor modifications to the original experimental system.

In the present study the same Quistor/mass filter combination was

employed but due to the nature of some of the proposed experiments it was necessary to redesign and modify the Quistor mounting assembly and parts of the electronic control system.

3.3.1.1 Construction and Mounting of the Original Quistor

A diagram of the original stainless steel Quistor as mounted in place of the normal ion source of an Electronic Associates Inc. Quad 250A mass filter is shown in Figure 3.6.

Figure 3.6 Diagram of the Original Quistor as Mounted on the Quadrupole Mass Filter

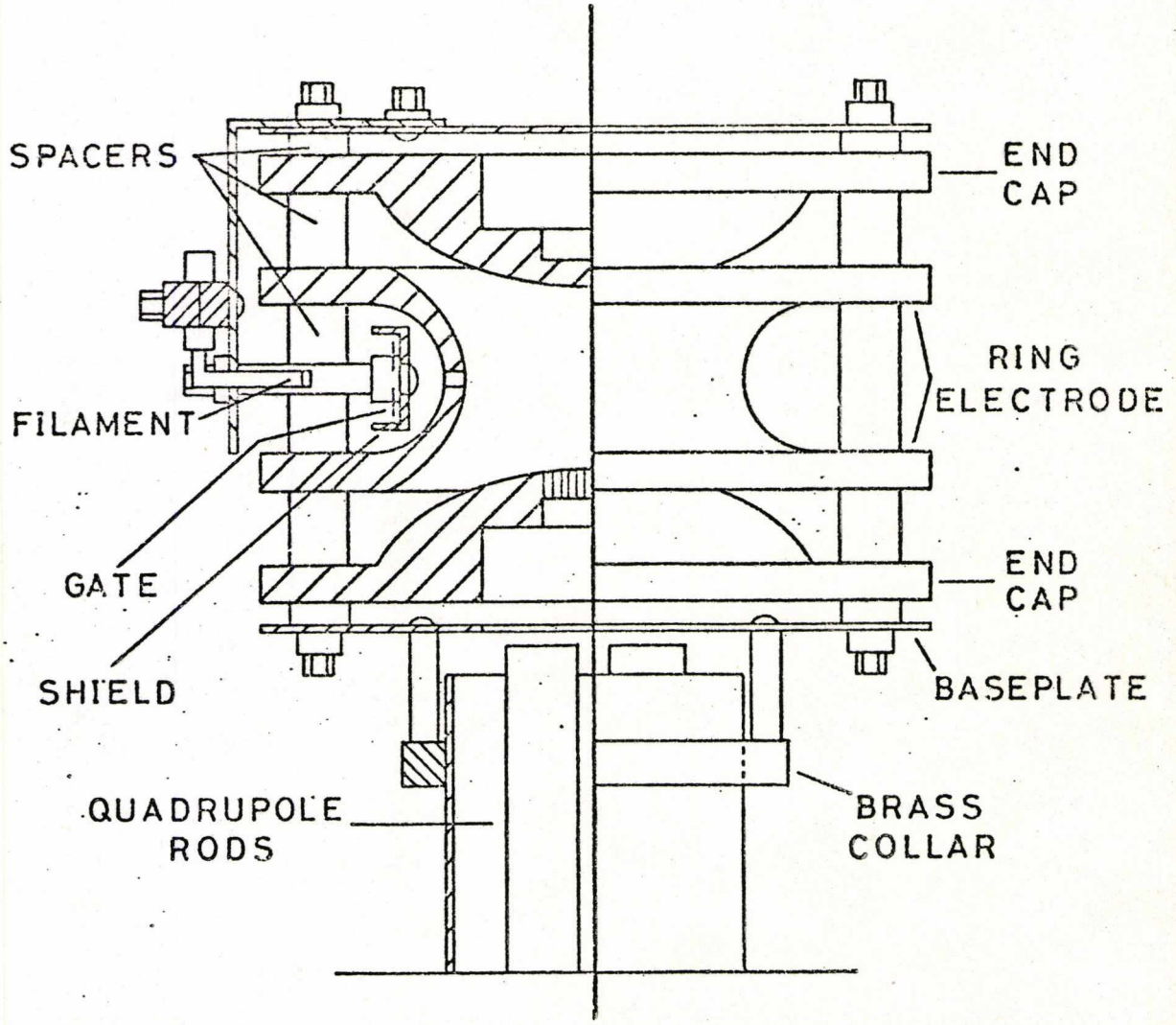

The ring electrode, which has an internal radius (r_o) of 1.008 cm, is recessed to accommodate the electron gun and has a 0.15 cm electron entrance hole drilled central to this recess. The central region of the lower end-cap is perforated with thirty 0.075 cm diameter holes to permit ion extraction into the mass filter. A stainless steel plate fixed above the Quistor supports the electron gun which consists of a support bracket, heated tungsten filament and gating electrode surrounded by an earthed shielding electrode. The correct spacing and electrical insulation between electrodes is provided by spacers machined from pyrophólite. The entire assembly is bolted to a stainless steel base plate in which there is a 2.5 cm diameter aperture which allows the Quistor to be mounted with the minimum separation between the lower end cap and the entrance to the mass filter. Four bolts secure this base plate to a brass collar which is attached to the mass filter housing. Electrical connections to the Quistor are made via barrel connectors to wires spot-welded to stainless steel tags fixed to the edges of the electrodes by 10 B.A. stainless steel screws in tapped holes.

The Quistor/mass filter combination was mounted vertically inside the vacuum chamber described in Section 3.3.1.5.

3.3.1.2 Modifications to the Quistor Mounting Assembly

Although the original system had been operated successfully for a number of years, the Quistor had to be remounted for the following reasons:

(i) The assembled Quistor structure was not very rigid because: the base plate and the plate above the Quistor which supported the electron gun, were made of stainless steel sheet only 0.05 cm thick, and the pyrophólite spacers were worn and did not fit tightly into the holes in the Quistor electrodes. This meant that it was impossible to align the Quistor accurately in the vertical plane.

(ii) If the Quistor required maintenance such as filament replacement, the entire Quistor/mass filter assembly had to be removed from the vacuum system which meant exposing the electron multiplier to the laboratory atmosphere for long periods of time.

(iii) Certain experiments, the results of which were required for this study, could not be performed with the Quistor mounted in its original configuration.

The major factor that influenced the design of the new mounting assembly was the intention to incorporate an additional electron multiplier into the system at a later date, such that ions contained in the Quistor could be pulsed either into the mass filter or directly onto the first dynode of the electron multiplier. In order to allow for this modification the Quistor assembly was removed from the mass filter housing and re-mounted on a specially constructed column as shown in Figure 3.7. The Quistor was re-assembled with new pyropholite spacers on a base plate which was 0.4 cm thick. This made the whole assembly more rigid and its vertical alignment more accurate. The base plate has a central aperture 1.2 cm in diameter to permit the passage of ions from the Quistor to the electron multiplier which would be housed in the upper chamber of the support column. A new electron gun support bracket was constructed which was secured to the base plate by two 8 B.A. stainless steel screws. The support column was made in two sections from 4.4 cm diameter stainless steel tube. These two cylinders were attached to the Quistor base plate, central support disc and column base plate by 6 B.A. stainless steel screws as shown in Figure 3.7. The complete column was mounted on a 15 cm vacuum flange fitted with nine electrical feed throughs. A photograph of the assembled Quistor on its base plate is shown in Figure 3.8.

In order to arrange for ions to be pulsed from the Quistor into the mass filter, the Quistor, on its support column, and the mass filter housing

Figure 3.7 Section Through the Quistor Secured to the New Support Column

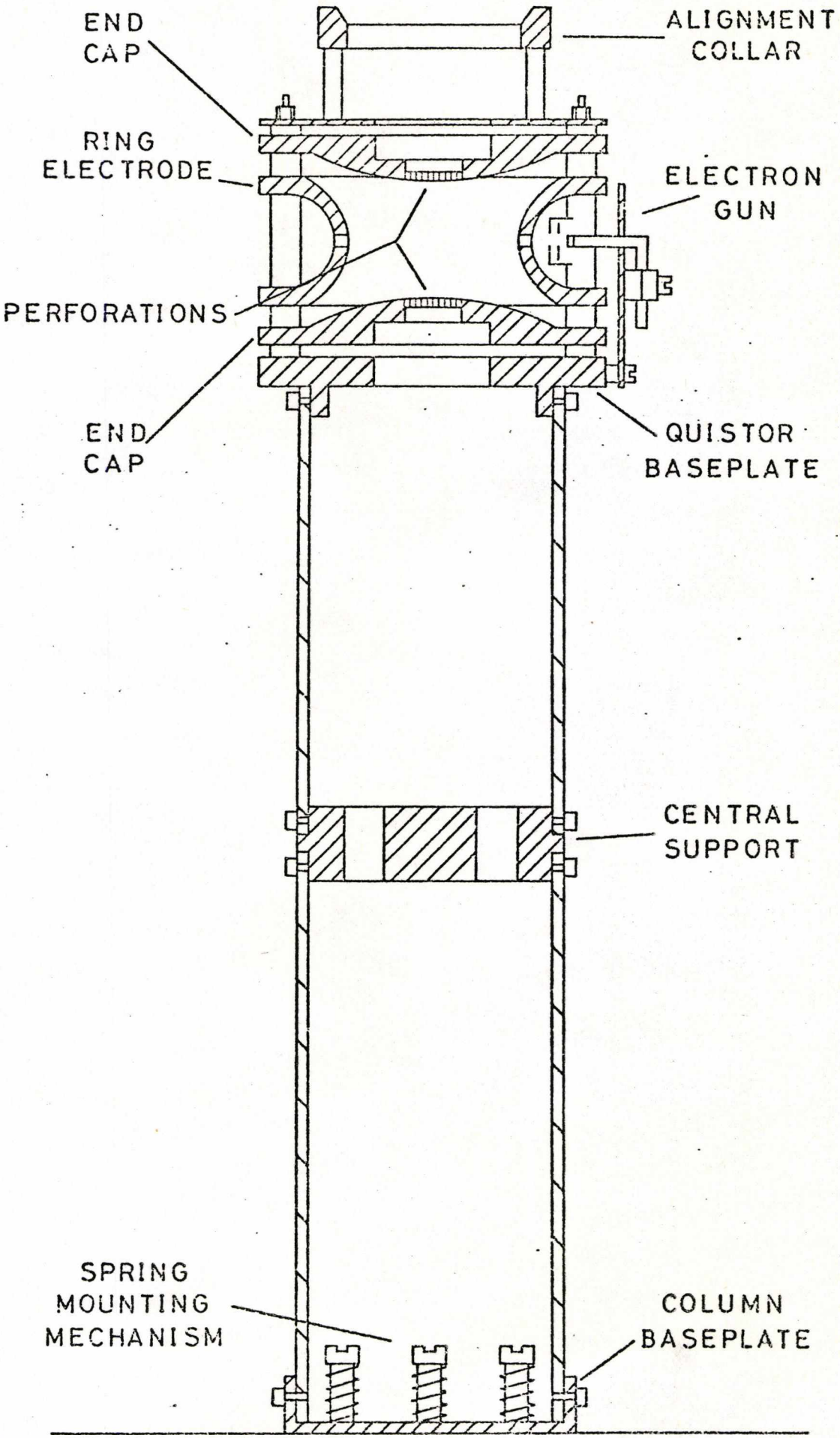

Figure 3.8 Photograph of the Assembled Quistor

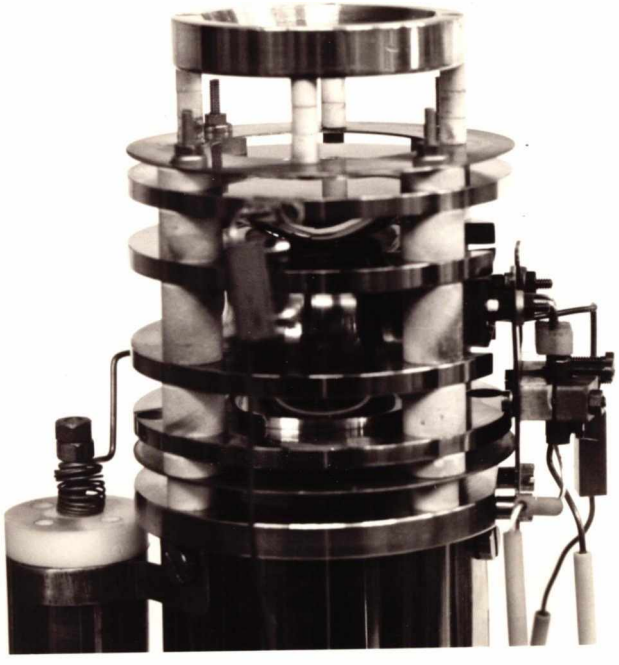

Figure 3.9 Diagram of the Horizontally Mounted Quistor/Quadrupole Mass Filter Combination

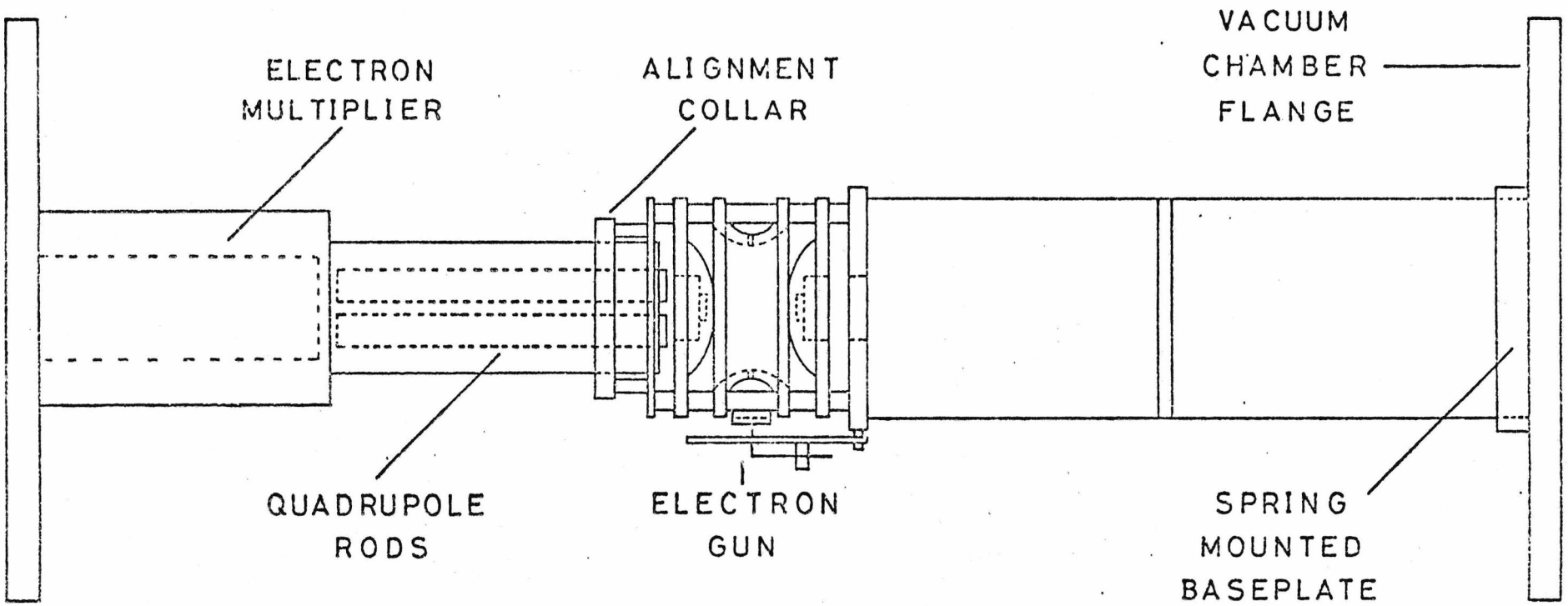

had to be inserted horizontally into opposite ends of the vacuum chamber as shown in Figure 3.9. To ensure that the central axis of the Quistor was accurately aligned with that of the mass filter, a brass collar was attached to the top of the Quistor assembly as shown in Figure 3.7. When the Quistor was inserted into the vacuum chamber the brass collar slid over the mass filter housing, automatically aligning the perforations in the Quistor end-cap with the mass filter aperture. The Quistor support column was not attached rigidly to the vacuum flange but was spring-loaded such that it could be tilted up to 5^{o} from its central axis in any direction. This ensured that if the central axis of the Quistor/mass filter assembly did not correspond exactly with that of the vacuum chamber, then the act of tightening the vacuum flanges at the ends of the vacuum chamber would result in just tilting the support column rather than distorting the whole structure. A photograph of the Quistor/mass filter combination as it would be assembled inside the vacuum tank is shown in Figure 3.10.

3.3.1.3 Electronic Apparatus

The experimental system consisted of the following electronic apparatus:

(i) The EAI Quadrupole power supply, which includes: the r.f./d.c. control unit for the mass filter, the multiplier power supply and the filament power unit which was used to drive the Quistor filament.

(ii) The Quistor r.f. power supply which was a copy of the EAI unit except that the output was controlled manually. This could deliver up to 2400V peak to peak at switched frequencies of nominally 0.8, 1.6 and 2.8 MHz. The output could be floated to any potential from 0 to ±200V d.c. using an r.f./d.c. interface unit.

(iii) Two Hewlett Packard Model 214A pulse generators. The output of

Figure 3.10 Photograph of the Quistor/Quadrupole Mass Filter Combination

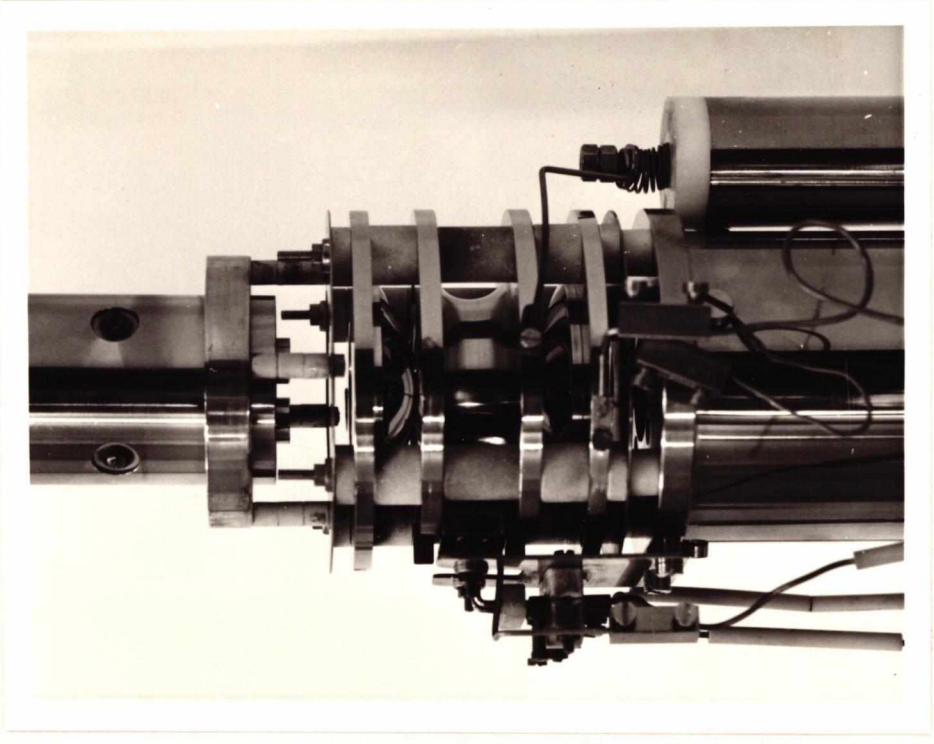

one of these units was connected to a pulse/d.c. interface such that the output pulse could be biased to any d.c. level in the range 0 to -140V d.c.

(iv) A Brookdeal Box Car detector Model 9415. This comprises two units: a scan delay generator, and a linear gate.

(v) A Bryans Southern Instruments Model 26000 XY pen recorder.

(vi) A Tektronix Model 585A dual beam oscilloscope.

The function and operation of these units is described in Section 3.3.2.

3.3.1.4 Modifications to the Electronic Apparatus

In the original system the 100V power supply, which was used to control the drive valve of the r.f. generator, was mounted in close proximity to the r.f./d.c. and pulse/d.c. interface circuitry. These units were connected to their respective power supplies and output sockets by long and usually unshielded wires. This situation gave rise to pulse modulation of the r.f. waveform and excessive r.f. pick-up on the outputs of the pulse generators. In order to remedy this situation these units were remounted inside an aluminium box and each one was carefully shielded from the other. The complete circuit diagram for this control unit is shown in Figure 3.11. All of the Quistor operating potentials with the exception of the filament supply were controlled and monitored using this control unit.

3.3.1.5 The Vacuum System

A schematic diagram of the vacuum system and the sample introduction system is shown in Figure 3.12. The vacuum chamber was pumped by an Edwards E02 oil vapour diffusion pump, backed by an Edwards ES35 rotary pump. The diffusion pump was surmounted by a liquid nitrogen cold

Figure 3.11 Circuit Diagram of the Quistor Electronic Control Unit

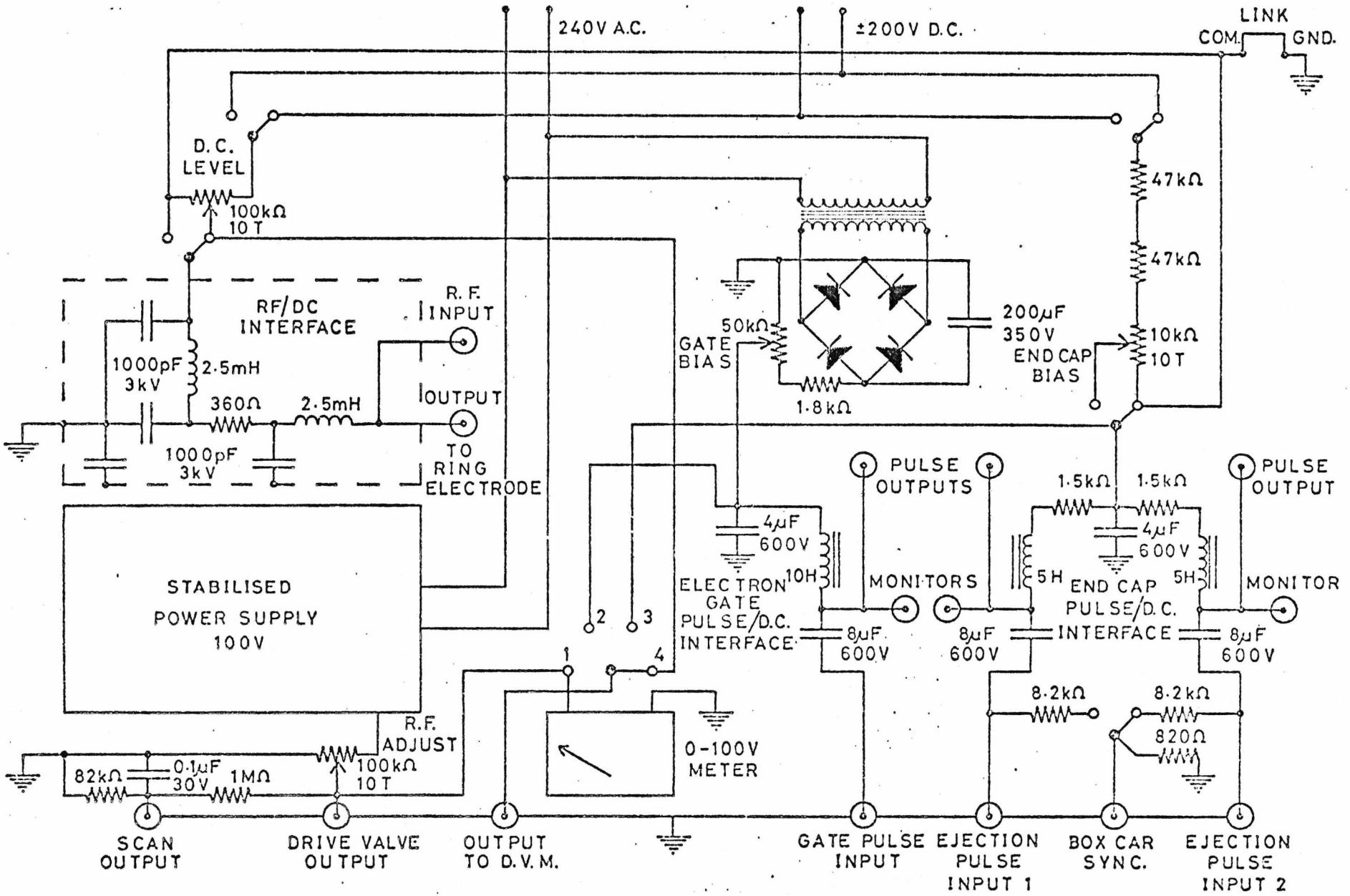

Figure 3.12 Schematic Diagram of the Vacuum Chamber and Sample Inlet System

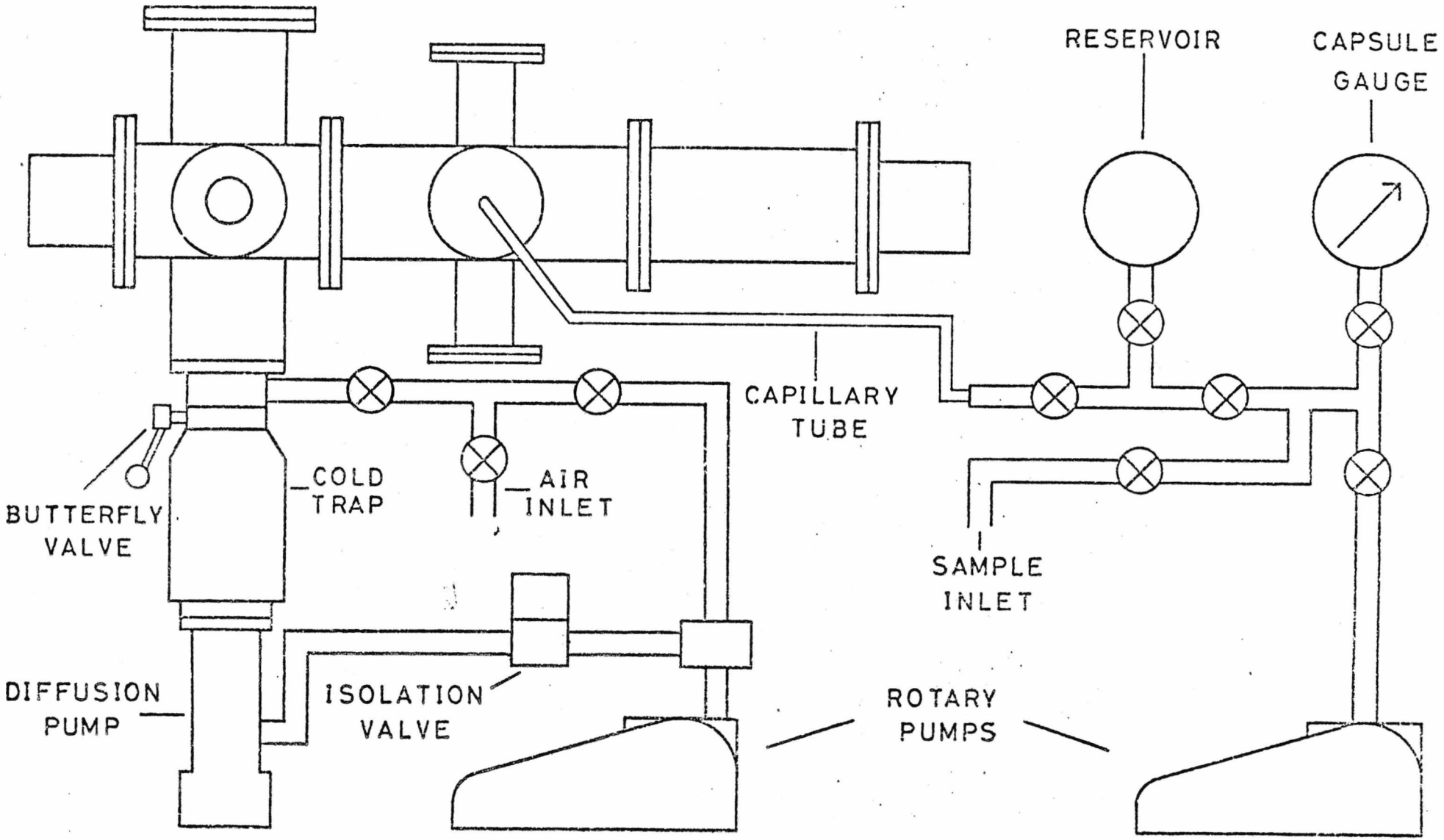

trap and a quarter-swing butterfly valve. The pressure in the vacuum chamber was monitored by a pirani gauge and a Vacuum Generators VIG 20 ion gauge and IGP2 control unit.

The sample introduction system was pumped by an Edwards ES50 rotary pump and the pressure monitored with a 0 to 20 Torr capsule gauge. Since the inlet system could not be heated only gases and volatile liquids could be introduced into the vacuum chamber.

3.3.2 Technique for the Operation of the Quistor as an Ion Storage Source

In order to characterise the Quistor as an ion storage source it was necessary to employ a number of different operating procedures, but the basic experimental technique and the configuration of the experimental system was the same for all experiments and is illustrated in the schematic block diagram and pulse timing sequence shown in Figure 3.13.

Ions are created inside the Quistor by a pulse of electrons from the electron gun, which pass through the hole in the ring electrode. This electron pulse is formed by the application of a 90 volt pulse from the ion creation pulse generator to the gate electrode which is biased at a potential of -130 volts. Since the filament is maintained at a level of -50 volts, electrons only pass through the gate for the duration of the ion creation pulse which is typically 20 μs wide. The ions are stored in the Quistor by application of suitable r.f. and d.c. potentials to the ring electrode. For operation in the total pressure mode the d.c. level is set to zero. After a pre-determined time, the storage time ions are ejected from the Quistor into the mass filter by application of either a negative pulse to the end-cap nearest to the mass filter aperture such that the ions are effectively 'sucked out' (SO), or by a positive pulse applied to the other end-cap in which case the ions are 'pulsed out' (PO). The ejection pulse which is typically 20 μs wide and 90 volts high, is provided by the ion ejection pulse generator which is triggered from the ion creation

Figure 3.13 Schematic Block Diagram of the Experimental System and Pulse Timing Sequence

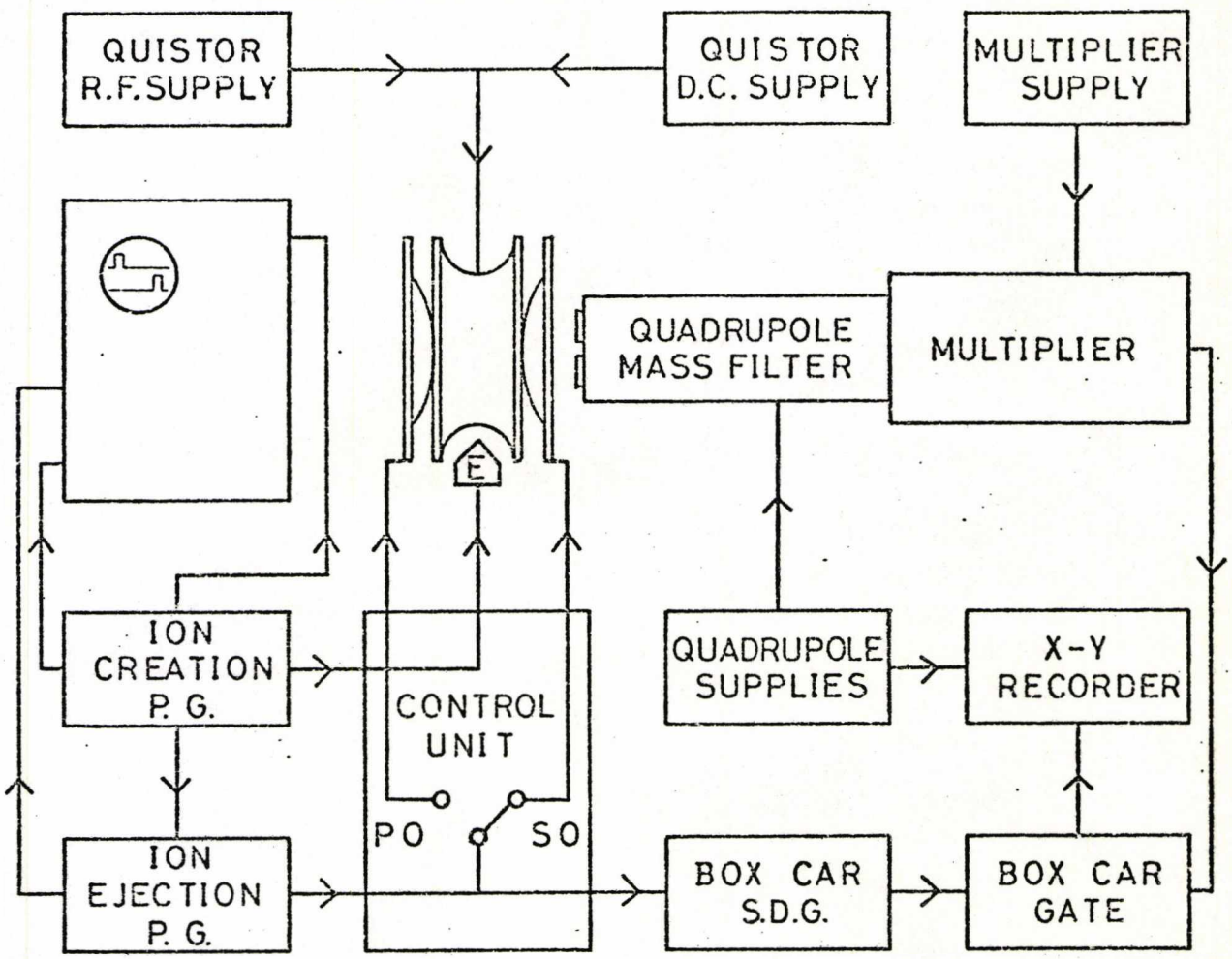

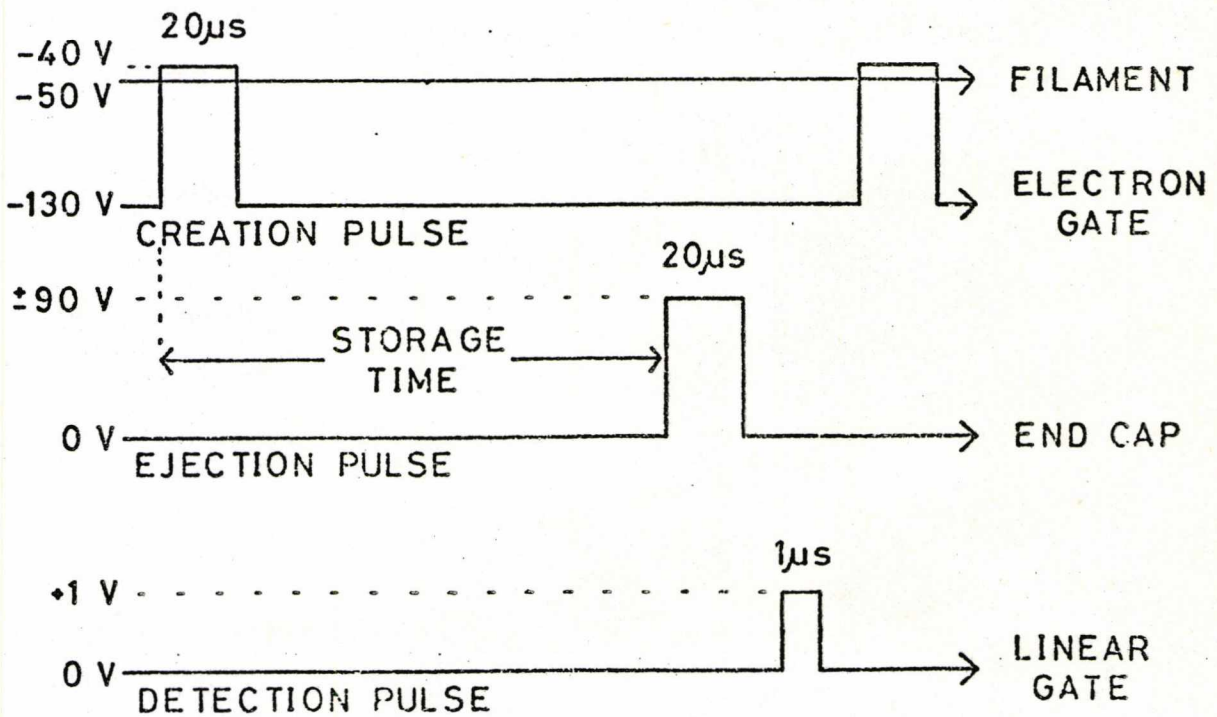

pulse generator. The ejected ions are mass analysed by the mass filter and the transmitted ion current is then amplified by the electron multiplier, the output of which is integrated and further amplified by the box car detector. As noted previously, the box car consists of two units, a scan delay generator which is triggered by the ejection pulse, and a linear gate. After a pre-set delay the scan delay generator produces a 1 volt pulse (the detection pulse) which opens the input to the linear gate for a specified duration, typically 1 μs, to sample the ion signal. The entire pulse sequence is repeated every 10 ms which corresponds to a repetition frequency of 100 Hz.

A mass spectrum of ions stored in the Quistor after a particular storage time was recorded on the X-Y recorder by setting the delay on the ion ejection pulse generator to the required storage time and scanning the mass filter slowly over the desired mass range. The scan rate was limited to a maximum of 1 amu/sec such that the signal produced on the X-Y recorder for a particular m/e value corresponded to the mean of at least 100 ion creation, storage and ejection events.

3.3.2.1 Pressure Calibration

In order to determine rate constants of ion-molecule reactions using the Quistor it was essential to be able to determine the pressure in the vacuum system as accurately as possible. The ionisation gauge was unsuitable for this purpose since it required recalibration for each separate gas employed, so the system pressure was determined indirectly using the inlet system capsule gauge and the following accepted calibration reaction:

$$CH_4^+ + CH_4 \longrightarrow CH_5^+ + CH_3$$

The calibration procedure comprised the measurement of the intensity of CH_4^+ peak expressed as a percentage of the total ion current recorded against increasing storage time for different fixed pressures of methane in the

sample inlet reservoir. By measuring the gradient of a line drawn through these points and assuming a value for the loss of CH_4^+ in the above reaction of 1.2×10^{-9} cm^3 mol^{-1} s^{-1} the pressure in the vacuum system could be determined for any known pressure in the inlet system.

The original calibration was performed by R.F. Bonner[127] and was checked periodically during the course of this work by determining the rate constant of the above reaction for a particular pressure. The values obtained were always within 20 per cent of the assumed value.

Unless otherwise stated, all pressure measurements reported in this chapter were determined from the above calibration.

3.3.2.2 Note on Quistor Cleaning Procedure

The storage characteristics of the Quistor were found to be quite critically dependent on the cleanliness of the electrode surfaces (see Section 3.4.1.2), and to a lesser extent of the pyropholite spacers. These were cleaned periodically using the following procedure:

(i) electron burns were removed from the electrode surfaces by polishing with 'Duraglit', similar burns on the spacers could only be removed by washing briefly in hydrofluoric acid;

(ii) both electrodes and spacers were immersed in a 1:1:1 mixture of hydrogen peroxide, formic acid and distilled water, for several hours;

(iii) after washing in water, acetone and trichloroethylene the electrodes were finally polished using paper towelling.

3.4 Physical Characteristics of the Quistor when Employed as an Ion Storage Source

The theoretical treatment of ion containment in the Quistor given in Section 3.2 is limited in that it assumes there is only one ion trapped at any particular time and also that this ion moves in an absolute vacuum. In practice, ion densities may be as high as 10^8 ions cm^{-3} and since the Quistor is operated at *ca.* 10^{-5} Torr, the density of gaseous molecules is of the order 10^{11} molecules cm^{-3}. Clearly this theoretical treatment cannot be employed to predict either the effect of space charge, induced by the mutual interaction of ions stored in the Quistor, or the effect of ion-molecule collisions between stored ions and gaseous molecules, on the storage capabilities of the Quistor. In order to investigate these effects and other physical characteristics, the following series of experiments were performed in an attempt to establish ideal operating conditions for the Quistor as a low pressure CI ion source.

3.4.1 The Experimental Limits of Ion Stability

In order to operate the Quistor as a low pressure CI ion source it is essential to be able to store ions possessing a wide range of m/e values simultaneously. For this purpose the Quistor is normally operated in the total pressure mode[69] which corresponds to working along the q_z axis of the stability diagram shown in Figure 3.5. It is possible to evaluate the theoretical mass range of the Quistor for a fixed value of the applied r.f. potential V_o and frequency Ω by substituting the values of q_z, corresponding to the limits of stability on the q_z axis, into equation (3.16). Since these limits are $q_z = 0$ and 0.91, the theoretical mass range has a lower limit of ~$4.5\ e\ V_o/r_o^2\ \Omega^2$ and an upper limit of infinity. Previous experience had shown that there was a definite upper limit to the mass range for a particular set of experimental conditions and so it was decided to investigate the experimental limits of stability in order to establish the real mass range of the Quistor. This and other

information on storage efficiency as a function of q_z was obtained from a study of the total pressure curve for the Quistor.

3.4.1.1 The Total Pressure Curve

The total pressure curve for the Quistor is exactly analogous to that for the quadrupole mass filter and is obtained by plotting the intensity of the stored ion signal for a particular mass as a function of the applied r.f. potential (V_o). Experimentally the sample, usually an inert gas, was introduced into the vacuum system at a known pressure and the mass filter tuned to the parent ion of the sample. The total pressure curve was recorded on the X-Y recorder (Figure 3.13) by manually rotating the potentiometer that controlled the output of the r.f. generator. This potentiometer actually controlled the potential on the grid of the drive valve of the r.f. generator and since the relationship between this drive potential and the output of the r.f. generator was linear over the range employed for these experiments, the drive potential was also used to drive the x axis of the X-Y recorder.

A total pressure curve for krypton (mass filter tuned to m/e 84) is shown in Figure 3.14(a). This was recorded at zero storage time, that is where the ion ejection pulse follows immediately after the ion creation pulse. The other operating conditions were:

Krypton pressure	2×10^{-5} Torr
Operating frequency ($f = \Omega/2\pi$)	0.8 MHz
Ion creation pulse width (ICPW)	20 μs
Ion ejection pulse width (IEPW)	20 μs
Ion ejection pulse height (IEPH)	90 V
Electron energy	50 eV

Unless otherwise stated, the above operating conditions were employed for all experiments described in this section. The zero storage total pressure curve for krypton is clearly a doublet but as can be seen from Figure 3.14(b) and (c), recorded at 10 μs and 60 μs storage time

Figure 3.14 Total Pressure Curves for Krypton (m/e 84)

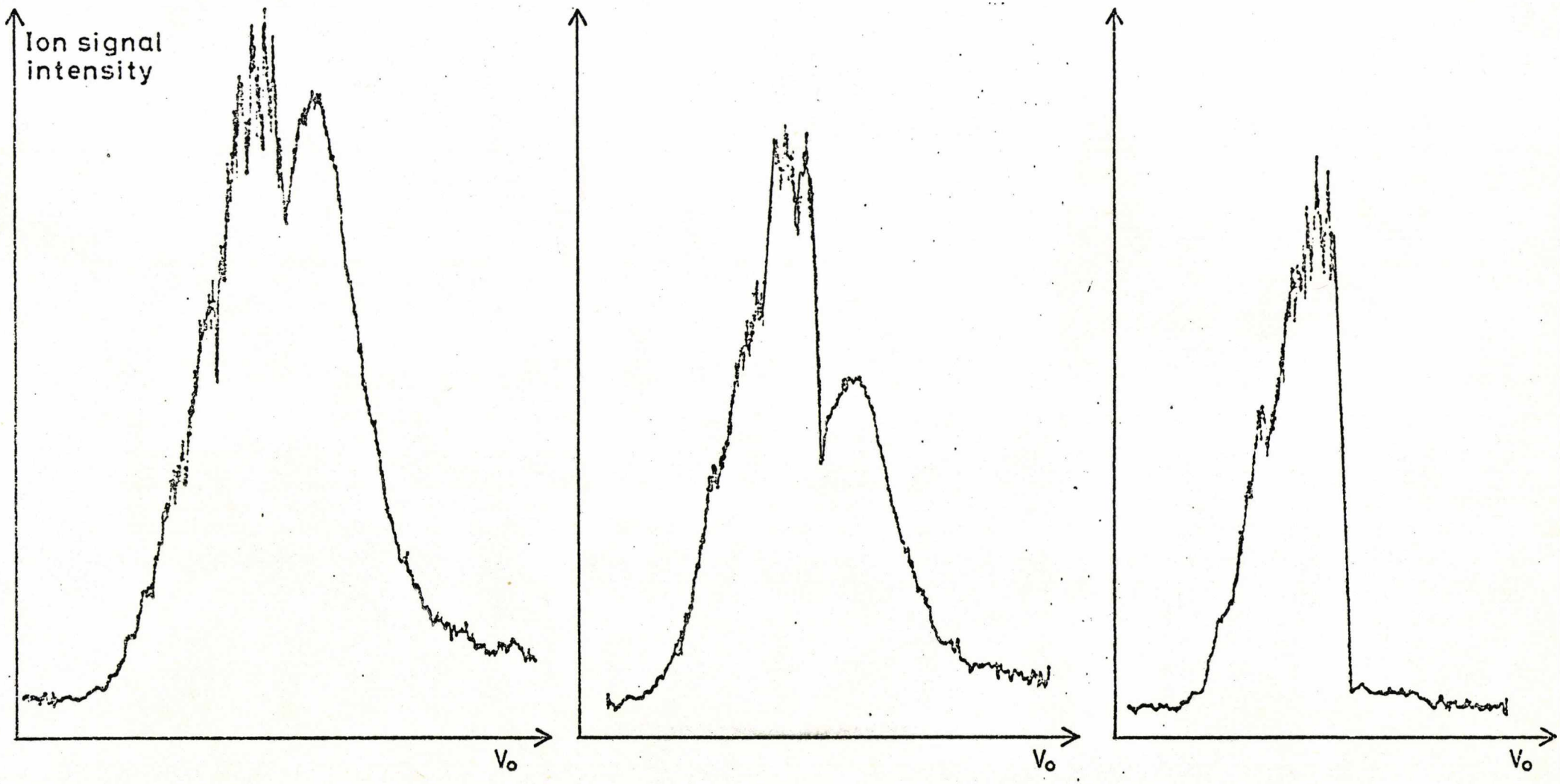

(a) zero storage time (b) 10μs storage time (c) 60μs storage time

respectively, on increasing the storage time the right-hand portion of the curve disappears. An explanation for this behaviour was obtained by observing the output of the electron multiplier on the oscilloscope. This revealed that pulses of ions were being ejected from the Quistor at times coinciding with both the ion ejection pulse and the ion creation pulse. Since under conditions of zero storage the two ion pulses were ejected almost simultaneously, they both arrived at the detector at a time when the box car linear gate was open and thus the zero storage total pressure curve was made up of ions ejected coincident with both the ion creation and ejection pulses. The ions ejected coincident with the ion creation pulse are 'unstable' ions, that is ions which are created under such initial conditions that their subsequent trajectories are unstable. These ions, being unbounded, either effectively 'fall out' of the Quistor or collide with its electrodes. Under the conditions employed to produce the total pressure curves shown in Figure 3.14, these 'unstable' ions clearly took up to *ca.* 60 μs to be lost from the Quistor and under certain conditions they may take as long as 100 μs to be lost. This places a lower limit on the useful storage time of the device since at storage times of below 100 μs, unstable ions will contribute to the 'stable' or stored ion signal which may lead to erroneous results especially when the Quistor is employed to study the kinetics of ion-molecule reactions. The total pressure curve shown in Figure 3.14(c) is the real total pressure curve for krypton ions since it shows the variation in the number of stored or stable ions as a function of the applied r.f. potential.

The experimental limits of stability were determined from the total pressure curves by measuring the value of the applied r.f. potential, V_o, where the intensity of the stored ion signal approached zero. These points correspond to the experimental stability boundaries on the q_z axis since outside of these boundaries ions are not stable and so cannot be stored. Two total pressure curves, one for krypton (m/e 84) and the other for argon (m/e 40) both recorded at an applied r.f. frequency of 0.8 MHz and a storage

Figure 3.15 Total Pressure Curves for Krypton (m/e 84) and Argon (m/e 40)

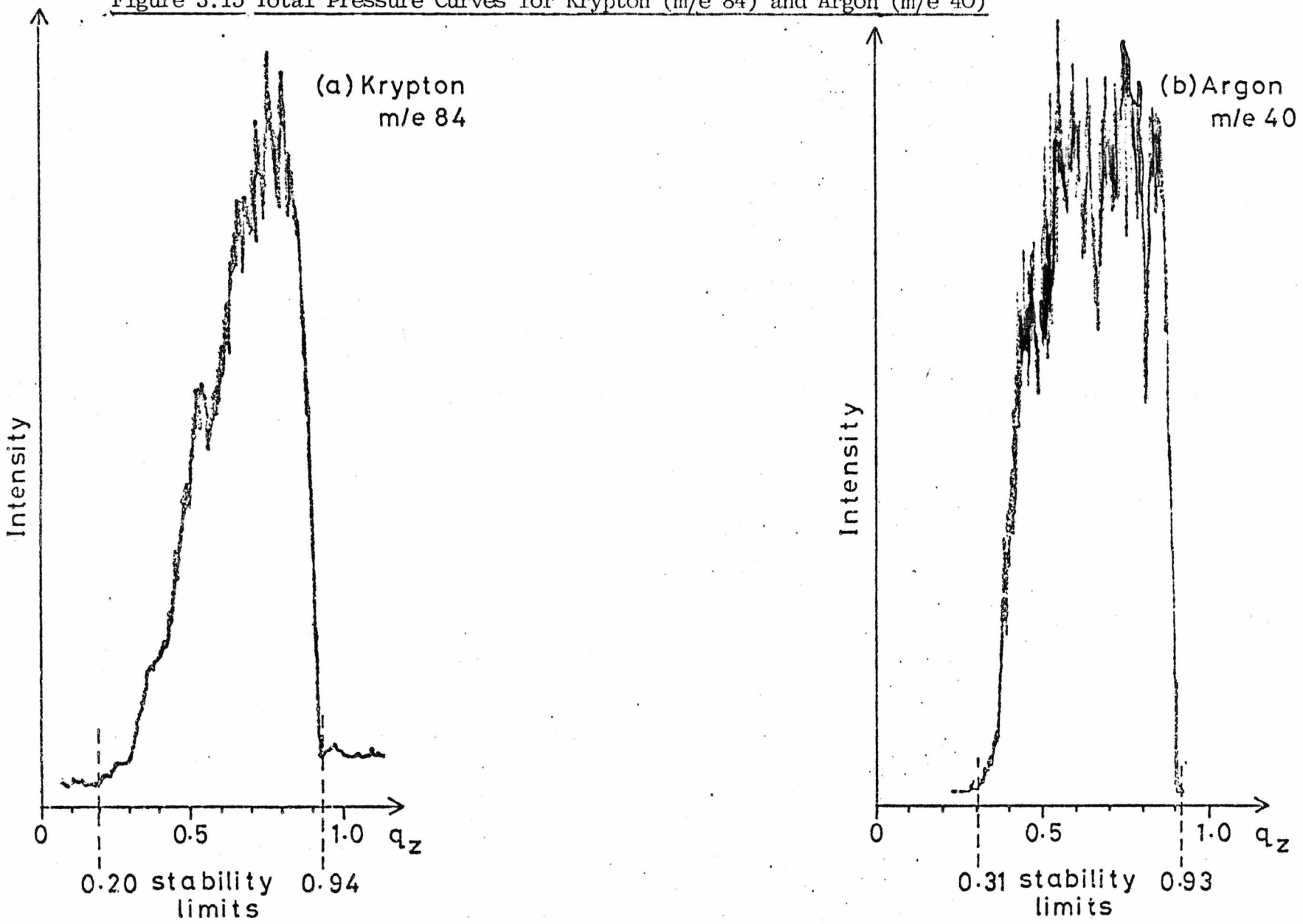

time of 100 μs are shown in Figure 3.15(a) and (b) respectively. The x axes of these curves have been transformed from V_o to q_z by substitution into equation (3.16). It was immediately apparent from these total pressure curves that the stability boundary on the q_z axis did not extend as far as $q_z = 0$. In fact, compared to the theoretical boundaries the experimental stability limits exhibited a general shift towards higher values of q_z. In addition to this the position on the q_z axis of the experimental stability limits, especially at low q_z, was dependent, on the m/e value of the stored ions as is clearly shown in Figure 3.15. The shifts in the stability limits on the q_z axis are thought to be caused by the space-charge potential of ions stored within the Quistor and were expected since the theoretical treatment given in Section 3.2 only considers the containment of one ion. The effects of space-charge are considered in more detail in Section 3.4.1.2.

Similar shifts in the stability limits were observed when the Quistor was operated at the higher frequency of 2.8 MHz. Unfortunately, the maximum output of the r.f. generator (2400 V) was insufficient to enable complete total pressure curves to be obtained for either krypton or argon in order to make direct comparison with those recorded at 0.8 MHz. However, a partial total pressure curve obtained for argon recorded at 100 μs storage time is shown in Figure 3.16(a). By comparison with the total pressure curve for argon recorded at 0.8 MHz shown in Figure 3.15(b) it appears that the shift in the stability limit at low q_z becomes smaller at higher frequencies of operation, a fact which is discussed further in the next section. A complete total pressure curve for helium (m/e 4) recorded at 100 μs storage time, at an operating frequency of 2.8 MHz, is shown in Figure 3.16(b). This illustrates that the stability limits exhibit the same general shift towards higher values of q_z for both operating frequencies.

The fact that the experimentally determined stability limit at low q_z was found not to extend as far as the theoretically predicted value of $q_z = 0$, placed a definite upper limit on the range of m/e values of ions

Figure 3.16 Total Pressure Curves Recorded at an Operating Frequency of 2.8 MHz

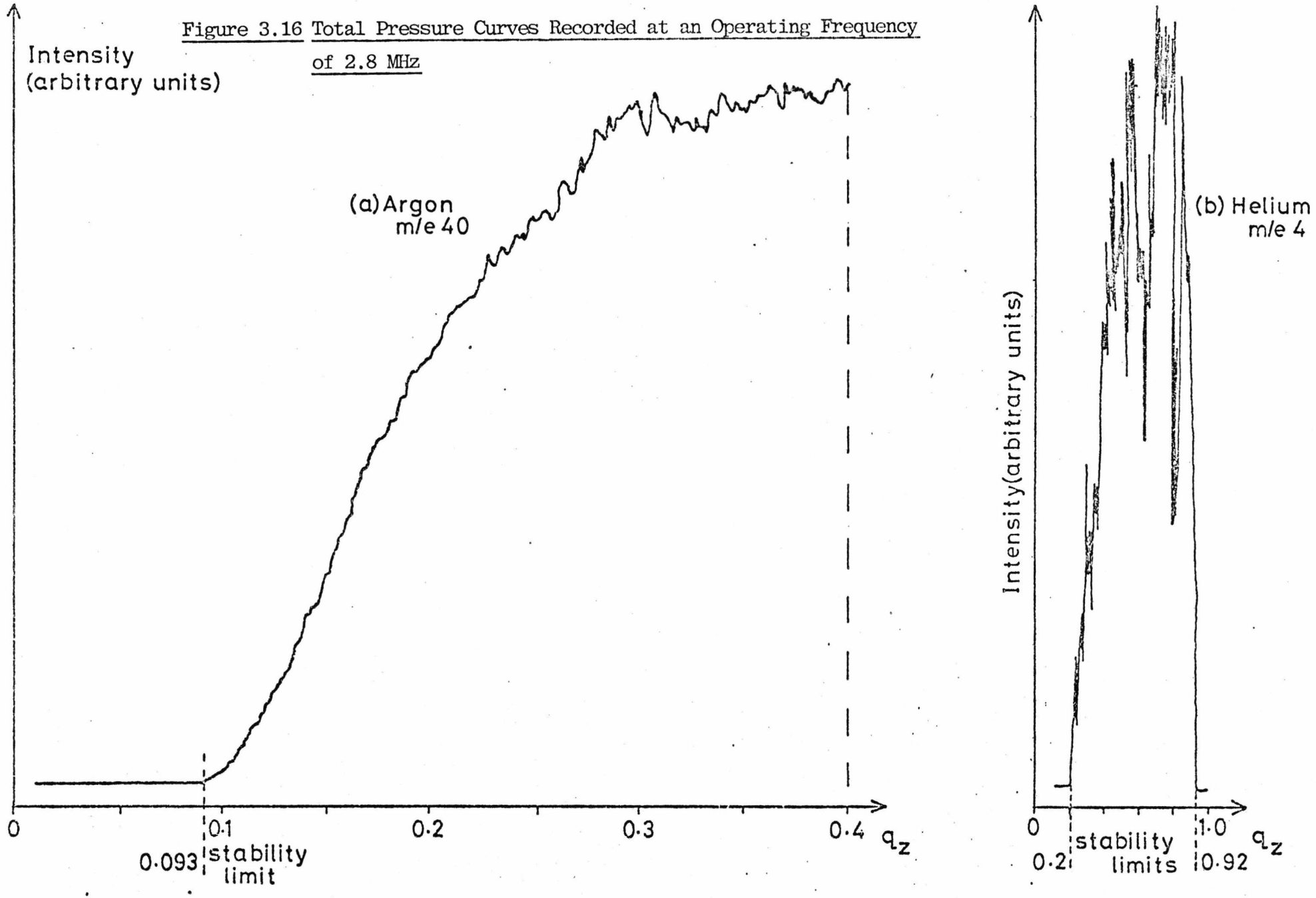

which could be stored simultaneously for a particular set of operating conditions. It was impossible to evaluate the actual mass range for ion storage for any given set of operating conditions because of the dependence of the experimental stability limits on the m/e value of stored ions. However, as an example of the mass range limitation, if the Quistor were operated under the conditions employed to record Figure 3.15(a) and the amplitude of the applied r.f. set such that m/e 84 was stored at $q_z \simeq 0.2$, then the ion of lowest mass which could be stored simultaneously, assuming a value of $q_z = 0.92$ for the high q_z stability limit, would be given by: $84\times(0.2/0.92) \simeq$ m/e 18. Therefore, under these conditions, all ions in the range m/e 18 to m/e 84 should be stable simultaneously. The consequences of this mass range limitation as regards the operation of the Quistor as a low pressure CI ion source are discussed in Chapter 4.

In order to examine the operation of the Quistor at other points in the stability diagram, and also to investigate how space charge affects the position of the stability boundaries, the method of determining experimental stability limits was extended to allow complete experimental stability diagrams to be plotted.

3.4.1.2 Experimental Stability Diagrams

In order to operate the Quistor at points in the stability diagram other than on the q_z axis, a positive or negative d.c. potential (supplied from the d.c. supply shown in Figure 3.13) was applied to the ring electrode in addition to the r.f. potential. Both end-caps were maintained at earth potential except for the duration of the ejection pulse.

Two different methods were employed to determine the boundaries of the experimental stability diagrams:

(i) The d.c. level on the ring electrode was set at a particular value and a plot of ion intensity *vs* r.f. potential was obtained in a similar manner to that described for total pressure curves. This procedure was repeated for various positive and negative values of the d.c. potential

such that the complete experimental stability diagram was covered. The value of the r.f. potential was measured at the points where the ion intensity approached zero for each ion intensity *vs* r.f. potential plot. In this way pairs of values of the d.c. potential, U and the r.f. potential, V_o were obtained which corresponded to points on the experimental stability boundaries.

(ii) The output of the electron multiplier, and the ejection pulse were displayed simultaneously on the screen of a dual trace oscilloscope. 'Stable' ions, ejected from the Quistor, appeared as a peak on the ion trace which coincided approximately with the ejection pulse. The values of U and V_o were then varied systematically to determine the points at which this ion peak just disappeared. These points corresponded to the experimental stability boundaries as for method (i).

Although both of these methods produced virtually identical stability diagrams within experimental error, the procedure employed with method (ii) permitted a more definitive assignment of the actual position of the stability boundaries, whereas with method (i) the observed position of the stability boundaries was, to a limited extent, dependent on the width and position in relation to the ion signal, of the Box Car detection pulse. However, with method (i) additional information was obtained from the general shape of the ion intensity *vs* r.f. potential plots (see Section 3.4.1.3) and so in practice the position of the stability boundaries was first determined using method (i) and verified using method (ii). The values of U and V_o determined in this way were converted into values of a_z and q_z according to equations (3.15) and (3.16) respectively. These may be re-written in the form shown below by making the substitutions: $\Omega = 2\pi f$, $V = 2V_o$. Other symbols have the same definitions as previously but in more convenient units, f, the frequency of the applied r.f. in MHz, r_o in cm, m in atomic mass units and V is the peak-to-peak amplitude of the applied r.f. in volts.

$$a_z = \frac{0.194\ U}{m\ r_o^2\ f^2} \tag{3.38}$$

$$q_z = \frac{0.0485\ V}{m\ r_o^2\ f^2} \tag{3.39}$$

An experimental stability diagram for argon ions (m/e 40), determined while operating under the following conditions, is shown in Figure 3.17

Argon pressure	2×10^{-5} Torr
Operating frequency	0.8 MHz
Storage time	100 μs

The dotted line represents the theoretical stability boundaries and the continuous line is drawn arbitrarily through the experimental points which are represented by open circles. This clearly demonstrates that the previously observed shift of the stability limits on the q_z axis, arises due to a general shift of the stability boundaries of the experimental stability diagram.

The shift in the stability boundaries on the q_z axis has also been observed by Fischer[64], who proposed an explanation for the phenomenon based on a consideration of the space charge of the ion cloud contained within the Quistor, an effect which is not taken into account in the basic theory described in Section 3.2. Fischer's model assumes that as the ion density builds up the resultant fields are equivalent to applying additional defocussing d.c. potentials $\Delta U/2$ to the end cap and ring electrodes. Thus, from equations (3.11) and (3.12)

Figure 3.17 Experimental Stability Diagram for Argon Ions (m/e 40)

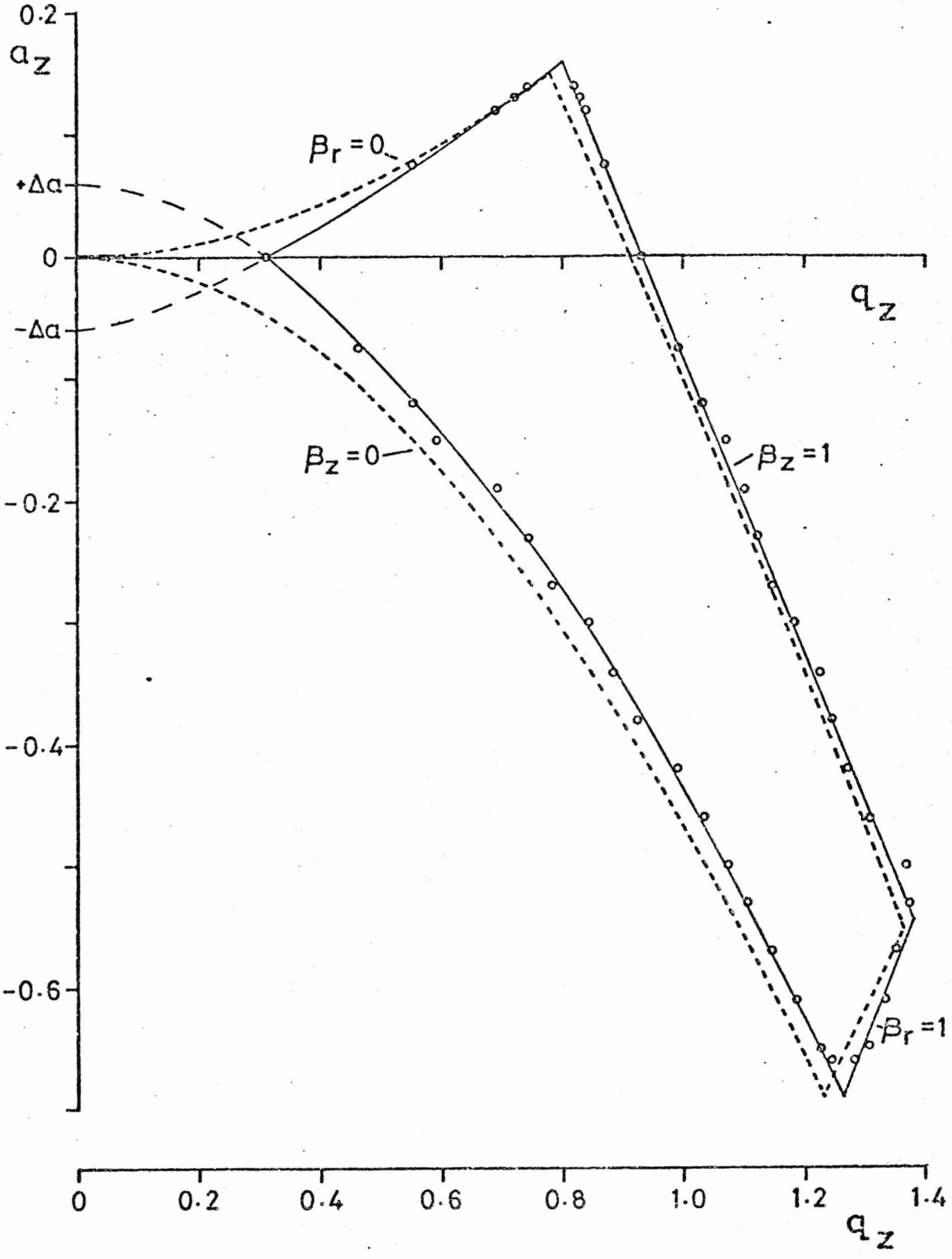

$$-2U_z \cdot \frac{z}{r_o^2} = \frac{\rho z}{2\epsilon_o}$$

and

$$\Delta U_r \cdot \frac{r}{r_o^2} = \frac{\rho r}{4\epsilon_o}$$

giving

$$\Delta U_z = -\Delta U_r = \frac{-\rho r_o^2}{4\epsilon_o} \qquad (3.40)$$

where ρ is the charge density and ϵ_o the permittivity. The net effect is that the space charge acts as a defocussing force in both the r and z directions; the d.c. potentials experienced by the ions are greater than they should be so that unstable trajectories result. This may be viewed as an apparent shift in the boundaries of the stability diagram which was in fact the effect observed as shown in Figure 3.17.

In order to relate equation (3.40) to the observed shift in the stability boundaries, the boundaries corresponding to $\beta_z = 0$ and $\beta_r = 0$ were extrapolated to give a very approximate value for the intercepts on the a_z axis $\pm \Delta a$. Then by combining equation (3.15) with equation (3.40) we obtain

$$\Delta a = \pm \frac{e}{\epsilon_o m \Omega^2} \rho \qquad (3.41)$$

From this expression it appears that for a given ion density more favourable operation of the Quistor (i.e. lower values of Δa) should be obtained for higher values of m and Ω. Although a general check on the validity of equation (3.41) was not performed, experimental evidence suggests that in terms of general trends it is valid. For example, referring to the total pressure curves shown in Figure 3.15, the stability

limit at low q_z is clearly closer to the a_z axis for m/e 84 than for m/e 40 and therefore Δa (m/e 84) is less than Δa (m/e 40) in agreement with equation (3.41). During the course of this investigation it was noticed that ions of low mass such as He^+(m/e 4) could not be stored in the Quistor when it was operated at low frequencies, *ca.* 0.8 MHz, unless its electrode surfaces had recently been cleaned. This behaviour was attributed to a combination of two effects: firstly, the space charge shift of the stability boundaries, since according to equation (3.41) large values of Δa are expected for low values of m and Ω and hence the stability diagram would be expected to be very narrow, and secondly, to the build-up of charge on non-conducting layers of material, such as diffusion pump oil, condensed onto the electrode surfaces or the pyrophollite spacers. This explanation for the variation in the storage capabilities of the Quistor with cleanliness must only be regarded as tentative. However, irrespective of operating conditions, its performance showed a definite deterioration with time until a stage was reached where no ions could be stored at all. This situation could only be rectified by thorough cleaning of the Quistor electrodes and spacers.

As was the case for the total pressure curve, power supply limitations did not permit a complete experimental stability diagram to be plotted for argon at an operating frequency of 2.8 MHz. However, a partial stability diagram recorded under the following conditions is shown in Figure 3.18

Argon pressure	2×10^{-5} Torr
Operating frequency	2.87 MHz
Storage time	800 μs
ICPW	20 μs

The stability boundaries are clearly not shifted as much as those in the stability diagram obtained for argon ions when operating at 0.8 MHz (Figure 3.17), and consequently the value of Δa is considerably lower, as

Figure 3.18 Partial Experimental Stability Diagram for Argon Ions Recorded an Operating Frequency of 2.87 MHz

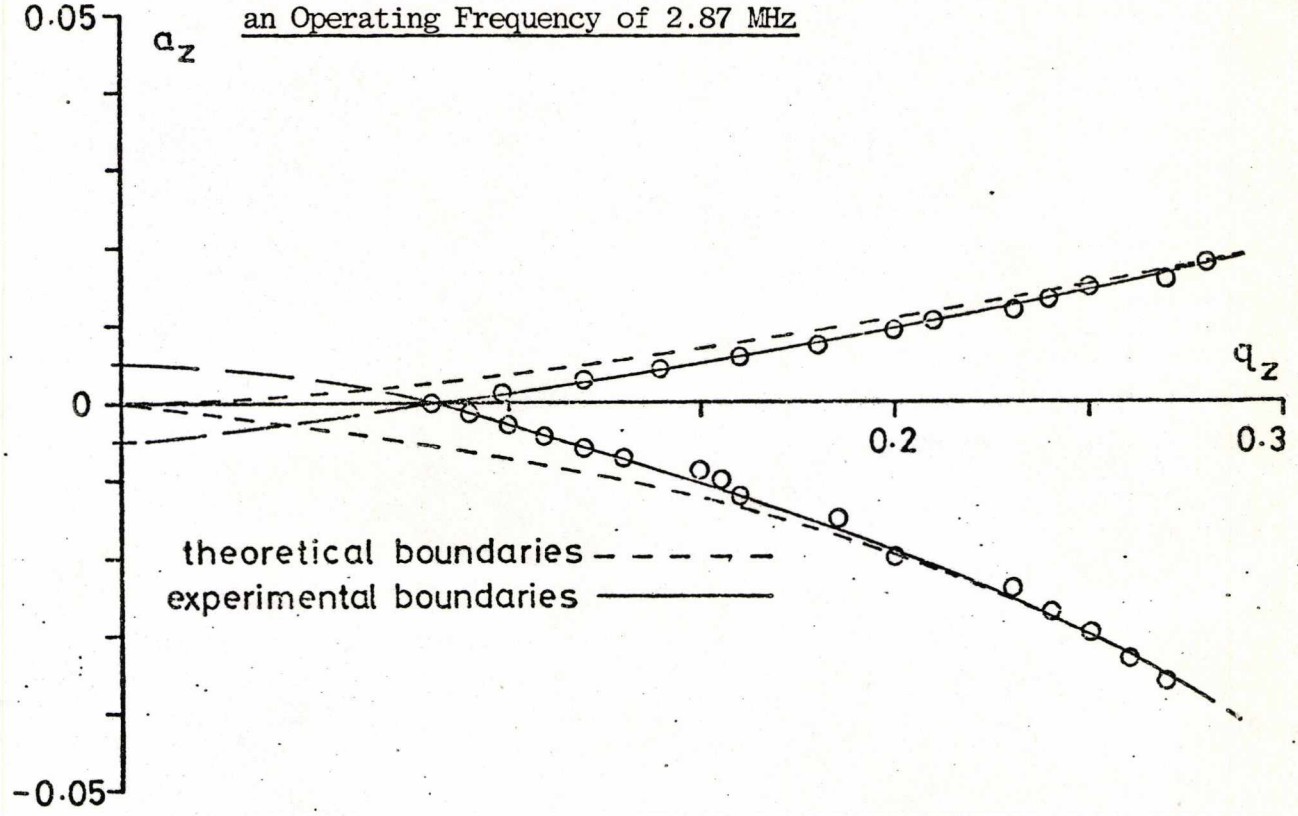

Figure 3.19 Graph Showing Variation in Position of the Stability Limit at Low q_z with Ion Creation Pulse Width

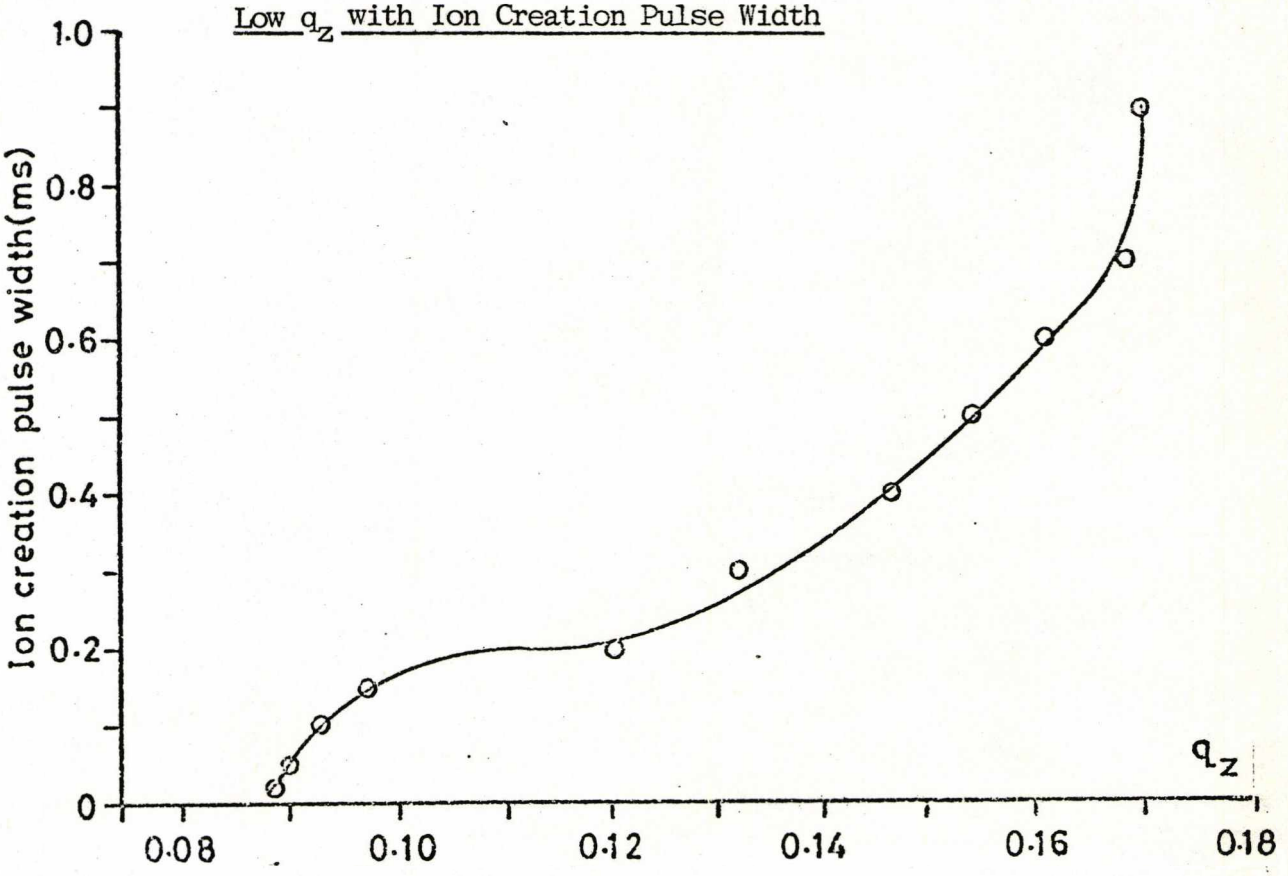

KENT UNIVERSITY LIBRARY

was expected from equation (3.41).

If the space charge of the ion cloud was the major contributing factor to the shift of the stability boundaries then their position should also be a function of the number of ions stored in the Quistor. This was investigated by determining the position of the stability limit at low q_z for different values of the ion creation pulse width (ICPW), while operating under identical conditions to those employed to obtain Figure 3.18. The results of this investigation are depicted in Figure 3.19. This clearly shows that the stability limit shifted towards higher values of q_z as the ICPW as increased. Unfortunately, it was impossible to deduce from this experiment the form of the relationship between the number of ions stored and the shift in the stability limit because the number of ions stored is not directly proportional to the ICPW. No further shift was observed beyond an ICPW of 900 μs and none was expected since ion build-up data (Section 3.4.2.4) indicated that under these conditions the device was saturated. At very low values of the ICPW the number of ions stored is correspondingly small and so the position of the stability limit would be expected to approach the theoretical value of $q_z = 0$; however, this was not observed experimentally. Although at low values of the ICPW the position of the stability limit was very difficult to determine, due to lack of sensitivity, the graph shown in Figure 3.19 appears to intersect the q_z axis at a value of *ca.* 0.085. One possible explanation for this behaviour is that the electron gate was not totally effective in shuttering the electron beam at times other than when creation pulse was applied, which would result in continuous ionisation. The space charge of ions formed in this way would give rise to the observed shift at an ICPW of zero. The standard method of testing the electron gate was to observe the output from the multiplier corresponding to the 'stored' ion signal on an oscilloscope set at maximum sensitivity, and then disconnect the ion creation pulse from the electron gate. Any 'stored' ions observed must then have been formed by electrons 'leaking' through the electron

gate. This test was performed before every experiment and usually the electron gate was found to be functioning properly. However, a simple calculation revealed that the number of stored ions required to produce an observable 'ion peak' on the oscilloscope screen when operated at its maximum sensitivity was *ca.* 1000. This implies that continuous ionisation could be occurring and not be detected, which makes the above explanation feasible.

3.4.1.3 Storage Efficiency

Besides providing information on the limits of stability, total pressure curves such as those illustrated in Figures 3.15(a), 3.15(b) and 3.16(b) give a direct indication of the 'ion storage efficiency' as a function of q_z. These curves all maximise at a q_z of *ca.* 0.7 at which point considerably more ions can be stored than for a q_z of, for example, 0.35. When ions possessing a range of m/e values are stored simultaneously at a particular fixed value of the applied r.f. potential, those with different m/e values will be stored at different values of q_z as given by equation (3.16), and since storage efficiency varies with q_z there will be an inherent mass discrimination. Experimental evidence for this effect is given in Chapter 4.

A theoretical explanation for the shape of the total pressure curve has been given by Lawson *et al*[121]. According to this treatment the shape arises due to a combination of two factors: the space charge limited maximum ion density, and the initial acceptance volume within which ions must be formed in order to remain stable. The space charge-limited density of ions *at rest*, which can be contained within a potential well of the form described in Section 3.21, may be estimated by first invoking the Poisson relation

$$\left[\begin{array}{c}\text{electrostatic} \\ \text{potential, } \phi_i\end{array}\right] + \left[\begin{array}{c}\text{pseudo-} \\ \text{potential, } \psi\end{array}\right] = \text{constant}$$

such that

$$-\nabla^2\phi_i = \nabla^2\psi = 4\pi\ \rho_{max} \tag{3.42}$$

where ρ_{max} is the theoretical space-charge limited density. For operation in the total pressure mode, the potential $\psi_{x,y,z}$ at a point x,y,z is

$$\psi_{x,y,z} = \frac{\overline{D}_r}{r_o^2}(x^2 + y^2) + \frac{\overline{D}_z}{z_o^2}\ z^2 \tag{3.43}$$

then by substitution of $\overline{D}_r = \overline{D}_z/2$ and $r_o^2 = 2z_o^2$ and applying the operator ∇^2

$$\nabla^2\psi = \frac{3\overline{D}_z}{z_o^2}$$

Equating this with equation (3.42) and making the substitution $\rho_{max} = e\ N_{max}$

$$N_{max} = \frac{3\overline{D}_z}{4\pi\ e\ z_o^2} \tag{3.44}$$

Making the substitutions, $\overline{D}_z = e\ V_o^2/4m\ z_o^2\ \Omega^2$ and $V_o = (m\ z_o^2\ \Omega^2/2e)q_z$, equation (3.44) becomes

$$N_{max} = \frac{3}{64\pi}\frac{m\Omega^2}{e^2} \cdot q_z^2 \tag{3.45}$$

From this it would appear that the space charge-limited ion density N_{max} should increase as a function of q_z^2. The second factor arises, briefly, due to the fact that for a particular value of q_z there is an 'acceptance' volume within which an ion must be formed, with a given initial velocity, in order that the amplitude of its subsequent trajectory does not exceed the physical dimensions of the device and be lost. This volume decreases

to zero as the value of β approaches 1.0. For operation in the total pressure mode the value of β_z increases from 0 to 1.0 as the value of q_z increases from 0 to *ca.* 0.91 (Figure 3.5). Therefore, when a total pressure curve is obtained the acceptance volume decreases to zero as the q_z = *ca.* 0.91 stability limit is approached. By combining these two factors Lawson *et al*[121] obtained a theoretical total pressure curve which had a similar shape to those determined experimentally and maximised at the same value of q_z = *ca.* 0.7.

In order to investigate storage efficiencies at other points in the stability diagram, a series of ion intensity *vs.* applied r.f. potential (V_o) curves were plotted for different values of the applied d.c. potential (U) using method (i) described in Section 3.4.1.2. A series of these curves is shown in Figure 3.20

Argon pressure	2×10^{-5} Torr
Operating frequency	0.81 MHz
Storage time	1 ms
ICPW	20 μs

These, in fact, represent the variation in ion storage efficiency for a series of horizontal sections through the stability diagram at fixed values of a_z. It is immediately apparent from these curves that the position of maximum storage efficiency is not on the q_z axis but appears to occur at the point a_z = -0.074, $q_z \simeq 0.75$. Dehmelt[131] has suggested that optimum storage may occur under conditions where the depths of the pseudo-potential wells in the r and z directions are equal. He reasoned that under conditions where $\bar{D}_r = \bar{D}_z/2$ (as is the case for operation on the q_z axis) an ion formed with a large amplitude of oscillation in the z direction, may, as a result of collisions with either other ions or molecules (Section 3.4.2.1) be deflected and subsequently collide with the

Figure 3.20 Series of Ion Intensity *vs* R.F. Potential Curves for Different Values of a_z

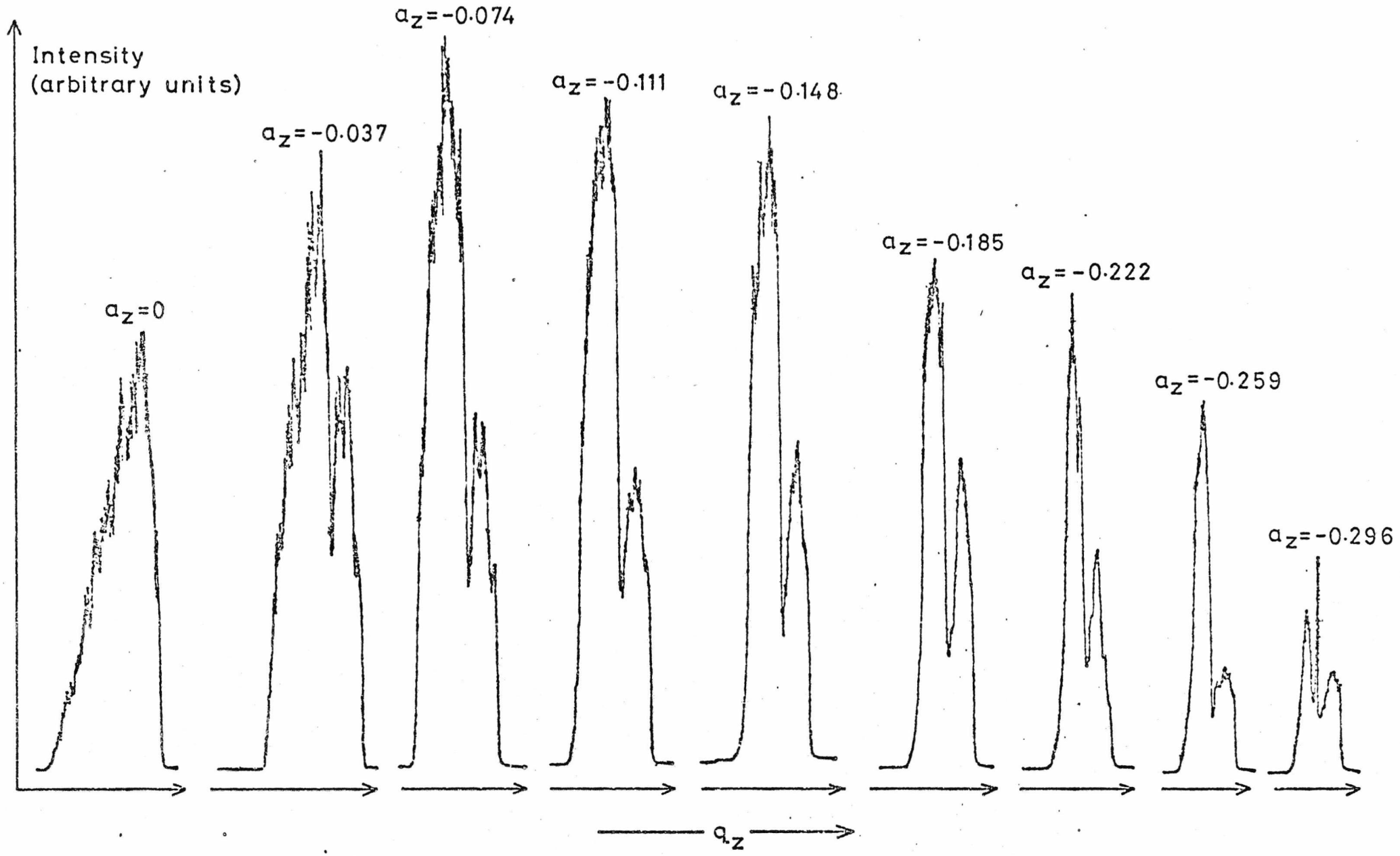

ring electrode. This would be less likely to occur if the depths of the pseudo-potential wells in the r and z direction were equal. Substitution into equation (3.29) for the case where $a_z \neq 0$ gives an expression for the depths of the pseudo-potential well at any point in the stability diagram:

$$\overline{D}'_z = \frac{e V_o^2}{4m z_o^2 \Omega^2} - \frac{U}{2} \qquad (3.46\ a)$$

and for the r-direction

$$\overline{D}'_r = \frac{e V_o^2}{4m r_o^2 \Omega^2} + \frac{U}{2} \qquad (3.46\ b)$$

Substituting for U and V_o (equations (3.15) and (3.16)) and equating $\overline{D}'_z$ with $\overline{D}'_r$ yields

$$a_z = - q_z^2/8 \qquad (3.47)$$

Thus, according to this treatment, the point of optimum storage efficiency should fall on the locus given by equation (3.47). For $a_z = -0.074$ the value of q_z given by this equation is 0.77 and so the point of maximum storage efficiency determined from the curves shown in Figure 3.20 ($a_z = -0.074$, $q_z \simeq 0.75$) is extremely close to this locus, which lends strength to the validity of this type of theoretical approach. The fact that the point of maximum storage efficiency occurred at this particular point on the locus may be explained in the same terms as those employed by Lawson *et al*[121] to explain the shape of the total pressure curve.

A theoretical value for the point of optimum operation (maximum storage efficiency) has been calculated by Baril and Septier[132] using the methods of phase space dynamics[129]. This point was $a_z = -0.35$, $q_z = 0.495$ which also falls on the locus given by equation (3.47). However, since space charge was not taken into account for this calculation no agreement

between this value and that determined experimentally was expected.

3.4.1.4 Non-Linear Resonances

All of the curves shown in Figure 3.20, with the exception of that recorded at $a_z = 0$, were found to be partially split into doublets or in the case of that recorded at $a_z = -0.296$, a triplet. Peak splitting of a similar nature has been observed by Dawson and Whetten[133,134] when operating the Quistor as a mass spectrometer. This phenomenon is well characterised since similar effects are observed with the quadrupole mass filter[134,135]; it is caused by field imperfections which give rise to so-called non-linear resonances. In practical devices the fields are not the perfect quadrupole fields which are described exactly by the Mathieu equation. Errors in the field result from imperfect electrode geometry, errors in spacing of the electrodes, charging of insulators and non-sinusoidal waveforms. In a perfect field, the expression for the potential at any point (equation (3.6)) contains only second order terms involving the coordinates of that point, and the restoring force on an ion is linearly proportional to its displacement from the centre of the device. The effect of geometric errors in the field is to introduce higher than second order terms in the expression for potential so that the restoring forces are non-linear. The actual form of the higher order terms may be derived from the theory of spherical harmonics[136]. (A spherical harmonic is any homogeneous polynomial which satisfies Laplace's equation). Considering only geometric errors and only retaining terms with rotational symmetry the potential for the Quistor may be expressed as the series

$$\phi_{r,z} = \frac{1}{4z_o^2}(U-V\cos\Omega t)\left[(r^2-2z^2) + \frac{A}{z_o}(3r^2z-2z^3)\right.$$

$$\left. + \frac{A'}{z_o^2}(r^4 + 8/3\ z^4 - 8r^2z^2) + \ldots\right] \qquad (3.48)$$

where A and A' are the weighting factors for the third and fourth order distortions respectively. Dawson and Whetten[137] have shown that an error in the spacing of one end-cap electrode with respect to the ring electrode introduces a large third-order distortion and a symmetrical error in the spacing of both end-caps with respect to the ring electrode introduces a large fourth-order distortion. The presence of either of these distortions gives rise to resonances at particular points in the stability diagram. For the third order distortion these occur at $\beta_r = 2/3$ and $\beta_r + 1/2\ \beta_z = 1$ and for the fourth order distortion at $\beta_r = 1/2$, $\beta_r + \beta_z = 1$ and $\beta_z = 1/2$[138]. An ion with a_z, q_z coordinates corresponding to one of these resonance lines would absorb power from the field, become unstable and subsequently either collide with an electrode or be ejected from the Quistor. It is this effect which produces the 'dips' in curves such as those shown in Figure 3.20.

The following experiment was performed to determine the location in a_z, q_z space of the observed resonance 'dips' in an effort to establish whether they were caused by a third or fourth order distortion. This would identify the particular electrode spacing errors in the Quistor which could then be corrected to eliminate the distortion. A series of ion intensity *vs.* r.f. potential (V_o) curves were recorded at different values of the d.c. potential (U) using the same method as that employed in the determination of the experimental stability diagram (Section 3.4.1.2). The value of V_o was measured at points corresponding to the stability limits, and also where any resonance dips occurred. The U and V_o values were then transformed into a_z and q_z using equations (3.15) and (3.16) and the results are presented in the form of a partial experimental stability diagram in Figure 3.21. The operating conditions were:

Figure 3.21 Partial Experimental Stability Diagram for Argon Ions (m/e 40) showing Position of Resonance 'Dips'

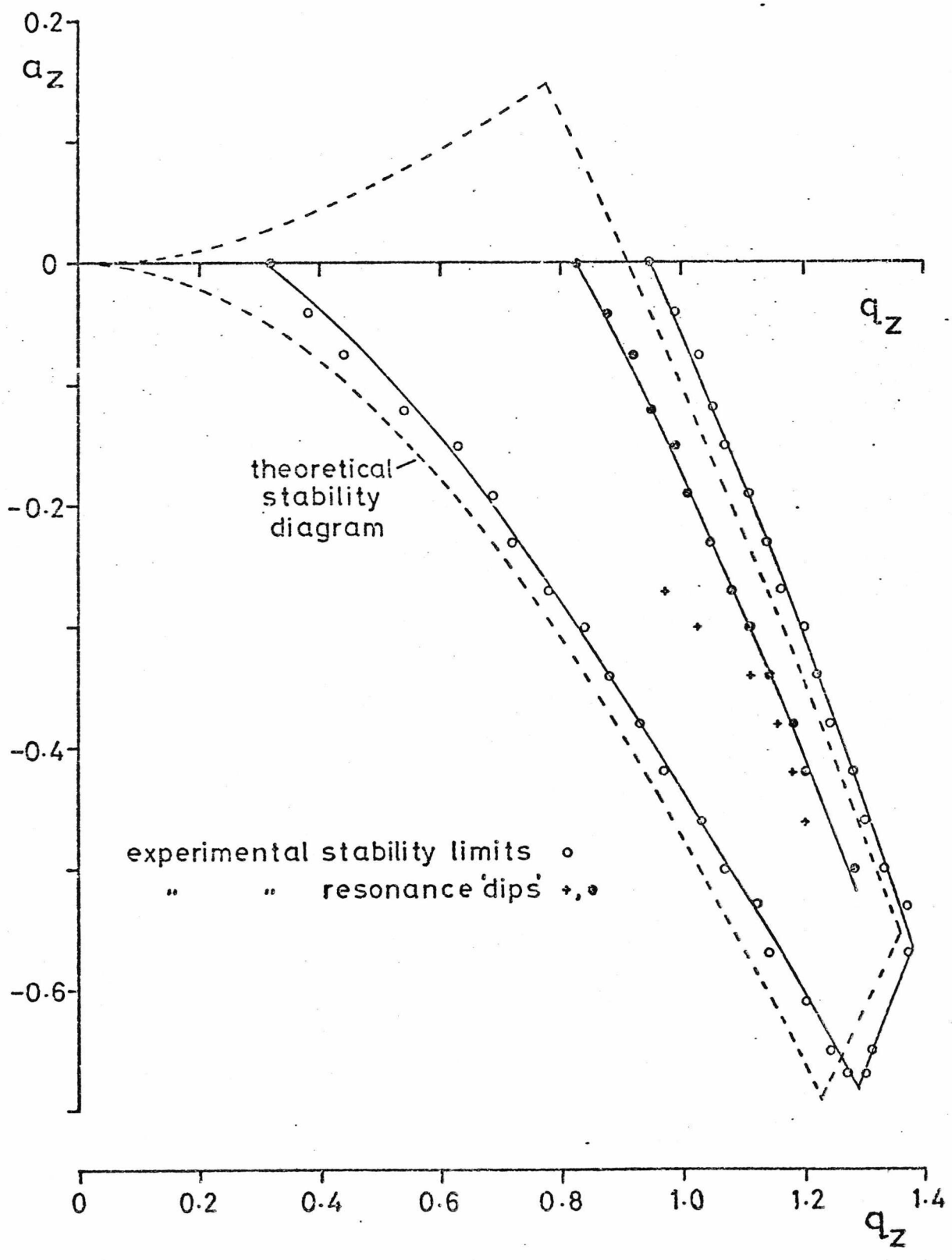

Argon pressure	2×10^{-5} Torr
Operating frequency	0.81 MHz
Storage time	100 μs
ICPW	20 μs

Allowing for the shift in the experimental stability diagram, the major resonance 'dips' (indicated by closed circles) were found to fall approximately on a line corresponding to $\beta_z = 2/3$. Some other minor resonance 'dips' were present (indicated by crosses) but these did not all appear to fall on a particular resonance line. The appearance of major resonance 'dips' on the line $\beta_z = 2/3$ was surprising since these did not correspond to either a third or a fourth order distortion. The only possible explanation for the occurrence of resonances at this point is that they were caused not by geometric errors but by the presence of sub-harmonics in the applied r.f. waveform. Unfortunately this explanation could not be confirmed since no frequency analyser was available. Although some of the minor resonances occurred at points in the stability diagram, which would indicate the presence of a third order distortion, the resonance 'dips' were so insignificantly small that they did not warrant an attempt to correct the electrode spacing.

This section on experimental limits of stability may be summarised as follows:

(i) There is a definite limit to the range of m/e values of ions which may be stored simultaneously. This 'mass range' is dependent on the operating frequency and also on the number of ions stored.

(ii) For any fixed set of operating conditions, ions with different values of m/e are not stored with the same efficiency and so the Quistor possesses an inherent mass discrimination when operated in the total pressure mode.

(iii) There appears to be no great advantage in operating the Quistor at any other point in the stability diagram besides the q_z axis when it is employed as an ion storage source. Although the storage efficiency is marginally higher when operating just below the q_z axis, the 'mass range' is narrower and non-linear resonances become more pronounced.

3.4.2 Ion Loss Processes

In this section the processes by which ions possessing 'stable' trajectories may be lost from the Quistor are considered in detail. The rapid loss of 'unstable' ions has already been discussed in Section 3.4.1.1. Ion loss processes and the kinetics of ion loss have been examined by several authors[64,67,123,131,133,139] and the available kinetic data has been summarised by Lawson *et al*[121]. Only one of these studies[121] was concerned with the operation of the Quistor in the total pressure mode and this consisted of the determination of ion loss parameters for only one particular set of operating conditions. Since it was intended to operate the Quistor in this mode as a low pressure chemical ionisation ion source, a greater knowledge of these parameters was clearly of interest. The following experiments were performed in order to investigate ion loss kinetics in the Quistor when operated in the total pressure mode for a range of different operating conditions.

3.4.2.1 Mechanisms of Ion Loss

Loss of stable ions from the Quistor may occur by two processes: (i) ion-neutral molecule interactions and (ii) ion-ion interactions.

(i) There are a number of different types of ion-neutral molecule interactions which could result in ion loss, these include: elastic scattering, inelastic scattering, charge transfer and ion-molecule reactions. In the first two of these it is possible that a stable ion could be deflected in such a way that its subsequent trajectory is unstable and so it would be lost. In the charge transfer process an ion with a stable trajectory is replaced with a new ion, probably with zero initial velocity, but this may be created outside of the acceptance volume and so it would be rapidly ejected from the trap. Any ion-molecule reaction results in the loss of the ion of interest.

(ii) The collision of a pair of like-charged stable ions may result in one or both of their subsequent trajectories becoming unstable. In addition to this, the trapping field may be modified by the space charge potential which develops as the number of stored ions increases. One manifestation of this effect, namely the shift of the experimental stability boundaries has already been described in Section 3.4.1.2.

3.4.2.2 The Kinetics of Ion Loss

During the ion creation period (that is for the duration of the ion creation pulse) the rate of change of the number of stored ions N with time may be represented by the expression[66]

$$\frac{dN}{dt} = k_1 p - k_2 N^2 - k_3 N p \qquad (3.50)$$

where k_1 is the "rate constant" for ion creation, k_2 the rate constant for ion loss by ion-ion interactions, k_3 the rate constant for ion loss

by ion-neutral molecule interactions and p the pressure. At the saturation level where the rate of ion creation is exactly balanced by the rate of ion loss; i.e. $dN/dt = 0$, equation (3.50) becomes

$$k_1 p = k_2 N_\infty^2 + k_3 N_\infty p \tag{3.51}$$

where N_∞ is the ion density at saturation. It is possible to evaluate k_1 for a particular pressure by determining the initial slope of a 'build-up' curve obtained by plotting the stored ion intensity against the length of the ionisation period, since for small N equation (3.50) becomes

$$\frac{dN}{dt} = k_1 p \tag{3.52}$$

The values of k_2 and k_3 may be evaluated by considering the situation after the electron beam has been suppressed, such that $k_1 p = 0$ and

$$\frac{dN}{dt} = -(k_2 N^2 + k_3 N p) \tag{3.53}$$

This may be rearranged to

$$\frac{dN}{N(k_2 N + k_3 p)} = -dt \tag{3.54}$$

which on integration[139] becomes

$$\frac{1}{k_3 p} \ln\left(\frac{k_2 N + k_3 p}{N}\right) = t + \text{constant} \tag{3.55}$$

The constant may be evaluated by assuming that at $t = 0$, $N = N_o$, then equation (3.55) becomes

$$\frac{1}{k_3 p} \ln\left(\frac{N_o(k_2 N + k_3 p)}{N(k_2 N_o + k_3 p)}\right) = t \qquad (3.56)$$

which rearranges to

$$\frac{1}{N} = \left(\frac{k_3 p + k_2 N_o}{k_3 p\ N_o}\right) \exp(k_3 p t) - \frac{k_2}{k_3 p} \qquad (3.57)$$

By using a standard curve fitting procedure on the decay data when plotted as $1/N$ *vs.* t, the values of k_2 and k_3 may be determined for a particular pressure.

In order to evaluate the rate constants in appropriate units the value of N, which experimentally is obtained as a signal height in volts, must be converted to absolute units. This may easily be achieved from a knowledge of the gain of the electron multiplier, the transfer efficiency of the quadrupole mass filter and the ratio of the number of ions ejected from the Quistor to the number which actually enter the mass filter. Unfortunately, the latter two quantities are very difficult to determine accurately and so this introduces considerable uncertainties into the absolute values of the rate constants. The value of N is normally quoted as an ion density in ions cm^{-3} by assuming that the ions are contained within the inscribed oblate spheroid having a volume $4\pi\ r_o^2\ z_o/3$.

3.4.2.3 Experimental Aspects of the Determination of k_1, k_2 and k_3

The build-up curves required to evaluate k_1 were obtained by determining the stored ion intensity for a range of values of the ion creation pulse width, with a fixed delay time between the falling edge of the creation pulse, and the ejection pulse. This delay time was set at 100 μs to ensure that all unstable ions were lost before the stable ions were ejected into the mass filter. The ion intensity was determined by scanning the mass filter over the range corresponding to the m/e of the stored ion and then measuring the height of this ion peak in volts so that

it could be converted into the ion density N.

Two different methods were employed to obtain decay data which could be analysed using the method described in Section 3.4.2.2 to evaluate k_2 and k_3 :

Method (i) - the ion creation pulse width was fixed and the ion intensity was determined, using the method described above, for a range of values of the storage time. A decay curve could then be obtained by plotting the ion intensity against storage time.

Method (ii) - this method required a rearrangement of the experimental system shown in Figure 3.13 and the inclusion of a third pulse generator. A block diagram of the modified configuration is shown in Figure 3.22. In this system the ion creation pulse is used to trigger the box car scan delay generator (S.D.G.) which after a preset delay time produces a pulse which triggers the ion ejection pulse generator and a third 'initial delay' pulse generator. After a certain initial delay the latter pulse generator produces a 1 volt pulse, the detection pulse, to open the box car linear gate. The scan delay generator is set to ramp the delay time at a specified rate for a specified period, and simultaneously produces a voltage ramp that is directly proportional to the delay time, which is used to drive the x axis of the pen recorder. Since the ion ejection pulse is produced at the end of the delay time this system effectively ramps the storage time and so it is possible, by connecting the y axis of the pen recorder to the output of the electron multiplier via the linear gate, to obtain directly, a plot of the change in ion intensity as a function of storage time.

The relative advantages of these two methods are discussed in Section 3.4.2.4(i).

Figure 3.22 Schematic Block Diagram of Experimental System for Storage Time Scanning

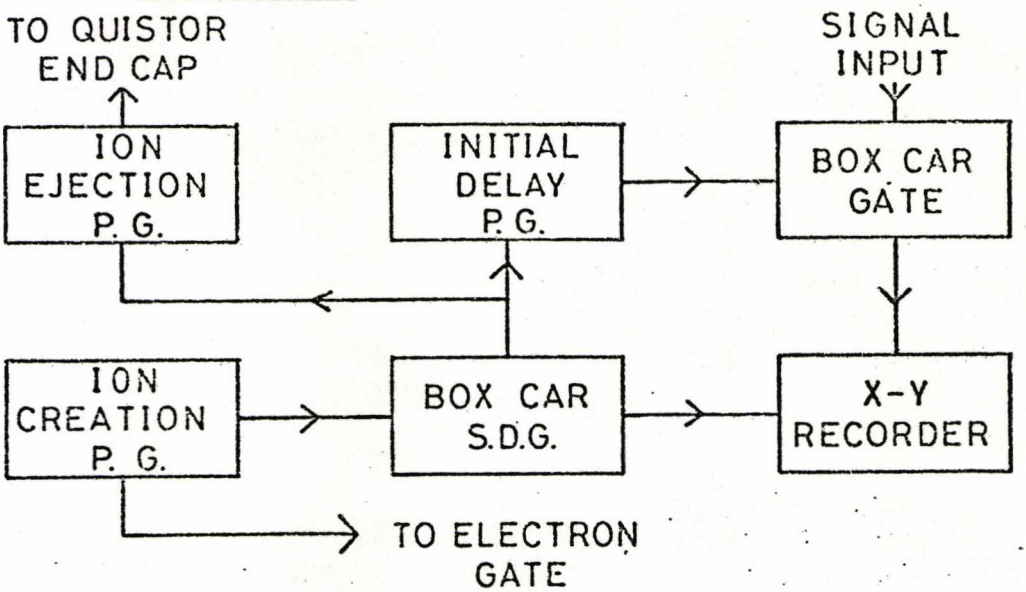

Figure 3.23 Build-up Curve for Argon Ions (m/e 40)

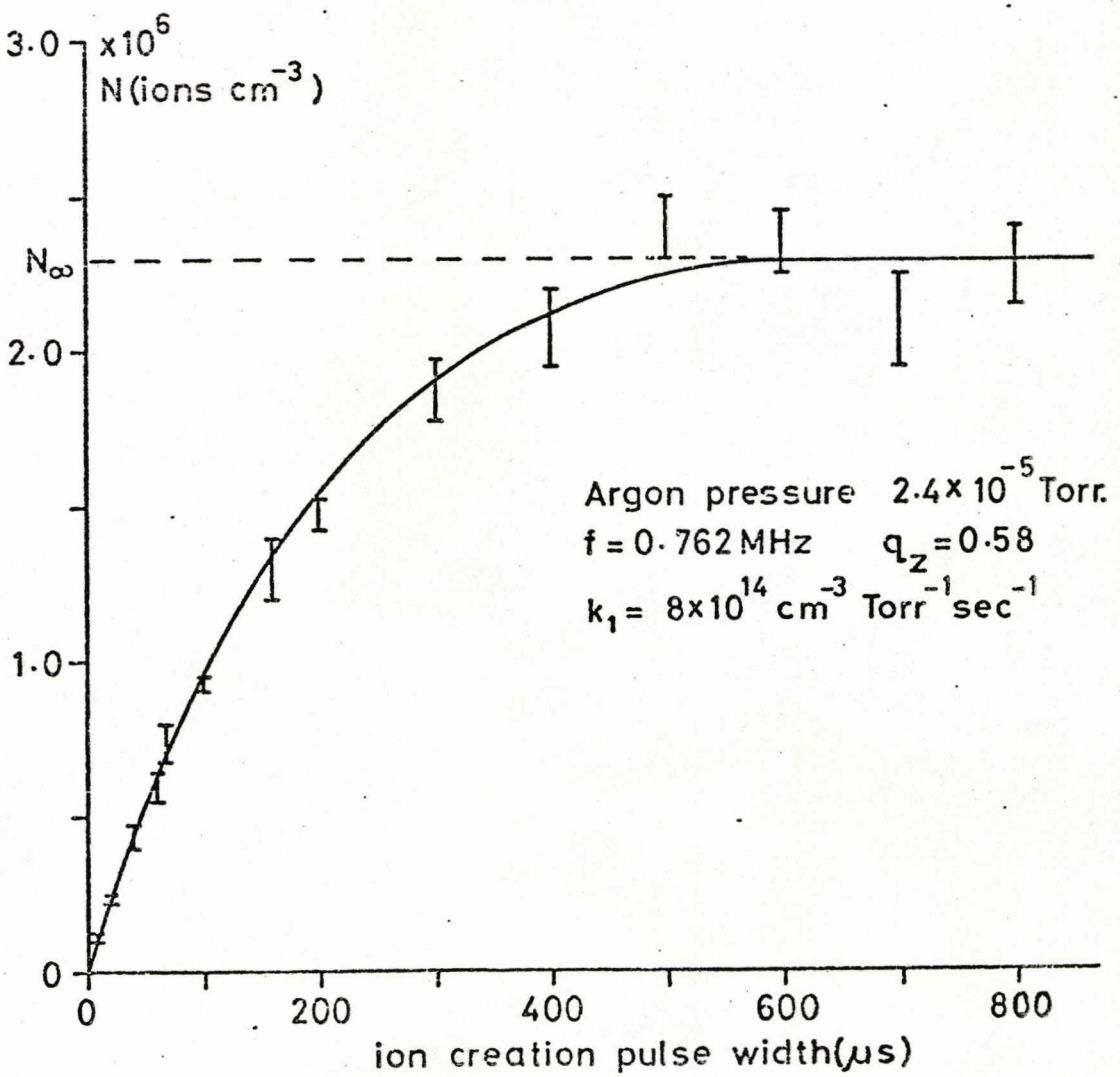

3.4.2.4 Results of Investigation into Ion Loss Processes

This investigation consisted mainly of the experimental determination of values for the rate constants for ion loss k_2 and k_3, for various different sets of operating conditions. The value of the ion creation "rate constant" k_1 was determined for only one particular set of operating conditions.

An ion build-up curve for argon ions recorded at a constant storage time of 100 μs is shown in Figure 3.2 3. The output from the box car linear gate in volts was converted into terms of the number of ions contained within the Quistor by using the factor, 1 volt output ≡ 5×10^4 ions cm^{-3}. This factor was calculated from the measured gain of the electron multiplier, which at the time this particular experiment was performed was found to be 1×10^5, and an assumed value of 10^{-3} for the transfer efficiency of ions from the Quistor to the first dynode of the electron multiplier. (This value of the transfer efficiency was estimated from experimental results by previous workers[126-7]). Under the conditions employed to record the build up curve shown in Figure 3.23 the value of N_∞ determined from the saturation level is 2×10^6 ions cm^{-3} and the value of k_1 calculated from the initial slope is 8×10^{14} cm^{-3} $torr^{-1}$ sec^{-1}. These values are in reasonable agreement with other literature values for these parameters summarised by Lawson *et al*[121], and so the value of the conversion factor for output volts to ions cm^{-3} was assumed to be correct within an order of magnitude. The value of k_1 was not determined for other sets of operating conditions since this parameter is expected to be dependent on such factors as the electron current and electron optics and not on the operational characteristics of the device. Due to the large uncertainties involved in the determination of N_∞ no further quantitative measurements of this parameter were made. However, total pressure curves recorded when the Quistor was operated at saturation were found to have a similar shape to those shown in Figures 3.14(c), 3.15(a) and (3.15(b) which gives a good indication of how N_∞ varies with q_z. Lawson *et al*[121] have determined the

value of this parameter for various different values of the applied r.f. frequency and found that its value increases sharply as the r.f. frequency increases.

All subsequent experiments on ion loss processes were performed when the gain of the electron multiplier had fallen to 1×10^4. Consequently, the conversion factor which applies to these experiments is: 1 volt output from box car $\equiv 5\times10^5$ ions cm^{-3}.

3.4.2.4(i) The Dependence of k_2 and k_3 on Pressure

In an effort to establish whether the values of the ion loss rate constants were dependent on pressure and also to determine values for these constants while operating the Quistor under conditions which may be used when it is employed as a low pressure CI ion source, a number of ion decay curves were obtained at different pressures. A minimum storage time of 100 μs was used for these studies to ensure that errors did not occur due to 'unstable' ions contributing to the stored ion signal. For a fixed value of the ion creation pulse width the number of ions created and, if the device is operated below the saturation level, the number of ions stored, increases as the operating pressure is increased. This means that the value of N_o would be different for experiments performed at different pressures. In order to fix as many variables as possible the experiments were performed in such a way that the value of N_o was approximately independent of pressure. This was achieved by adjusting the ion creation pulse width for each experiment such that the value of N (in practice the output from the box car in volts) at 100 μs storage was constant. Since this procedure could not be performed at zero storage time the value of N_o was not actually constant but its approximate independence of pressure was sufficient for these experiments.

Two series of decay curves for argon ions (m/e 40) obtained while operating at an r.f. potential of 1000V p-p with a frequency of 2.86 MHz are shown in Figures 3.24 and 3.25 and the results of a computer analysis

Figure 3.24 Decay Curves for Argon Ions (m/e 40) Recorded using Experimental Method (i)

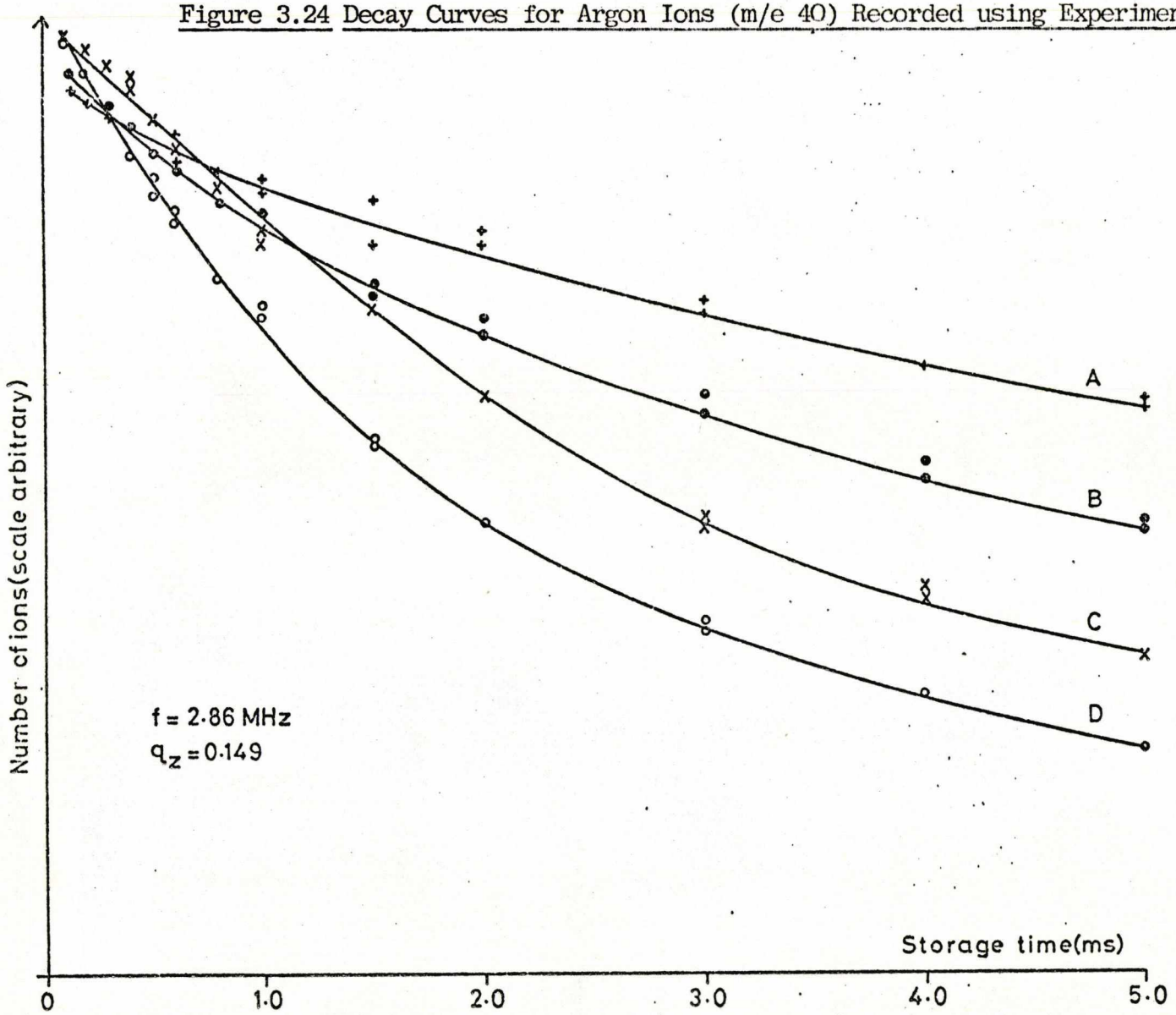

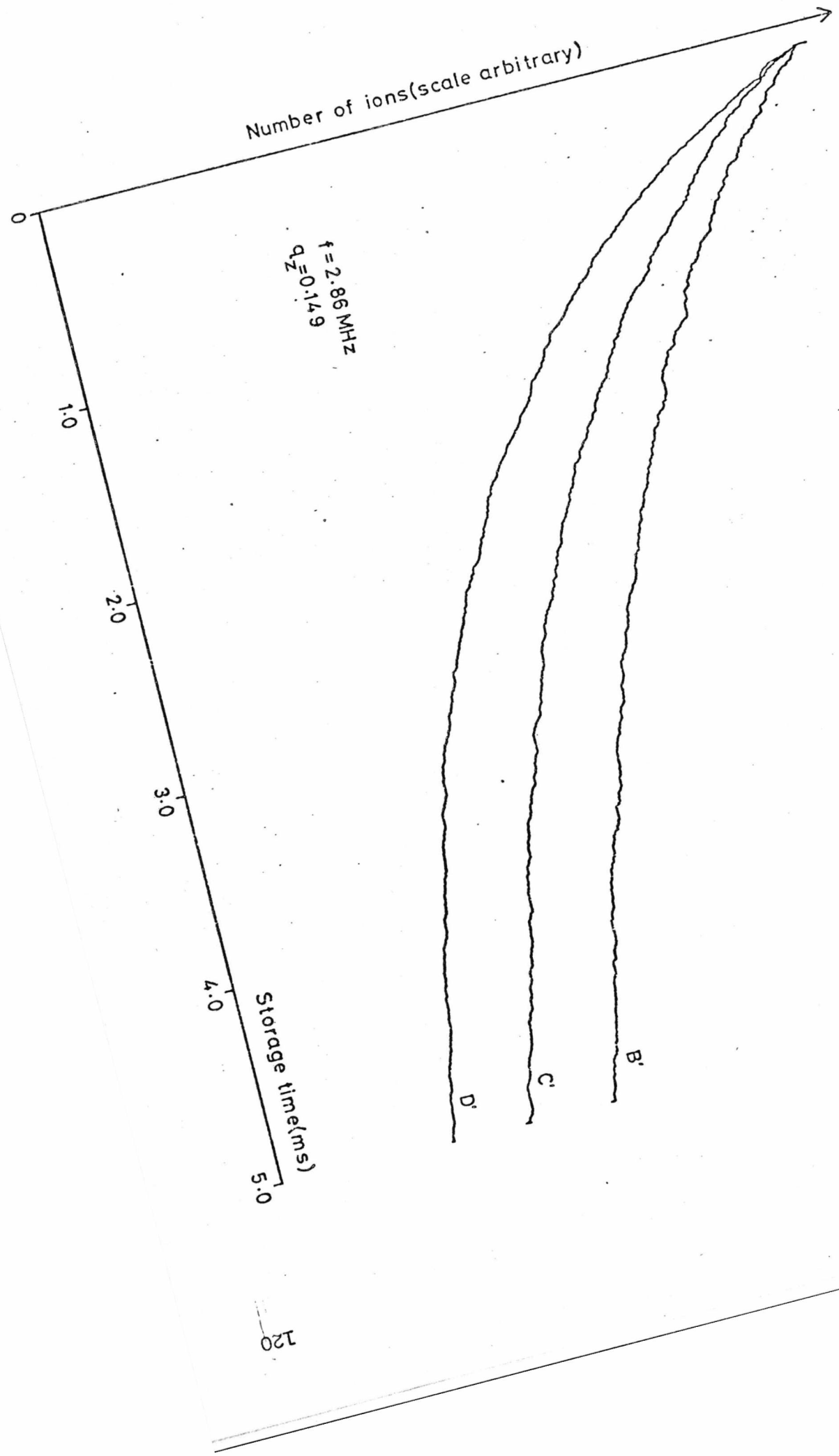

Figure 3.25 Decay Curves for Argon Ions (m/e 40) Recorded using Experimental Method (ii)

of these curves are presented in Tables 3.1 and 3.2 respectively. The two series were recorded under identical operating conditions but by different experimental methods ((i) and (ii) respectively as described in Section 3.4.2.3). The computer program employed for this study was based on the standard method of non-linear least-squares. The data was input in the form of the reciprocal of the number of ions (in terms of volts^{-1}) at a particular storage time in seconds, and the program calculated a value of k_2 in volts^{-1} sec^{-1} and $k_3 p$ in sec^{-1} and also the statistical error in these parameters. The value of k_2 was converted into units of cm^3 sec^{-1} by dividing by the conversion factor (1 volt $\equiv$ 5×10^5 ions cm^{-3}). The errors given for the values of k_2 do not include the error in the conversion factor which could be appreciable. Similarly, the errors given for the values of k_3 do not include possible contributions from pressure measurement errors. Some of the values of k_2 and k_3 listed in Tables 3.1 and 3.2 have a rather large uncertainty associated with them. The two principal contributing factors thought to be responsible for this were: firstly, due to r.f. and a.c. mains 'pick-up', there was a large amount of noise superimposed on the ion signal, this gave rise to random fluctuations in the output from the box car and consequently a distribution of values for N at a particular storage time, and secondly, the mathematical nature of the rate expression (equation (3.57)) was such that for any small uncertainty in the value of N there was a large uncertainty in the values of the rate constants, especially k_3.

From a comparison of Tables 3.1 and 3.2 it is clear that experiments performed using the two different experimental methods did not give identical values for the rate constants, but considering the great number of independent variables and the large inaccuracies involved in these experiments the agreement is excellent. Experimental method (ii) had a great advantage over method (i) in that a complete decay curve could be obtained in 100 seconds whereas with method (i) this took up to 15 minutes. Method (ii) was therefore less susceptible to errors arising from drift of

Table 3.1 Ion Loss Data for Ar^+ Ions at Various Pressures

(Experimental Method (i))

	Pressure* ($mol.cm^{-3}$)	k_2 ($cm^3\ sec^{-1}$)	k_3p (sec^{-1})	k_3 ($cm^3\ mol^{-1}\ sec^{-1}$)	q_z
A	3×10^{11}	$2.0 \pm 1.3\times10^{-4}$	26 ± 42	$9 \pm 14\times10^{-11}$	0.149
B	8.4×10^{11}	$3.0 \pm 0.9\times10^{-4}$	52 ± 26	$6.2 \pm 3.1\times10^{-11}$	
C	15.8×10^{11}	$5.4 \pm 0.7\times10^{-4}$	90 ± 14	$5.7 \pm 0.9\times10^{-11}$	
D	23.3×10^{11}	$9.9 \pm 0.6\times10^{-4}$	87 ± 15	$3.7 \pm 0.6\times10^{-11}$	

Table 3.2 Ion Loss Data for Ar^+ Ions at Various Pressures

(Experimental Method (ii))

	Pressure* ($mol.cm^{-3}$)	k_2 ($cm^3\ sec^{-1}$)	k_3p (sec^{-1})	k_3 ($cm^3\ mol^{-1}\ sec^{-1}$)	q_z
B'	8.4×10^{11}	$5.2 \pm 0.4\times10^{-4}$	72 ± 8	$8.6 \pm 1\times10^{-11}$	0.149
C'	15.8×10^{11}	$9.3 \pm 0.3\times10^{-4}$	72 ± 8	$4.6 \pm 0.5\times10^{-11}$	
D'	23.3×10^{11}	$12.1 \pm 0.8\times10^{-4}$	129 ± 10	$5.6 \pm 0.4\times10^{-11}$	

* The pressure in Torr has been converted to the equivalent molecular density at 293^0K using the conversion factor 1 Torr $\equiv 3.3\times10^{16}\ mol.cm^3$

the r.f. potential and long term pressure variations. However, it was necessary with the latter method to plot more than one decay curve for a particular set of operating conditions in order to obtain an estimate of the uncertainty in N for a particular storage time.

The values for k_3 given in Tables 3.1 and 3.2 are in reasonable agreement with other literature values for this parameter[64,121], but it is not totally meaningful to make direct comparisons of this kind since these values were obtained using different sets of operating conditions and it has not as yet been established whether the values of k_3, or k_2, are dependent on the operating conditions. From the data shown in Table 3.1 it appears that the value of k_3 decreased as the operating pressure was increased, but the errors in k_3 were so large that it was not possible to determine from this data alone whether this was a real effect. The same trend was not evident in the data shown in Table 3.2. A variation of this kind would not be expected from theoretical considerations, over such a small pressure range, if the only neutral species present were argon atoms. However, for these studies argon gas was introduced into the vacuum chamber surrounding the Quistor via the calibrated inlet system such that the argon pressure was in the range 1×10^{-5} to 1×10^{-4} Torr, the actual value depending on the particular experiment. The background pressure in the vacuum chamber was *ca.* 1×10^{-6} Torr as measured on the ion gauge, so the 'atmosphere' within which the ion loss processes were studied did not consist solely of argon atoms. The background gases comprised mainly nitrogen, oxygen and water together with small amounts of hydrogen and carbon dioxide. The relative proportions of these gases varied over a wide range and depended on which gases had been introduced into the vacuum chamber for other experiments performed prior to these studies. All of the above mentioned gases undergo exothermic charge transfer or ion molecule reactions with Ar^+ ions as follows:

Reaction	Rate constant[140] ($cm^3\ mol^{-1}\ sec^{-1}$)	
$Ar^+ + N_2 \longrightarrow N_2^+ + Ar$	6.6×10^{-11}	(a)
$Ar^+ + O_2 \longrightarrow O_2^+ + Ar$	1.1×10^{-10}	(b)
$Ar^+ + H_2O \longrightarrow H_2O^+ + Ar$ $\longrightarrow ArH^+ + OH\cdot$	1.4×10^{-9}	(c)
$Ar^+ + H_2 \longrightarrow ArH^+ + H\cdot$	1.7×10^{-9}	(d)
$Ar^+ + CO_2 \longrightarrow CO_2^+ + Ar$	7×10^{-10}	(e)

Although the partial pressure of these gases was two or three orders of magnitude lower than the argon pressure, the rates of some of the possible ion-molecule reactions are so high that the sum $\sum_i k_i p_i$ where p_i is the partial pressure of the i*th* background gas and k_i the rate constant for its reaction with Ar^+, may make a significant contribution to the value of $k_3 p$. An estimate of the extent to which ion-molecule reactions with the background gases were contributing to the loss of argon ions was obtained from the following considerations. If k_3' is the rate constant for ion loss due to interactions between argon ions and argon molecules alone and $\sum_i p_i$ is the background pressure then

$$k_3(p + \sum_i p_i) = k_3' p + \sum_i k_i p_i \tag{3.58}$$

making the assumption that $p >> \sum_i p_i$ and dividing through by p

$$k_3 = k_3' + \frac{\sum_i k_i p_i}{p} \tag{3.59}$$

From equation (3.59) it appears that a plot of k_3 against 1/p should be a

straight line with an intercept at k_3'. The results of such an analysis on the data presented in Table 3.1 is shown in Figure 3.26 along with the results of a similar analysis on an additional set of data shown in Table 3.3. This latter set of data was recorded under identical conditions to those employed to obtain the decay curves shown in Figures 3.24 and 3.25 using method (ii) but over a wider pressure range. The errors in two of the values of k_3 shown in Table 3.1 are so large that no positive conclusions could be derived from this set of data plotted in Figure 3.26. However, the errors in the data shown in Table 3.3 are very much smaller and it is clear from Figure 3.26 that there is a definite linear relationship between k_3 and $1/p$ for this set of data. Values for k_3' of 1×10^{-11} cm^3 mol^{-1} sec^{-1} and for $\Sigma\, k_i p_i$ of 33 sec^{-1} were obtained from a straight line drawn through these points using a least squares method. From the value of $\sum_i k_i p_i$ it is evident that up to a pressure of *ca.* 10^{-4} Torr ($\simeq 3.3\times10^{-10}$ mol cm^{-3}) the major contribution to the value of $k_3 p$ was ion losses due to ion-molecule and charge transfer reactions of Ar^+ ions with molecules of the backround gases, this probably accounts for the variation in k_3 with the pressure of argon. Due to the large errors involved in these experiments and the presence of backround gases it was impossible to establish whether k_3' was independent of argon pressure with certainty or investigate whether this parameter was dependent on other operating conditions.

From Tables 3.1, 3.2 and 3.3 it appears that the value of k_2 increased as the argon pressure was increased. It is possible that this effect was in some way caused by the presence of ions formed from the backround gases present in the vacuum chamber, but the total number of these ions compared to the number of Ar^+ ions was so small that this was thought to be unlikely. When argon gas is ionised by electrons with an energy of 50 eV, Ar^{2+} ions are formed (and also Ar^{3+} but since these ions were not observed during this study they will not be considered further) in addition to Ar^+ ions. Under the conditions employed to perform these

Figure 3.26 Plot of k_3 against 1/p

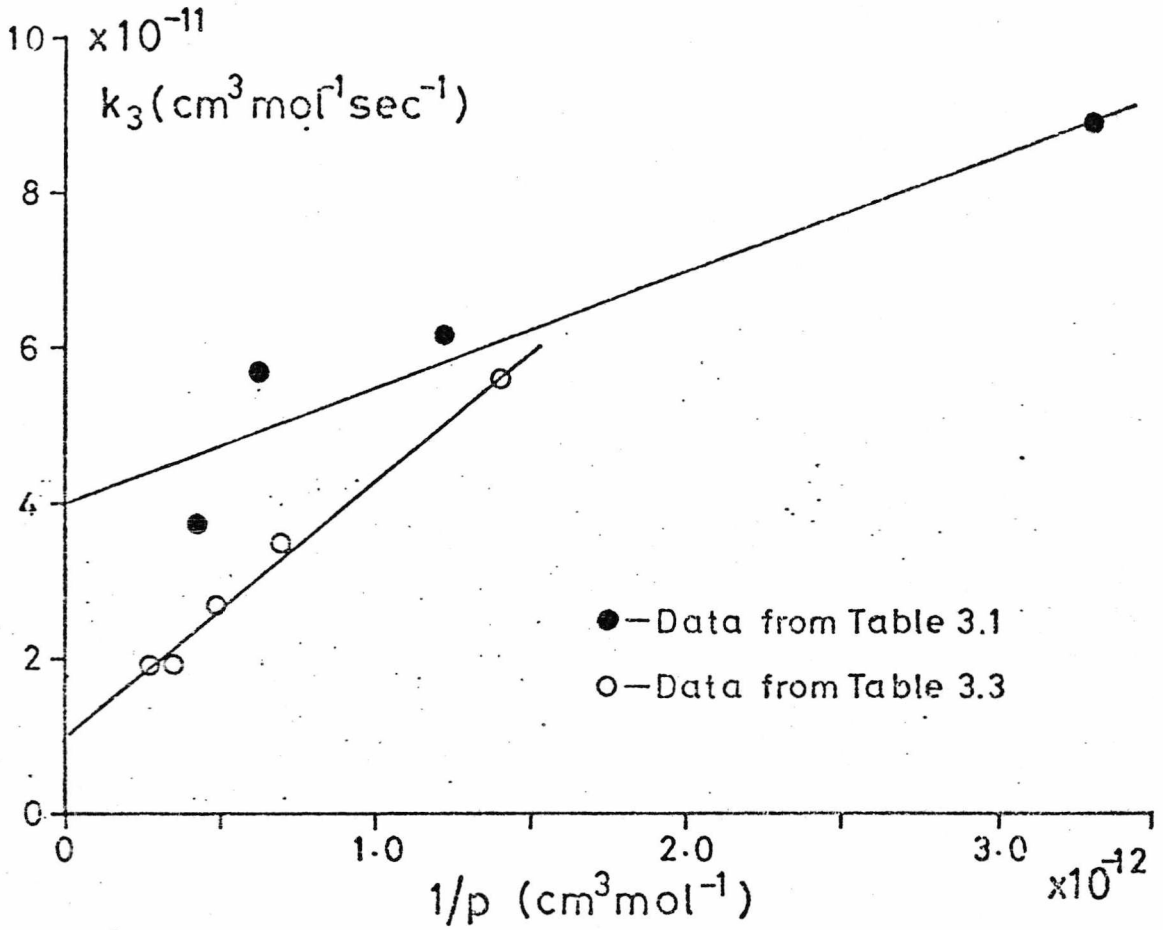

Table 3.3 Additional Ion Loss Data for Ar^+ Ions at Various Pressures

(Experimental Method (ii))

Pressure* ($mol.cm^{-3}$)	k_2 ($cm^3\ sec^{-1}$)	k_3p (sec^{-1})	k_3 ($cm^3\ mol^{-1}\ sec^{-1}$)	q_z
7.1×10^{11}	$4.7\pm0.8\times10^{-4}$	40±19	$5.6\pm2.6\times10^{-11}$	
14.2×10^{11}	$7.0\pm0.7\times10^{-4}$	50±13	$3.5\pm0.9\times10^{-11}$	
21.2×10^{11}	$9.6\pm0.7\times10^{-4}$	58±12	$2.7\pm0.6\times10^{-11}$	0.149
28.3×10^{11}	$13.0\pm0.5\times10^{-4}$	54±8	$1.9\pm0.3\times10^{-11}$	
35.4×10^{11}	$18.6\pm0.7\times10^{-4}$	68±8	$1.9\pm0.2\times10^{-11}$	

* The pressure in Torr has been converted to the equivalent molecular density at 293^0K using the conversion factor 1 Torr ≡ 3.3×10^{16}mol.cm^3

experiments both of these ions were stable simultaneously and at a pressure of 2×10^{-5} Torr at 100 μs storage the ratio Ar^{2+}/Ar^{+} was *ca.* 0.1. This ratio was not monitored throughout these experiments but Todd *et al*[141] have shown that its value increases as the argon pressure is increased. Since the number of Ar^{+} ions at zero storage was kept approximately constant as the pressure was increased, so the number of Ar^{2+} ions increased with pressure. This would cause an increase in space charge which will modify the trapping field and result in the loss of ions from the trap. This effect could have produced the observed increase in k_2 with pressure.

No further experiments were performed on the variation of k_2 and k_3 with pressure because effects arising due to the presence of backround gases and ions formed from them could not be eliminated. However, this study demonstrates that the presence of backround gases can give rise to a significant increase in the rate of ion loss.

3.4.2.4(ii) The Dependence of k_2 and k_3 on q_z

For this investigation a series of decay curves was obtained, each curve being recorded at a different value of the r.f. potential. In order to fix as many other variables as possible, the pressure was held constant and the value of N_o was fixed by adjusting the ion creation pulse width using the same method as was described in Section 3.4.2.4(i). Argon was introduced into the vacuum chamber at a pressure of 2.4×10^{-5} Torr ($\equiv 8.4\times10^{11}$ mol.cm^3) and the decay curves were obtained using experimental method (i) for two different operating frequencies: 2.86 MHz, and 0.796 MHz. The results of the computer analysis of this data are shown in Tables 3.4 and 3.5 respectively. Due to excessive noise superimposed on the ion signal caused by r.f. 'pick-up', the statistical errors in the values of k_2 and k_3 were over 100% when the Quistor was operated above a potential of 1000V p-p at 2.86 MHz and above 350V at 0.796 MHz. This set an upper limit to the range of q_z over which these experiments could be

Table 3.4 Ion Loss Data for Ar^+ Ions at Various Values of q_z.

Operating Frequency 2.86 MHz

Pressure* ($mol.cm^{-3}$)	k_2 ($cm^3\ sec^{-1}$)	k_3p (sec^{-1})	k_3 ($cm^3\ mol^{-1}\ sec^{-1}$)	q_z
$8.4\ 10^{11}$	$11.1 \pm 3.5\times10^{-4}$	120 ± 28	$14.3 \pm 3.3\times10^{-11}$	0.111
	$10.2 \pm 2.1\times10^{-4}$	83 ± 34	$9.8 \pm 4.0\times10^{-11}$	0.120
	$3.1 \pm 0.5\times10^{-4}$	53 ± 14	$6.3 \pm 1.7\times10^{-11}$	0.149

Table 3.5 Ion Loss Data for Ar^+ Ions at Various Values of q_z.

Operating Frequency 0.796 MHz

Pressure* ($mol.cm^{-3}$)	k_2 ($cm^3\ sec^{-1}$)	k_3p (sec^{-1})	k_3 ($cm^3\ mol^{-1}\ sec^{-1}$)	q_z
8.4×10^{11}	$9.0 \pm 6.0\times10^{-4}$	183 ± 40	$22 \pm 5\times10^{-11}$	0.424
	$7.9 \pm 1.7\times10^{-4}$	70 ± 41	$8.3 \pm 5\times10^{-11}$	0.540
	$3.9 \pm 0.6\times10^{-4}$	54 ± 38	$6.4 \pm 5\times10^{-11}$	0.656

* The pressure in Torr has been converted to the equivalent molecular density at 293^0K using the conversion factor 1 Torr $\equiv 3.3\times10^{16} mol.cm^3$

performed and a lower limit was set by the shifted stability boundaries at low q_z.

Although the errors in the values of k_2 and k_3 shown in Tables 3.4 and 3.5 are substantial, there appears to be a general decrease in the value of both of these parameters with increasing values of q_z over the range studied. In order to gain an insight into how the rate of ion loss varied over a wider range of q_z, a number of decay curves were obtained, using experimental method (ii), for values of q_z in the range 0.43 to 0.92, while operating at a frequency of 0.796 MHz and a pressure of 4×10^{-5} Torr (argon). These decay curves are presented in the form of a three-dimensional "storage surface" in Figure 3.27. The decay curves shown on this surface were obtained by drawing a "best curved line" through the experimental curves. The decay curves represented by dashed lines were not obtained from experimental data but were estimated for completeness. This diagram shows clearly how, for a fixed value of N_o, the rate of ion loss varies as a function of q_z. Although the values of k_2 and k_3 were not calculated from this data, it was possible to deduce from Figure 3.27 and the results shown in Tables 3.4 and 3.5 that the values of these parameters gradually decrease with increasing values of q_z and minimise at a q_z of *ca.* 0.65, this corresponding to the maximum of a section taken through the "storage surface" perpendicular to the storage time axis. Beyond this point their values increase and become very large as the value of q_z approaches the stability limit. The general shape of the storage surface may be explained in the same terms as those for the total pressure curves discussed in Section 3.4.1.3. Indeed, the shaded section through the "storage surface" in Figure 3.27 is equivalent to a total pressure curve recorded at 5 ms storage time and is similar in shape to those curves shown in Figure 3.15.

Ion loss processes and the dependence of these processes on operating conditions are extremely difficult to discuss in theoretical terms. The effect of elastic collisions on a population of charged particles stored in a Quistor have been described theoretically by Dawson[142] using the

Figure 3.27 Three-Dimensional "Storage Surface" for Argon Ions (m/e 40)

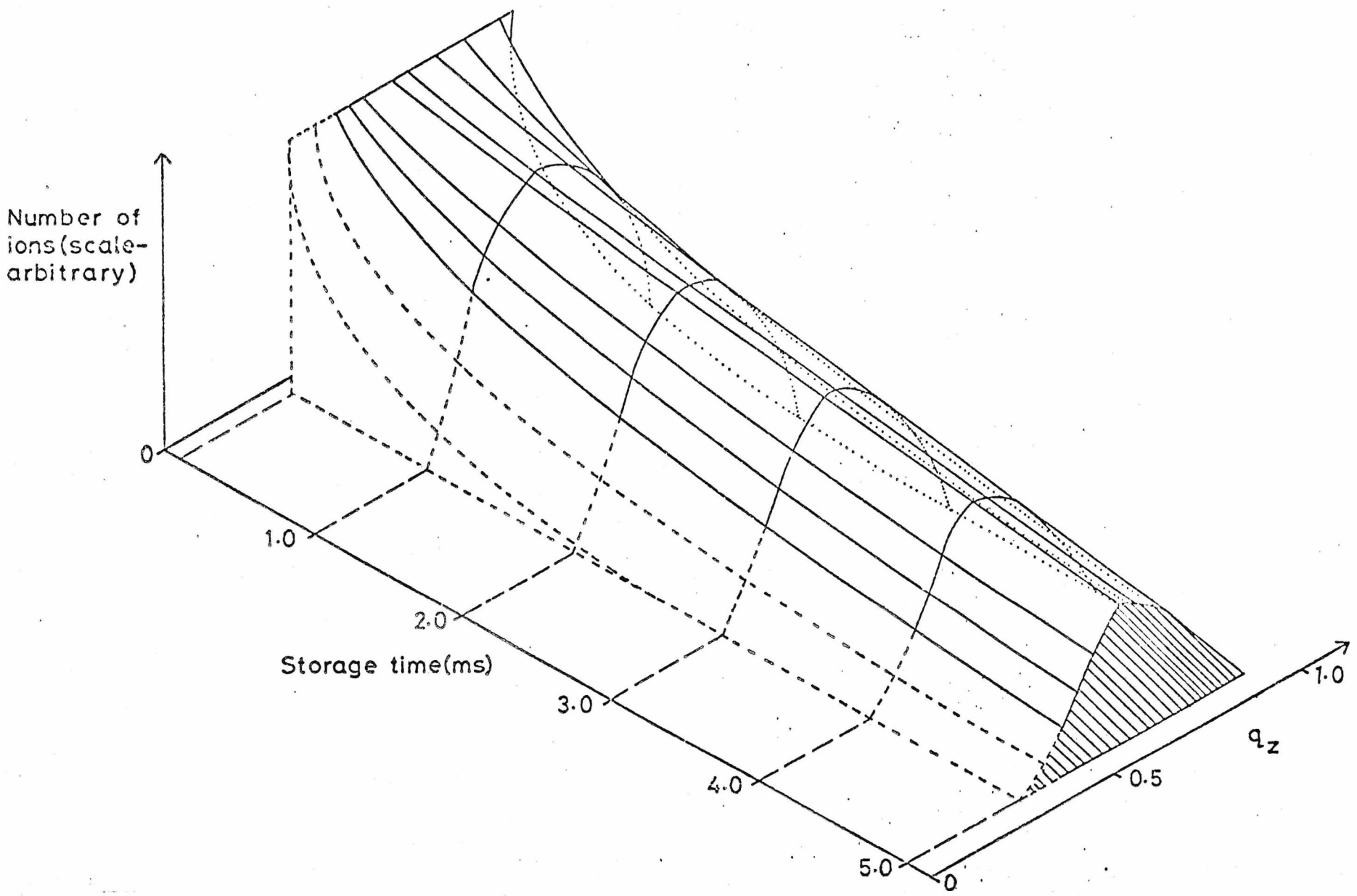

method of phase space dynamics and also by André[143] who employed a statistical method. However, neither of these studies considered ion-ion interactions or space charge.

3.4.2.5 The Relative Importance of the Mechanisms of Ion Loss

The rate data for ion loss presented in Tables 3.1, 3.2 and 3.3 was analysed further in an effort to discover how the relative importance of the two mechanisms of ion loss changed as a function of pressure and ion density. The rate of ion loss due to ion-ion and ion-molecule interactions was estimated by calculating values for k_2N^2 and $k_3'Np$ respectively and the relative importance of the two ion loss mechanisms was determined by evaluating $k_2N/k_3'p(\equiv k_2N^2/k_3'Np)$. The value of k_3' used in this investigation was that determined from Figure 3.26 (1×10^{-11} cm^3 mol^{-1} sec^{-1}).

The values of $k_2N/k_3'p$, calculated for each of the values of k_2 presented in Tables 3.1, 3.2 and 3.3, are shown in Figure 3.28 plotted as a function of pressure (in terms of molecular density). The value of N was chosen arbitrarily as 10^5 ions cm^{-3} and it is clear that under these conditions ion loss by ion-ion interactions is the dominant ion loss process. It was impossible to draw any positive conclusions about the nature of the relationship between $k_2N/k_3'p$ and pressure from Figure 3.28 because of the scatter in the experimental points and the large uncertainties associated with them. However, it appears that over the pressure range studied the value of $k_2N/k_3'p$ changed by less than a factor of two.

The variation in the rate of ion loss with ion density is shown in Figure 3.29 for the case where $k_2 = 5.4\times10^{-4}$ cm^3 sec^{-1} and $p = 5\times10^{-5}$ Torr ($\equiv15.8\times10^{11}$ $mol.cm^{-3}$) from Table 3.1. The rates of ion loss for the two mechanisms are in this case equal at an ion density of *ca.* 2×10^4 ions cm^{-3} and at higher ion densities ion-ion scattering is the more dominant effect. From Figure 3.29 it is apparent that at an ion density equal to the value of N_{max}, the space charge-limited ion density calculated from equation

Figure 3.28 Plot of $k_2N/k_3'p$ against Pressure

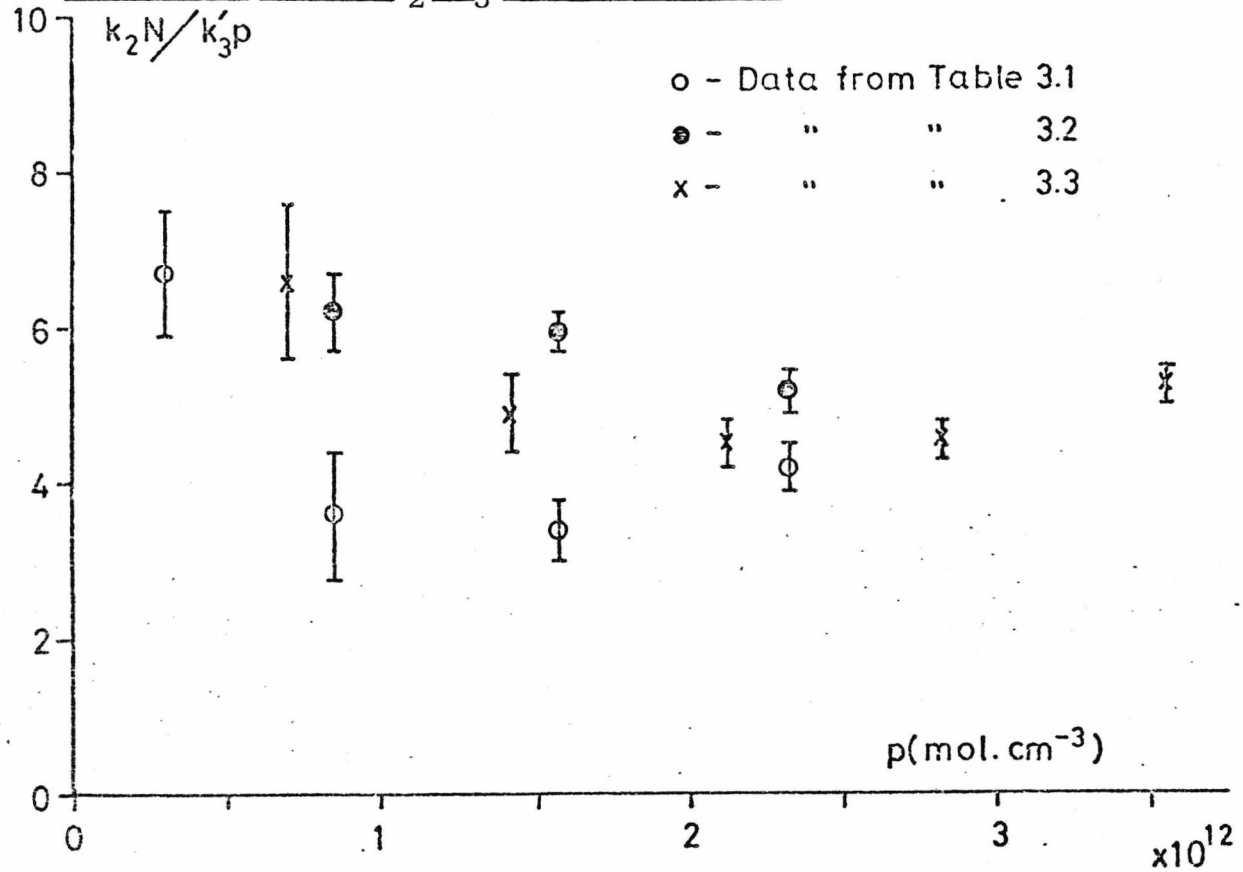

Figure 3.29 Graph showing the Variation of the Rate of Ion Loss with Ion Density

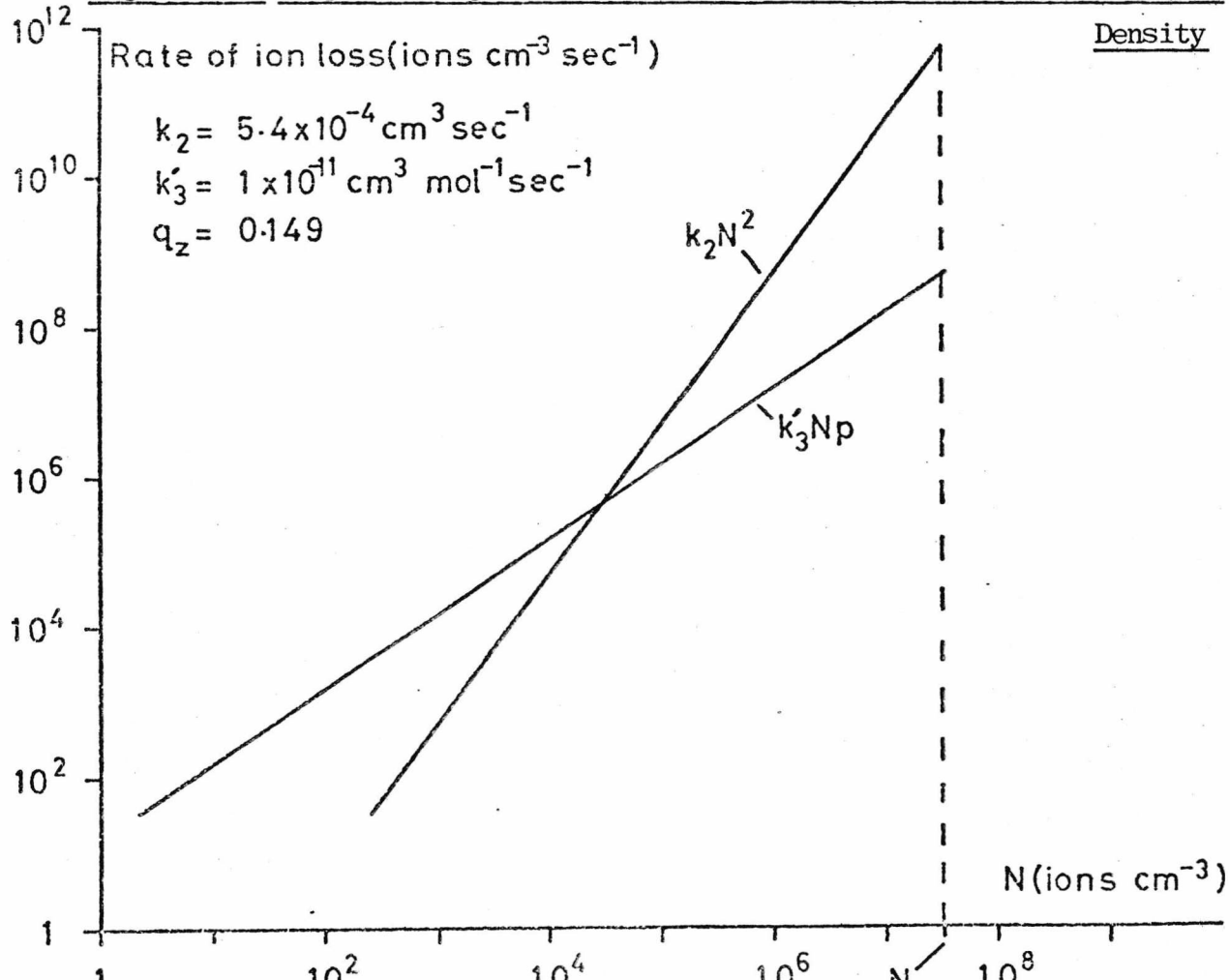

(3.45), the rate of ion loss due to ion-ion interactions is 1000 times faster than that due to ion-molecule interactions.

In this section on ion loss processes the values of the ion loss rate constants k_2 and k_3 determined over a range of operating conditions were found to be dependent on pressure and the value of q_z. The dependence on pressure was unexpected and although a plausible explanation was given for the variation of k_3 with this parameter, a thorough investigation into these effects was precluded due to limitations of the experimental system.

3.4.3 The Ion Ejection Process

In using the Quistor as an ion storage source for a mass spectrometer, whether for the determination of the rates of ion-molecule reactions or for chemical ionisation, it is essential that the amplitude of the ejection pulse is sufficient to remove all of the ions from the trap. Failure to do this will result in erroneous values for rate constants and a general lack of sensitivity.

In order to investigate how the amplitude of the ejection pulse required to *(a)* just eject some ions and *(b)* to remove all of the ions from the Quistor depended on the value of q_z, two types of experiment were performed. In the first, Ne^+ ions were stored for a certain time before being ejected by applying a negative going ('suck-out') pulse to the end-cap nearest to the mass filter which was set to transmit this species. A series of ion intensity *vs.* r.f. potential plots was obtained with the amplitude of the ejection pulse maintained at a series of fixed levels, using the same method as was employed to record the total pressure curves described in Section 3.4.1.1. In the second type of experiment, Ar^+, Ar^{2+} or Ne^+ ions were stored and then mass analysed with ejection being achieved by a double-pulsing technique the pulse timing sequence of which is illustrated in Figure 3.30. The basic configuration of the

Figure 3.30 Pulse Timing Sequence for Double-Pulsing Technique

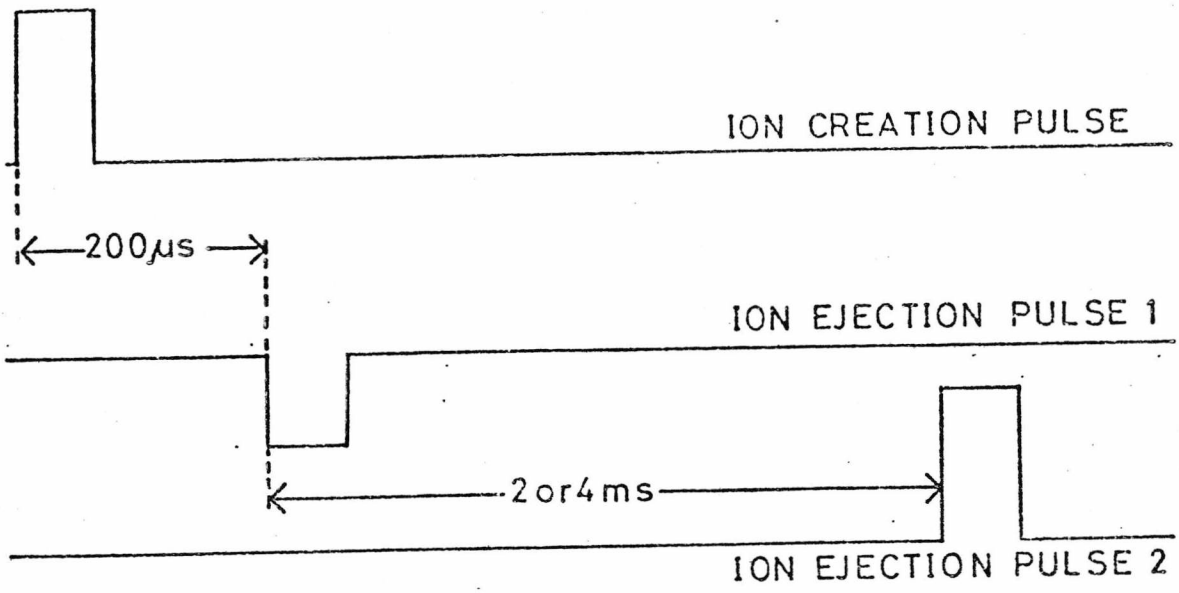

experimental system for these experiments was identical to that illustrated in Figure 3.13 except that a second ion ejection pulse generator was incorporated such that ejection pulses could be applied to either of the end-caps. By operating in this manner a first negative-going pulse of variable amplitude could be applied to the end-cap nearest to the mass filter to 'suck-out' the ions. The effectiveness of this was then monitored by applying a second large (+100V) positive pulse to the other end-cap to see whether further ions could be detected leaving the trap. The observation therefore comprised setting the r.f. potential to a given level and observing the ion signal trace on the oscilloscope which simultaneously displayed the two ejection pulses. The magnitude of the first pulse was then slowly increased until the signal co-incident with the second pulse just disappeared, from which it was concluded that the pulse height at this point was just sufficient to eject all the ions.

The conditions employed in the experiments were as follows:

Sample pressure (neon or argon)	*ca.* 2×10^{-5} Torr
Operating frequency	2.8 or 2.88 MHz
ICPW	20 μs
IEPW's	20 μs
Storage time to first ejection	200 μs
Interval between ejection pulses	2 or 4 ms
Range of V_o (zero to peak)	0 - 1500V

The results from the first experiment, on the threshold for ion ejection took the form of the series of traces shown in Figure 3.31, in which the magnitude of the detected signal is displayed as a function of V_o for different ejection pulse heights. Evidently there is a range of V_o extending from zero to *ca.* 200V where apparently ions are not stored. This is the same type of effect as was observed with the total pressure curves described in Section 3.4.1.1, and has been attributed to the shift in the stability boundaries due to the effects of space charge. At the onset of stability the signals rise steeply, the greatest rate of increase being observed for the smallest ejection pulse height. After maximising, the signals fall sharply and then finally tail to zero at a V_o of *ca.* 1500V, corresponding to the stability limit of $q_z \approx 0.91$. One interesting feature is that the traces change shape dramatically in the direction of reduced intensity with increasing ejection pulse height, an effect which could be caused by defocusing of the ion beam in the region between the Quistor and the mass filter. The value of V_o at which the sharp decrease in ion intensity after the maximum occurred was determined from oscilloscope observations and the results are shown in Table 3.6. The values of q_z and $\bar{D}_z$ shown in Table 3.6 were calculated using equations (3.16) and (3.35) respectively.

Figure 3.31 Total Pressure plots for Ne^+ Ions at Different Ejection Pulse Heights

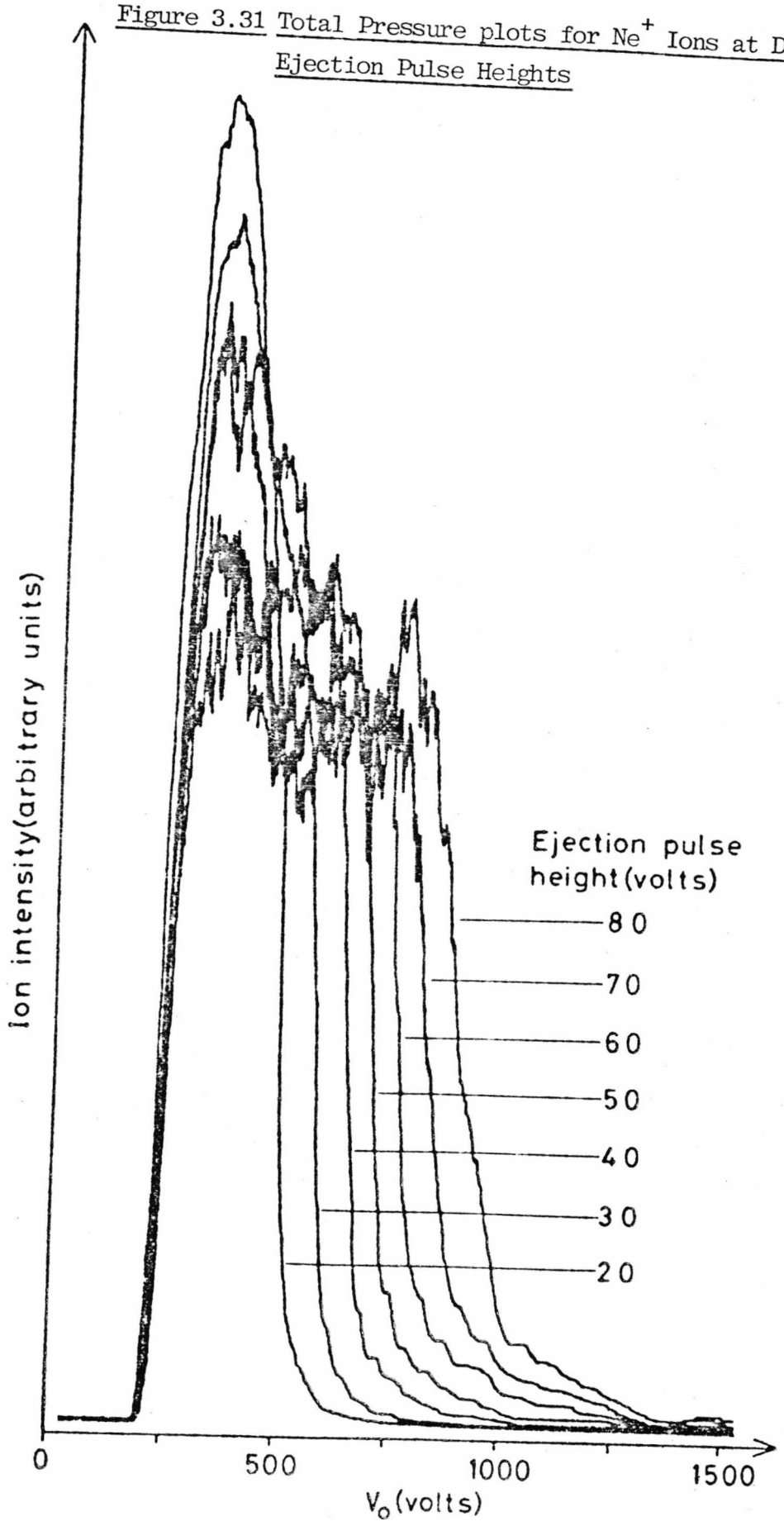

Table 3.6 Threshold Ejection of Ne^+ Ions

Ejection Pulse Height (EPH) (Volts)	V_o (Volts)	q_z	$\bar{D}_z$ (Volts)	EPH/$\bar{D}_z$
10	400	0.24	11.85	0.84
20	500	0.30	18.51	1.08
30	600	0.36	26.65	1.12
40	675	0.40	33.73	1.18
60	825	0.49	50.39	1.19
80	950	0.56	66.82	1.20

Table 3.7 Results of Double Pulsing Experiment for Ar^+ Ions

First Ejection Pulse Height (Volts) (a)		V_o (Volts)	q_z	$\bar{D}_z$ (Volts)	EPH/$\bar{D}_z$
14(b)	12(c)	400	0.116	5.80	2.2 ± 0.3
19.5	18	450	0.131	7.34	2.6
24	24	500	0.145	9.06	2.6
32	32	550	0.160	10.97	2.9
37	39	600	0.174	13.05	2.9
48	44	650	0.189	15.32	3.0
53	52	700	0.203	17.76	3.0
64	60	750	0.218	20.39	3.0
66	68	800	0.232	23.20	2.9

Note (a) estimated precision of observation ±2V

(b) second pulse at 2 ms delay

(c) second pulse at 4 ms delay

Table 3.8 Results of Double Pulsing Experiment for Ar^{2+} and Ne^{+} Ions (m/e 20)

First Ejection Pulse Height (Volts) (a)		V_o (Volts)	q_z	$\bar{D}_z$ (Volts)	EPH/$\bar{D}_z$	
Ne^{+}(b)	Ar^{2+}(b)				Ne^{+}	Ar^{2+}
9	8	300	0.178	6.66	1.4	1.2
15.5	13	350	0.207	9.07	1.7	1.4
24	17.5	400	0.237	11.85	2.0	1.5
30	24	450	0.267	14.99	2.0	1.6
36	31	500	0.296	18.51	2.0	1.7
-	36	550	0.326	22.40	-	1.6
-	45	600	0.355	26.65	-	1.7
-	50	650	0.385	31.28	-	1.6
-	56	700	0.415	36.27	-	1.5

Note (a) estimated precision of observation ±2V

(b) second pulse 2 ms delay

The results of four sets of experiments on the total ejection of ions for m/e 40 (Ar^+) and m/e 20 (Ar^{2+} and Ne^+) are presented in Tables 3.7 and 3.8 respectively. Two sets of data for Ar^+ are included to demonstrate that changing the interval between the two ejection pulses from 2 ms to 4 ms had little effect on the observations. This data is presented in graphical form, ejection pulse height *vs.* q_z, in Figure 3.32. From this it appears to be approximately twice as easy to remove all the ions with m/e 20 as with m/e 40.

It is convenient to discuss these results in terms of the pseudo-potential well model described in Section 3.2.1. From Figure 3.31 and and Table 3.6 it is apparent that even at minimal ejection pulse heights some ions are ejected from the trap and at pulse heights approximating to the depth of the potential well $\overline{D}_z$, there is a rapid increase in the efficiency of ejection. The data in Tables 3.7 and 3.8 suggests that in order to achieve total ejection of ions a pulse height some two or three times the value of $\overline{D}_z$ may be required. The latter observation may not in fact represent the real situation since in addition to the force on the ion cloud exerted by presence of the ejection pulse there are also the forces associated with the space-charge within the stored ion cloud which may also contribute to the ion ejection process. This may be quantified as follows. The intercepts on the q_z axis of the graphs in Figure 3.32 represent the shifts in the stability boundaries attributed in Section 3.4.1.2 to the presence of an additional defocusing potential induced by the space charge of the ion cloud. The value of this potential may be estimated by determining the shift in the a_z coordinate, Δa_z, at the value of q_z corresponding to the stability limit as determined by comparison with the theoretical stability diagram shown in Figure 3.5, and then using equation (3.15) re-written in the form

$$\Delta a_z = \frac{8e\ U'}{m\ z_o^2\ \Omega^2} \qquad (3.60)$$

Figure 3.32 Plots of Pulse Height for Total Ion Ejection *vs* q_z for Ar^+, Ne^+ and Ar^{2+} Ions

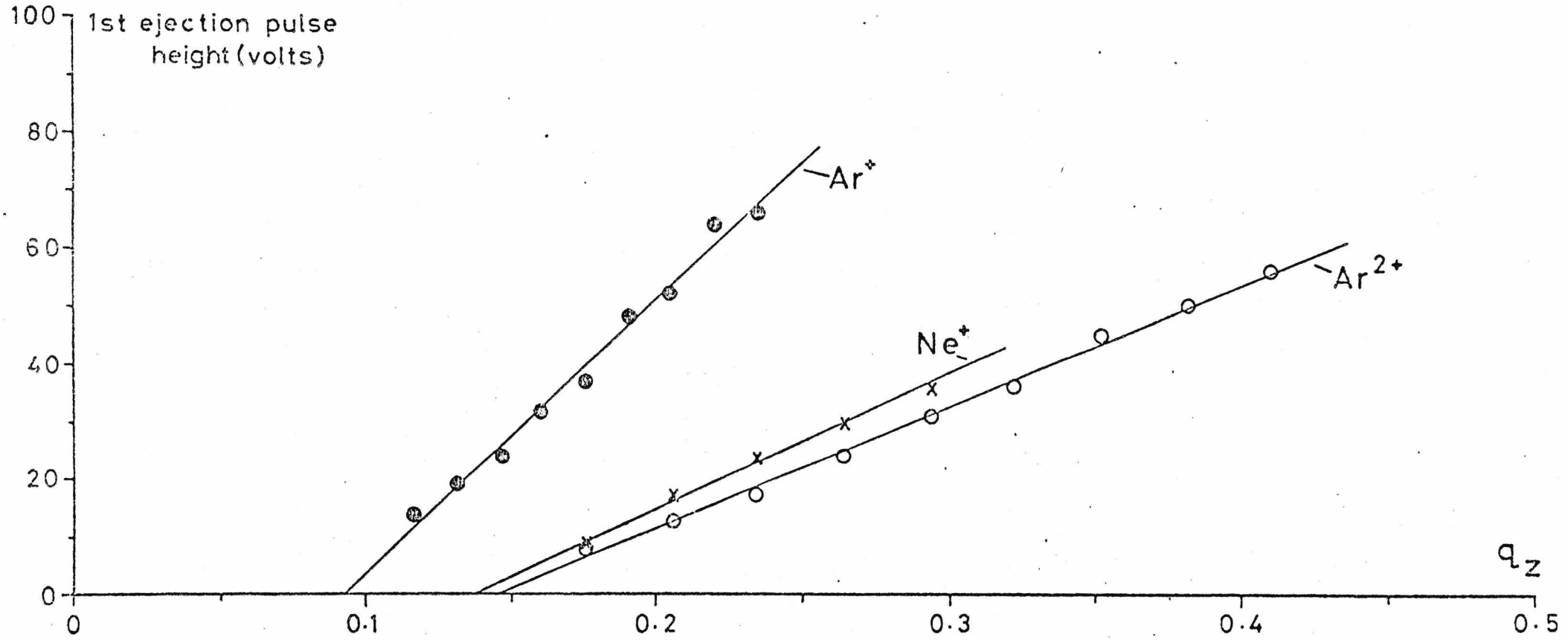

where U' is the additional potential apparently established between the end-cap electrodes and the centre of the trap. The results of these calculations along with the values of $\overline{D}_z$ at the stability limit are shown in Table 3.9.

Table 3.9 Comparison of Destabilising Potential with $\overline{D}_z$

Stability Limit q_z		Δa_z	U'(Volts)	$\overline{D}_z$(Volts)
Ar^+	0.093	0.006	5.1	3.5
Ar^{2+}	0.146	0.012	5.1	4.5
Ne^+	0.136	0.011	3.7	3.9

This fairly close agreement between the observed values of U' and the calculated depths of the pseudo-potential well lends some support to this type of approach, the assumption being that when the potential equivalent to the charge density of the stored ions equals or exceeds the well depth no ions are stored. As a result it may be envisaged that the actual ejection pulse height is effectively increased by a value equivalent to U'; in other words the space-charge repulsion within the trapped ion cloud contributes to the ejection process.

The somewhat surprisingly large pulse heights required for total ion ejection may be explained in terms of the following simple model. Assuming that ions oscillating along the z axis do so within a parabolic potential well of depth $\overline{D}_z$ situated between the end caps as in Figure 3.33, then on subsequent application of a negative going pulse of $-W = \overline{D}_z$ the form of the well is changed to that shown in Curve 1. From this it is evident that a well, albeit of reduced depth, remains which could cause the retention of those ions which initially had low amplitudes of oscilla-

Figure 3.33 Representation of the Potential along the z-Axis of the Quistor when a Pulse of Magnitude -W is Applied to One End-Cap Electrode

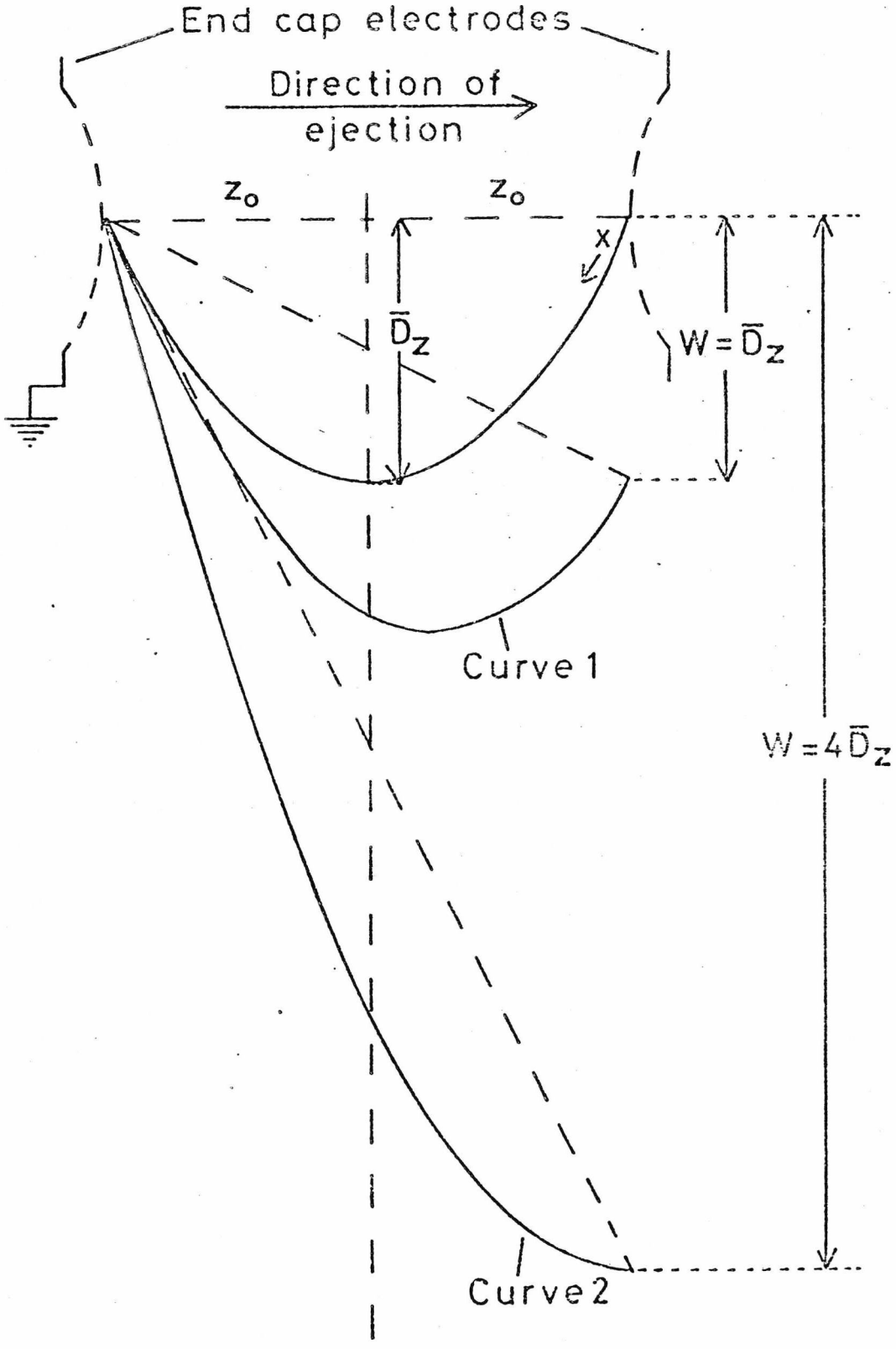

tion around the centre. In fact, for total ejection the most difficult ion to remove should be one at point X i.e. experiencing the maximum restoring force directed away from the direction of ejection. The force experienced by an ion of mass m at a point z is from equations (3.33) and (3.34)

$$m \frac{d^2z}{dt^2} = - e \cdot \frac{d\bar{D}_z}{dz}$$

$$= - \frac{2e \bar{D}_z \cdot z}{z_o^2}$$

At the inner surface of the end-cap ($z = z_o$) it is assumed that when the ejection field is applied for such an ion to just be ejected the force is balanced by an equal and opposite force $eW/2z_o$ so that

$$\frac{eW}{2z_o} = \frac{2e \bar{D}_z \cdot z_o}{z_o^2}$$

therefore $$W = 4\bar{D}_z$$

This situation is represented by Curve 2 in Figure 3.33 and shows that the application of an ejection potential of the above magnitude causes the minimum of the well to co-incide with the end-cap electrode. This conclusion can also be reached by simple algebraic considerations of the equations of a parabola combined with a straight line. From this model it appears that for total ion ejection the amplitude of the ejection pulse should be equal to four times the value of $\bar{D}_z$ whereas experimentally observed ratios vary from 2.2 to 3.0 for m/e 40, and 1.2 to 2.0 for m/e 20.

There are a number of possible explanations for the discrepancy between the observed and expected ratios. The effect of space-charge on the ion ejection process has already been mentioned. An equivalent approach is to envisage the effective depth of the well available for trapping being

reduced by the space charge potential. Since, for a given value of q_z, the well depth $\bar{D}_z$ is proportional to m/e and assuming that at the same q_z the charge density of trapped ions is of the same order regardless of the species, the destabilising influence caused by the space-charge will be relatively greater at lower m/e so that the observed ratios (EPH/D_z) will tend to lower values particularly at low values of $\bar{D}_z$.

A further argument relates to the possible limit placed upon the effective depth of the pseudo-potential well in the z-direction through scattering into the r-direction. Major and Dehmelt[144] have argued that, since the well depth in the r-direction, $\bar{D}_r$, is half that in the z-direction, (equation (3.37)), then collisional energy interchange will place a limit on the maximum kinetic energy of the stored ions equal to $\bar{D}_r$. This is equivalent to saying that the ion motion in the z direction corresponds to that in a well of reduced depth equal to $\bar{D}_z/2$.

In conclusion, these experiments have demonstrated that there is a linear relationship between the amplitude of the ejection pulse required for total ion ejection and the value of q_z associated with these ions. This relationship is m/e dependent and trends indicate that the $EPH/\bar{D}_z$ ratio increases with m/e.

3.5 Conclusion

Besides adding to the body of knowledge on the physical characteristics of the Quistor, the results of the experiments described in this chapter have established some of the limitations to its use as an ion storage source and have also shown the conditions under which it must be operated for optimum performance. The most important results may be summarised as follows:

(i) There is a definite limit to the range of m/e values of ions which may be stored simultaneously in the Quistor, this being primarily dependent on the value of the applied r.f. potential and r.f. frequency.

(ii) There appears to be no great advantage in operating at any other value of a_z except $a_z = 0$.

(iii) Since storage efficiency is a function of q_z, ions of different m/e values stored simultaneously will not be stored with the same efficiency which in effect amounts to an inherent mass discrimination.

(iv) Due to non-linear resonances points of instability occur within the stability boundaries.

(v) The optimum point of operation appears to be at a q_z of *ca.* 0.7.

(vi) The presence of backround gases can apparently have a significant effect on the rate of ion loss.

(vii) In order to eject all of the ions from the Quistor the ejection pulse height must be between 3 and 4 times the depth of the potential well, $\overline{D}_z$, the actual value being dependent on the m/e value.

CHAPTER 4

THE DEVELOPMENT OF THE QUISTOR AS A LOW PRESSURE CHEMICAL IONISATION ION SOURCE FOR A MAGNETIC SECTOR MASS SPECTROMETER

4.1 Introduction

The original work on the use of the Quistor, operated in the total pressure mode, as a low pressure chemical ionisation ion source was performed by Bonner and colleagues[69,127] of this Laboratory with the apparatus described in Section 3.31. They showed that when mixtures of methane with either methanol or ethanol at a total pressure of *ca.* 2×10^{-5} Torr were ionised and these ions stored in the Quistor for *ca.* 5 ms, chemical ionisation reactions took place which were exactly analogous to those reactions which occur in conventional high pressure CI ion sources.

As an example of the use of the Quistor/quadrupole mass filter combination as a CI mass spectrometer, the low pressure CI mass spectrum of butan-2-ol is shown in Figure 4.1. This was obtained using methane as the reagent gas with a reagent gas to sample ratio of *ca.* 5:1 and a storage time of 8 ms. Some of the characteristic features of CI mass spectra, namely, the protonated parent ion (m/e 75) and the alkyl ion formed by the loss of a water molecule from the protonated parent ion (m/e 57), are clearly present in this spectrum. Although, as this demonstrates, the Quistor/quadrupole mass filter combination could be successfully employed as a CI mass spectrometer, no further development work was performed on this apparatus for the following reasons:

(i) Quadrupole mass filters possess an inherent discrimination against high mass ions which was a distinct disadvantage in this particular application since CIMS often involves the analysis of high molecular

weight compounds. Although there are a number of methods of eliminating mass discrimination, none of these facilities were available on the E.A.I. Quad 250A mass filter.

(ii) The sample inlet system could not be heated and so it was only suitable for the introduction of volatile samples. A solid sample introduction probe was available but there was no convenient way of mounting this such that the probe tip was in close proximity to the Quistor. In addition to this the Quistor was mounted inside a large vacuum chamber which could not be conveniently baked so that if involatile samples were introduced they condensed on the vacuum chamber walls which resulted in serious contamination.

(iii) For this project it was intended to make a comparison between high pressure CI using a conventional high pressure ion source and low pressure CI using the Quistor, and for this purpose it would be necessary to mount these ion sources on the same type of mass analyser. The available vacuum chamber could not be easily converted to incorporate the different pumping system which would be required in order to use a high pressure ion source in conjunction with the quadrupole mass filter.

For these reasons and also in order to make the most meaningful comparison between high and low pressure CIMS it was decided to build two separate ion sources for an A.E.I. MS9 magnetic mass spectrometer : a conventional high pressure ion source and a Quistor ion source. The high pressure ion source is described in Chapter 5.

4.2 The Design and Construction of a Quistor Ion Source for a Magnetic Mass Spectrometer

The ion source described in this section is a modified version of one constructed from an original design by Dr. G. Lawson. It was designed such that it had similar external dimensions to a standard A.E.I. electron bombardment ion source and could be mounted on the standard A.E.I. source

Figure 4.1 Low Pressure Methane CI Mass Spectrum of Butan-2-ol

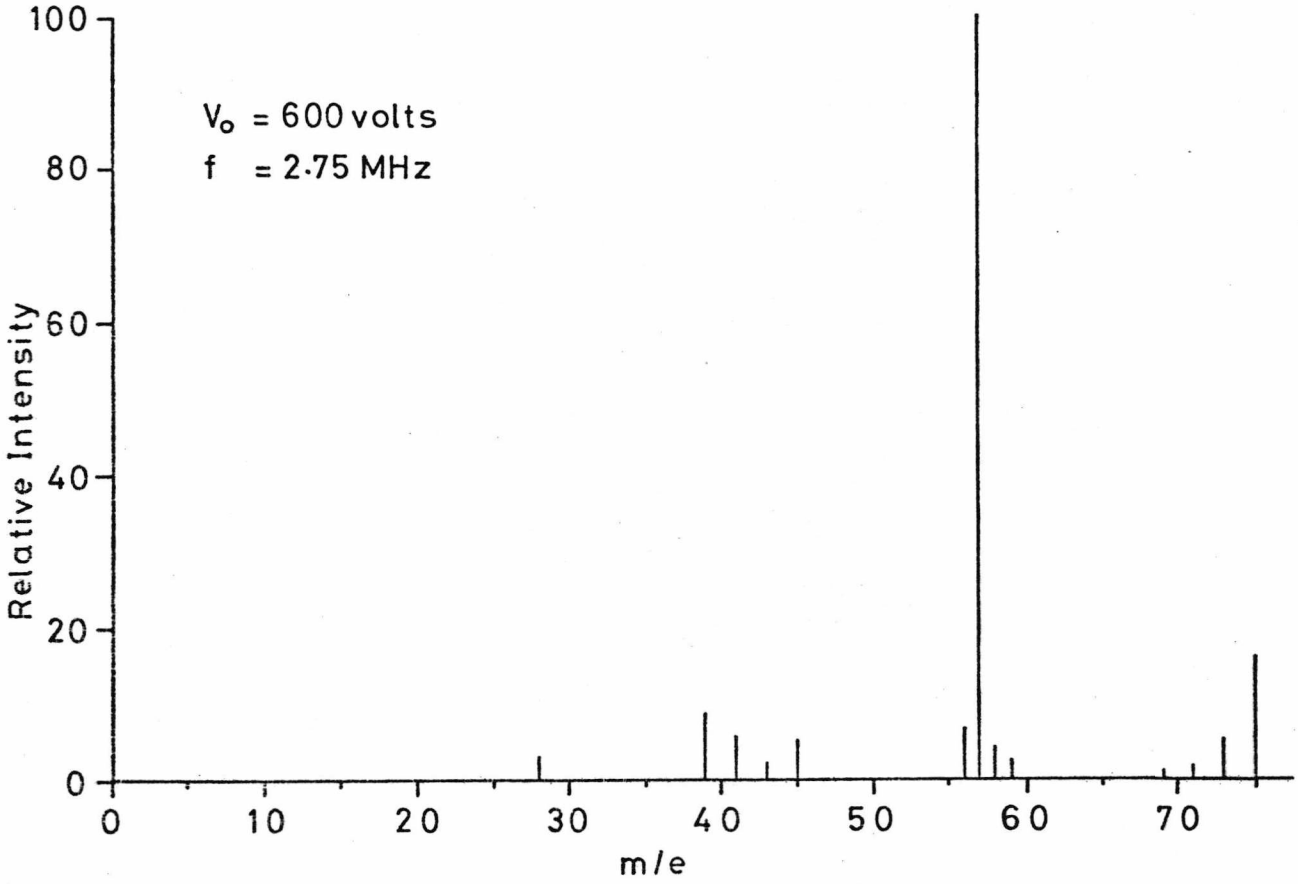

Figure 4.2 Central Section Through the Assembled Quistor

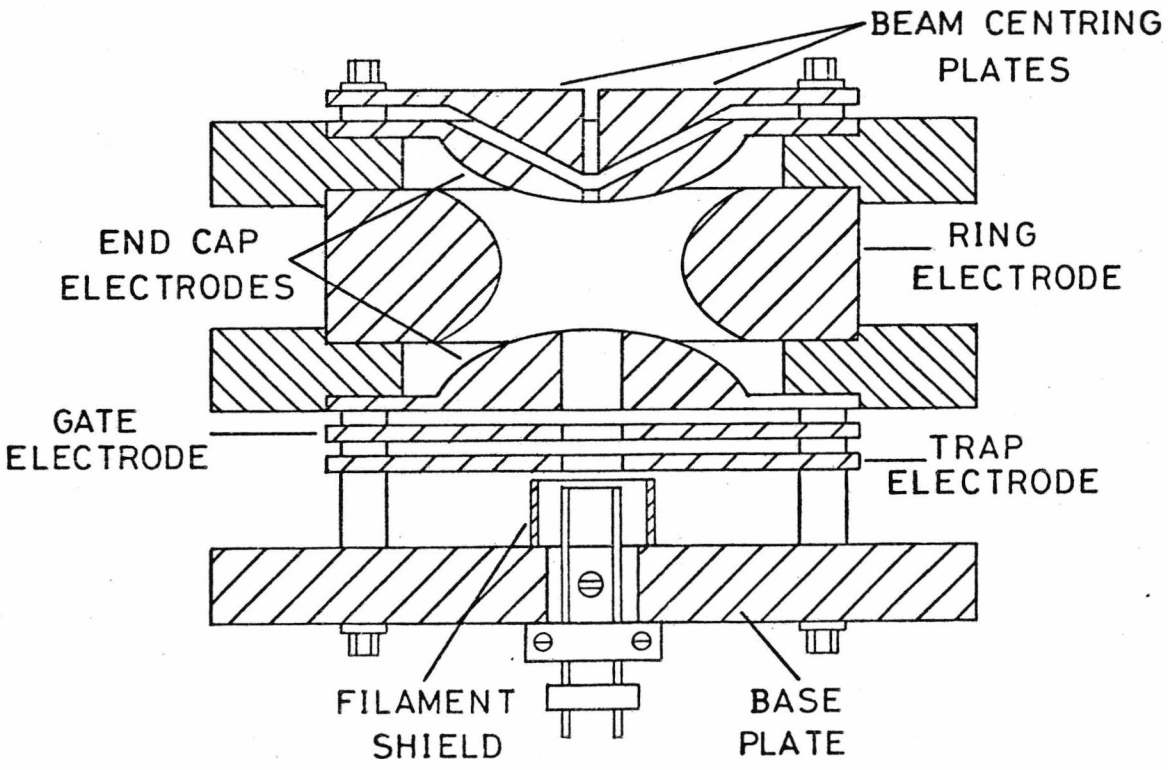

flange. A central section and a complete drawing of the assembled ion source are shown in Figures 4.2 and 4.3 respectively. It has the same basic structure as the Quistor described in Chapter 3, two end-caps and a ring electrode with the value of r_o chosen in this case as 0.7 cm, which was the maximum value that space limitations allowed. Both of the end-caps have 1.0×0.1 cm slits milled through them to permit electron entrance and ion extraction. The ion source has two beam centring electrodes which are shaped such that they form a Pierce-lens[145] arrangement with the upper end-cap. This was incorporated in an effort to improve ion focussing between the Quistor and the analyser. The electron gun comprises a standard MS9 filament, which is surrounded by a shielding electrode, and two electron beam control electrodes each having a 1.0×0.1 cm slit milled through them, such that they matched up with the slit in the lower end-cap. All electrodes were machined from stainless steel. The correct spacing and electrical insulation between the ring and two end-cap electrodes was provided by spacers manufactured from boron nitride. This material was chosen because of its mechanical strength, its excellent electrical insulation properties and its good outgassing characteristics under vacuum conditions. Two 0.15 cm diameter holes were drilled in the upper spacer, such that when the source was in place inside the MS9 source housing, they were in exact alignment with the heated glass re-entrant and the solid sample probe vacuum lock. All other spacers were made from either ceramic or pyropholite. The entire structure was mounted on a standard MS9 source baseplate and held together by four 10 B.A. threaded rods. This assembly was then secured to an MS9 source flange using standard components. Electrical connections to the Quistor were made by push-fit connectors to tabs spot-welded to the various electrodes. Four alignment holes were drilled through the entire assembly, such that it could be aligned using the MS9 source alignment jig.

There are two major differences between this and the original Quistor in Chapter 3. Firstly, in the former, the boron nitride spacers

Figure 4.3 Front Elevation and Plan View of the Quistor

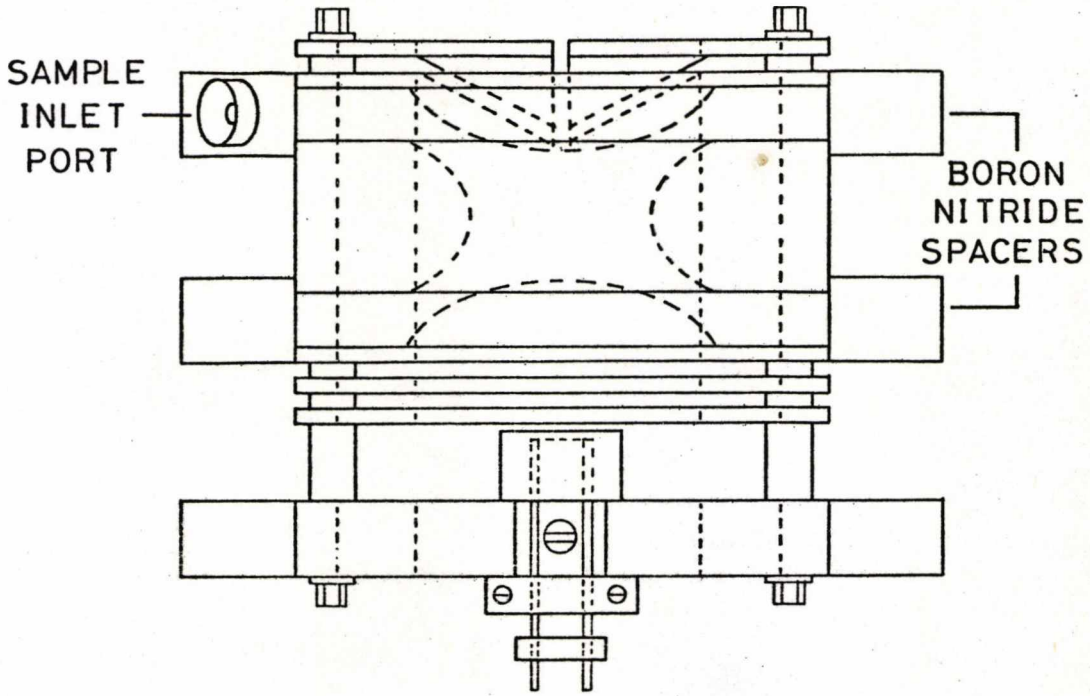

FRONT ELEVATION

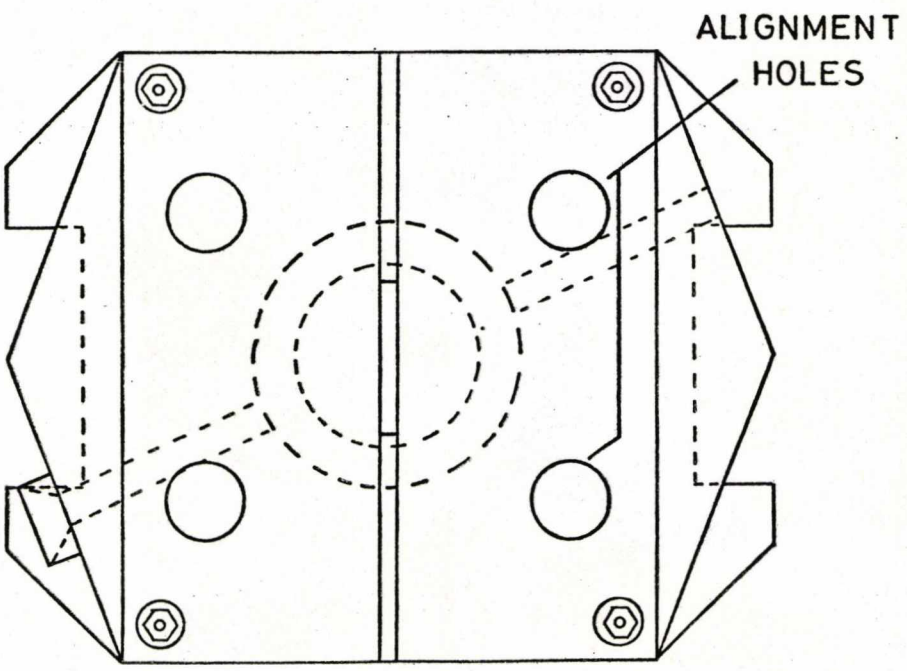

PLAN

between the ring and end-cap electrodes were made in the form of complete rings such that the hyperbolic surfaces of the electrodes were completely enclosed. This feature was incorporated in an effort to improve the alignment of the electrodes and also to prevent the sample from being pumped away to quickly. Secondly, the new Quistor has an axial electron gun, that is the electron beam is directed along the z axis of the trap, whereas in the original Quistor the electron beam was directed radially through a hole in the ring electrodes. Besides being easier to construct and mount, the axial electron gun is less susceptible to problems arising from r.f. pick-up since it is physically further from the ring electrode and easier to shield from these effects. The problem of r.f. pick-up prevented any form of emission current stabilisation in the original Quistor.

Two photographs of the assembled ion source are shown in Figures 4.4(a) and 4.4(b). Another photograph of the ion source with the beam centring plates and upper end-cap removed is shown in Figure 4.5. The hyperbolic electrode structure and the electron entrance slit in the lower end-cap are clearly visible.

4.3 The Characterisation of the New Quistor Ion Source

Before attempting to operate the new Quistor as an ion storage source for the MS9, it was necessary to characterise the axial electron gun and to determine whether the new device was capable of ion storage. These experiments were performed by mounting the new Quistor on the quadrupole mass filter in place of the original Quistor. The basic characterisation was performed in this way rather than when the new device was installed on the MS9, because the Quistor/quadrupole mass filter combination is a well characterised system and the experiments were technically easier to perform.

For all of the experiments described in this section the new Quistor was secured to the support column (Figure 3.7) and placed inside

Figure 4.4 Photographs of the Assembled Quistor

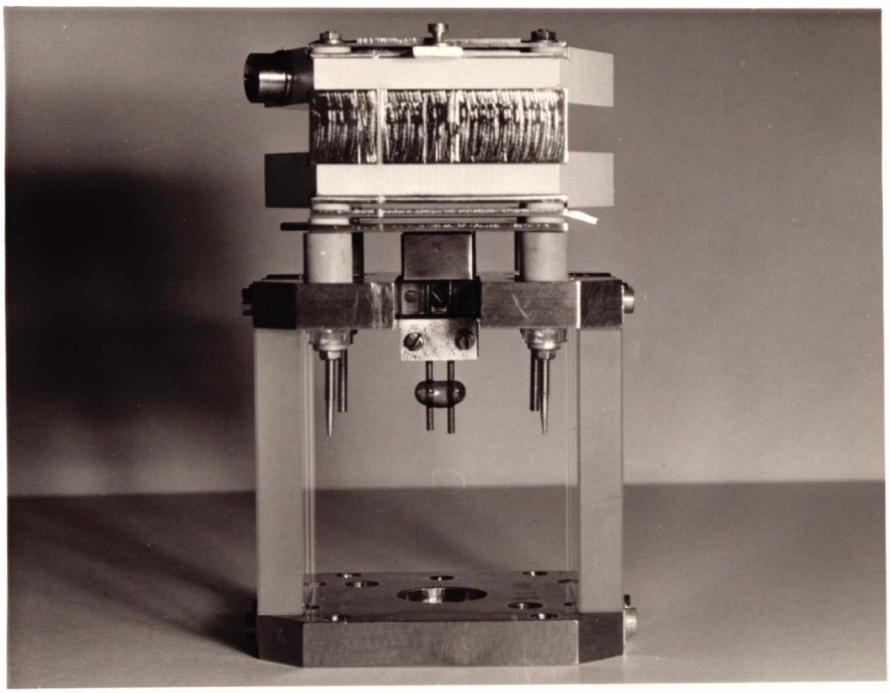

(a)

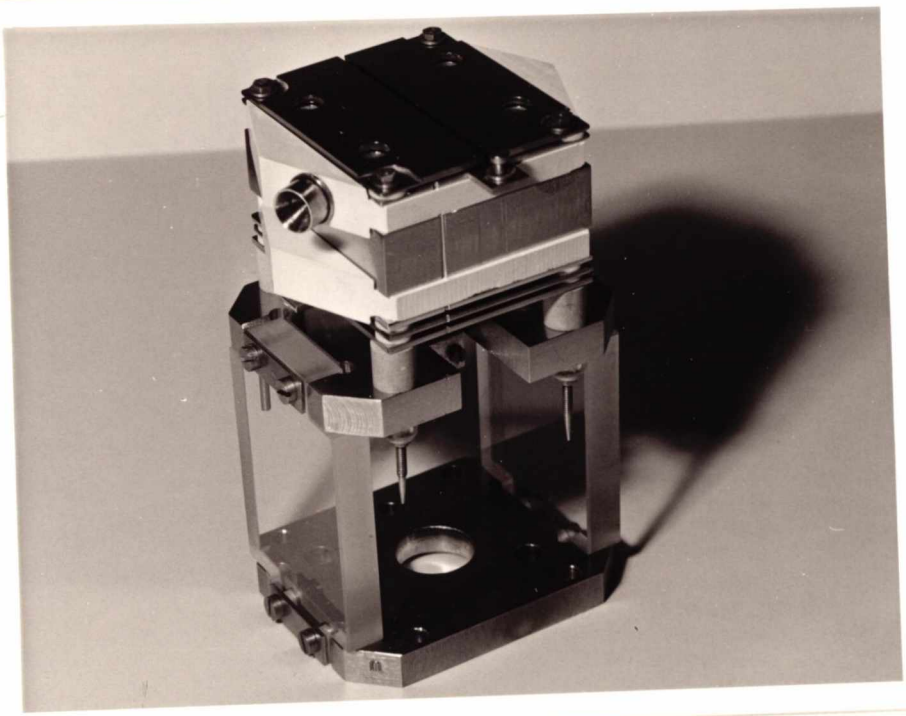

(b)

Figure 4.5 Photograph of the Quistor with Beam Centring Plates and Upper End-Cap Removed

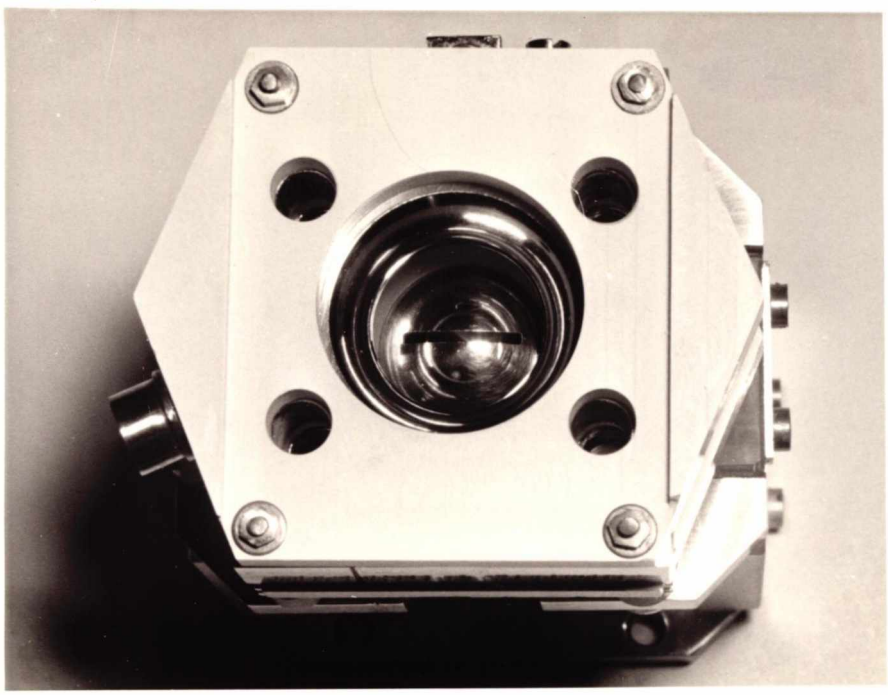

Figure 4.6 Schematic Diagram of the Quistor

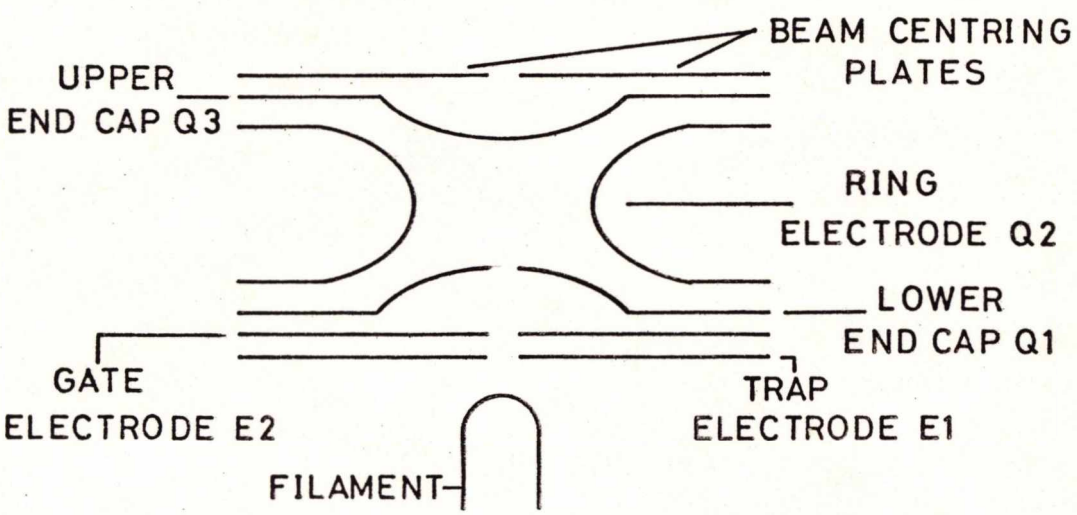

the vacuum chamber such that the beam centring plates were 0.1 cm away from the quadrupole rods.

4.3.1 The Electron Gun

When operating the Quistor as a pulsed ion source it is necessary to gate the electron beam by applying suitable potentials to the gating electrodes placed between the filament and the Quistor. The method of gating the electron beam employed in the original Quistor (Section 3.3.2) was unsuitable for the new device because the two electron guns were of a different design. The following experiments were therefore performed in order to establish the optimum conditions for the operation of the new electron gun.

From the schematic diagram of the new Quistor shown in Figure 4.6 it is evident that there are two methods of gating the electron beam from the filament : earth E1 and apply the gating potential to E2 or earth E2 and apply the gating potential to E1. Both of these possibilities were investigated by applying a negative potential to the gating electrode and then determining the effect of this potential on the number of electrons entering the Quistor by measuring the current collected on the ring electrode, Q2 and the upper end-cap, Q3, which were shorted together, using an Avometer.

These measurements were made for increasing negative values of the gating potential until the collected electron current decreased to zero. The results of this investigation for three fixed values of the electron energy are shown in Figure 4.7 plotted as the collected electron current *vs* (filament minus gate potential)(electron energy is defined as the potential of the filament with respect to earth).

(i) E1 earthed and E2 gated - From Figure 4.7(a) it is apparent that a gating potential greater than the electron energy (electron energy in this case being the potential difference between E1 and the filament) is required to completely attenuate the electron beam. This was probably

Figure 4.7 Plots Showing the Effectiveness of the Electron Gate

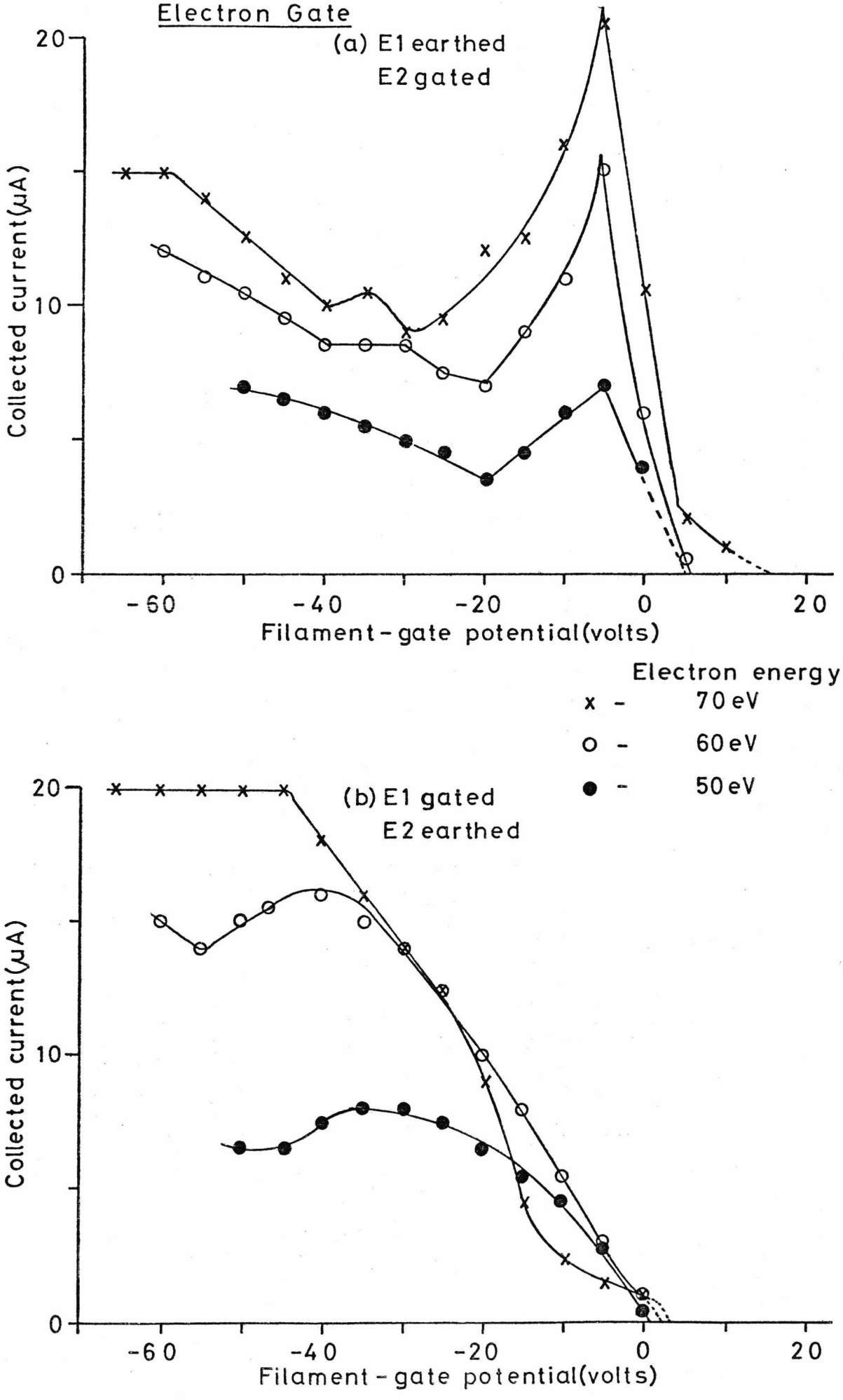

due to the energy spread of the electron beam. The peak which occurs at the same value of the (filament minus gate potential) for each of the curves shown in Figure 4.7 could represent the maximum of the electron energy distribution or may have been caused by a focussing effect.

(ii) E1 gated and E2 earthed - In this case as the potential difference between E1 and the filament decreases the effective electron energy also decreases so that when this difference is zero electrons are no longer accelerated towards the Quistor. This accounts for the gradual decrease in collected electron current as the gating potential is increased as shown in Figure 4.7(b).

Although both of these methods were effective in gating the electron beam method *(i)* was adopted for reasons discussed in Section 4.4.1.

For pulsed operation of the Quistor the electron gate is opened by superimposing a positive going pulse, the ion creation pulse, on the gating potential. When E2 is gated the amplitude of this pulse is adjusted such that during the time the electron gate is open the potential on the gating electrode corresponds to the position of the maxima of the curves shown in Figure 4.7(a). In this way the electron current is maximised for the duration of the creation pulse. The actual value of the gating potential required to gate the electron beam was determined from observations of the stored ion signal on an oscilloscope as described in the next section.

4.3.2 Ion Storage Characteristics

The ion storage characteristics of the new device were investigated using the same experimental system as that shown in Figure 3.13. For these experiments the two beam centring plates, the lower end-cap (Q1) and E1 were earthed, the ion ejection pulse was applied to the upper end-cap (Q3) and the ion creation pulse to E2.

After establishing that the new device was capable of storing ions

the value of the gating potential required to shut the electron gate was determined by setting the ion creation pulse amplitude to zero and observing the output from the electron multiplier corresponding to the stored ion signal (i.e. that which was co-incident with the ion ejection pulse) on an oscilloscope, while the gate potential was slowly increased. At an electron energy of 50 eV the stored ion signal disappeared at a gate potential of -100V indicating that under these conditions the electron beam was totally attenuated.

The stability limits on the q_z axis were determined while operating the new Quistor under the following conditions

Argon pressure	2.4×10^{-5} Torr
Operating frequency, f	0.82 MHz
ICPW	20 μs
IEPW	20 μs
Storage time	500 μs

For m/e 40 the lower stability limit was $q_z = 0.29$ and the upper stability limit was $q_z = 0.92$. These values are in excellent agreement with those determined for the original Quistor under similar operating conditions (Section 3.4.1.1).

A build-up curve and a decay curve for Ar^+ (m/e 40) ions recorded under the following conditions are shown in Figures 4.8(a) and 4.8(b) respectively.

Argon pressure	2.4×10^{-5} Torr
Operating frequency, f	0.82 MHz
Applied r.f. potential, V_o	90V (zero-peak)
ICPW	20-500 μs
IEPW	20 μs
Storage time	0.1-5 ms

Figure 4.8 Build-Up and Decay Curves for Ar^+ (m/e 40) Ions

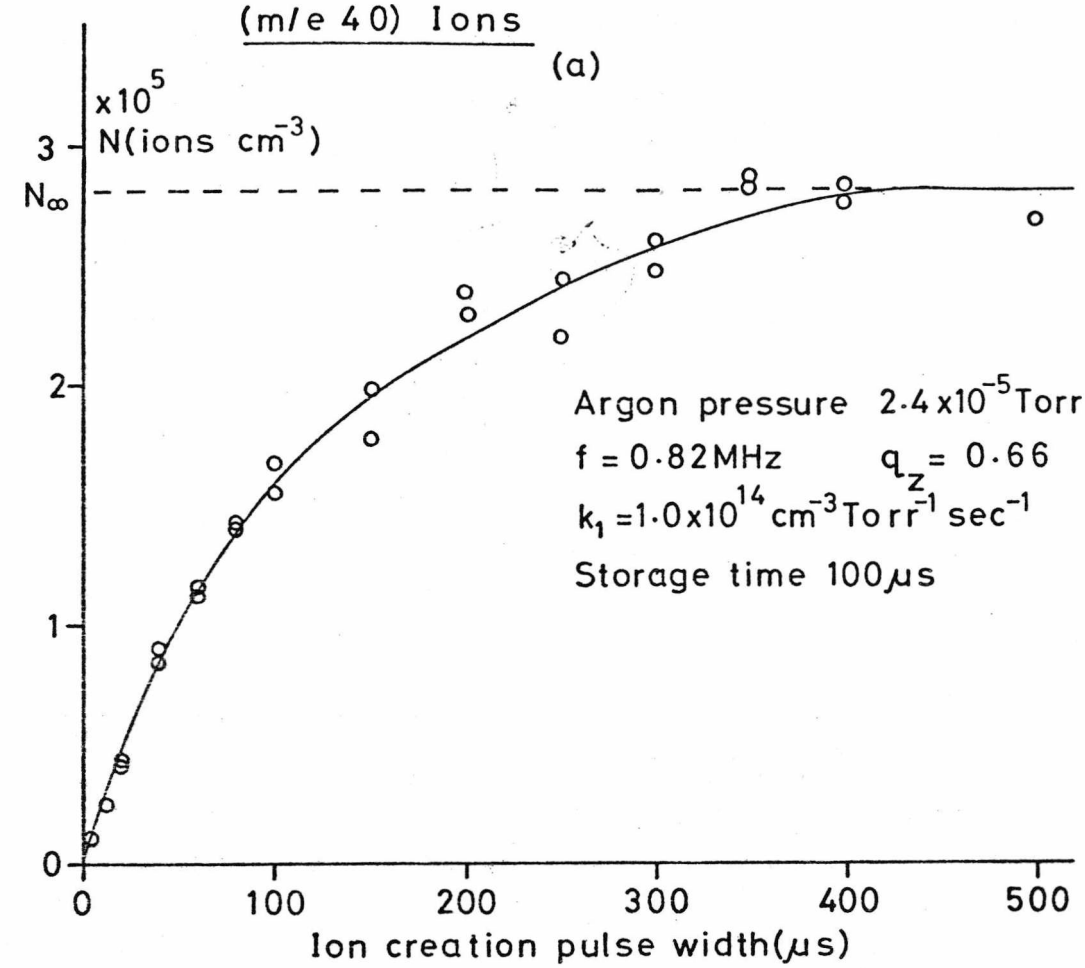

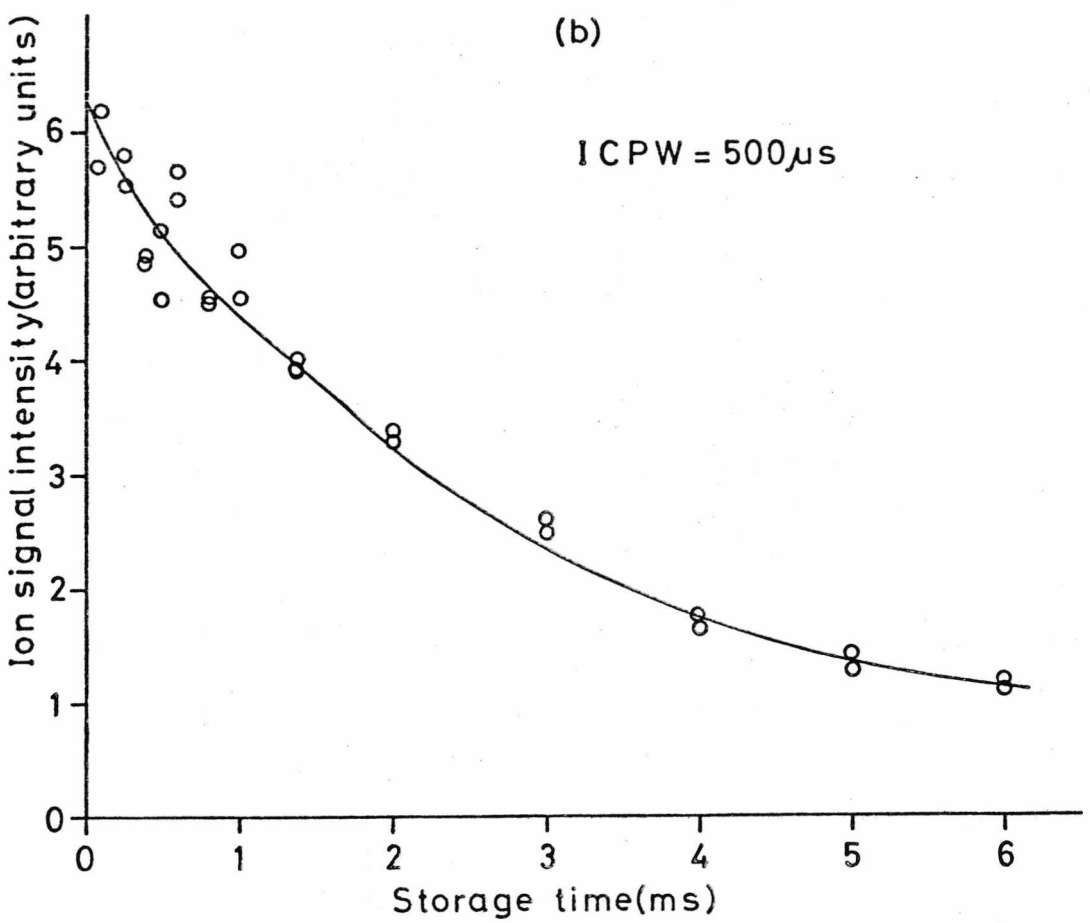

Comparing the build-up curve shown in Figure 4.8(a) with that shown in Figure 3.23 which was obtained using the original Quistor while operating under similar conditions, the values of k_1 (1.0×10^{14} and 8.0×10^{14} cm^{-3} $Torr^{-1}$ sec^{-1} respectively), determined from the initial slope, differ by a factor of eight. However, this was expected since the value of k_1 is dependent on the electron optics and current which will be different for the two devices because the electron guns are not of the same design. From the values of N_∞ determined from these two curves it appears that the original Quistor is capable of storing more ions than the new device. However, the large uncertainties involved in the calculation of N_∞, and also k_1 make it impossible to draw any positive conclusions from this comparison. The values of the ion loss parameters determined from the decay curve shown in Figure 4.8(b) are: $k_2 = 2.0\pm0.4\times10^{-4}$ cm^3 sec^{-1} and $k_3 = 6.0\pm4.0\times10^{-11}$ cm^3 mol^{-1} sec^{-1}. These values are in reasonable agreement with those determined for the original Quistor when operated at a q_z of 0.66 (Table 3.5).

As a further confirmation that the new Quistor was functioning correctly as an ion storage source the ion storage mass spectrum of methane was studied as a function of storage time. The results of this study are presented in Figure 4.9. The rapid decrease in the intensity of the ions at m/e's 15 and 16 and the appearance of ions at m/e 17 and 29 indicated that the following two well-known ion-molecule reactions were occurring

$$CH_4^+ + CH_4 \longrightarrow CH_5^+ + CH_3 \qquad \text{R.4.1}$$

$$CH_3^+ + CH_4 \longrightarrow C_2H_5^+ + H_2 \qquad \text{R.4.2}$$

The rate constants for these two reactions determined from Figure 4.9 are 13×10^{-10} cm^3 mol^{-1} sec^{-1} and 5.6×10^{-10} cm^3 mol^{-1} sec^{-1} respectively. These values are in excellent agreement with those determined by Lawson *et al*[68] from a study of the methane system using the original Quistor.

Figure 4.9 Plot Showing the Relative Intensities of the Ions in Methane as a Function of Storage Time

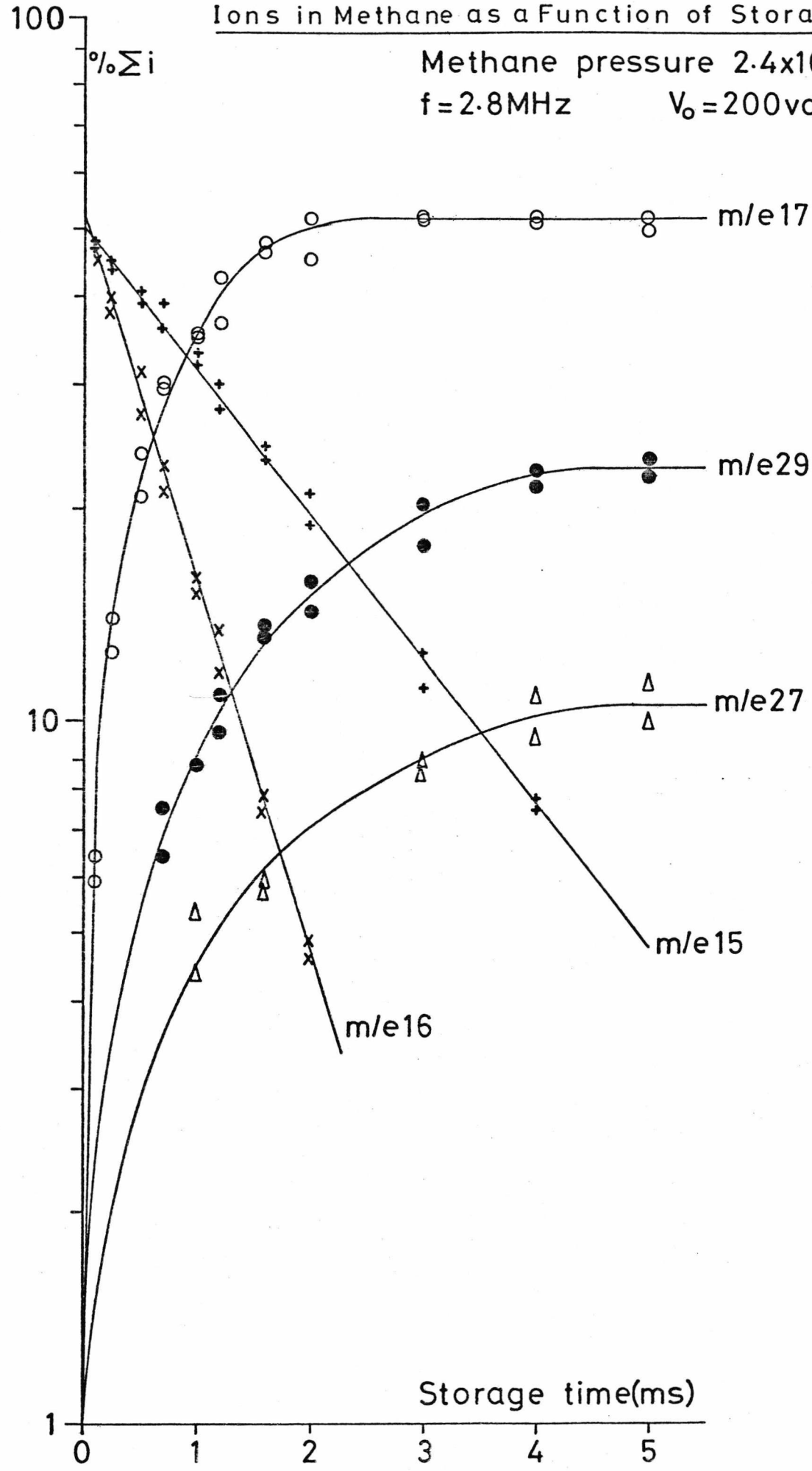

Ion-molecule reactions occurring in other gases studied using the Quistor are discussed in more detail in Chapter 6.

From this brief study it is apparent that the new Quistor was functioning correctly as an ion storage source with storage characteristics very similar to those of the original Quistor. One important difference between the new device and the original Quistor are the values of r_o which are 0.7 cm and 1.008 cm respectively. Because of this difference in internal dimensions the value of V_o required to store an ion such that it has a particular value of q_z in the new Quistor is approximately half of that required for the original device, since $q_z \propto V_o/r_o^2$ (equation 3.15). This effectively doubles the range of operating conditions available with the existing r.f. power supply.

4.4 Interfacing the Quistor with the MS9

When the Quistor is employed as an ion source for the quadrupole mass filter all of the necessary operating potentials are referenced to earth. However, in order to use it as an ion source for the MS9 these operating potentials must be referenced to the ion accelerating potential which may be as high as 8000 volts. For this purpose an interface unit was introduced between the Quistor, the Quistor power supplies and the MS9 source supply chassis. In addition to this the operation of the Quistor as an ion source for the MS9 required several minor electronic modifications to the source supply chassis and the incorporation of a box car detector into the signal amplification circuitry.

4.4.1 The Interface and Source Supply Chassis Modifications

There are two possible methods of referencing the Quistor operating potentials to the accelerating potential of the MS9. Firstly, the Quistor power supplies, comprising the r.f. generator and the two pulse generators, could be isolated from earth and connected to the mains supply via a high voltage isolation transformer. These supplies could

then be floated to accelerating potential and their outputs connected, using suitably insulated and screened cables, directly to the Quistor electrodes. Secondly, since the majority of the Quistor operating potentials are time varying in nature the outputs of the power supplies could be connected to the Quistor electrodes via suitable high voltage capacitors. In this way the power supplies and one side of the capacitors could be maintained at earth potential and the other side of the capacitors and the Quistor electrodes floated to accelerating potential. The latter method was chosen because when operating the Quistor it is essential to be able to adjust and monitor, using an oscilloscope, the large number of different operating parameters. This is most conveniently achieved when the power supplies are earthed and would be extremely difficult if they were at a high potential and mounted inside a cumbersome insulated cage of the type that would be required if the alternative method was used.

A schematic block diagram and pulse timing sequence of the experimental system is shown in Figure 4.10. This system is basically the same as that employed to operate the original Quistor except that the two pulse generators and the r.f. generator are connected to the Quistor electrodes via the high voltage interface and all d.c. operating potentials are derived from the MS9 source supply chassis. A circuit diagram of the interface is shown in Figure 4.11. This was mounted inside a box made from 'Paxolin' sheet and connections between the interface, the ion source and the power supplies were made by either P.E.T. or H.T. B.N.C. co-axial connectors. These shielded connectors were securely earthed to the frame of the mass spectrometer. The zener diodes were included in an effort to protect the pulse generators from high voltage transients which are produced when the accelerating potential is switched on and off and also when high voltage arcing occurs.

Although the ion ejection pulse could be applied to either Q1 or Q3 a negative going 'suck out' pulse was normally applied to Q3 and Q1 was set to the accelerating potential. The ion creation pulse was connected

Figure 4.10 Schematic Block Diagram and Pulse Timing Sequence of the Quistor/MS9 System

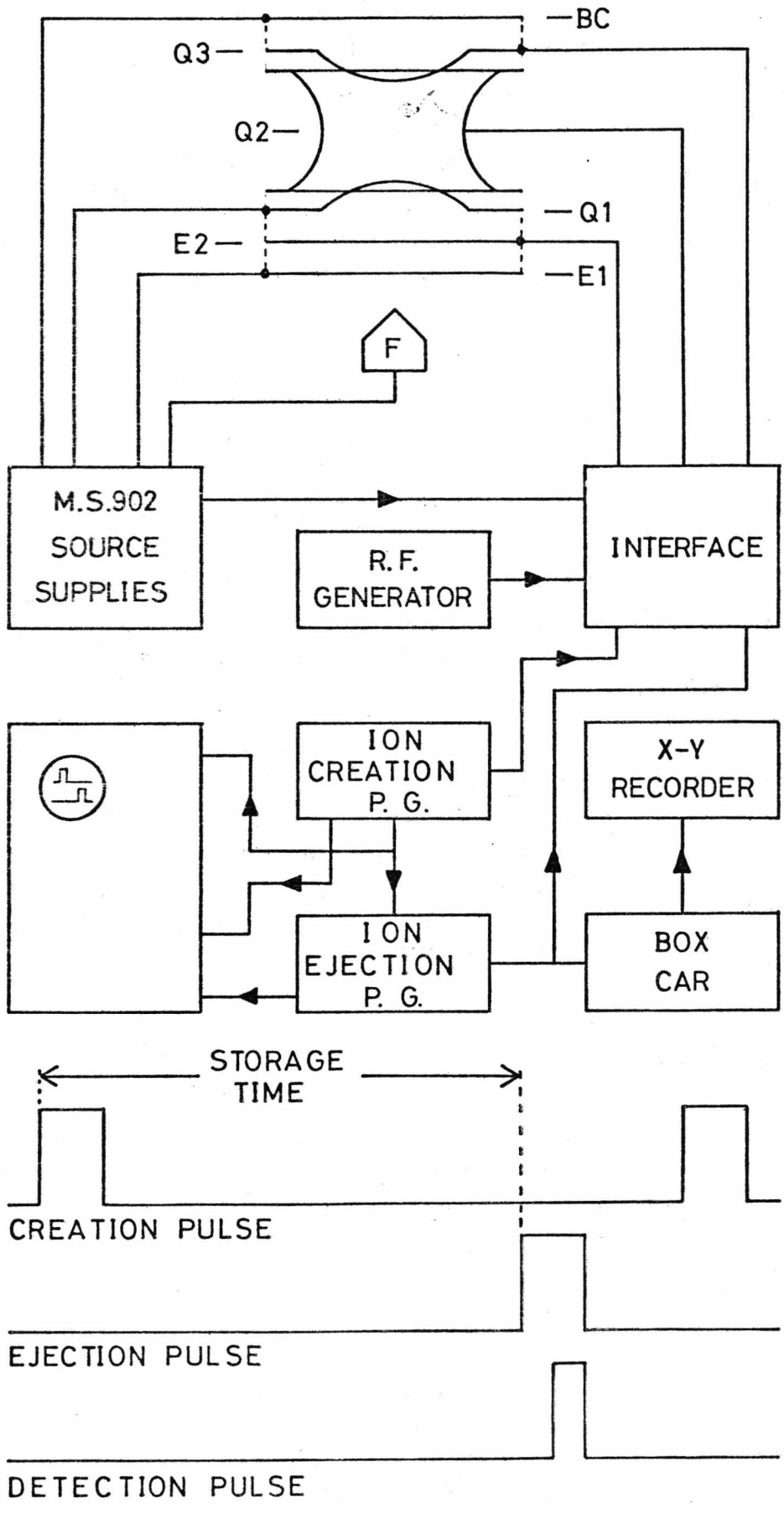

to E2 which was biased at -100 volts with respect to the accelerating potential. This d.c. bias was derived from a potential divider in the source supply chassis.

The filament power supply did not require any modification because standard MS9 filaments were employed in the Quistor electron gun; it was, however, necessary to modify the emission current stabilisation circuit. This involved changing the value of the trap potential such that it was variable in the range -25V to +25V instead of being fixed at +60V with respect to accelerating potential. This was necessary because, since the Quistor has no trap electrode, the emission current must be stabilised with reference to the current collected on E1 and if this electrode was maintained at +60V the electron gate would not operate correctly. The facility of a variable 'trap potential' was incorporated to permit focussing of the electron beam. Satisfactory stabilisation of the emission current could only be achieved if E1 was used as the emission collector, and so the alternative method of gating the electron beam using E1, discussed in Section 4.3.1, could not be employed because some form of filament current control is essential.

These modifications to the source supply chassis were made in such a way that it was possible to change the values of the various potentials to those values required to operate the Quistor using one single switch.

4.4.2 Modifications to the Signal Amplification System

Since the Quistor is operated as a pulsed ion source it was necessary to incorporate a Brookdeal box car integrator into the MS9 signal amplification circuitry. The box car linear gate was connected between the MS9 head amplifier and the bandwidth filter as shown in Figure 4.12 and was triggered from the scan delay generator in the same way as for the Quistor/quadrupole mass filter system (Figure 3.13). Since the maximum output of the head amplifier is 100V and that of the box car linear gate 10V, the dynamic range of the signal amplification system was

Figure 4.11 Circuit Diagram of the High Voltage Interface

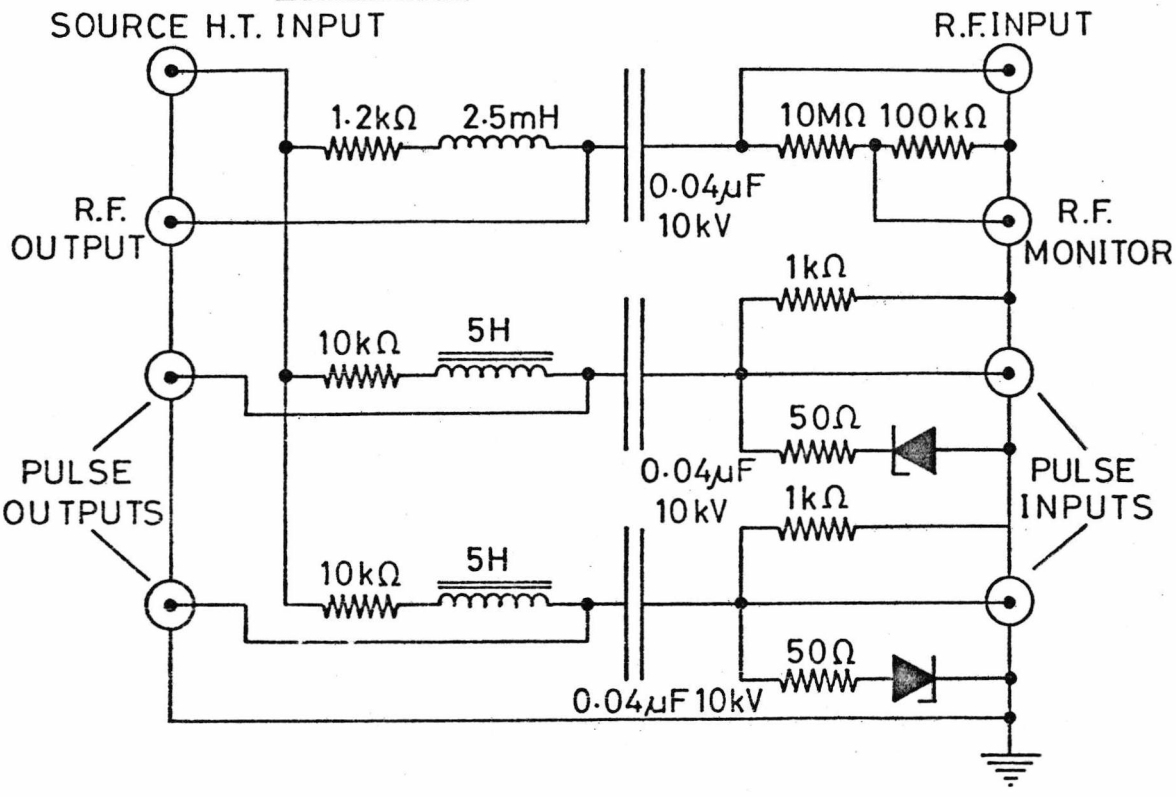

Figure 4.12 Block Diagram of the Modified Signal Amplification System

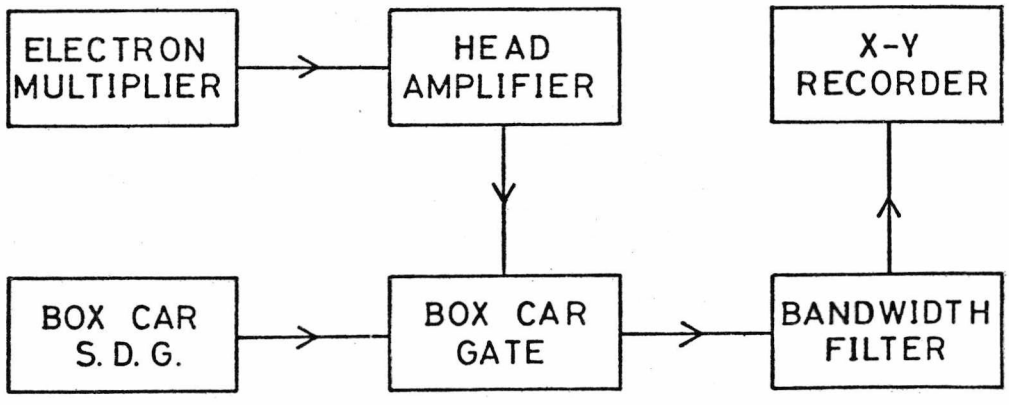

reduced by a factor of ten.

Mass spectra were recorded on a Bryans 26000 series X-Y pen recorder, the X axis (m/e) being driven by an internal scan unit.

4.5 The Operation of the Quistor as an Ion Storage Source for the MS9

The basic operating procedure was identical to that for the Quistor/mass filter combination. An operating frequency of 2.5 MHz (nominal) was employed since the results of experiments described in Section 3.4.1 indicated that of the two available frequencies, this one allowed the simultaneous storage of ions with a wider range of m/e values. Under certain conditions the maximum available ejection pulse amplitude (90 volts, from the Hewlett Packard 214A) was found to be insufficient to effect the ejection of all the ions from the trap. This was remedied by incorporating a pulse amplifier between the ejection pulse generator and the interface (Figure 4.10) which produced pulses with amplitudes of up to 800V. In practice an ejection pulse amplitude of 250V was found to be sufficient for most experiments. An electron energy of 70 eV was employed for all low pressure CI studies.

The MS9 mass spectrometer was operated at an ion accelerating potential of 8 kV and usually with both the source and collector slits wide open, under which conditions the resolution was between 500 and 1000 (10% valley definition). According to the manufacturer's specifications, at a resolution of 500 the scan time per mass unit for a magnet scan rate corresponding to 9.6 minutes per decade in mass is 500 ms. Since the Quistor pulse sequence was normally repeated at 10 ms intervals the signal produced on the X-Y recorder for a particular m/e value corresponded to the mean of 50 ion creation, storage and ejection events. This was found to be the minimum value which would give reproducible mass spectra, thus, since the resolution could not be reduced and any increase in the repetition rate would limit the maximum available storage time, the maximum scan rate was limited to 9.6 minutes per decade.

For low pressure CI studies the reagent gas was normally introduced via the standard A.E.I. cold inlet system and the sample through either the All Glass Heated Inlet System or on the solid sample probe. Pressure measurements quoted in this chapter were obtained using the source housing ionisation gauge and must therefore only be regarded as approximate.

Since the Quistor ion source was mounted on an A.E.I. source flange its installation was no more complicated than exchanging normal ion sources except that the electron beam collimating magnets had to be removed. The complete operation including the connection of the interface unit and the box car detector took less than one hour.

4.6 Low Pressure CI Studies with the Quistor as an Ion Source for the MS9

For low pressure CI studies with the Quistor the operating conditions must be arranged such that all ions with m/e values between those of the reagent gas primary ions and the quasi-parent ion of the sample are stored simultaneously. This represents the minimum 'storage range' requirement since, depending on the reagent gas employed and the chemical nature of the sample, ions may be formed with m/e values above that of the quasi-parent ion.

The experiments described in this section were performed to ensure that the new Quistor could be operated as a CI ion source and to establish optimum conditions for its operation in this mode.

4.6.1 The Ion Storage Mass Spectrum of Methane

From the brief study of the ion-molecule reactions occurring in methane at a pressure of 2×10^{-5} Torr in the Quistor, the results of which were presented in Figure 4.9, it is clear that after a storage time of 5 ms the two major product ions are CH_5^+ and $C_2H_5^+$. These are the methane CI reagent ions which are also produced in a high pressure CI

ion source operated at 1 Torr. Lawson *et al*[68] have used the Quistor/mass filter combination to investigate the methane system in more detail. They found that the relative intensities of the product ions were dependent not only on pressure and storage time but also on the amplitude of the r.f. potential (V_o). Since any change in the product ion, or in this case reagent ion, distribution could affect the relative intensities of ions in a CI mass spectrum, this effect was investigated in more detail before proceeding with methane CI studies.

The series of mass spectra shown in Figure 4.13 were recorded at a pressure of 2×10^{-5} Torr and a fixed storage time of 5 ms for various different values of the r.f. potential. Values of q_z for the ions of m/e 17 and 29 are listed in Table 4.1 for each of the values of V_o employed.

Table 4.1 Values of q Calculated for m/e 17 and 29 for Different Values of V_o (f = 2.48 MHz)

V_o(volts)	q_z(m/e 17)	q_z(m/e 29)
75	0.139	0.082
85	0.158	0.092
95	0.176	0.104
100	0.186	0.109
105	0.195	0.114
125	0.232	0.136
135	0.250	0.147
170	0.315	0.185

The general increase in the total number of ions stored as the r.f. potential is increased was expected, since the storage efficiency increases up until a value of q_z of *ca.* 0.7 (Section 3.4.1.3). The change in the relative intensity of m/e 17 and 29 is an example of the mass discrimination effect discussed in Section 3.4.1.3. At very low values of the r.f. potential m/e 29 was stored at a value of q_z, which from the results of experiments described in Section 3.4.1.1, would be

Figure 4.13. Mass Spectra of Methane Recorded at 5ms Storage Time for Various Values of the r.f. potential (V_o in volts)

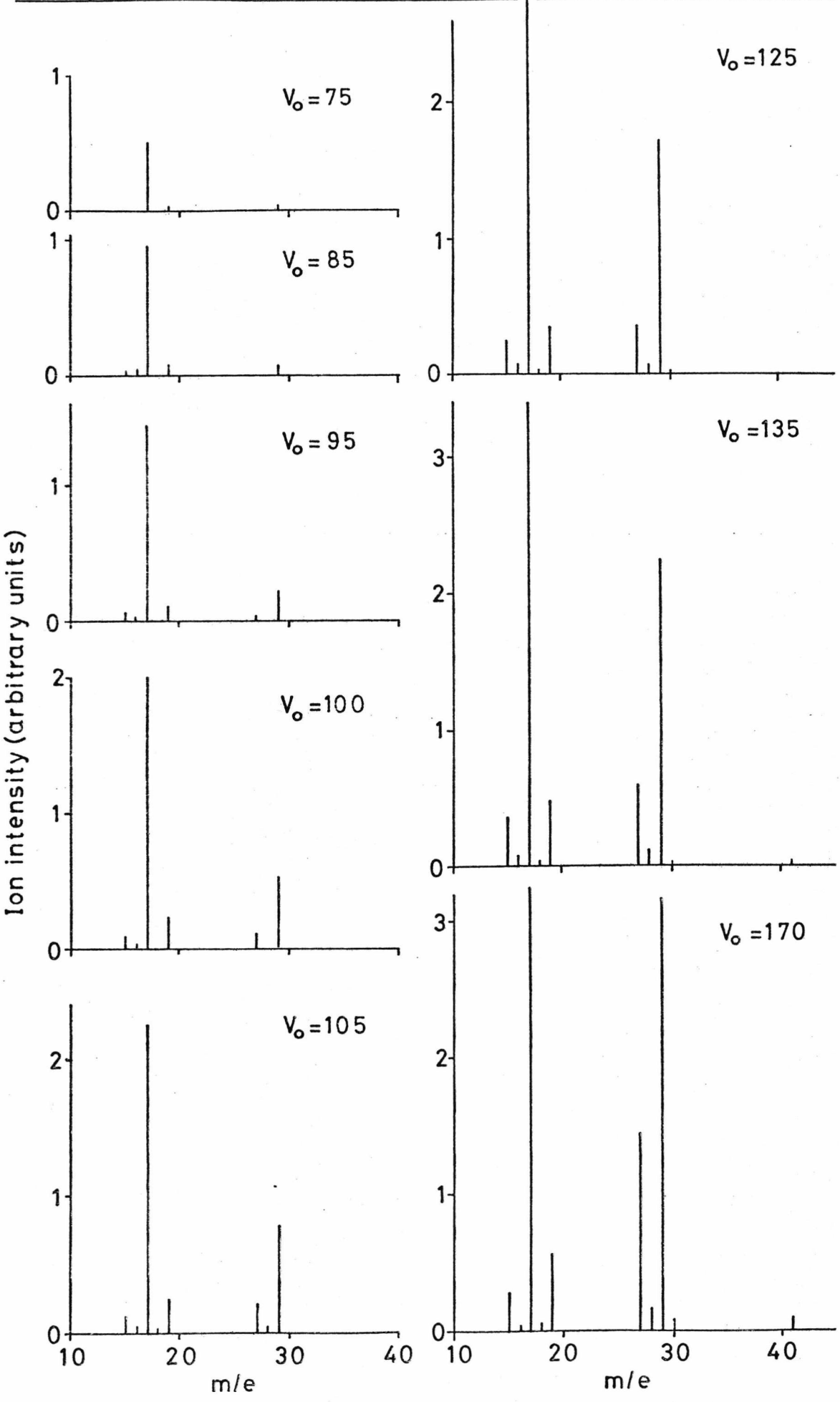

expected to be very close to the stability limit where the maximum number of ions that can be stored is small. Under these conditions the number of ions stored may only represent a small fraction of the total number of ions created (in this case by reaction R.4.2). As the r.f. potential is increased a greater proportion of the ions formed is actually stored and therefore the observed relative intensity of m/e's 17 and 29 is more representative of the actual relative numbers of these ions created by reactions R.4.1 and R.4.2 respectively.

There are a number of other factors which may also contribute to the observed changes in the relative intensities of stored ions at different values of the r.f. potential. Firstly, in the case of methane the relative intensities of CH_5^+ and $C_2H_5^+$ will be dependent on the relative proportions of their precursor ions CH_4^+ and CH_3^+ stored in the Quistor, which will also be a function of the amplitude of the r.f. potential. Secondly, since the primary ion kinetic energy of any ion-molecule reaction occurring in the Quistor is dependent on the value of V_o (see Section 3.2.1 and Chapter 6) then any change in the relative intensities of product ions with this parameter may reflect differences in the kinetic energy dependence of the rates of the respective ion-molecule reactions. For the case of methane the exact nature of the kinetic energy dependence of the reactions producing CH_5^+ and $C_2H_5^+$ is still a matter of some conjecture[146] and will not be discussed here. Finally, if a particular ion may be produced by two different ion-molecule reactions and one of these reactions is endothermic then the relative intensity of this ion may change drastically as the primary ion kinetic energy approaches the threshold energy for this reaction. In methane the ion $C_2H_3^+$ (m/e 27) may be produced by two reactions

$$CH_2^+ + CH_4 \longrightarrow C_2H_3^+ + H_2 + H \qquad \text{R.4.3}$$

$$CH_3^+ + CH_4 \longrightarrow C_2H_3^+ + 2H_2 \qquad \text{R.4.4}$$

Reaction R.4.3 occurs at thermal energies but the latter reaction is endothermic with a primary ion kinetic energy threshold of *ca.* 1.5 eV[68] for the ground state precursor ion. This may explain the observed increase in the relative intensity of m/e 27 in Figure 4.13 since Lawson *et al*[68], who have investigated these reactions in more detail using the Quistor, estimated that under similar operating conditions to those employed to produce the data shown in Figure 4.13 the average kinetic energy of the CH_3^+ species was in the range 1 to 4 eV. Under the thermal energy conditions prevalent in a high pressure CI ion source operated at a pressure of 1 Torr, reaction R.4.3 is the only pathway by which the $C_2H_3^+$ ion may be produced.

From this investigation it is clear that ideally the amplitude of the applied r.f. potential should be fixed such that the relative intensities of the major reagent ions in methane were constant for particular values of the pressure and storage time.

4.6.2 The Use of Methane as the Reagent Gas

For these experiments the value of V_o was adjusted so as to maximise the intensity of the ion at m/e 17 when the Quistor was operated at a storage time of 5 ms. This maximum occurred where the value of q_z for this ion was *ca.* 0.56.

The low pressure CI mass spectra of methanol and ethanol using methane as the reagent gas are shown in Figures 4.14 and 4.15 respectively. These were obtained by introducing a 10:1 (approximately) mixture of methane to alcohol into the Quistor-MS9 combination such that the total pressure, as measured by the source region ionisation gauge, was 2×10^{-5} Torr. Figure 4.14a was recorded at 100 μs storage time and is in effect a combination of the electron impact mass spectra for methane and methanol, except that m/e 17 is present through the formation of CH_5^+.

Figure 4.14 Mass Spectra of a 10:1 Mixture of Methane and Methanol Recorded at (a) 100μs and (b) 2ms Storage Time

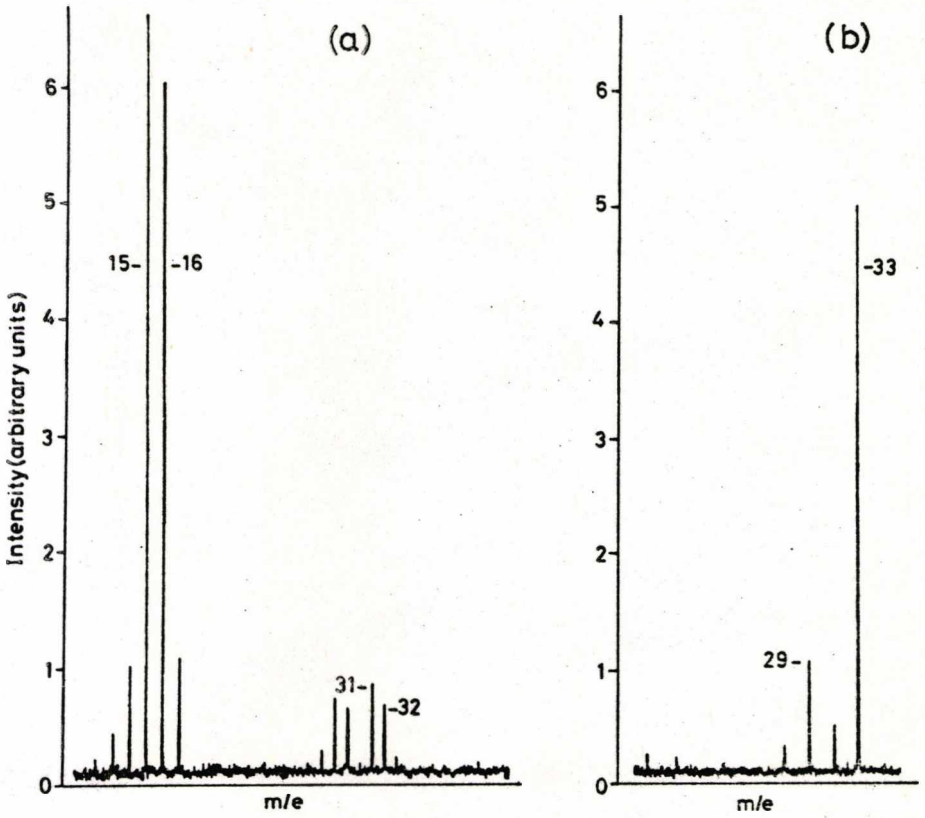

Figure 4.15 Mass Spectra of a 10:1 Mixture of Methane and Ethanol Recorded at (a) 100μs and (b) 2ms Storage Time

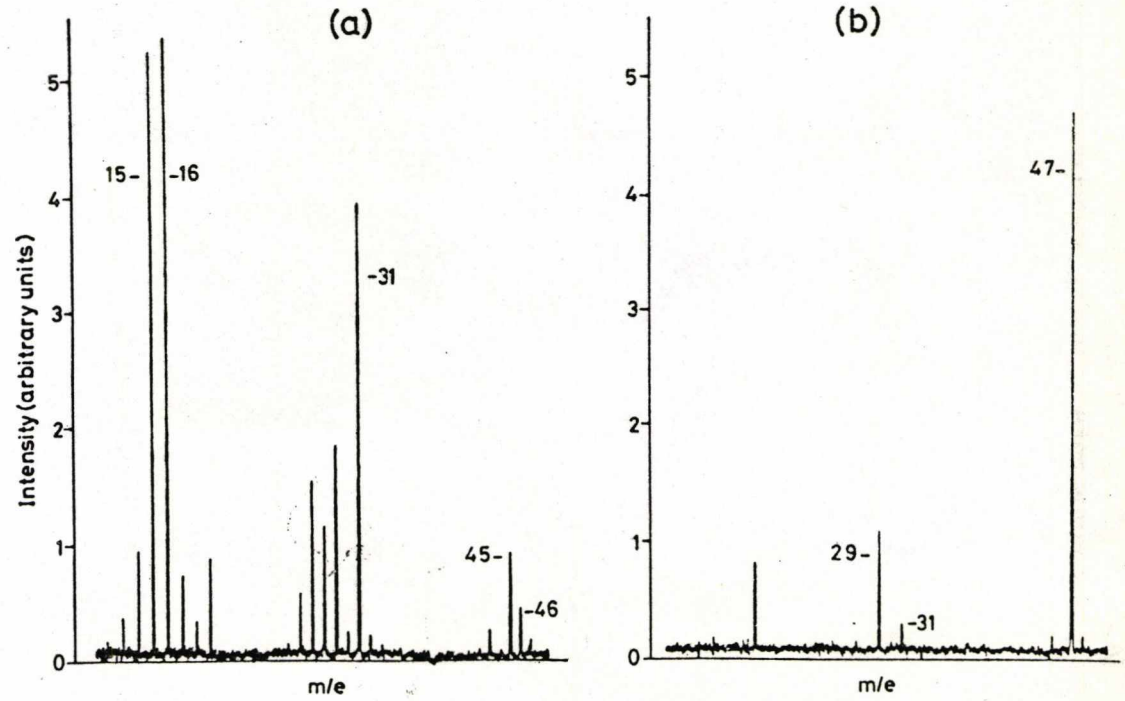

Figure 4.14b shows the mass spectrum of the same mixture recorded at 2 ms storage time. The peak at m/e 33 which accounts for 75% of the total ionisation in this mass spectrum is due to the protonated methanol ion $(M+1)^+$. Similarly for the methane-ethanol mixture the mass spectrum shown in Figure 4.15a is really a combination of the electron impact mass spectra of the two separate compounds but the mass spectrum recorded at 2 ms storage time has the ion at m/e 47 as the base peak which is assigned as the species $C_2H_5OH_2^+$. These spectra are similar to those obtained in the original work on the use of the Quistor as a low pressure CI ion source[69].

The performance of the Quistor with samples of higher molecular weight was initially quite promising. Figure 4.16a shows the zero storage (coincident ion creation and ion ejection pulses) mass spectrum of a 10:1 mixture of methane and butan-2-ol. Above m/e 20 this mass spectrum is similar to that obtained using a conventional electron impact ion source[147]. The low pressure CI mass spectrum recorded at 2 ms storage time shown in Figure 4.16b has its base peak at m/e 57 which corresponds to the alkyl fragment ion formed by the loss of a water molecule from the protonated parent ion. The low relative intensity of the $(M+1)^+$ ion at m/e 75 is typical of that for the CI mass spectra of secondary alcohols recorded under high pressure conditions[148]. However, an attempt to obtain the methane - low pressure CI mass spectrum of cyclohexanone resulted in a mass spectrum containing only a few low intensity ions with m/e values corresponding to those of the fragement ions present in the EI mass spectrum of this compound. No ions were observed with m/e values greater than *ca.* 80. The reason for this behaviour becomes clear after further consideration of the experimental limits of stability and storage efficiency which were discussed in Sections 3.4.1.1 and 3.4.1.3 respectively.

In Section 3.4.1.1 it was shown how the experimentally observed shifts in the stability boundaries limited the mass (i.e. m/e) range of

Figure 4.16 Mass Spectra of a 10:1 Mixture of Methane and Butan-2-ol Recorded at (a) zero and (b) 2ms Storage Time

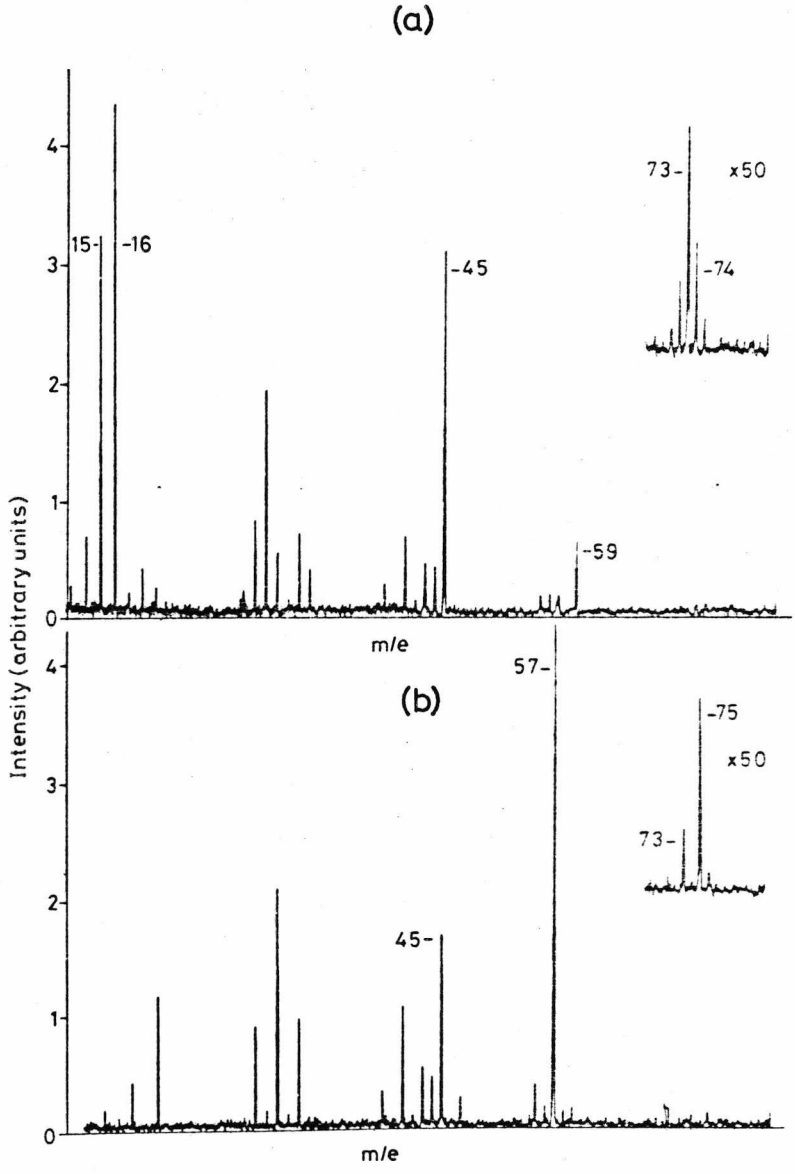

ions which could be stored simultaneously in the Quistor. Due to instrumental limitations the experimental stability limits could not be determined for the new Quistor at the operating frequency of 2.48 MHz. However, since these limits determined at the lower frequency of 0.8 MHz were found to be almost identical for both the new and the original Quistor (Section 4.3.2) it is reasonable to assume that they would be similar at the higher frequency of operation. Taking these limits as $q_z \simeq 0.1$ to 0.9 it is possible to calculate that the ion with the highest value of m/e that would be stable under the conditions employed for the above experiments (i.e. such that m/e 17 is stored at $q_z = 0.56$) is $17\times(0.56/0.1) = 95$. This suggests that the reason the low pressure methane CI mass spectrum of cyclohexanone could not be obtained under these conditions was because the quasi-parent ion of cyclohexanone at m/e 99 was unstable and therefore ejected from the trap almost immediately after its formation. From this it would appear that one possible remedy to this situation would be to increase the value of V_o such that the value of q_z associated with m/e 99 was greater than 0.1. However, since the storage efficiency is very low in the vicinity of the stability boundaries, for the practical purpose of storing a large number of ions, the useful range of q_z is reduced even further. Consequently, it would be necessary to increase the value of V_o such that the value of q_z associated with m/e 99 is *ca.* 0.2 but under these conditions the methane primary ions would be unstable. The useful range of q_z is limited further by the fact that it was found experimentally that the optimum conditions for obtaining low pressure CI mass spectra were when the reagent gas primary ions were stored at a value of q_z where the storage efficiency is a maximum, i.e. in the range $q_z = 0.5$ to 0.7.

In conclusion the use of methane as a low pressure CI reagent gas in the Quistor is limited to samples with a molecular weight of less than *ca.* 80. However, the low pressure CI mass spectra of samples with

higher molecular weights were obtained using other reagent gases as is discussed in the next section.

4.6.3 The Use of Propane as the Reagent Gas

The major ion-molecule reactions occurring in propane were briefly investigated using the Quistor/mass filter combination. As is shown in Figure 4.17 the major product ion after a storage time of 5 ms was $C_3H_7^+$ which is produced by the following hydride abstraction reactions of propane primary ions with propane molecules[149]:

$$C_2H_5^+ + C_3H_8 \longrightarrow C_3H_7^+ + C_2H_6 \qquad \text{R.4.5}$$

$$C_2H_4^+ + C_3H_8 \longrightarrow C_3H_7^+ + C_2H_5 \qquad \text{R.4.6}$$

The rate constants for these reactions determined from the data shown in Figure 4.17 are 8.4×10^{-10} cm^3 mol^{-1} s^{-1} and 4.6×10^{-10} cm^3 mol^{-1} s^{-1} respectively, in excellent agreement with values obtained by other workers who employed the space charge trapping technique[150].

If, for the purpose of low pressure CI studies, the applied r.f. potential V_o was set such that the ion $C_2H_5^+$ (m/e 29) was stored at a $q_z \simeq 0.7$, then the ion of highest m/e value that could be stored simultaneously would be $29\times(0.7/0.1)$ = m/e 203 where 0.1 is the assumed value for the lower stability limit. From this it was inferred that even after taking into account the further limitations on the useful range of q_z discussed in the previous section it should be possible to employ propane as the reagent gas for compounds with molecular weights considerably above the limit of 80 found for methane. This was confirmed by the mass spectrum shown in Figure 4.18 which is of a 200:1 (approximately) mixture of propane and cyclohexanone recorded at a storage time of 5 ms, a total pressure of 2×10^{-5} Torr and with the applied r.f. potential set at 600V p-p. The peak at m/e 99 is the quasi-parent ion $(M+1)^+$ which may

Figure 4.17 Plot Showing the Relative Intensities of the Major Ions in Propane as a Function of Storage Time

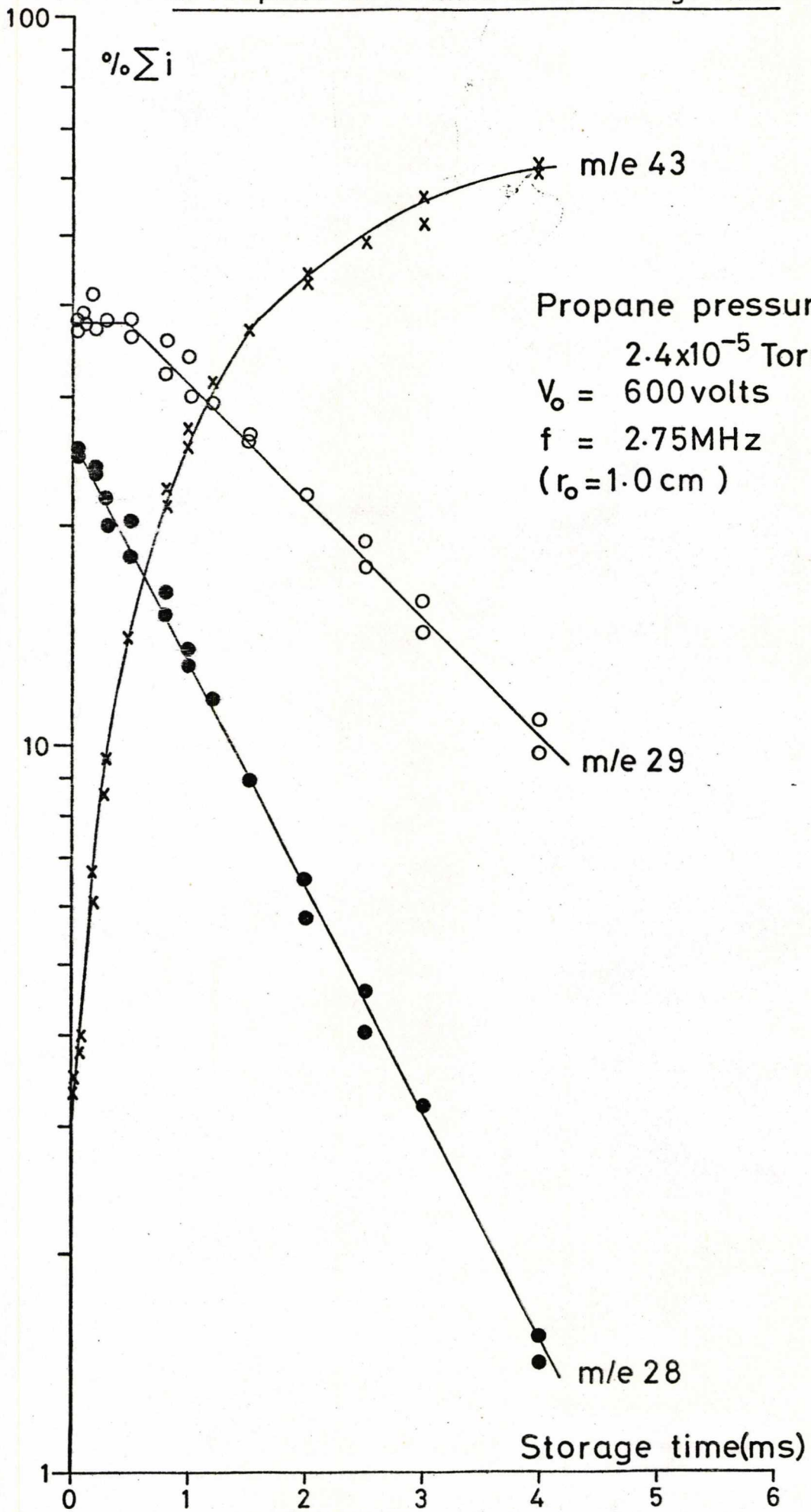

Figure 4.18 Mass Spectrum of a 200:1 Mixture of Propane and Cyclohexanone Recorded at 5ms Storage Time

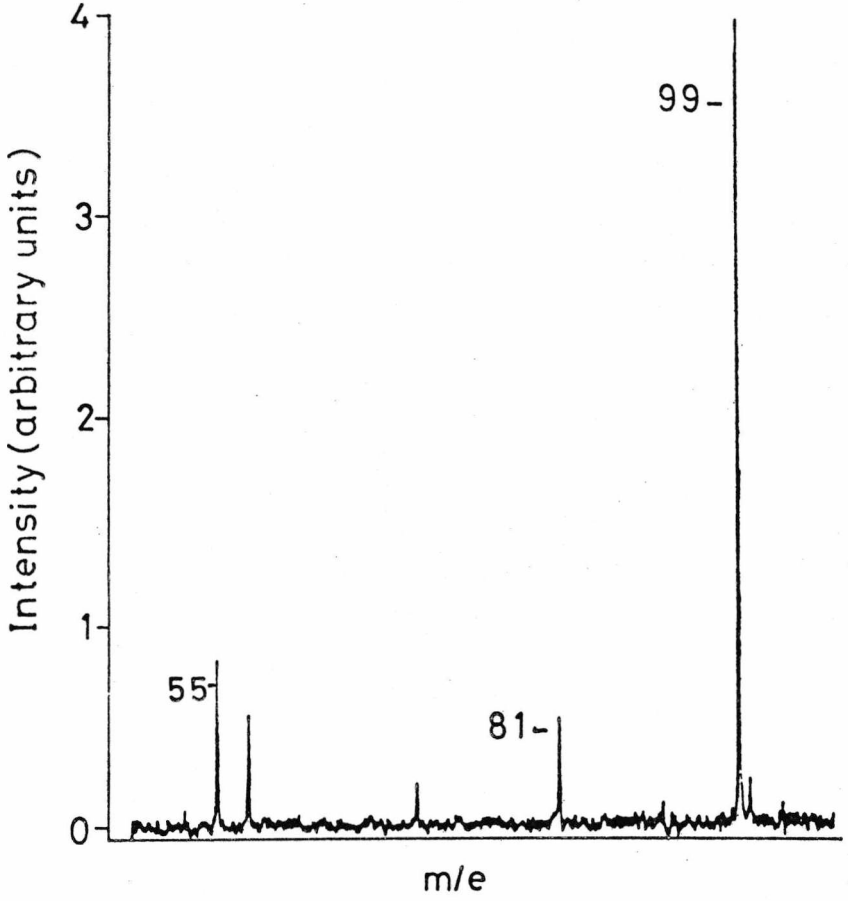

Figure 4.19 Mass Spectrum of a 200:1 Mixture of Propane and Benzaldehyde Recorded at 5ms Storage Time

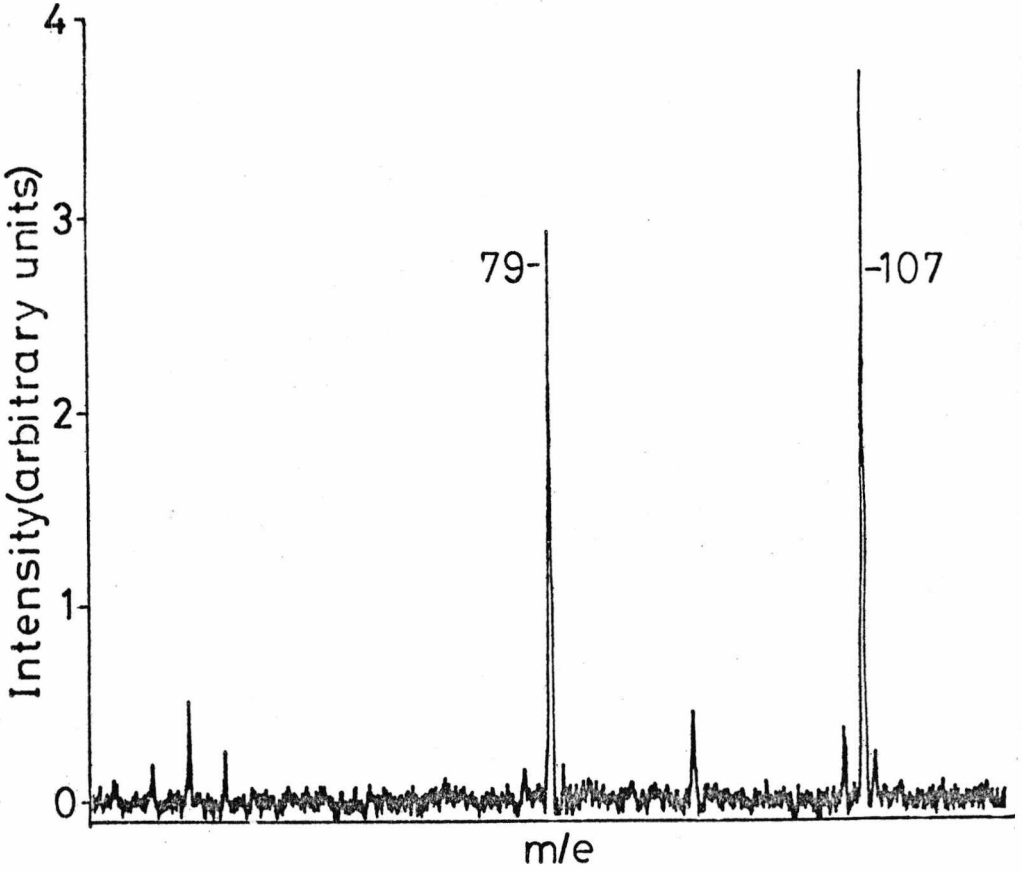

subsequently lose a water molecule to form the $(M+1 - H_2O)^+$ ion at m/e 81. The m/e values of the other ions in this spectrum correspond to some of those present in the EI mass spectrum of cyclohexanone. The major propane reagent ion $C_3H_7^+$ (m/e 43) constitutes 70% of the total ionisation in the ion storage mass spectrum of pure propane recorded under the above conditions, the remainder being made up of $C_3H_5^+$, $C_3H_3^+$ and $C_2H_5^+$. As a further example of the use of propane as a reagent gas, the low pressure propane CI mass spectrum of benzaldehyde is shown in Figure 4.19. This was recorded under identical conditions to those employed to obtain the mass spectrum shown in Figure 4.18. The base peak is at m/e 107 which corresponds to the quasi-parent ion of benzaldehyde $(M+1)^+$. This mass spectrum is discussed in more detail in Chapter 6 along with further examples of the use of the Quistor as a low pressure CI ion source with other reagent gases.

4.7 Conclusion

In summary the results presented in this chapter have established that:

(i) although the new and the original Quistors were of a different design the ion storage characteristics are very similar;

(ii) the new Quistor functions correctly as an ion storage source for the MS9;

(iii) in order to fix the relative intensities of the reagent ions it is necessary to hold both the pressure and the amplitude of the r.f. potential constant;

(iv) it is possible to obtain low pressure CI mass spectra with the Quistor/MS9 combination but the use of methane as a reagent gas is limited to samples with molecular weights below *ca.* 80;

(v) ideally, the Quistor should be operated such that the reagent gas primary ions are stored at a q_z of 0.5 to 0.7.

CHAPTER 5

THE MODIFICATION OF A MAGNETIC SECTOR MASS SPECTROMETER TO OPERATE IN THE HIGH PRESSURE CHEMICAL IONISATION MODE

5.1 Introduction

This chapter describes the design and construction of the parts required to modify an AEI MS9 double focusing mass spectrometer to permit its operation in the high pressure CI mode, and the performance of the modified instrument as a CI mass spectrometer. The general instrumental requirements, and the modifications necessary, to operate a mass spectrometer in the high pressure CI mode have been described in detail in Chapter 2. For the MS9 the necessary modifications may be divided into four sections:

1. The replacement of the existing source pumping system with one of higher capacity, to permit differential pumping of the source and analyser regions.
2. The construction of a gas-tight ion source capable of operating at an internal pressure of *ca.* 1 Torr.
3. The construction of a combined reagent gas/sample inlet system.
4. The uprating of the electron energy supply and the conversion from trap to emission control of the filament.

5.2 Instrumental Modifications

5.2.1 The Vacuum System

The modifications to the MS9 source pumping system described in this section were designed by Dr. J.M.B. Bakker of Shell Research Ltd.

and were implemented before the commencement of this project.

The standard MS9 source pumping system consists of a 130 $l\ s^{-1}$ vapour diffusion pump, with a liquid nitrogen cold trap, backed by a 1 $l\ s^{-1}$ rotary pump. The source envelope is pumped through a small aperture which results in an overall pumping speed at the ion source of only 22 $l\ s^{-1}$. Approximate calculations show (see Section 5.2.2.1) that because of the relatively high gas flow rates from a typical CI ion source a pumping speed of over 100 $l\ s^{-1}$ is required in order to keep the pressure in the source envelope down to a workable level. It was therefore necessary to uprate the source pumping system and also to increase the conductance between this and the ion source. The new system is shown schematically in Figure 5.1. The pumping aperture in the source housing was enlarged from 2.5 to 7.5 cm in diameter. A length of 7.5 cm O.D. stainless steel tube was argon-arc welded at one end to the enlarged pumping aperture and at the other end to a length of 10 cm O.D. stainless steel tube. One end of the latter tube was blanked off and the other welded to a 15 cm flange for connection to the pumping stack. The new pumping system consisted of an Edwards 10 cm E04 oil vapour diffusion pump with an Edwards NTM4 liquid nitrogen cold trap and an Edwards QSB4 quarter swing butterfly valve. The stack was surmounted by a 5 cm spacer and bolted directly to the 15 cm flange. Two ionisation gauge heads were incorporated into the system, one mounted directly opposite the source pumping aperture and the other above the butterfly valve. The diffusion pump was backed by an Edwards ES200 rotary pump and the two were connected via the original AEI 1.25 cm O.D. backing line which also serves the analyser diffusion pump. The manufacturer's specification for this pumping system is 150 $l\ s^{-1}$ for air at the top of the stack. Taking into consideration the conductance of the tubing connecting this to the source housing the overall pumping speed at the ion source was estimated at 125 $l\ s^{-1}$.

The design of the MS9 is such that only a small pin hole connects

Figure 5.1 Schematic Diagram of Source Vacuum System

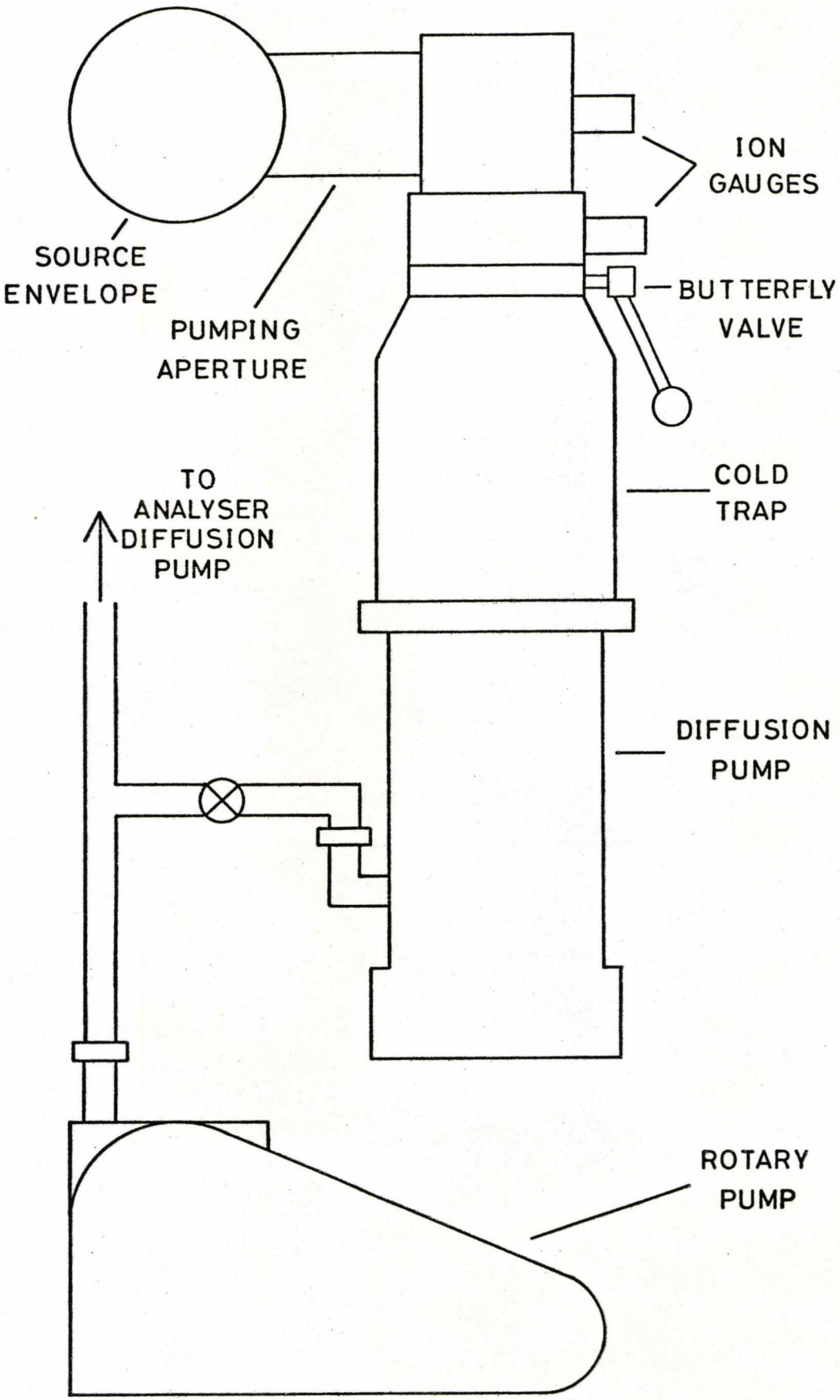

the source and analyser vacuum regions. Consequently no modification of either the analyser or its pumping system was required.

5.2.2 The Design and Construction of the Ion Source

5.2.2.1 Basic Design Considerations

In designing the high pressure CI ion source one of the first decisions to be made was whether to construct a single purpose CI ion source or a combined CI/EI ion source. Since this work involved the comparison of high and low pressure CIMS, it was decided that a single purpose CI ion source would be constructed as this would allow a more representative comparison of the two techniques. If EI mass spectra were required the standard EI ion source could be installed and operational within three hours.

A very important factor in the design of the ion source was the selection of the dimensions of the electron entrance hole and ion exit slit. These should be made as large as possible for optimum ion source sensitivity but in practice the total area of these apertures is limited by the capacity of the source pumping system. For the MS9 the pressure in the source envelope must not be allowed to rise above 5×10^{-4} Torr under normal operating conditions and since the estimated pumping speed of the new pumping system was 125 $l\ s^{-1}$ the maximum permissible gas flow rate from the ion source was 0.0625 Torr $l\ s^{-1}$. In many commercial CI ion sources the dimensions of the source apertures are 0.03 cm diameter and 0.5×0.005 cm respectively. It is possible to calculate approximately an upper limit to the rate of gaseous effusion from such an ion source as follows:

The total aperture area is:

$$(0.005\times0.5) + \pi(0.015)^2\ cm^2$$

$$= 0.0032\ cm^2$$

The number of molecules striking unit area in unit time can be calculated

from the kinetic theory:

$$N = 1/4\ N_D\ \bar{\nu}$$

where N_D is the number density of the gas and $\bar{\nu}$ is the average velocity of the molecules. Assuming that the back pressure outside of the ion source is negligible, the rate of volume flow out of a unit area aperture i.e. the conductance, is $1/4\ \bar{\nu}$. Since for nitrogen at $288^{\circ}K$ $\bar{\nu} = 4.6 \times 10^4$ cm sec^{-1}, the gas flow rate from the ion source at an internal pressure of 1 Torr is

$$\frac{1 \times 0.0032 \times 4.6 \times 10^4}{4 \times 1000}$$

$$= 0.037 \text{ Torr } l\ s^{-1}$$

As this is well within the maximum permissible flow rate for the MS9 with the new pumping system the above aperture dimensions were adopted for the ion source designed for this work.

Another important factor in the design of the ion source was the distance between the centre of the electron beam and the ion exit slit as set by the position of the electron entrance hole in the ion chamber wall. If this distance is too short, then ions formed near the centre of the electron beam will not undergo a sufficient number of ion-molecule collisions for CI purposes, before drifting out of the ion exit slit under the combined influence of the electric fields produced by the repeller potential and penetration of the accelerating potential. Conversely if this distance is too long ions formed near the electron beam may diffuse towards the ion chamber walls and not reach the ion exit slit. Since the exact form of the electric field inside an ion source is very difficult to evaluate and calculations concerned with ion drift and residence times in CI ion source are prone to large errors, it was impossible to calculate an ideal value for this distance and so a value

Figure 5.2 Drawing of the Ion Source Block

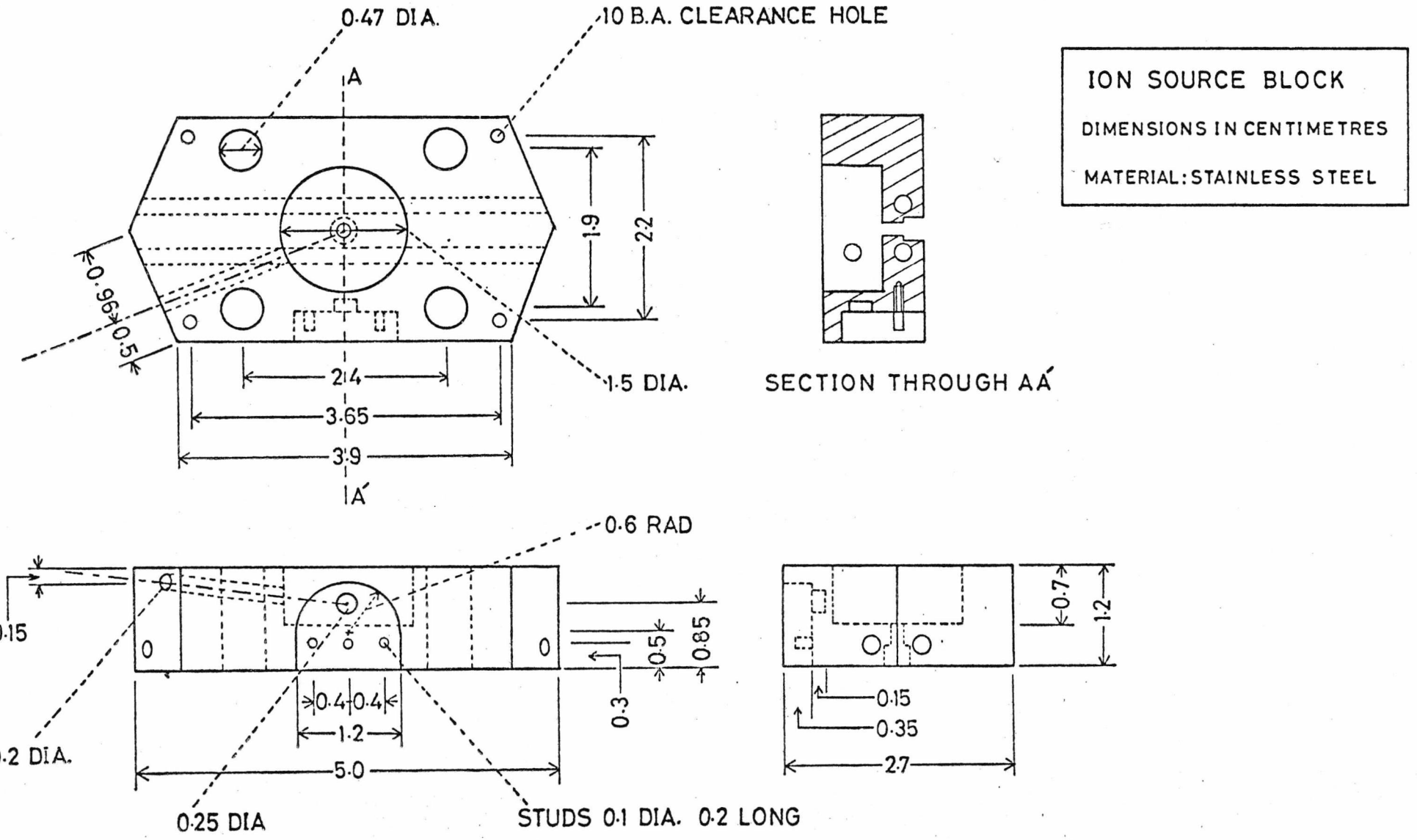

of 0.35 cm was chosen which is in fact an average of various literature values.

The ion source was designed such that it had the same external dimensions as the standard AEI EI source block. In this way the new CI source block could be mounted using standard AEI source mounting components. For purposes of description the ion source may be divided into two parts: the source block which includes the repeller electrode and ion exit plate, and the electron gun.

5.2.2.2 The Source Block

For ease of machining the source block, a dimensioned drawing of which is shown in Figure 5.2, was designed with a circular ion chamber. A recess was provided for the electron gun with two studs to facilitate its alignment. No provision was made for a trap electrode since the ion source was not intended for EI operation. Four alignment holes were drilled through the source block such that the standard AEI source alignment jig could be used to align the new CI ion source. Besides the electron entrance hole the only other apertures in the ion chamber wall were the electrical feedthrough for the repeller and the sample/reagent gas inlet port. The latter aperture was drilled such that it was pitched at an angle of 8.5° to the horizontal plane of the source block. This ensured that the sample/reagent gas mixture was directed toward the central axis of the electron beam at the centre of the ion source. Two holes were drilled through the length of the source block both parallel to the longitudinal axis, into which standard AEI ion source heaters were inserted. The entire source block was machined from stainless steel.

The repeller electrode was constructed from a circular stainless steel plate which was spot-welded to a tapped 10 B.A. rod. This was inserted through the hole in the source block from which it was electrically insulated by two Rulon spacers as shown in Figure 5.3. When the

Figure 5.3 Detail of Repeller Mounting

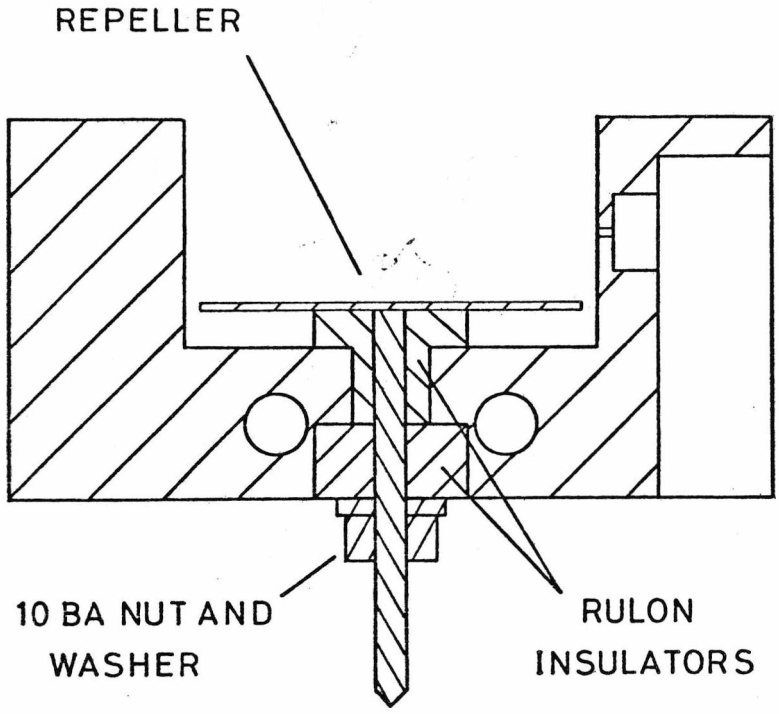

Figure 5.4 Drawing of Ion Exit Plate

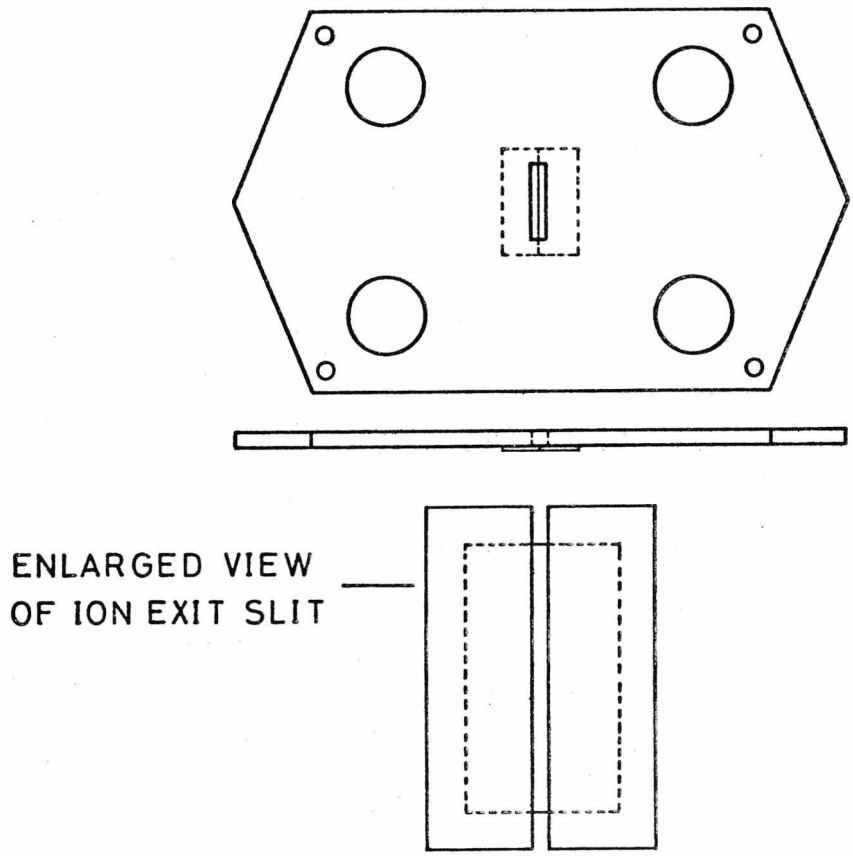

Figure 5.5 Three Dimensional View of Source Block and Ion Exit Plate

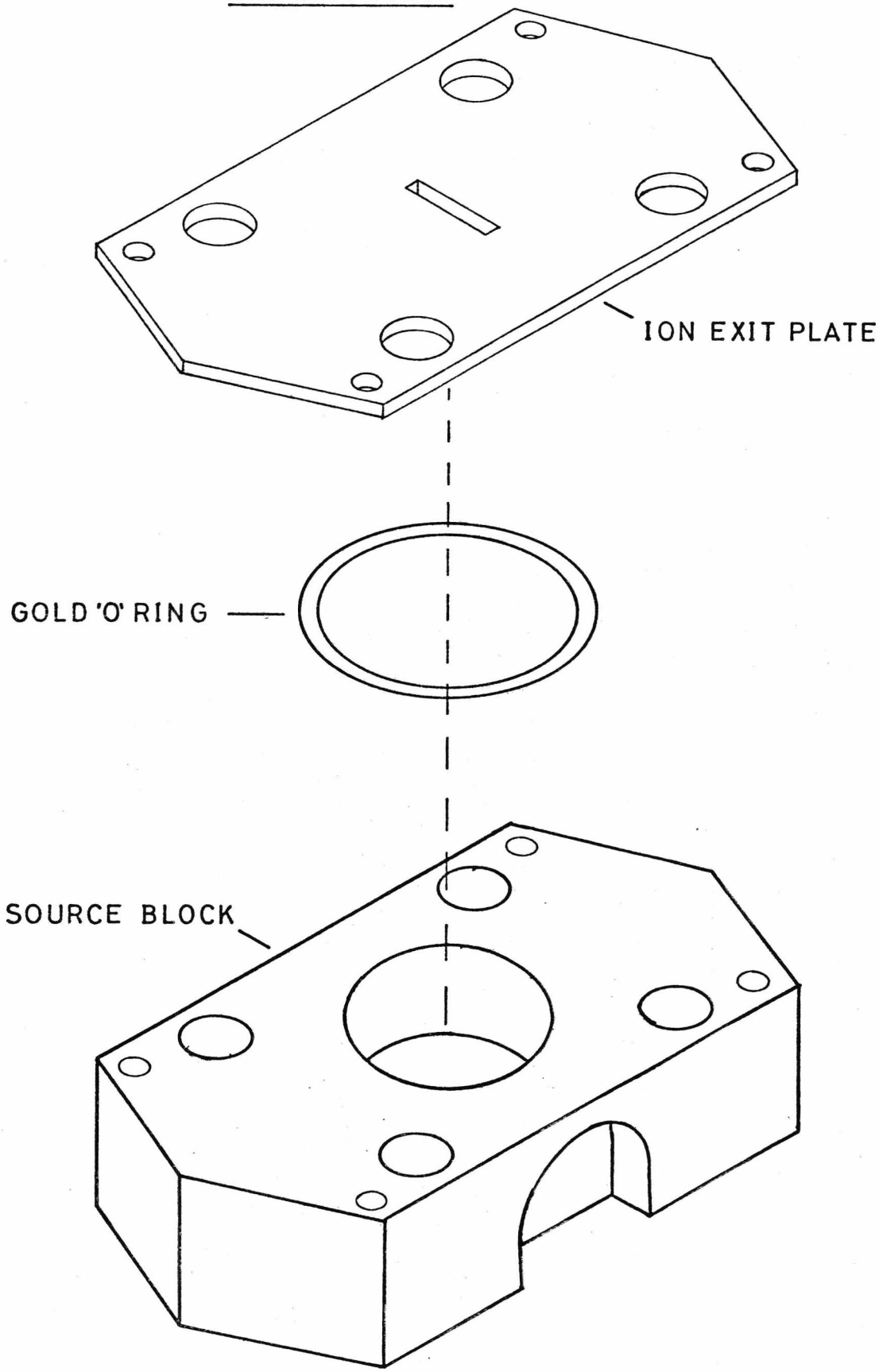

10 B.A. nut is tightened the repeller feedthrough is essentially gas-tight. Above operating temperatures of 280°C the Rulon spacers had to be replaced with ones made from boron nitride.

The top of the ion chamber was 'closed' with an ion exit plate constructed from 0.1 cm stainless steel sheet as shown in Figure 5.4. The very narrow exit slit was formed by firstly spark eroding a 0.5×0.1 cm slit through the plate and then over this, spot welding two pieces of 0.0125 cm thick stainless steel sheet such that there was a gap of 0.005 cm between them as shown in the enlarged inset in Figure 5.4. In order to make a gas tight seal between the top of the ion source block and the underside of the ion exit plate both surfaces were ground with carborundum paste on a flat glass plate until highly polished. The two were then bolted together with a 0.005 cm thick gold 'O' ring placed between them as shown in Figure 5.5.

5.2.2.3 The Electron Gun

The electron gun was designed to include a total emission collector such that the filament could be controlled with reference to the emission current rather than the trap current, since the latter mode of control is unreliable for CI ion sources. An exploded diagram of the complete electron gun appears in Figure 5.6. Electrical insulation between the baseplate and the total emission collector was provided by a thin piece of mica sheet. The filament support rods were sandwiched between two ceramic spacers and secured to the baseplate with two 10 B.A. screws. The assembly was shaped such that it fitted into the recess in the source block and was held in place by a single 10 B.A. screw. Filament alignment was achieved simply by lining the filament up with the centre of the hole in the baseplate prior to attaching the electron gun to the source block. The alignment studs on the source block ensured that when the electron gun was in position the filament was in exact alignment with the electron entrance hole.

Figure 5.6 Exploded Diagram of the Electron Gun

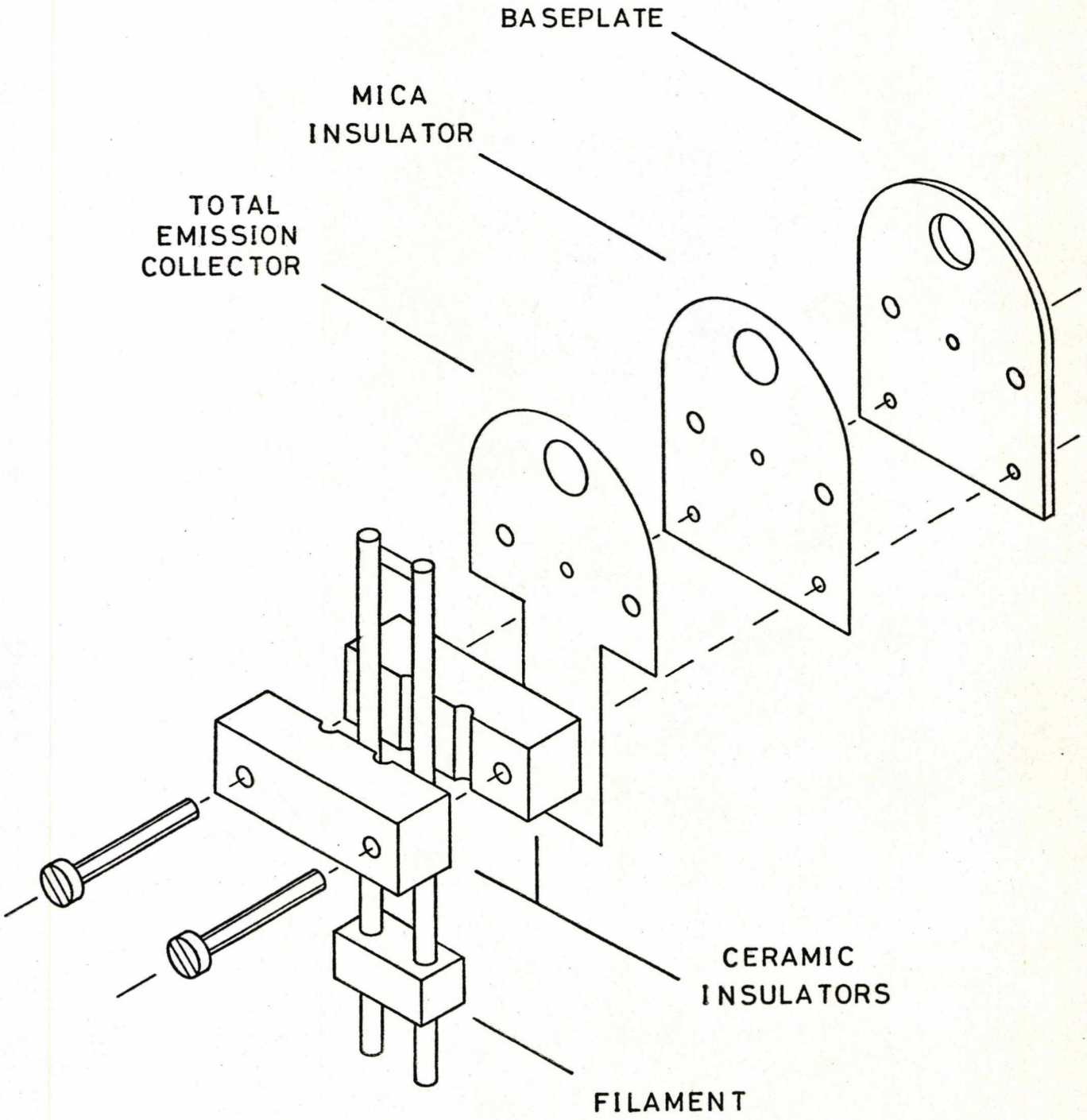

5.2.2.4 Assembly and Alignment of the Ion Source

Before assembly all ion source components were subjected to scrupulous cleaning using normal ion source cleaning procedures. Since the CI ion source block was mounted using standard AEI source mounting components the order of assembly was identical to that for a standard EI ion source. It was essential ensure that the gold 'O' ring was arranged concentrically around the lip of the ion chamber before the ion exit plate was secured in place. The entire ion source assembly was mounted on a source endplate which had provision for water cooling of the ion source, and was aligned using the standard AEI source alignment jig. All electrical connections were the same as for the EI ion source except that the 'trap' wire was connected to the total emission collector. A specially constructed probe guide was push-fitted into the sample/ reagent gas inlet port (described in Section 5.2.3.1). A photograph of the assembled high pressure CI ion source is shown in Figure 5.7.

5.2.3 The Inlet System

The introduction of both the sample and the reagent gas into a CI ion source must be achieved in such a way as to maintain its 'gas tightness'. However, any gas tight connection between the CI inlet system and ion source must also be easily demountable to permit ion source removal for cleaning and maintenance. As none of the standard MS9 sample introduction systems could be mated directly to the ion source, they were unsuitable for CI purposes and so it was decided to construct a completely separate inlet system for the CI ion source. In order to minimise the probability of leaks in the ion source, the inlet system was designed such that the reagent gas and the sample were introduced through a single inlet port. The new CI inlet system consists of two basic components : a specially modified direct introduction solid sample probe, and a reagent gas flow control system.

Figure 5.7 Photograph of Assembled Ion Source

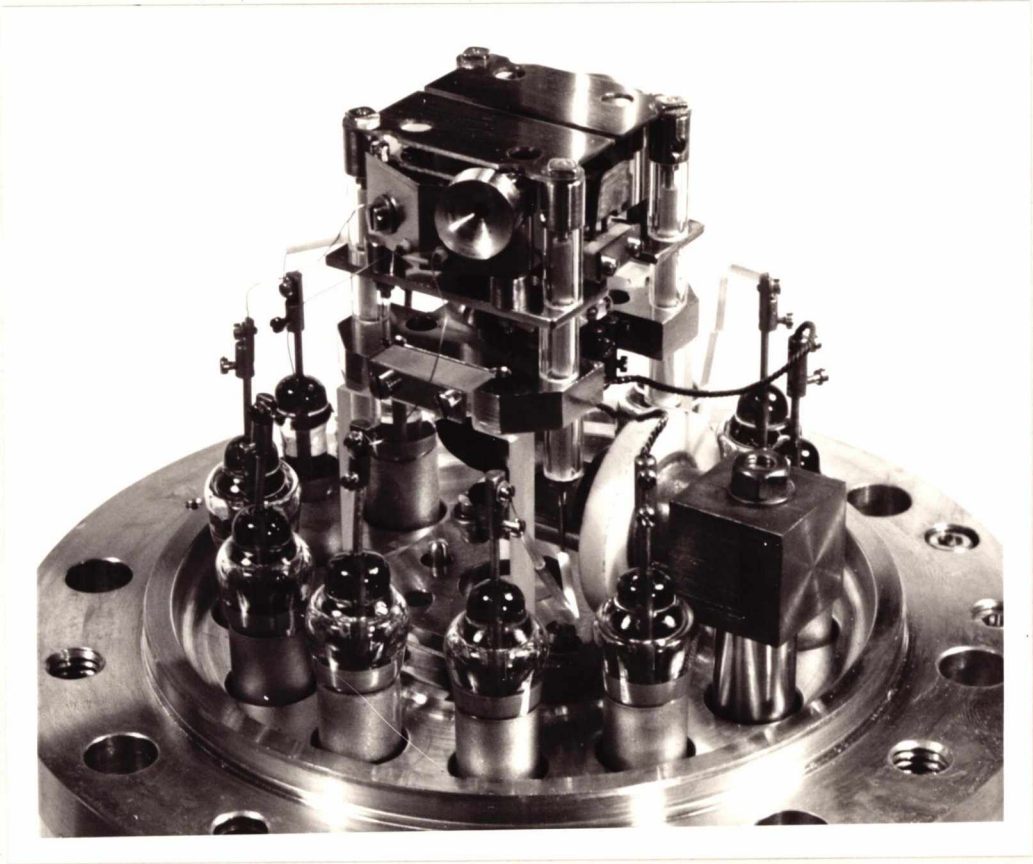

5.2.3.1 The Combined Sample and Reagent Gas Introduction Probe

The probe was designed to be introduced into the source vacuum region via the MS9 probe vacuum lock and is similar to that described by Garland *et al*[20] in that it is based on an AEI concentric direct insertion probe. A drawing of the assembled probe is shown in Figure 5.8. The stainless steel shaft was fitted at one end with a fluted Teflon support disc and to the other end a Cajon 4UTA6-BT vacuum coupling was welded. Two rectangular sections were machined from the chromium plated brass handle to permit adjustment of the Cajon coupling. A piece of 0.7 cm O.D. Pyrex glass tubing was passed through the length of the probe and terminated at one end with a 1.2 cm diameter Pyrex glass ball. This ball was ground together with a spherical stainless steel probe guide, which is attached to the inlet port on the ion source as shown in Figure 5.9 in order to make an efficient gas tight seal between inlet system and ion source. A 0.25 cm O.D. Pyrex glass rod was passed through the centre of the glass tube. This was fitted at one end with a small steel spring and the other end was attached to a piece of 'soft' iron via a Teflon sleeve. By altering the position of the probe magnet this rod could be made to move along the probe shaft such that the sample which was placed in a sample cup attached to the steel spring, could be introduced directly into the ion source.

In order to protect the reagent gas flow control system from electrical discharges of the type discussed in Chapter 2, a small leak constructed from an orifice plate was placed in the handle end of the Pyrex tube, an enlarged section of which is shown in Figure 5.10. From similar considerations to those described in Section 5.2.2.1 it was calculated that at the expected flow rate the size of orifice required to maintain a pressure differential of 50:1 between the reagent gas flow control system and the ion source was 0.003 cm diameter. In this way the pressure on the high pressure side of the leak could be kept at above 50 Torr in the region where electrical discharge cannot be sustained.

Figure 5.8 Drawing of the Probe Assembly

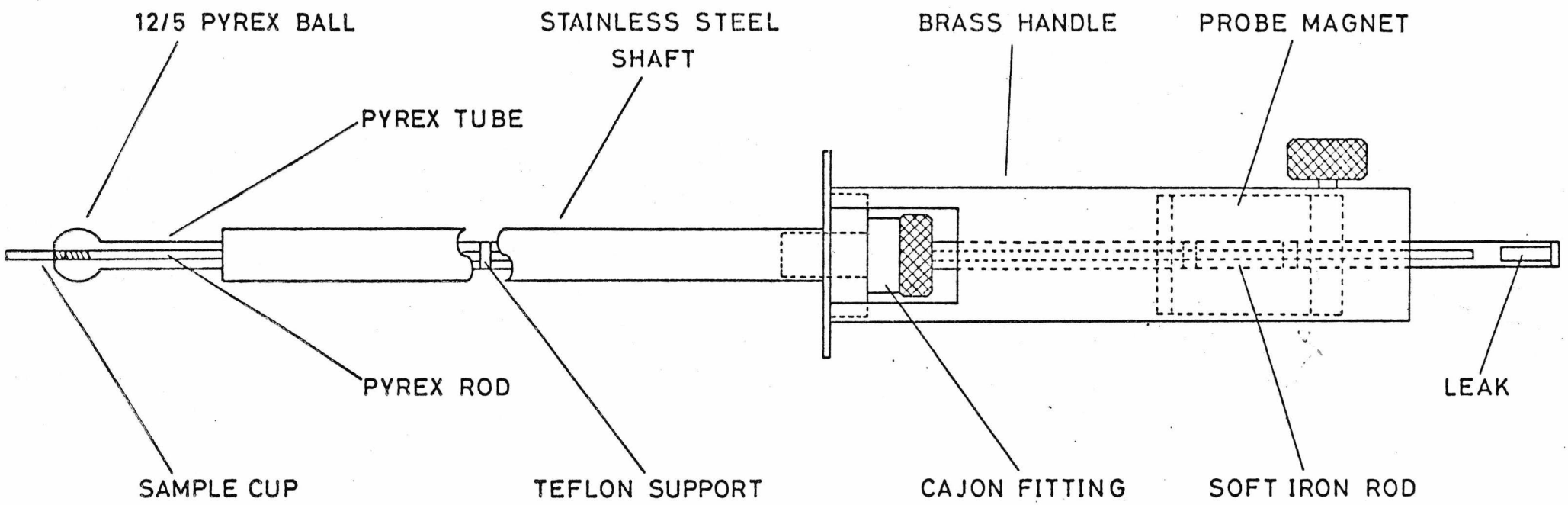

Figure 5.9 Detail of the Ion Source -Probe Mating

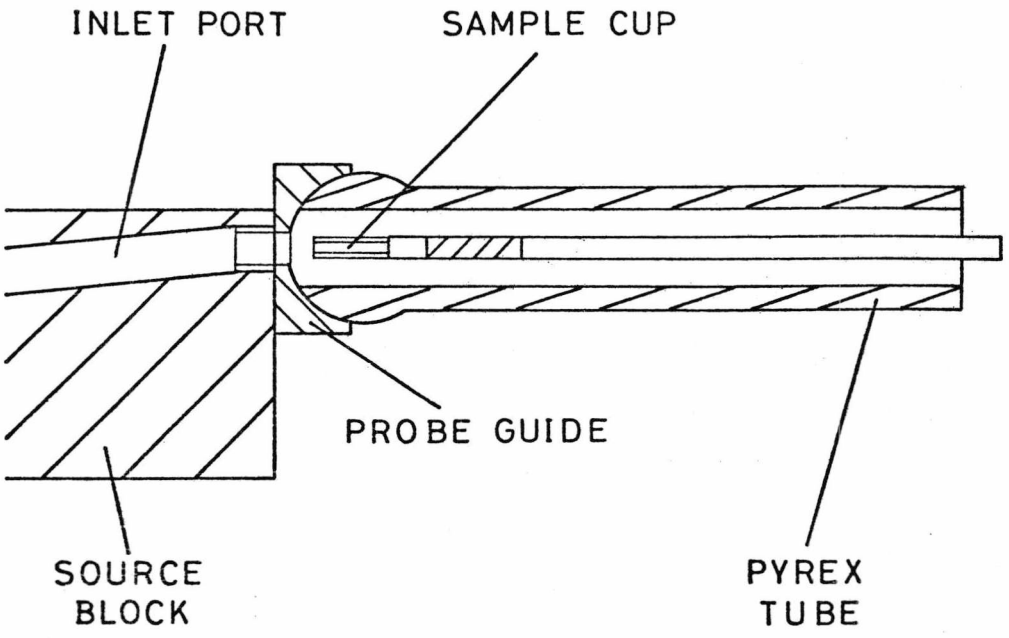

Figure 5.10 Section through the End of the Probe

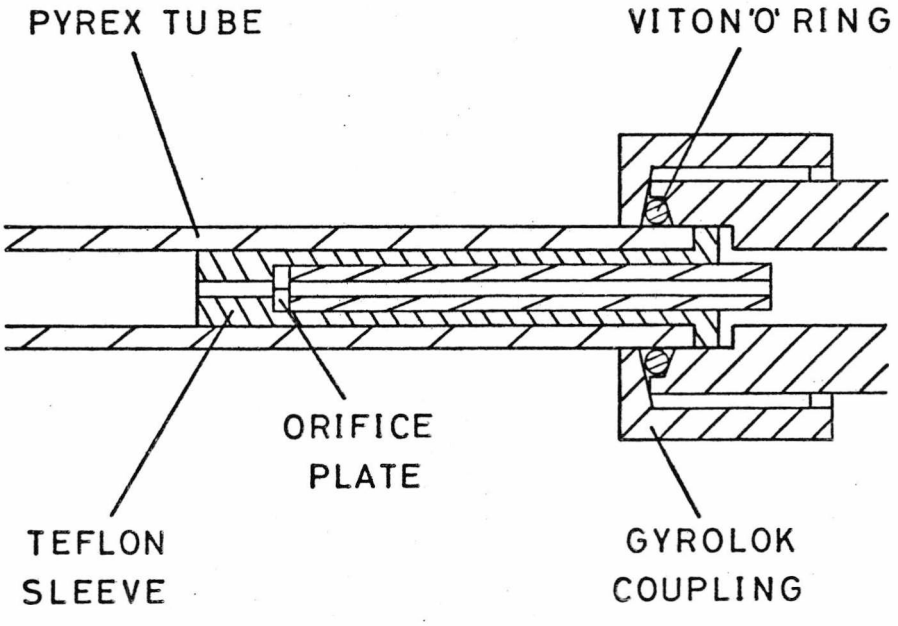

The leak was sealed into the Pyrex tube using a drilled-out Gyrolok coupling and a Viton 'O' ring. The other end of the coupling was connected to a piece of Teflon tubing which was attached to the reagent gas flow control system.

5.2.3.2 The Reagent Gas Flow Control System

Since the relative concentrations of reagent ions in a CI ion source may vary considerably with reagent gas pressure, it was essential to be able to control the pressure of the reagent gas in the ion source such that it could be kept constant over a long period of time. This was achieved, using the system shown schematically in Figure 5.11, simply by controlling the flow rate of reagent gas into the ion source through the probe.

The reagent gas, supplied from a lecture bottle fitted with a single stage regulator, was introduced on the high pressure side of the Matheson model 49 vacuum regulator. This could be preset to maintain the pressure in the 3 litre reservoir to any value between 0 and 760 Torr. The flow of reagent gas through the probe was controlled by metering valve 5 and the pressure at this point was monitored by an Edwards CG3 capsule gauge. The reservoir and probe could be evacuated independantly, using valves 2 and 4 respectively, which were connected to the MS9 inlet system rotary pump. Volatile samples and additional reagent gases could be introduced via metering valve 3 which was connected to the standard AEI cold inlet system. All valves were Hoke types D3212 G4Y (throttling) and 1315 G4Y (metering) made of stainless steel and fitted with 0.6 cm Gyrolok couplings. Interconnections between these valves were made with 0.6 cm O.D. stainless steel tubing.

5.2.4 Electronic Modifications

In order to operate the MS9 in the CI mode two simple modifications to the source supply chassis were necessary : the uprating of

Figure 5.11 Schematic Diagram of the Reagent Gas Flow Control System

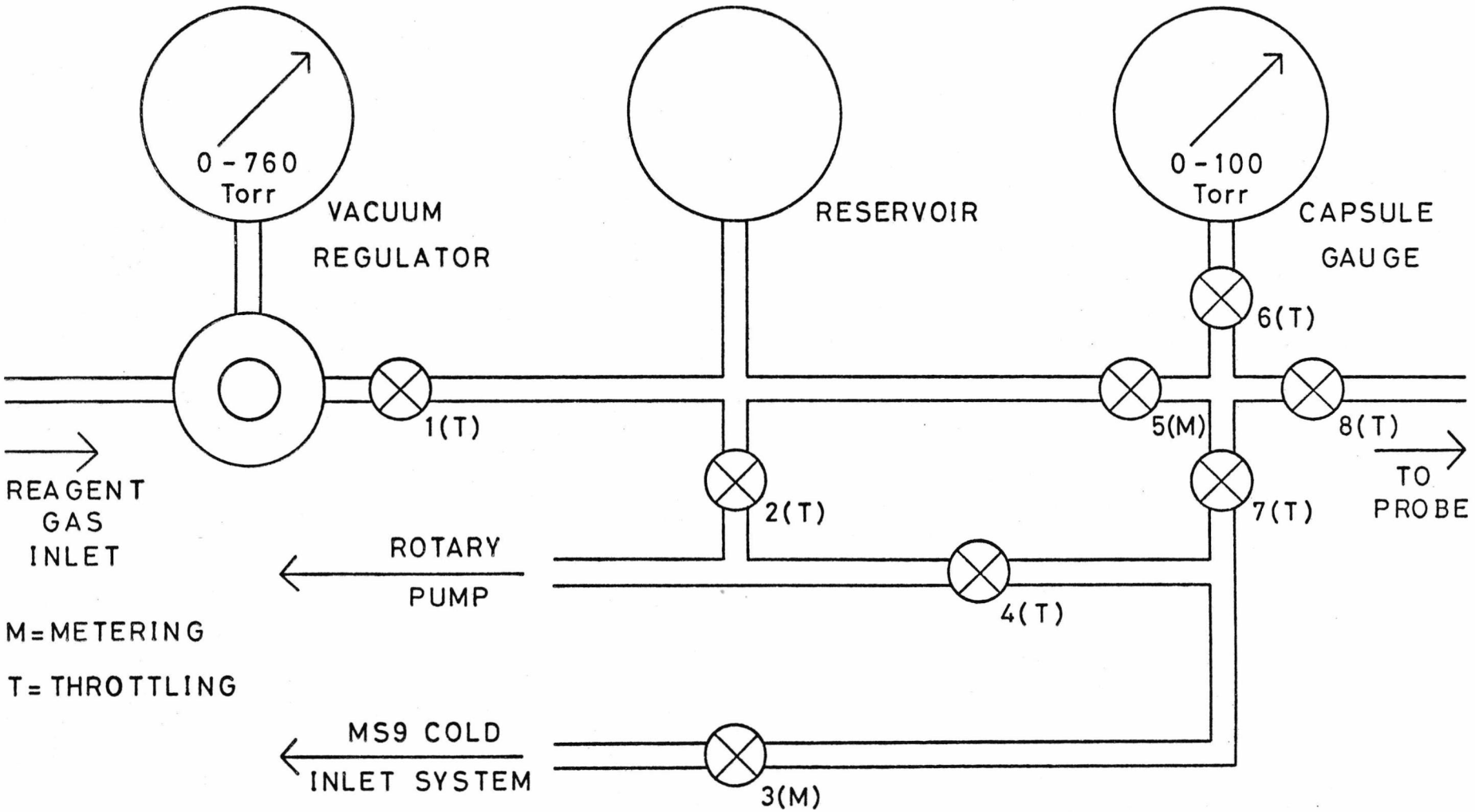

the electron energy supply and conversion from trap to total emission stabilisation of the filament current.

The maximum available electron energy was increased by incorporating a floating 420V power supply into the source supply chassis. The output of this supply could be varied in 68V steps, and was wired in series with the existing 0 → 80 eV electron energy supply such that for operation in the CI mode the electron energy was continuously variable in the range 0 → 500 eV. An additional position on the electron energy meter switch was provided so that the electron energy could be monitored over this range.

The conversion from trap to emission control of the filament current was achieved by firstly changing the trap potential, which is normally fixed at a value of +60V with respect to the source block, such that it was variable in the range 0 → ±25V. This was derived from a potential divider in the source supply chassis. Secondly, the wire normally attached to the trap electrode was connected to the total emission collector on the new electron gun. The filament was then controlled with reference to the electron current collected by the total emission collector and by varying the potential on this electrode it was possible to focus the electron beam on to the small electron entrance aperture.

These modifications were implemented in such a way that it was possible to change all of the necessary potentials from the EI to the CI configuration in one simple switching operation.

5.3 The Operation of the MS9 in the Chemical Ionisation Mode

5.3.1 Installation of the Ion Source and Inlet System

The procedure for installing the new CI ion source was identical to that for the exchange of any two EI ion sources since it was mounted on a standard MS9 source endplate. The installation could be completed and the source region evacuated to 1.0×10^{-6} Torr in less than two hours but for reasons discussed in Section 5.4.1, the system could not be operated satisfactorily until the ion source had been baked for

several hours.

In order to ensure that no leaks occurred between the probe guide on the ion source and the probe, its length was carefully adjusted in the following manner. The Cajon fitting (Figure 5.8) was loosened and the Pyrex tube retracted such that the Pyrex ball was adjacent to the stainless steel shaft. The probe was then inserted through the probe vacuum lock in the normal way and the Pyrex tube pushed towards the ion source until the probe guide cup and Pyrex ball were tightly mated together. The Cajon fitting was then re-tightened.

The reagent gas flow control system was installed by making a vacuum connection between this and the MS9 inlet system rotary pump, and connecting the required reagent gas supply to the Matheson gas regulator.

5.3.2 Pressure Calibration

For CI studies it is essential to have a knowledge of the pressure inside the ion source. Since no direct means of ion source pressure measurement was available this was determined indirectly by pre-calibrating the source region ionisation gauge against a known pressure of a particular reagent gas in the ion source as measured by a McLeod gauge. This was accomplished by removing both the pyrex rod and the leak from the probe and attaching a T-piece to the top end of the pyrex tube. One side arm of the T-piece was connected to a McLeod gauge and the other to the reagent gas flow control system. The calibration was performed by inserting the probe and recording the pressure measured by both the ionisation and McLeod gauges for various fixed values of the reagent gas flow rate.

A pressure calibration graph for methane obtained by the above method is shown in Figure 5.12(a), from which it was determined that in order to operate at an ion source pressure of 1 Torr it would be necessary to increase the methane flow rate until the pressure indicated by the ionisation gauge was *ca.* 3×10^{-4} Torr. The pressure in the analyser region,

Figure 5.12 Pressure Calibration Graphs for Methane

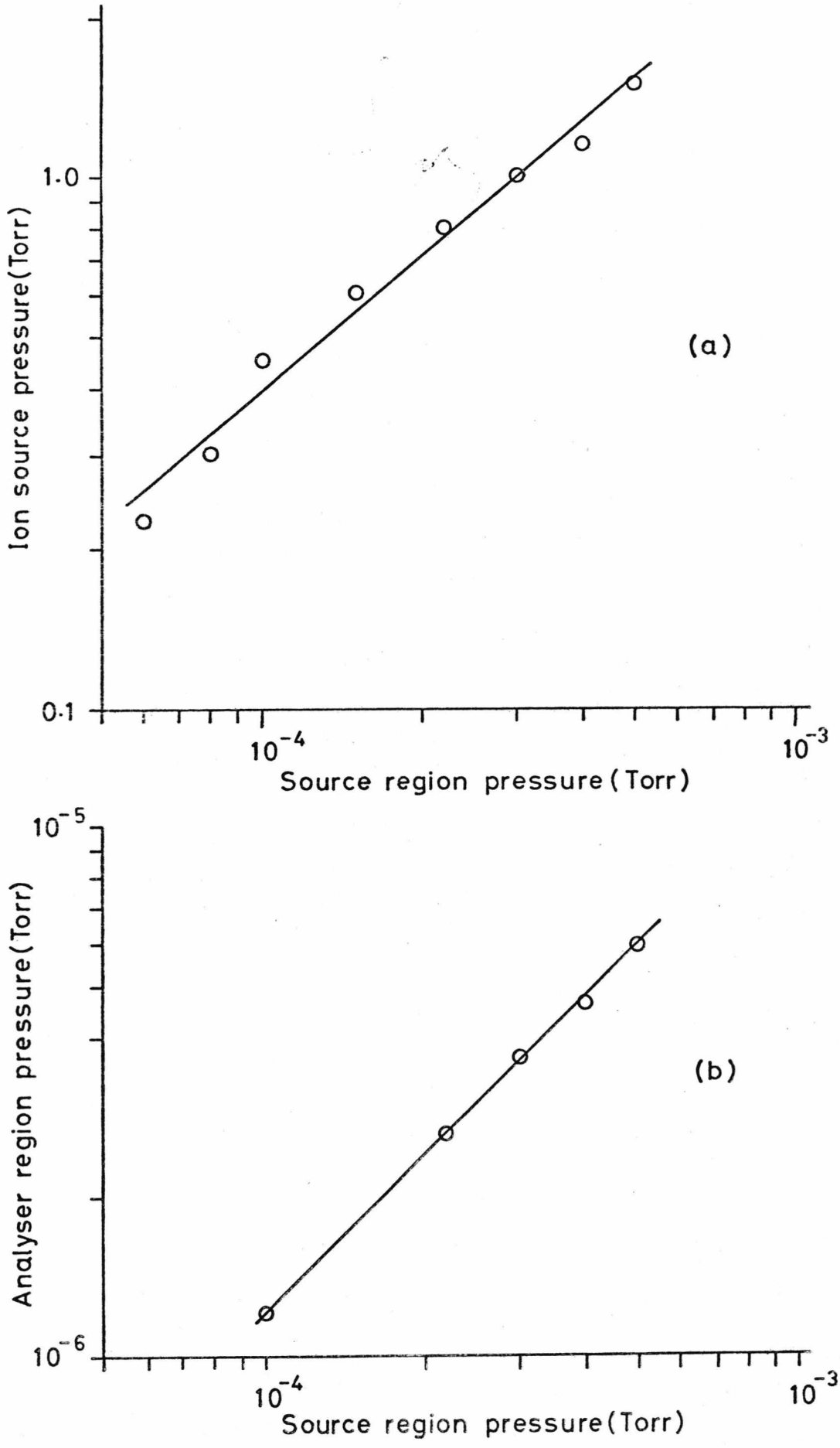

which was recorded simultaneously with the calibration for methane, was always a factor of *ca.* 100 times lower than the pressure in the source region as shown in Figure 5.12(b). Since the sensitivity of an ionisation gauge is dependent on the nature of the gas in which it is employed for pressure measurement, the calibration procedure had to be repeated for each reagent gas used.

One source of error in this method of determining the pressure in the ion source arose due to the fact that the reagent gas was actually flowing during the calibration and therefore there was a pressure drop between the top of the Pyrex shaft and the ion source. However, considering the internal diameter of the Pyrex shaft and the slow gas flow rate the error from this source was thought to be small compared to, for example, the error in reading the McLeod gauge which was ±0.05 Torr; taking into consideration other sources of error all ion source pressure measurements were subject to a total error of ±0.1 Torr.

The gas flow rate through the ion source was measured by inserting the probe and connecting a soap-bubble flow meter to the high pressure inlet of the Matheson gas regulator in place of the reagent gas supply. At a pressure of 5.0×10^{-5} Torr in the source region this was determined as 4 atm mls $min^{-1} \equiv 0.05$ Torr l s^{-1} which is very close to the value predicted in Section 5.2.2.1.

5.3.3 Method of Sample Introduction

The introduction of solid and involatile liquid samples was achieved by first placing them in a standard capillary sample tube and attaching this to the lower end of the Pyrex rod in the probe shaft. The Pyrex rod was then retracted, using the probe magnet until it was inside the probe shaft. The probe was inserted through the vacuum lock such that it mated tightly with the ion source and the sample tube lowered, again using the probe magnet, such that it was in contact with the sample introduction port on the ion source. The Matheson gas regulator was

adjusted such that the pressure of reagent gas in the reservoir was 100 Torr. Valve 8 on the reagent gas flow control system was then opened and the flow rate adjusted using Valve 5 until the required ion source pressure was attained. For methane an ion source pressure of 1 Torr (i.e. 3×10^{-4} Torr indicated on the source region ionisation gauge) corresponded to a pressure of *ca.* 65 Torr indicated on the capsule gauge.

The procedure for the introduction of volatile liquids was similar, except that these were placed in the reservoir of the MS9 cold inlet system and introduced via Valve 3 of the reagent gas flow control system.

Since the probe itself could not be heated the rate of evaporation of involatile samples into the ion source was wholly dependent on the temperature of the source block, which was normally maintained at a temperature of 150°C. This produced an adequate sample partial pressure for most samples but if necessary the source block temperature could be set to any value in the range 50 to 250°C using the source heaters or water cooling.

5.3.4 Optimisation of Ion Source Operating Parameters

Each time the CI ion source was installed its operating parameters had to be optimised by introducing the required reagent gas and tuning the mass spectrometer to one of its principal reagent ions, e.g. CH_5^+ or $C_2H_5^+$ for methane. The intensity of this ion was monitored on an oscilloscope and maximised by systematically adjusting the ion source operating parameters. The required value of these parameters varied with the nature of the reagent gas and to a greater extent on its pressure, however typical values were as follows: (potentials given are relative to the source block which is at accelerating potential)

Electron Energy	350 eV
Emission Current	750 μA
Repeller	+1 V
Total Emission Collector	+20 V

The optimum value for the repeller potential did not exceed ±2V irrespective of the nature of the reagent gas or the sample. This is consistent with reports by other workers[13,15]. The reason for this behaviour has already been discussed in Chapter 2. The ion source did not in general require re-optimisation after sample introduction as long as the total ion source pressure was approximately constant. However, for samples with a molecular weight of above *ca.* 350 the ion source operating parameters were re-tuned to maximise the intensity of the ion corresponding to the base peak in the mass spectrum of the sample.

5.4 The Performance of the MS9 when Operated in the High Pressure Chemical Ionisation Mode

One of the primary aims of this project was to compare low pressure CI mass spectrometry, as practised using the Quistor, with conventional high pressure CI mass spectrometry. Before using the high pressure CI system described in this chapter for such a comparison it was first necessary to ensure that it could be employed to produce representative CI mass spectra by comparing its performance with the results of CI studies performed by other workers.

5.4.1 High Pressure CI Mass Spectra Obtained using Methane as the Reagent Gas

A mass spectrum of methane recorded at a pressure of 1 Torr is shown in Figure 5.13. Although the major methane reagent ions CH_5^+, $C_2H_5^+$ and $C_3H_5^+$ are clearly present, the base peak in this spectrum is at m/e 19 which corresponds to the protonated water molecule H_3O^+. This ion is produced by the following reactions

$$CH_5^+ + H_2O \longrightarrow H_3O^+ + CH_4 \qquad \text{R.5.1}$$

$$C_2H_5^+ + H_2O \longrightarrow H_3O^+ + C_2H_4 \qquad \text{R.5.2}$$

Figure 5.13 Mass Spectrum of Methane Recorded Prior to Ion Source Bakeout

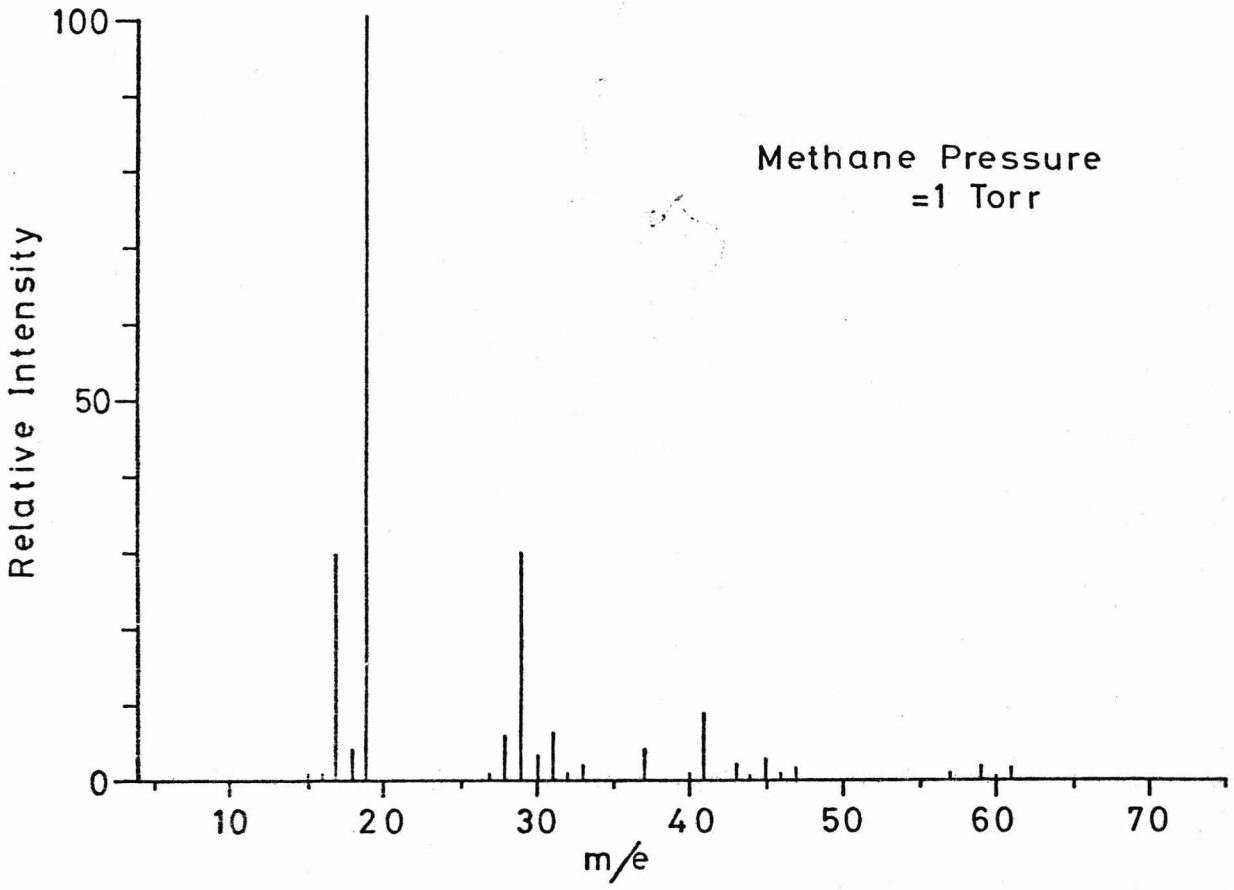

Figure 5.14 Methane CI Mass Spectrum of n-Decane

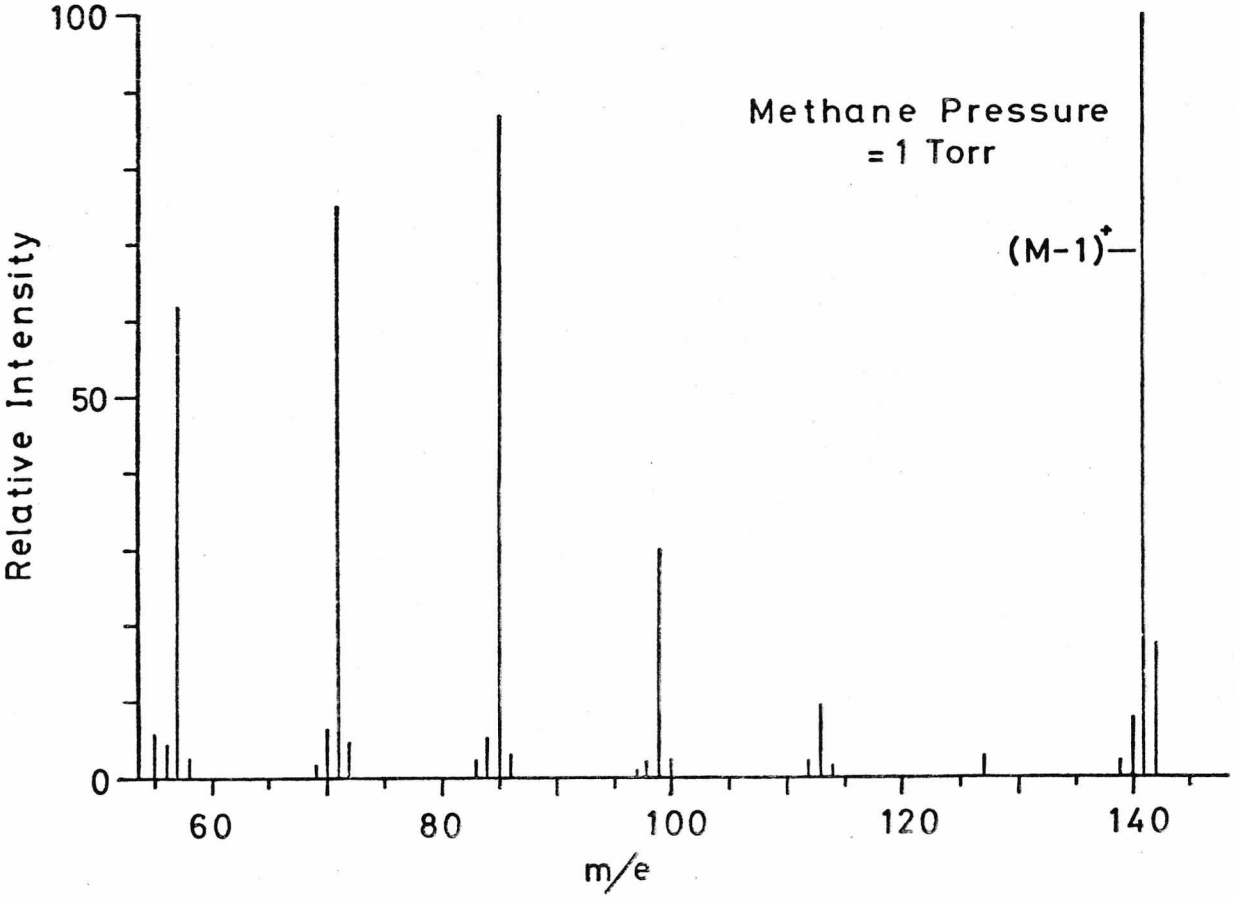

and the water molecules are present in this case, due to the fact that the mass spectrum was recorded only one hour after the ion source had been installed. It is for this reason, as was mentioned in Section 5.3, that the ion source had to be baked out for several hours after installation, a procedure which resulted in the reduction of the intensity of the H_3O^+ ion to less than *ca.* 3% of the total ionisation in the mass spectrum of methane recorded at 1 Torr. After baking, the major reagent ions CH_5^+ and $C_2H_5^+$ comprised *ca.* 90% of the total ionisation. Smaller amounts of the ions $C_2H_3^+$, $C_2H_4^+$, $C_3H_5^+$ and $C_3H_7^+$ were also present. The ion-molecule reactions which give rise to these ions have already been discussed in Chapters 1 and 4. It has been shown by Michnowicz and Munson[151] that the presence of small amounts of water may drastically change the relative intensities of ions in methane CI mass spectra, consequently a great effort was made to eliminate water, in addition to the above procedure, by baking the inlet system and pre-drying the reagent gas and the sample.

One of the first groups of compounds to be investigated by CIMS was the paraffin hydrocarbons[10] and so it was thought appropriate to commence this brief investigation by considering the CI mass spectrum of n-decane, which was recorded at a temperature of 200°C and is shown in Figure 5.14. This mass spectrum exhibits the characteristic features of the CI mass spectra of all straight chain alkanes. The $(M-1)^+$ ion is the most abundant ion and the only other ions present in significant abundance correspond to alkyl fragments $(C_nH_{2n+1})^+$.

A direct comparison of this mass spectrum with one recorded by other workers under similar operating conditions is shown in Table 5.1. The overall agreement between the two mass spectra is not particularly good. However, according to Munson *et al*[10], and also Hunt and McEwen[119], the relative abundances of ions in the CI mass spectra of hydrocarbons are dramatically affected by the temperature of the ion source. Therefore a small difference between the actual temperatures at which the two mass spectra were recorded may account for the discrepancies between the

values of percentage total ion current shown in Table 5.1.

Table 5.1 Comparison of CI Mass Spectra of n-Decane

(a) This Work (b) Hunt and McEwen[119]

Percentage of Total Ion Current

m/e	141 $C_{10}H_{21}^+$	127 $C_9H_{19}^+$	113 $C_8H_{17}^+$	99 $C_7H_{15}^+$	85 $C_6H_{13}^+$	71 $C_5H_{11}^+$	59 $C_4H_9^+$
(a)	23	0.7	2	6	20	17	14
(b)	31	0.5	1	10	22	22	14

The methane CI mass spectrum of cholesterol was obtained at an ion source temperature of 150°C and values of the percentage total ionisation for the major ions in this spectrum are listed in Table 5.2 along with results taken from an extensive study of the CI mass spectra of steroids, performed by Michnowicz and Munson[152,153]. There is reasonable agreement between these two sets of data except for the large difference in the values for the $(M-1)^+$ ion. However, since Michnowicz and Munson do not state the actual ion source temperature at which the data were recorded this discrepancy could also be due to a temperature effect.

From the above comparison it is clear that the high pressure CI system described in this chapter was producing characteristic CI mass spectra. No great importance was attached to the differences between the CI mass spectra produced by this system and those published by other workers since the relative intensities of ions in CI mass spectra are often dependent, not only on ion source temperature, but also on the value of the repeller potential and on the partial pressure of the sample in the ion source. Of the last two parameters the former is seldom stated in the literature and the latter is usually unknown, consequently it is

almost impossible to make a really meaningful comparison.

As a final example of the use of methane as a reagent gas the CI mass spectrum of cetyl alcohol recorded at an ion source temperature of 150°C is shown in Figure 5.15. The base peak is at m/e 225 which corresponds to the ion $(M+1 - H_2O)^+$ and the only other intense ion in the high mass region of the spectrum is at m/e 241 which corresponds to the $(M-1)^+$ ion. The ions in the low mass region of this spectrum occur mainly at m/e values corresponding to the two series $C_nH_{2n-1}^+$ and $C_nH_{2n+1}^+$. This mass spectrum is typical of the methane CI mass spectra of long chain primary alcohols[6], and is a good example of the utility of CI in the determination of molecular weight since ions in the molecular weight region of the EI mass spectra of this class of compounds are invariably of very low relative intensity or even non-existent.

The use of the high pressure system to obtain the CI mass spectra of a variety of different compounds with reagent gases such as isobutane and n-hexane is described in Chapter 6.

5.4.2 Instrumental Aspects of the Performance of the MS9 when Operated in the High Pressure CI Mode

The high resolution capability of the MS9 was unimpaired by its operation in the CI mode. However, due to the very narrow ion exit slit on the CI ion source the minimum resolution (i.e. that obtained when both the source and collector slits are fully open) was found to be higher than when the instrument was operated in the EI mode. This behaviour has been reported by other workers[18]. Most of the CI mass spectra obtained using this instrument were recorded at a resolution of *ca.* 2000 (10% valley definition).

The absolute sensitivity (in terms of the charge collected per mole of a particular sample) of the high pressure system was not determined, but the relative sensitivity of this and the low pressure CI system is discussed in Chapter 6. Typically, 1 µg of sample introduced into the

Cholesterol
M = 386

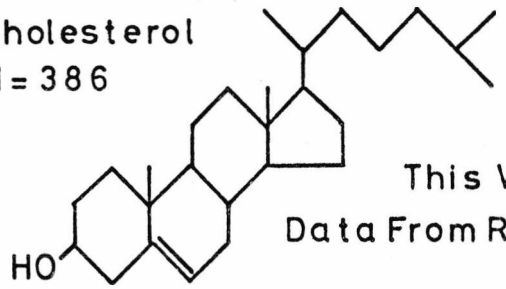

Table 5.2 Comparison of Methane CI Mass Spectra of Cholesterol

	% Total Ion Current					
	$(M+H)^+$	$(M)^+$	$(M-H)^+$	$(M+H-H_2O)^+$	$(M-H-H_2O)^+$	
This Work	5·4±1·2	2·5±0·8	10·7±2·1	48·0±5·2	5·7±0·9	a
Data From Ref. 152	5·0±1·0	3·2±1·6	20·0±3·8	52·0±4·7	4·2±0·8	b

Average of (a) 3, and (b) 9 Determinations

Figure 5.15 Methane CI Mass Spectrum of Cetyl Alcohol

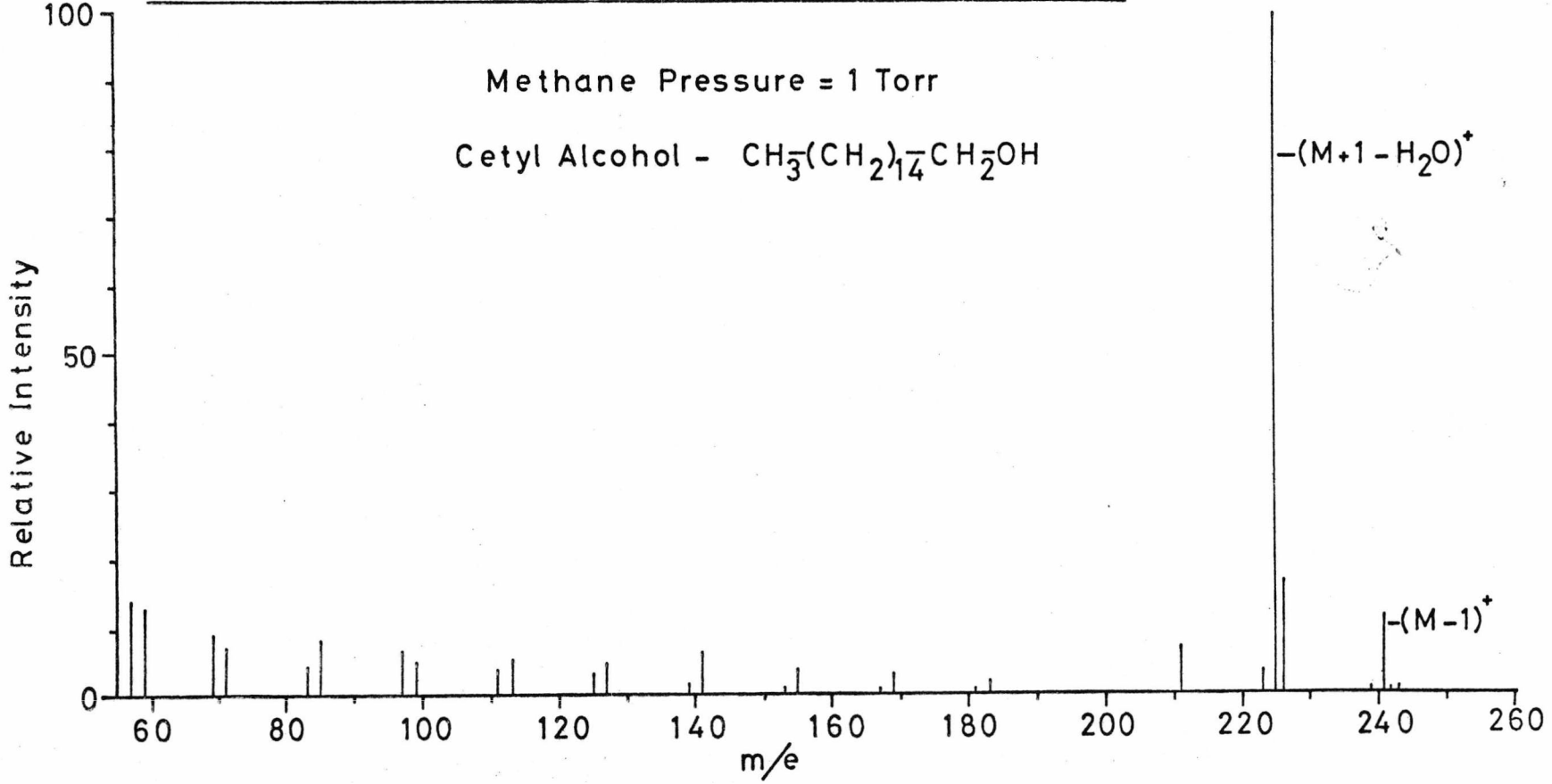

ion source on the direct insertion probe produced intense CI mass spectra for most of the samples investigated. Since there was no available means of measuring the sample partial pressure in the ion source the reagent gas to sample ratio was unknown. The sample partial pressure was infact very difficult to control since the probe could not be directly heated, however, it was usually possible to deduce whether this pressure was excessively high, from the occurrence of high relative intensities of cluster ions (i.e. $[2M+1]^+$ etc.) in the CI mass spectra. The formation of cluster ions under these conditions is discussed further in Chapter 6.

5.5 Conclusion

In summary, this chapter has described the relatively simple modification of a MS9 mass spectrometer to permit its operation in the CI mode and a brief characterisation of this instrument.

The CI mass spectra presented were found to be very similar to those obtained by other workers except for appreciable differences in the relative intensities of certain ions. However, this apparent discrepancy may have been caused by small differences in ion source operating conditions.

Contamination of the ion source and inlet system by water vapour was found to be a serious problem. This could only be solved by baking the system after installation of the ion source and pre-drying all samples.

CHAPTER 6

FURTHER LOW PRESSURE CI STUDIES WITH THE QUISTOR AND A COMPARISON OF ITS PERFORMANCE WITH THAT OF THE HIGH PRESSURE CI ION SOURCE

6.1 Introduction

The experimental results presented in Chapters 4 and 5 established that both the Quistor and the high pressure CI ion source were capable of producing characteristic CI mass spectra. In this chapter further examples of the use of the Quistor as a low pressure CI ion source are given and its performance is compared with that of the high pressure CI ion source. This comparison is prefaced by a theoretical study of the two ion sources.

For convenience of presentation all of the mass spectra described in this chapter are reproduced in the form of line diagrams. The reagent ions are usually omitted from these diagrams but all sample ions are included except for those with intensities below 1% of that of the base peak. Any significant ions of lower relative intensity are mentioned separately in the text.

6.2 A Comparative Theoretical Study of the Two Ion Sources

Although apparently identical CI processes have been shown to occur in both the Quistor and the high pressure ion source, the operating conditions under which these processes take place are vastly different. In this section the major differences, namely those in ion energy, ion residence time and pressure, are discussed in detail as are the possible effects of these differences on the CI mass spectra produced using the two ion sources.

6.2.1 Ion Energy

6.2.1.1 The Quistor

In discussing the energy of ions which are trapped in the Quistor it is, at first, convenient to ignore the possible effects of ion-ion and ion-molecule collisions on ion energy, and to consider only that which they possess as a result of their motion in the Quistor trapping field.

The energy of trapped ions may be estimated using a number of different methods:

(a) In the theoretical treatment of ion motion given in Section 3.2 a solution to the Mathieu equation was given (equation (3.21)) from which, for a given set of initial conditions (i.e. u_o, $\dot{u}_o$ and γ_o), it is possible to derive information on the trajectory of an ion when the device is operated under any particular set of operating conditions. Since the change in position of the ion as a function of time is then known an average ion velocity may be calculated by differentiating equation (3.21) and integrating over a certain time period. Hence from a knowledge of the ionic mass, the average ion kinetic energy may be estimated. (A more detailed account of this treatment is given in Reference 121). This method, however, is rather limited, since the value of the average ion energy obtained applies only to an ion in a trajectory associated with a particular set of initial conditions, and in practice ions are created with a distribution of values of the initial conditions.

(b) Another approach to the estimation of ion energies is based on the pseudo-potential well model which was described in Section 3.2.1. Consider the case where an ion is oscillating along the z axis of the Quistor from one end-cap to the other but without actually touching either of these electrodes. According to the model developed in Section 3.2.1 this ion would oscillate in a parabolic pseudo-potential well, a representation of which is shown in Figure 6.1, of depth $\overline{D}_z$ given by equation

Figure 6.1 Representation of the Parabolic Pseudo-Potential Wells

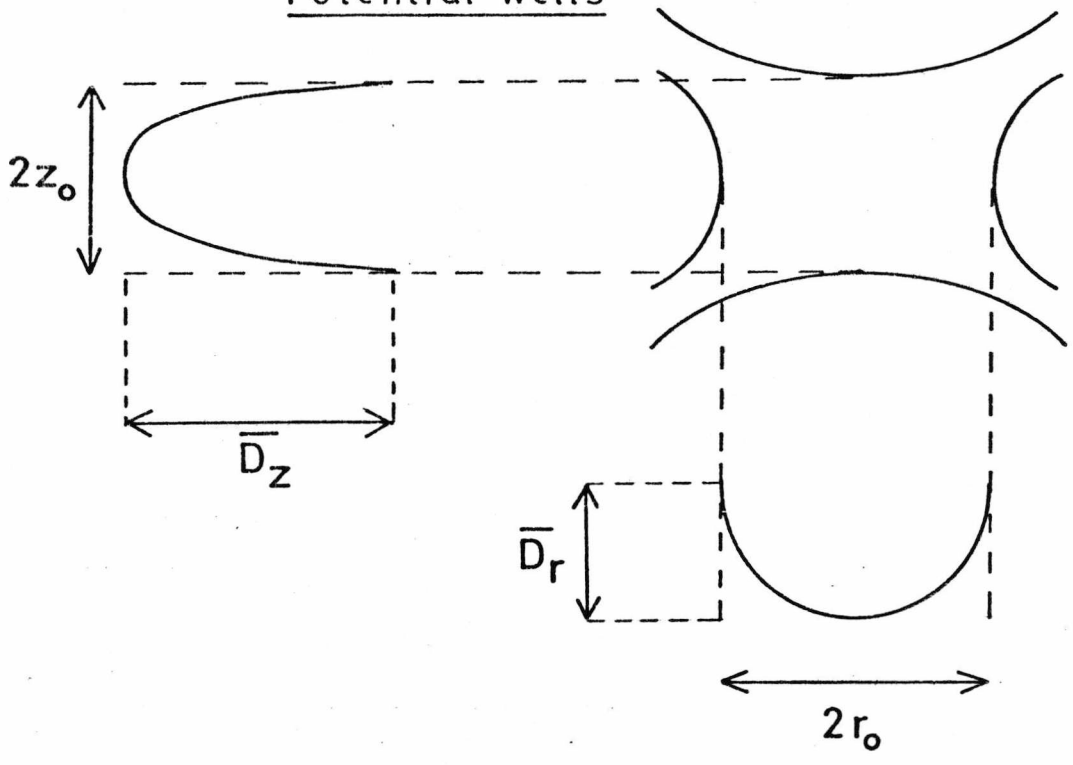

(3.35). If effects due to interactions with other ions and molecules are ignored, the total energy associated with this ion (i.e. potential energy + kinetic energy) is constant and given by $e\bar{D}_z$; however, the total instantaneous ion kinetic energy varies widely. Todd *et al*[123] have shown that it is possible to calculate a mean ion kinetic energy for the above case by integrating over one secular period as follows. For simple harmonic motion with an amplitude z_o and frequency ω_z

$$z = z_o \sin \omega_z t \tag{6.1}$$

and

$$\dot{z} = z_o \omega_z \cos \omega_z t \tag{6.2}$$

By integrating over a time interval π/ω_z the mean velocity is given by

$$\langle \dot{z} \rangle = \frac{2 z_o \omega_z}{\pi} \tag{6.3}$$

and the kinetic energy corresponding to this mean velocity is therefore

$$\tfrac{1}{2} m \langle \dot{z} \rangle^2 = \frac{2m z_o^2 \omega_z^2}{\pi^2} \tag{6.4}$$

which on substitution for ω_z^2 in terms of $\bar{D}_z$ (derived from equations (3.22) and (3.31))

$$\omega_z^2 = \frac{2e \bar{D}_z}{m z_o^2} \tag{6.5}$$

gives

$$\tfrac{1}{2} m \langle \dot{z} \rangle^2 = \frac{4}{\pi^2} e\bar{D}_z \tag{6.6}$$

$$= 0.405 \, e\bar{D}_z$$

As an example of the use of this method to estimate ion kinetic energies, consider an ion of m/e 16 in a trap where r_o = 0.7 cm powered with a potential V_o = 300V oscillating at 2.5 MHz. This corresponds to a q_z of 0.6 and, from equation (3.35) the depth of the pseudo-potential well is $\overline{D}_z$ = 22.5 eV, giving a mean ion kinetic energy of 9.1 eV. However, the model on which this calculation is based assumes that an ion can oscillate throughout the whole distance $2z_o$ without striking the electrodes. In practice, the r.f. ripple superimposed on such a trajectory would result in the ion being lost from the trap, so it is evident from equation (6.3) that using this value for the amplitude of the secular oscillation must necessarily give a high estimate of the mean ion kinetic energy.

It is possible using the above method to estimate a mean ion kinetic energy for the more realistic case of an ion with components of motion in both the z and r directions; however, this approach is only valid for low pressure conditions (i.e. $<10^{-8}$ Torr). Major and Dehmelt[144] have argued that at higher pressures ion scattering becomes important and the maximum permissible energy is determined by the lowest potential well, that given by $\overline{D}_r (= \overline{D}_z/2$ for a = 0 and $r_o^2 = 2z_o^2)$. For the above example this would reduce the mean ion kinetic energy to 4.55 eV.

The use of the pseudo-potential well model is by far the most convenient and simplest method of estimating ion kinetic energies, and the values obtained give a reasonable estimate of the maximum possible value for this parameter for a given set of operating conditions. However, as was stated in Section 3.2.1 this method is only valid for small values of q and, like the previous method, it can give no information on the ion energy distribution.

(c) A more exact approach to the determination of ion kinetic energies is possible using the recently developed application of phase space dynamics to quadrupole devices[128,154]. The full mathematical development of this approach is outside the scope of this thesis. (For

a recent review of these methods see Reference 129). Very briefly, with this method the position and velocity of an ion is represented in the form of a matrix and it is possible to calculate how the values of these parameters vary as a function of time using simple mathematical techniques such as matrix multiplication. It is then possible to calculate a mean velocity and hence the mean ion kinetic energy. This method has the advantage that from a knowledge of the initial distribution of values of u and $\dot{u}$, (i.e. the distribution of values of position and velocity at the point of ion creation) it is possible to derive information on the ion energy distribution for a particular set of operating conditions. Values of mean ion kinetic energies calculated using this method have been shown[154] to compare favourably with those calculated using the pseudo-potential well model.

(d) It is also possible to employ experimental methods for the determination of ion kinetic energies. Lawson *et al*[68] determined the rate constants for certain ion-molecule reactions occurring in ammonia while operating the Quistor under similar operating conditions as those employed in the above example. By comparison with rate data determined by other workers, using experimental methods where the ion energy is known, they were able to deduce that the mean primary ion kinetic energy was in the range 1 to 3 eV. Unfortunately, this method is very limited because the ion kinetic energy dependence of the rates of ion-molecule reactions have not been studied to any great extent, and even when this dependence is known the available data is not usually of a high accuracy.

From recent results by Waldren and Todd[155] it appears that it may be possible to derive information on ion kinetic energies from a study of the arrival time distributions of ions ejected from the Quistor.

Of all the above methods that utilising phase space dynamics is by far the most versatile and generally applicable. However, although this is the only method which gives any indication of the ion energy distribution, this in itself is limited since it is necessary to make an assumption

about the nature of the initial distribution.

When the Quistor is operated as a CI ion source the reagent gas pressure is normally of the order of 10^{-5} Torr ($\hat{=}$ 10^{11} mol.cm^3) and the density of stored ions may be as high as 10^8 ions cm^3. Under these conditions an ion, which may be stored in this case for up to 10 ms, may undergo a number of collisions with other ions and molecules. This will modify the trajectory of the ion and, depending on the exact nature of the collision and the colliding partners, may substantially change its kinetic energy.

The effects of ion-ion interactions have been discussed by Dehmelt[131] in terms of the pseudo-potential well model, but only for the low pressure case (i.e. $<< 10^{-5}$ Torr) and by making the assumption that the ensemble of ions is thermally isolated and that energy is neither lost to neutral molecules during collisions nor gained from the applied power by r.f. heating. Dehmelt proposed that under such conditions the ion temperature, T_i, is established by ion-ion interactions and derived a 'self collision time', t_c, which provides a measure of the time required for the distribution of ion kinetic energies to become Maxwellian. However, Todd *et al*[123] have shown that under conditions similar to those normally employed to operate the Quistor in the CI mode, t_c is of the order of one second and since this is 100 times greater than the usual maximum storage period of 10 ms, it may be assumed that ion-ion interactions have no significant effect on ion-kinetic energies.

The effects of ion-neutral collisions on the ion kinetic energy have been examined by Major and Dehmelt[144] who considered the problem in terms of elastic collisions of ions of mass m with particles of mass m_r at rest. They examined three particular cases in detail. When $m/m_r << 1$, the elastic scattering of ions by essentially fixed scattering centres gives rise to r.f. heating, leading to an exponential energy increase with time. For $m/m_r >> 1$, the light neutral particles cause a viscous drag on the ions and so reduce the average energy with time. Experimental

evidence has been obtained which supports the hypotheses made in both of these cases[156,157]. In the special case of $m = m_r$, Dehmelt argues that when averaged over a secular oscillation period, there is zero change in the energy of the colliding ion since in such a collision (considering the head-on collision case only) the ion will be brought to rest and subsequently take up its original energy again from the r.f. field. However, Bonner *et al*[158,159] have performed a theoretical investigation for the latter case using Monte-Carlo methods and they concluded that the effect of a series of ion-neutral collisions would be the migration of ions towards the centre of the device which necessarily implies a reduction in ion kinetic energy. This conclusion was supported by another theoretical study by Dawson[142] using the methods of phase space dynamics. Dawson also suggested that as the ions migrate closer to the centre of the device, space charge repulsion would become important so that an equilibrium situation may be reached. An extensive theoretical investigation into the influence of elastic collisions on a population of charged particles, trapped in a Quistor, has been performed by André[143], who employed a statistical method based on the Markov process to derive information on the evolution of the population in terms of the energy of the trapped ions. The results of this study were largely in agreement with those performed by Dawson[142], and Bonner *et al*[158,159] which have already been mentioned. André also showed that after sufficient elastic collisions the energy of the ions would become of the same order as the thermal energy of the backround molecules.

From the above discussion it is clear that, even for the relatively simple case of storing ions of a single m/e value in the presence of molecules of their parent gas, the kinetic energy of ions trapped in the Quistor is not well defined. Although there have been a number of theoretical studies of the problem, no single theory encompasses all of the factors which may influence the energy of the stored ions and also since these theories are often based on a number of assumptions it is

impossible to estimate with any accuracy the energy of an ion for a given set of storage conditions.

Using the method based on the pseudo-potential well model it was estimated that for the range of storage conditions normally employed to operate the Quistor in the CI mode the average ion kinetic energy was in the range 1 to 10 eV. It is unlikely that, at an operating pressure of 10^{-5} Torr and a maximum storage time of 10 ms, an ion will undergo sufficient collisions for it to become thermalised.

6.2.1.2 The High Pressure Ion Source

The techniques of chemical ionisation have been employed to determine rate constants for ion-molecule reactions[81,82] and to evaluate equilibrium constants for reversible reactions of gaseous ions[160,161]. As noted in Chapter 2 for kinetic studies it is essential to have an exact knowledge of the ion residence time in order to determine rate constants accurately, while equilibrium considerations demand that these times be sufficiently long to permit attainment of the equilibrium. It is also necessary to have a knowledge of ion energies and their distributions, because firstly, although rate constants for exothermic ion-molecule reactions are largely independent of energy, those for endothermic ion-molecule reactions are not, and secondly, the equilibrium position from which thermodynamic parameters are derived, shifts as a result of ion energy variation.

The residence time of an ion in an ion source may be estimated from ion drift considerations for which there are three distinct cases[162]:

(i) Low field - when the ratio of the electric field to the pressure (E/P) is < 1 V cm^{-1} $Torr^{-1}$. In this case the ion energy gained by the field is small compared with the thermal energy and the Maxwell-Boltzman distribution of ion velocities is not substantially perturbed. The drift velocity V_d is found to be proportional to the field E

$$V_d = K\,E \qquad (6.7)$$

where K is the ion mobility. When the only interaction impeding ion motion is an inverse fourth power potential $V(r) = -\alpha\, e^2/2r^4$, typical for ion-polarisable molecule encounters, the mean collision free time is constant and the Langevin drift equation[80] in the polarisation limit results. This can be expressed in the following convenient numerical relationship

$$V_d = (T/P)(E/\sqrt{\alpha\ \mu_r}) \qquad (6.8)$$

where T and P are the temperature and pressure respectively, α is the polarisability and μ_r the reduced mass of the ion-polarisable molecule encounter. The residence time τ is then given by $\tau = L/V_d$ where L is usually the distance between the centre of the electron beam and the ion exit slit. As was mentioned in Chapter 2 the use of Langevin drift theory to estimate τ often leads to erroneous results[81,82]. This parameter is best determined directly from arrival time distributions using a pulsed ion source[83].

(ii) High field - when E/P is typically > 50 V cm^{-1} $Torr^{-1}$. In this case the polarisation force between ion-molecule encounter partners becomes less important compared with other forces such as hard-sphere repulsion. In this field region the ion drift velocity is found to be proportional to $\sqrt{E}$.

(iii) Intermediate field - in this case the ion energy gained by the field is comparable or greater than the thermal energy and neither energy source can be neglected. The dependence of ion drift velocity on the field usually changes gradually from a power of 1 to ½ in this region.

The intermediate field case is of particular interest here because most chemical ionisation sources are operated in this field region.

Wannier[163] derived the following expression for the average ion kinetic energy in an ion source operated under such conditions,

$$\tfrac{1}{2} m\langle V^2\rangle = \tfrac{1}{2}(m + M)V_d + \frac{3}{2} kT \qquad (6.9)$$

where m and M are the masses of the ions and neutral molecules respectively and k is Boltzmans constant. The first term of the righthand side of this expression represents the sum of field energy associated with the drift motion, and the random energy which arises due to ion-neutral collisions. The last term represents the thermal energy. Wannier's approach was extended by Chang *et al*[162] to permit the estimation of ion energy distributions. This was based on the following two assumptions: (a) that thermal equilibrium is achieved independently in the x, y and z axes (the z axis is conventionally taken as that parallel to the direction of ion drift out of the ion source) respectively; it is then possible to define a transverse ion "temperature" (T_T) and a longitudinal ion temperature (T_L) as follows:

$$\tfrac{1}{2} k T_T = \tfrac{1}{2} m\langle V_x^2\rangle = \tfrac{1}{2} m\langle V_y^2\rangle = \frac{e D_T}{2K} \qquad (6.10)$$

$$\tfrac{1}{2} k T_L = \tfrac{1}{2} m(\langle V_z^2\rangle - \langle V_z\rangle^2) = \frac{e D_L}{2K} \qquad (6.11)$$

D_T and D_L are the transverse and longitudinal diffusion coefficients, (b) that the components of the velocity and energy in the x, y and z axes can be described by one-dimensional Maxwell distributions characterised by the "temperature" in their respective directions i.e. T_T for x and y axes, T_L for the z axis. The corresponding Maxwell velocity and energy distributions are then:

$$f(V_i) = \left(\frac{m}{2\pi k T_T}\right)^{\frac{1}{2}} \exp\left(\frac{-m V_i^2}{2 k T_T}\right) \quad i = x,y \qquad (6.12)$$

$$f(V_z) = \left(\frac{m}{2\pi\ k\ T_L}\right)^{\frac{1}{2}} \exp\left(\frac{-\ m(V_z - V_d)^2}{2\ k\ T_L}\right) \tag{6.13}$$

$$f(G_{xy}) = \left(\frac{1}{k\ T_T}\right)\ \exp\left(\frac{-\ G_{xy}}{k\ T_T}\right) \tag{6.14}$$

$$f(G_z) = \frac{1}{2}\left(\frac{1}{\pi\ k\ T_L}\right)^{\frac{1}{2}}\ G_z^{-\frac{1}{2}}\ \exp\left\{\frac{-(G_z - 2\sqrt{G_z G_d} + G_d)}{k\ T_L}\right\} \tag{6.15}$$

where $G_d = \frac{1}{2}\ m\ V_d^2$ and $G_{xy} = G_x + G_y$

The convolutions of equations (6.14) and (6.15) are

$$f(G)\ dG = \sum_{\substack{G_{xy}=G \\ G_z=0 \\ G_{xy}=0 \\ G_z=0}} f(G_{xy})\ f(G_z)\ dG \tag{6.16}$$

where $G = G_{xy} + G_z$.

Chang *et al*[162] showed by numerical evaluation of the above expressions that the effect of the electric field is to produce a displaced Maxwellian distribution of ion energies. As an example of the magnitude of the average ion energy estimated using the above method, for $C_2H_5^+$ ions in methane at a pressure of 0.567 Torr and a temperature of 170°C the average ion energy when there is no extraction field is 0.0579 eV and for an extraction field of 4.3 V cm^{-1} it is 0.0744 eV.

From the examples given for average ion energies it is apparent that the value of this parameter may be more than two orders of magnitude greater for ions trapped in the Quistor than for ions drifting in the high pressure ion source. Since reagent ions trapped in the Quistor will

have a relatively high average kinetic energy they may be able to react with the sample molecules by a number of endothermic reaction channels which are not energetically feasible for the 'thermal' energy reagent ions in the high pressure ion source.

Reagent ions produced as the result of ion-molecule reactions in both the Quistor and the high pressure ion source may be formed with a considerable amount of excess internal energy. However, as will be shown in the next section, an ion drifting in a high pressure ion source will undergo hundreds of ion-molecule collisions during its residence time and this will have the effect of rapidly reducing the internal energy of the excited ions to the thermal level. Since an ion trapped in the Quistor undergoes relatively few ion-molecule collisions this relaxation will not occur to the same extent. Consequently reagent ions trapped in the Quistor will not only have a higher kinetic energy, but also a higher internal energy than reagent ions in the high pressure ion source. These effects could give rise to differences in the CI mass spectra obtained using the two ion sources.

6.2.2 Kinetic Factors and Other Effects

The kinetics of chemical ionisation and the mathematical analysis of rate data to determine rate constants for the formation of CI product ions has been studied by a number of workers (see References 27, 40, 41, 81, 82, 83, 113 and 164) and will not be considered in detail here. However, since there are such large differences between the values of both the pressure of the reagent gas and the ion residence time for the Quistor and the high pressure ion source, it is of interest to consider the possible effects of these differences on the rates of formation of reagent and sample ions.

For kinetic studies using a high pressure ion source it is usual to assume[40,113] that the reagent ions are formed rapidly compared to their residence time in the ion source. Considering the reaction of $CH_4^{+\cdot}$ ions

with methane molecules to produce the CH_5^+ reagent ion which is known to proceed with a rate constant of *ca.* 1.2×10^{-9} cm^3 mol^{-1} sec^{-1}, the time to 90% reaction, assuming pseudo first order kinetics, is given by

$$t_{90\%} \simeq \frac{2.3}{k\ p}$$

where k is the reaction rate constant and p the methane pressure. If p = 1 Torr the equivalent number density is 2×10^{16} $mol.cm^3$ at a temperature of 150°C, therefore $t_{90\%} \simeq 10^{-7}$s. Ion residence times for CI ion sources are of the order of 10^{-5}s so the above assumption is reasonable. The value of $t_{90\%}$ for the above case may be estimated in the same way for the Quistor. Here the operating pressure is *ca.* 1.0×10^{-5} Torr and the equivalent number density at 25°C (the normal operating temperature) is 3.2×10^{11} $mol.cm^3$, therefore $t_{90\%} \simeq 6$ ms. The relatively fast formation of reagent ions and the corresponding rapid disappearance of primary ions in the high pressure ion source is partially responsible for the fact that the probability of a reaction occurring between a primary ion and a sample molecule is very remote. This is clearly not the case for the Quistor, where $t_{90\%}$ is of the same order as the residence (i.e. storage) time. It is possible therefore that reagent gas primary ions may react with the sample molecules as well as the reagent ions. In the case of methane this could lead to the production of M^+ ions in the CI mass spectra obtained using the Quistor due to charge transfer reactions occurring between, for example, CH_4^+ and the sample molecules. Another possible effect of the relatively slow rate of production of reagent ions is that if the partial pressure of the sample in the Quistor is maintained at a factor of *ca.* 10^3 lower than the reagent gas, as is standard practice is high pressure CIMS, then the rate of production of sample ions will be so slow that the number of these ions produced during the storage period (10 ms) may be insufficient for purposes of detection.

Another consequence of the large difference between the operating

pressures employed in the Quistor and the high pressure ion source is that there will be a corresponding difference in the number of collisions an ion will experience during its residence time. It is possible to estimate the number of collisions an ion will experience from the following expression which was mentioned previously in Chapter 2:

$$z_c = k_c \cdot N \cdot \tau$$

As before k_c is the collision rate constant, N the number density and τ the residence time. For example, proton transfer reactions between CH_5^+ ions and sample molecules will proceed with a rate constant of the order of 10^{-9} cm^3 mol^{-1} sec^{-1} and since such reactions are known to occur at almost every collision it is reasonable to use this as a value for k_c. Using the same values for N are were employed to calculate $t_{90\%}$ and assuming values of 10^{-5}s and 10^{-2}s for the residence time in the high pressure ion source and the Quistor respectively the corresponding numbers of collisions of CH_5^+ ions calculated using the above expression are ~200 and ~3 respectively. From this it is apparent that under the conditions normally employed to operate the Quistor in the CI mode an ion will in general undergo considerably fewer collisions than it would in a high pressure ion source, and the time between collisions will be much greater. Consequently, collisional stabilisation of ionic species such as cluster ions [e.g. $H^+(H_2O)_n$] and association ions [e.g. $(M + C_2H_5)^+$ and $(2m+1)^+$] is less likely to occur in the Quistor and they would therefore be expected to be of very low relative intensities or even non-existent in low pressure CI mass spectra.

An additional kinetic factor arises due to the fact that the average residence time of quasi-parent ions formed in the Quistor is generally two or three orders of magnitude longer than that for the high pressure ion. The first step in the production of the set of ions which comprise the CI mass spectrum of a particular sample, is the formation of

the quasi-parent ions by, for example, the transfer of a proton from the reagent ions to the sample molecules. The quasi-parent ions thus formed may then undergo decomposition reactions which may be looked upon as a set of parallel, competing first-order reactions, to produce a set of fragment ions:

$$\begin{array}{rcl} & & S_1^+ + F_1 \\ MH^+ & \xrightarrow{k_i} & S_2^+ + F_2 \\ & & \vdots \quad\quad \vdots \\ & & S_i^+ \quad F_i \end{array}$$

where MH^+ is the quasi-parent ion, k_i is the rate constant for the production of the i^{th} fragment ion, S_i^+, and F_i is the respective neutral fragment. Since the time available for fragmentation of the quasi-parent ions stored in the Quistor is, on average, considerably longer than for those drifting in the high pressure ion source it would be expected, from the above kinetic considerations alone, that the total intensity of fragment ions, relative to the intensity of the quasi-parent ion, in low pressure CI mass spectra should be greater than that in high pressure CI mass spectra.

6.3 The Comparison of High and Low Pressure CI Mass Spectra Obtained Using the Two Ion Sources

Although the CI mass spectra which were presented in Chapters 4 and 5 indicated that methane was a suitable reagent gas for both ion sources, it was not employed for this comparison because its use in the Quistor was limited to samples with molecular weights of less than *ca.* 80. Many of the CI mass spectra presented in this section were obtained using isobutane as the reagent gas. This was chosen because it has been extensively employed in the field of high pressure CIMS and also because its use as a reagent gas for the Quistor system allowed the low pressure CI mass spectra to be obtained of samples with molecular weights of up to 280.

The samples employed in this study were not necessarily those which were particularly suited to analysis by the CI technique. Instead, samples were chosen which were expected to react in a predictable fashion with the reagent ions and produce relatively simple CI mass spectra.

In some of the mass spectra presented in this section dotted lines are used to represent the relative intensity of the reagent ions.

6.3.1 The Use of Isobutane as a Reagent Gas

6.3.1.1 The High and Low Pressure Mass Spectra of Isobutane

The mass spectrum of isobutane recorded at a source pressure of 0.2 Torr using the high pressure system is shown in Figure 6.2(a). The source pressure, which corresponded to a reading of 4×10^{-4} Torr on the source housing ionisation gauge, was the highest at which the system could be operated with isobutane as a reagent gas, since above this value serious arcing occurred between the ion source and ground. The base peak in the high pressure mass spectrum of isobutane is at m/e 57 which corresponds to the well known CI reagent ion, t - $C_4H_9^+$. This species also gives rise to the base peak in the low pressure (or ion storage) mass spectrum of isobutane shown in Figure 6.2(b), which was recorded while operating the Quistor at an applied r.f. potential (V_o) of 500V oscillating at 2.5 MHz. Under these conditions the intensity of the t - $C_4H_9^+$ species was maximised.

The variation in the relative intensities of ions in the low pressure mass spectrum of isobutane as a function of storage time was investigated while operating at a fixed pressure of 1.0×10^{-5} Torr. The results of this study are presented in Figure 6.3. Clearly the major process which occurs in this system is the formation of the t - $C_4H_9^+$ ion by hydride abstraction. According to Munson *et al*[165] who have also studied this system the t - $C_4H_9^+$ species is formed by both second and third order processes and it is necessary that virtually all of the other ions react to produce this species in order to account for the large

Figure 6.2 (a) High Pressure and (b) Ion Storage Mass Spectra of Isobutane

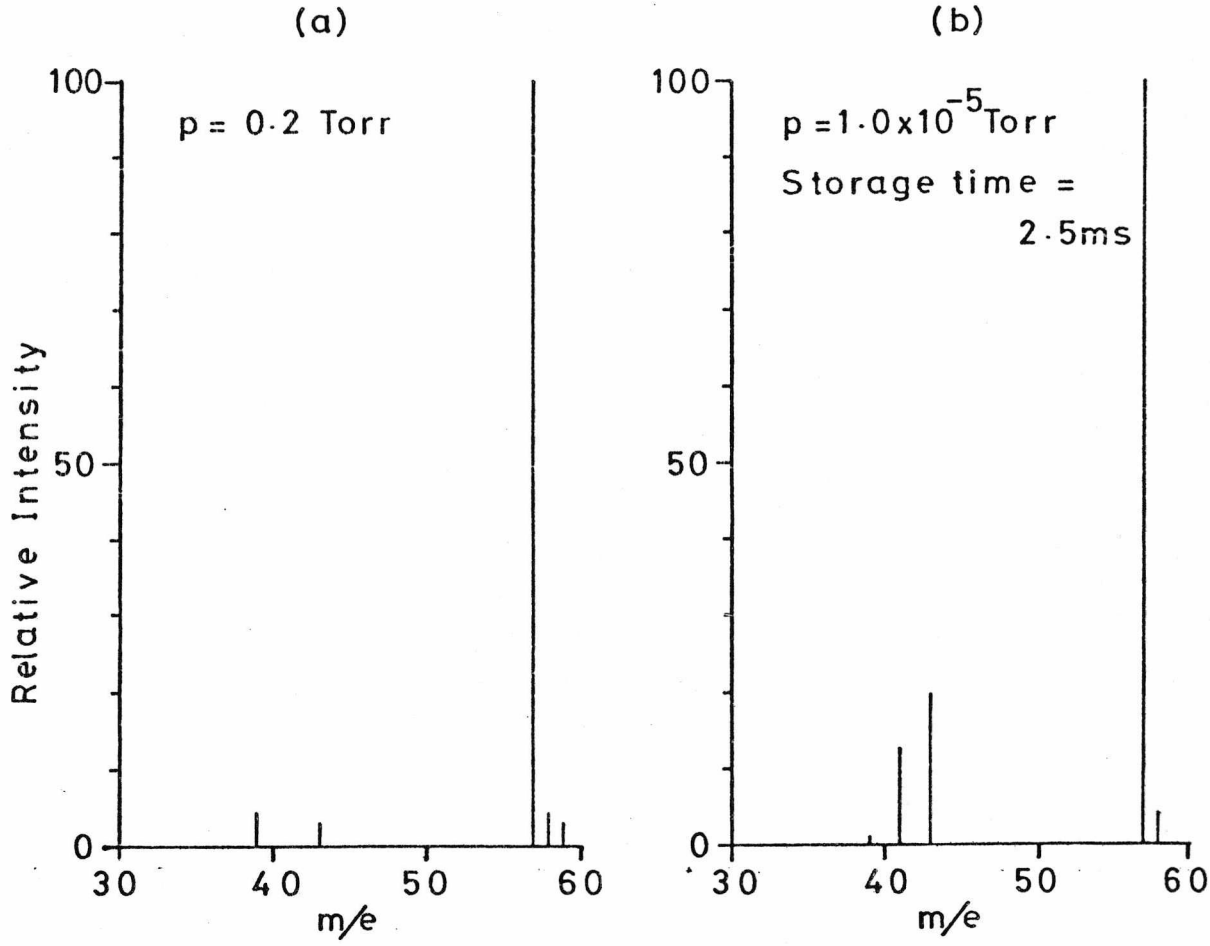

Figure 6·3 Plot Showing the Intensities of Ions in Isobutane as a Function of Storage Time

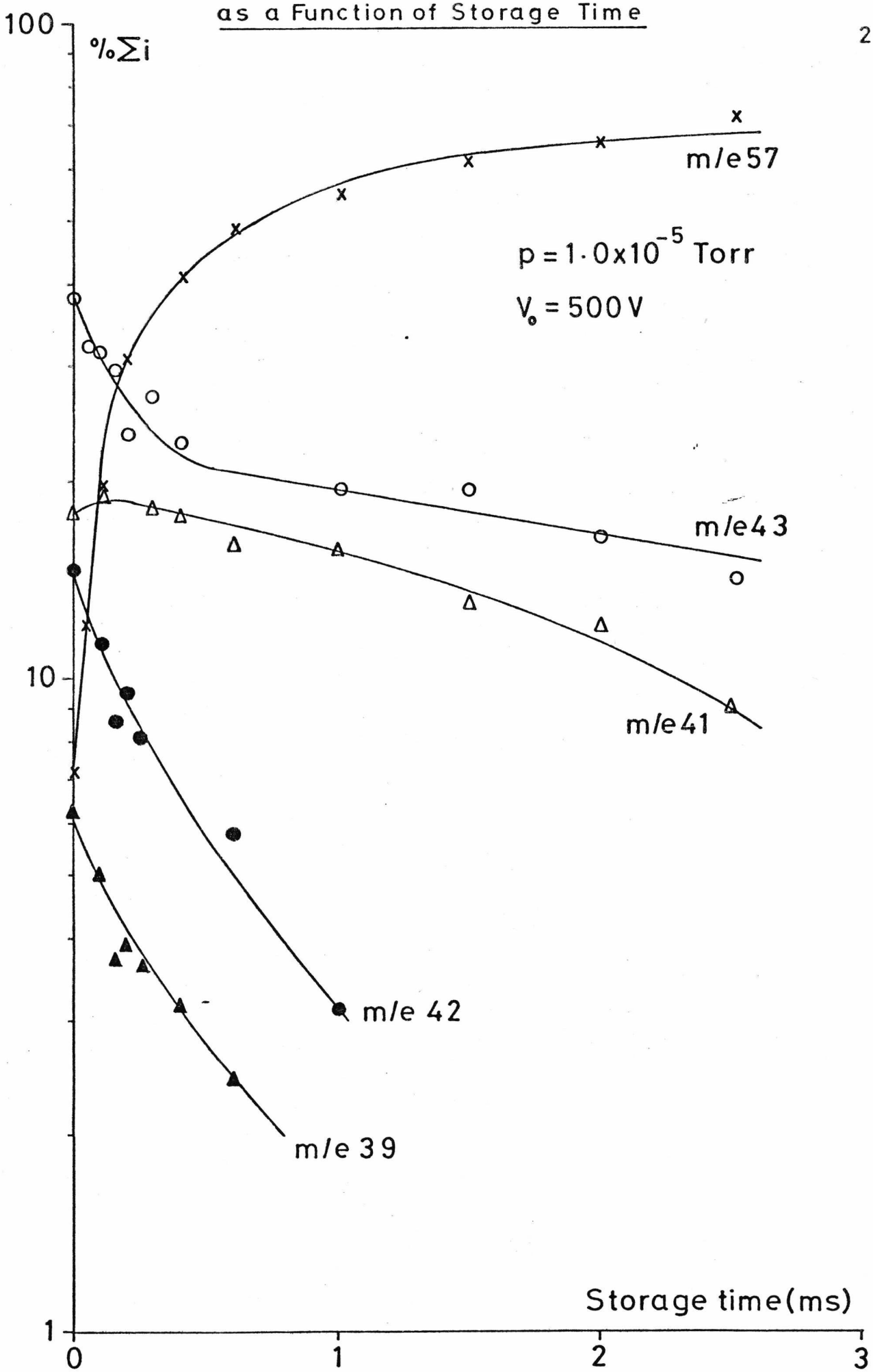

increase in its relative concentration. The general shape of the plots for m/e 41 and m/e 43 is indicative that these ions react in some other way, in addition to the second order hydride abstraction reaction.

6.3.1.2 Mass Spectra Obtained with Isobutane as the Reagent Gas

The operating conditions employed to obtain the mass spectra presented in this section are detailed below:

Low Pressure System (Quistor)	
Applied r.f. potential (V_o)	625 V_{z-p}
Frequency ($\Omega/2\pi$)	2.5 MHz
Pulse sequence repetition rate	100 Hz
Ion creation pulse width	20 μs
Ion ejection pulse width	10 μs
Ion ejection pulse amplitude	250 V
Storage time	zero, 5 ms or 9 ms
Isobutane pressure	1.0×10^{-5} Torr
q_z (for mass m in a.m.u.)	19.8/m

High Pressure System	
Electron energy	350 V
Emission current	1 mA
Repeller potential	+1 to +2 V
Source temperature	150-175°C
Isobutane pressure	0.2 Torr

All samples were introduced into the low pressure system using the A.G.H.I.S. The only available means of estimating the sample partial pressure with this system was the source region ionisation gauge and since the sensitivity of these instruments is dependent on the nature of the gas molecules present, the indicated pressure may differ from the true pressure

by more than an order of magnitude. However, for all of the more volatile samples the amount of sample entering the ion source was adjusted so that the indicated partial pressure was *ca.* 1×10^{-7} Torr. It was not possible to estimate the sample partial pressure in the high pressure ion source but an indication of an excessively high sample partial pressure could be obtained in some cases from the presence of high relative intensities of association ions (e.g. $[2M+1]^+$) in the CI mass spectra.

6.3.1.2(a) Benzyl Alcohol

In order to demonstrate the utility of using the Quistor as both an EI and a low pressure CI ion source, three mass spectra of an isobutane/benzyl alcohol mixture were recorded at different storage times. These are shown in Figure 6.4. Above m/e 58 the mass spectrum recorded at zero storage time is almost identical to the mass spectrum of benzyl alcohol obtained using a conventional EI ion source[166]. This was expected since under zero storage conditions the ions are ejected from the Quistor almost immediately after they are created and are not therefore under the influence of the r.f. electric field long enough for the mass discrimination effect to make significant changes to the relative ion intensities. As the storage time is increased to 9 ms (Figure 6.4(c)) the mass spectrum becomes more like a CI mass spectrum in character. The major CI process is that which produces the benzyl (or possibly tropylium) ion at m/e 91. There are two possible mechanisms for the formation of this ion[148] : either by the loss of a water molecule from the protonated parent molecule or by hydroxide ion abstraction from the parent molecule. It was not possible to determine with certainty whether the intensity of the ion at m/e 109 consisted solely of the ^{13}C isotope of the ion at m/e 108 or included a contribution from the $(M+1)^+$ species. However, the fact that the intensity of this ion was at most extremely small is indicative that if the ion at m/e 91 was formed by the former mechanism then the dehydration step is a very rapid process.

Figure 6.4 Mass Spectra of an Isobutane-Benzyl Alcohol Mixture (a)zero (b)5ms (c)9ms Storage Time

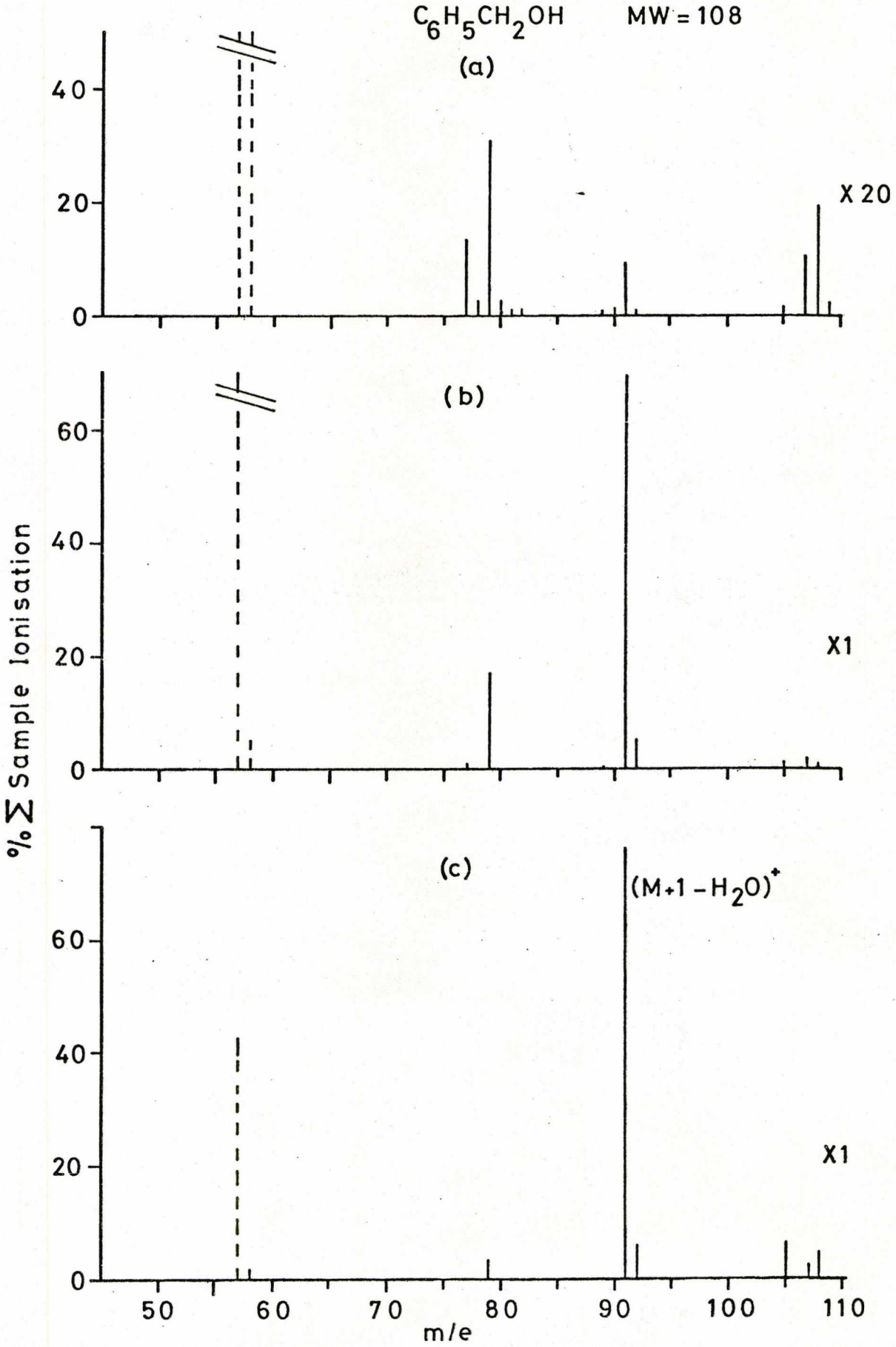

The data given in Table 6.1 indicates that there is a substantial increase in the total sample ion current as the storage time is increased from zero to 9 ms. This is not surprising since at zero storage the sample is ionised for 20 μs in a duty cycle of 10 ms, and at 9 ms storage time the sample is subject to ionisation by the reagent ions for 90% of the duty cycle. It is clearly advantageous therefore, as regards the sensitivity of this system, to operate at the maximum possible storage time. Also shown in Table 6.1 are the sums of the total reagent ion (i.e. m/e 57) and sample ion currents for the two spectra recorded at 5 ms and 9 ms storage time. The fact that this sum is almost identical for the two spectra is indicative that for this particular sample the reagent gas primary ions did not react directly with the sample molecules to any significant extent.

Table 6.1 Total Ion Current Data from Figure 6.4

Storage Time	Zero	5 ms	9 ms
Total Sample Ion Current (arbitrary units)	41.1	298	462
Relative Total Sample Ion Current	1	7.3	11.2
Total Reagent Ion Current (m/e 57)(arbitrary units)		360	200
Sum of Total Reagent and Sample Ion Currents	-	658	662

6.3.1.2(b) Benzaldehyde

The mass spectrum of an isobutane/benzaldehyde mixture recorded at zero storage, shown in Figure 6.5(a), provides a further example

Figure 6.5 Mass Spectra of an Isobutane-Benzaldehyde Mixture at (a) zero (b) 5ms (c) 9ms Storage Time and (d) High Pressure Mass Spectrum

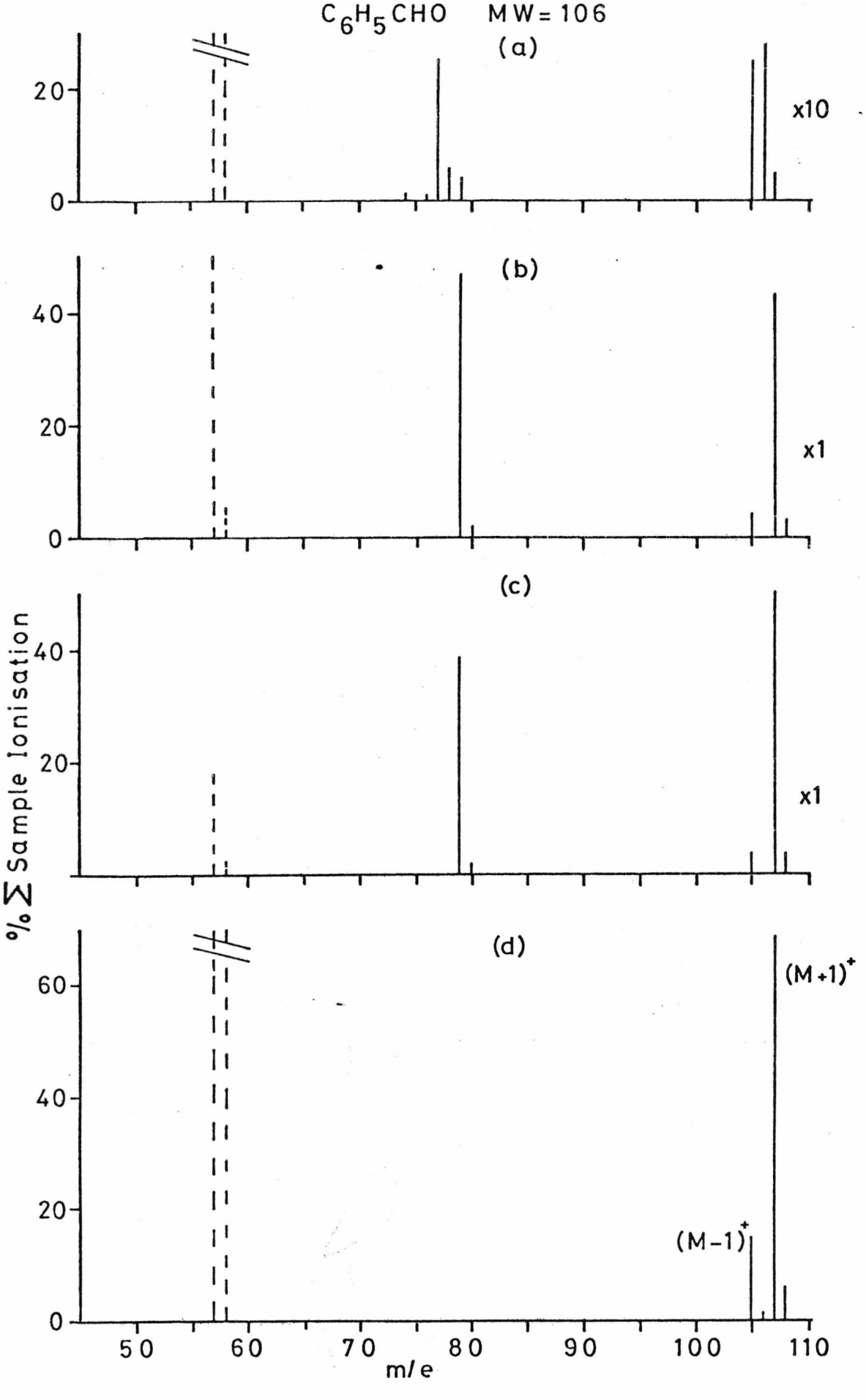

of the EI-type mass spectra obtained when the device is operated in this mode. The low pressure CI mass spectra of the same mixture recorded at 5 ms and 9 ms storage time are shown in Figures 6.5(b) and 6.5(c) respectively. From the total ion current data for these spectra summarised in Table 6.2 it is apparent that there is a substantial increase in the total sample ion current in going from the zero storage to the 9 ms storage, and also that the sum of the total sample and reagent ion currents is almost identical for the mass spectra recorded at 5 ms and 9 ms, as was the case for benzyl alcohol.

Table 6.2 Total Ion Current Data from Figure 6.5

Storage Time	Zero	5 ms	9 ms
Total Sample Ion Current (arbitrary units)	27.9	187	246
Relative Total Sample Ion Current	1	6.7	8.8
Total Reagent Ion Current (m/e 57)(arbitrary units)	-	97	37
Sum of Total Reagent and Sample Ion Currents	-	284	283

From the low pressure CI mass spectrum of benzaldehyde shown in Figure 6.5(c), it appears that the major CI process is protonation to form the $(M+1)^+$ ion at m/e 107. The $(M-1)^+$ ion at m/e 105 may have been formed as a result of a hydride abstraction reaction or possibly by the loss of a hydrogen molecule from the $(M+1)^+$ species. The fragment ion at m/e 79 probably arises due to the elimination of a carbon monoxide molecule

from the $(M+1)^+$ ion by the following mechanism originally proposed by Shannon[166] to explain the appearance of the m/e 79 species in the EI mass spectrum of benzyl alcohol.

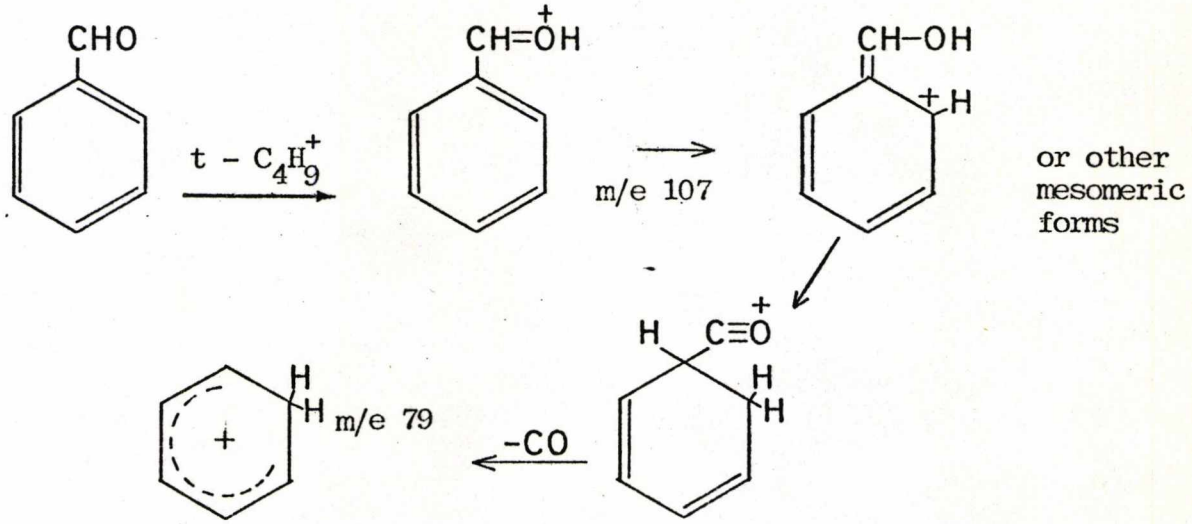

The fragment ion at m/e 79 is not present in the high pressure CI mass spectrum of benzaldehyde shown in Figure 6.5(d). This suggests that at the thermal energies prevalent in the high pressure ion source the energy transferred to the $(M+1)^+$ species as a result of its protonation by the t - $C_4H_9^+$ ion was insufficient to initiate the carbon monoxide elimination reaction. From this it was inferred that, as had already been suggested in Section 6.2.1.1, the energy associated with reagent ions trapped in the Quistor is considerably higher than the thermal energy reagent ions in the high pressure ion source. In fact, calculations based on the pseudo-potential well model indicate that the average kinetic energy of the t - $C_4H_9^+$ ion stored under the conditions employed to record Figure 6.5(c) is *ca.* 6 eV.

No ions with m/e values higher than the $(M+1)^+$ ion were detected in the low pressure CI mass spectrum of benzaldehyde but in the high pressure mass spectrum there was an ion at m/e 213 which corresponds to the $(2M+1)^+$ species. Although, in this case the absence of association ions in the low pressure CI mass spectra may be explained in terms of the arguments set out in Section 6.2.2, the formation of such ions in the Quistor has been reported by Fulford *et al*[174] in a study of the gas-phase ion-molecule

reactions occurring in dimethyl sulphoxide. However, this study was performed at pressures of *ca.* 10^{-4} Torr and at storage times of *ca.* 100 ms where the probability of collisional stabilisation is considerably greater than it is under the conditions employed in this work.

6.3.1.2(c) Methyl Benzoate

The zero storage and low pressure isobutane CI mass spectra of methyl benzoate are shown in Figures 6.6(a) and 6.6(b) respectively. In this case there is an increase of a factor 7.5 in the value of the total sample ion current in going from zero to 9 ms storage time. The low pressure CI mass spectrum contains an ion at m/e 137 corresponding to the $(M+1)^+$ species and a fragment ion at m/e 105 which corresponds to the ion formed as a result of the loss of a methanol molecule from the quasi-parent ion $(M+1 - CH_3OH)^+$. In the high pressure isobutane CI mass spectrum shown in Figure 6.6(c) the quasi-parent ion at m/e 137 constitutes almost 90% of the total ionisation. The only fragment ion in this spectrum is at m/e 105 as was the case with the low pressure mass spectrum. However, the relative intensity of this ion in the latter spectrum is considerably greater. It is unlikely that the mass discrimination inherent in the Quistor could alone effect such a large difference in relative intensities since the values of q_z for the two ions are such (q_z(m/e 137) = 0.14, q_z(m/e 105) = 0.19) that their storage efficiencies will be very similar.

It is extremely difficult to rationalise the differences between the relative intensities of ions in the low and high pressure CI mass spectra of a particular sample, because of the complexity of the situation as regards the energetics and kinetics of the CI process in the Quistor which were discussed in Section 6.2, and also because of other factors associated with the storage characteristics of the device. However, in simple terms there are basically two possible explanations for the differences in the relative intensities of the ions in the low and high pressure CI mass

Figure 6.6 Mass Spectra of an Isobutane-Methyl Benzoate Mixture Recorded at (a) zero (b) 9ms Storage Time and (c) at High Pressure

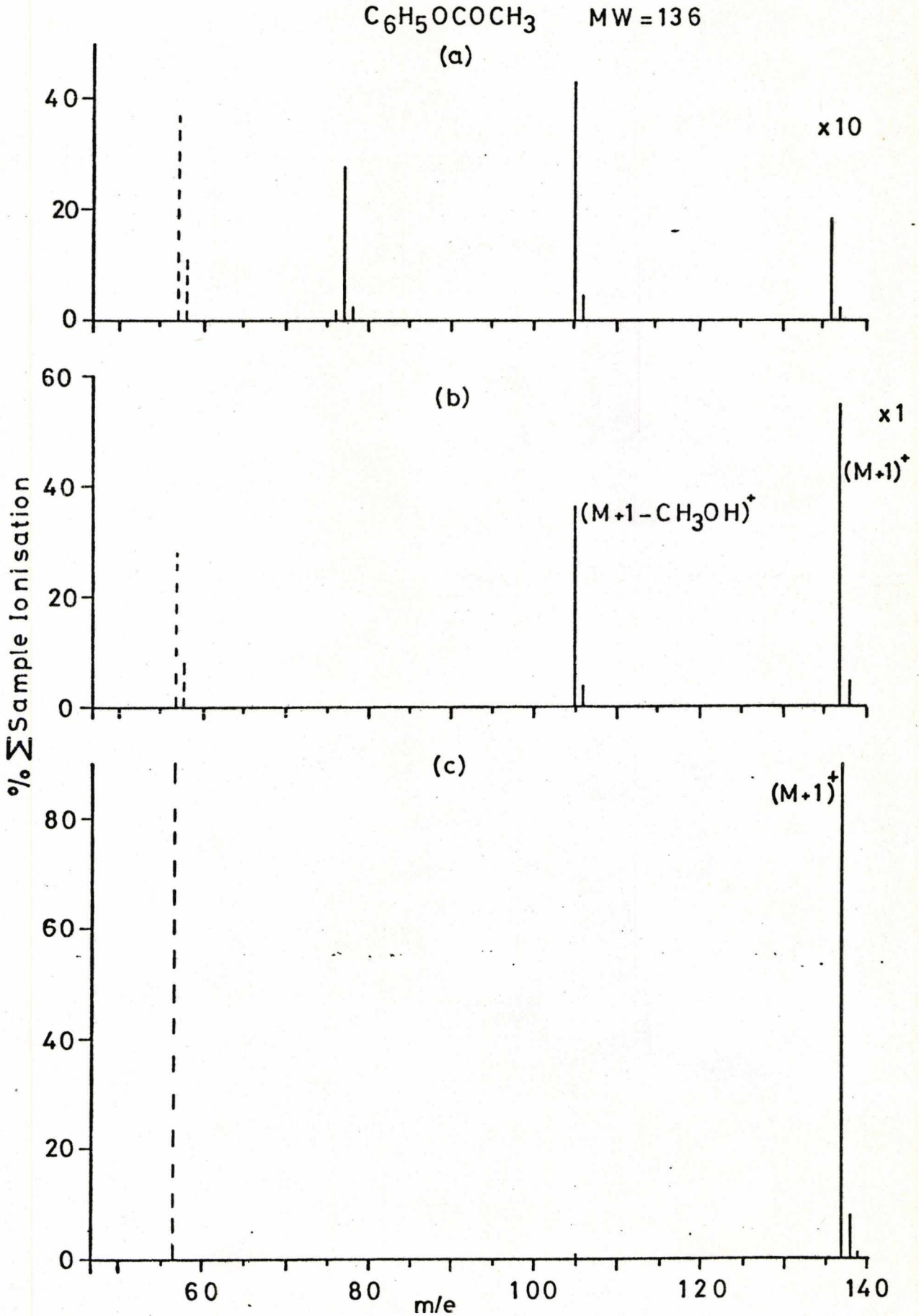

spectra of methyl benzoate. Firstly, in Section 6.2.1 it was suggested that reagent ions trapped in the Quistor will have a higher kinetic energy and also a higher internal energy than reagent ions drifting in the high pressure ion source. If this is so, it is reasonable to assume that quasi-parent ions formed, for example, by proton transfer reactions between reagent ions trapped in the Quistor and sample molecules, will have a higher internal energy than the same ions formed in the high pressure ion source. There will therefore be a greater tendency for the quasi-parent ions formed in the Quistor to fragment and consequently the relative intensity of fragment ions in low pressure CI mass spectra would be expected to be greater than that in high pressure CI mass spectra, as is the case with methyl benzoate. Secondly, as was discussed in Section 6.2.2, the fact that the average residence time of quasi-parent ions formed in the Quistor is considerably longer than that for the high pressure ion source, means that more time is available for the quasi-parent ions to undergo unimolecular decomposition reactions to produce the fragment ions. This effect will also lead to higher relative intensities of fragment ions in low pressure CI mass spectra.

6.3.1.2(d) Diethyl Succinate

The molecular ion and other ions in the high mass region of the EI mass spectra of dicarboxylic acid esters are invariably of very low relative intensity and it is often impossible to positively identify a particular ester from its EI mass spectrum alone. However, this class of compounds is particularly suited to analysis by CIMS since the quasi-parent ion in the isobutane-CI mass spectra of these compounds is often the base peak. Together with information derived from this and the fragment ions present in the spectra it is possible to identify a great number of the members of this class and even distinguish between geometrical isomers[167] using the CI-mass spectrum alone.

The low and high pressure isobutane-CI mass spectra of one of this

Figure 6.7 (a) Low and (b) High Pressure Isobutane-CI Mass Spectra of Diethyl Succinate

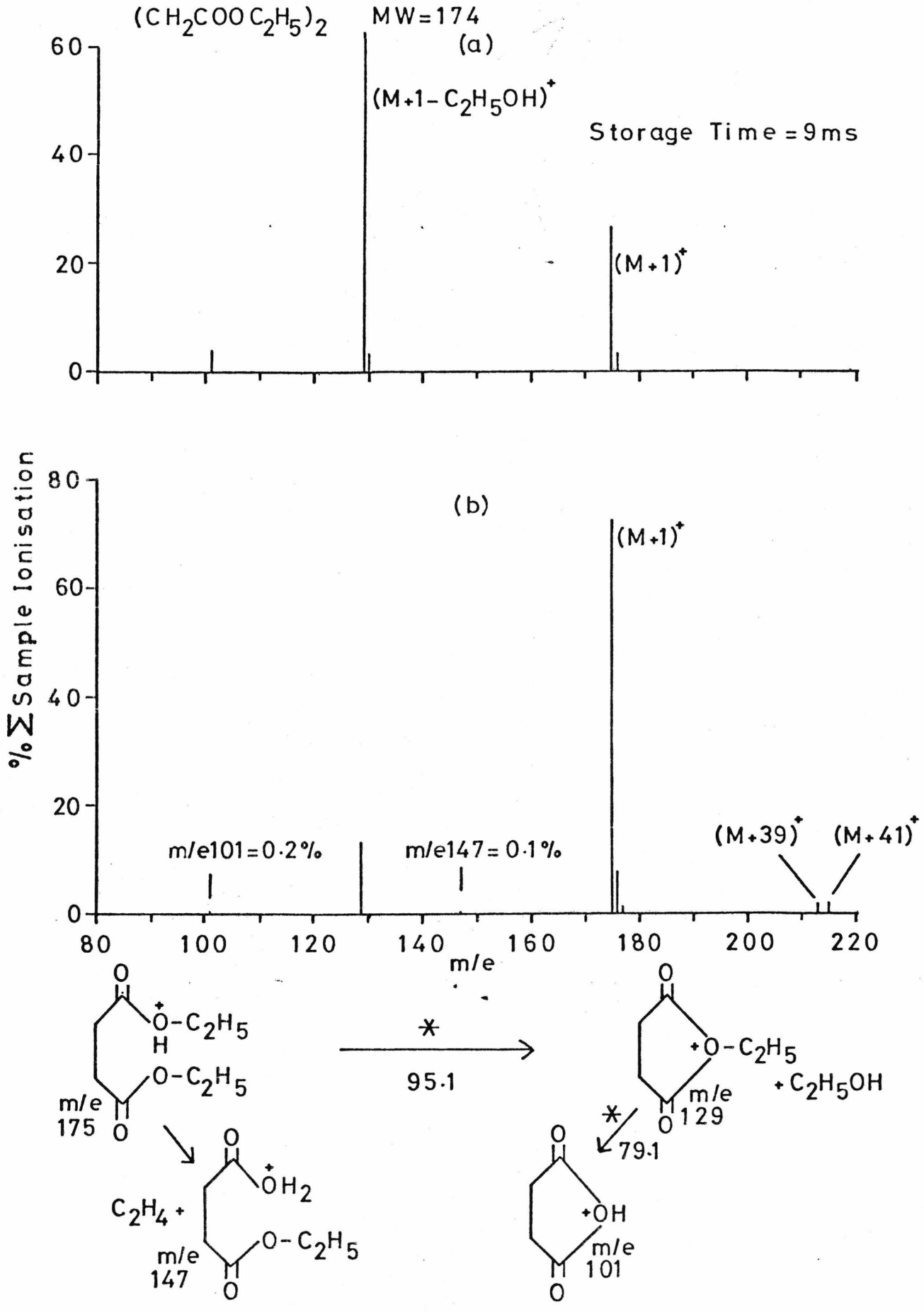

class of compounds, diethyl succinate is shown in Figure 6.7. The base peak in the low pressure mass spectrum is at m/e 129 which corresponds to the ion formed by the loss of an ethanol molecule from the $(M+1)^+$ species as is shown in Figure 6.7. The subsequent elimination of an ethylene molecule from the ion of m/e 129 gives rise to the formation of the only other fragment ion in this spectrum, at m/e 101. In the high pressure mass spectrum the quasi-parent ion is the base peak and in addition to the ions at m/e 129 and 101 there is also a fragment ion at m/e 147 corresponding to the species formed as a result of the loss of an ethylene molecule from the quasi-parent ion. As has been the case with the mass spectra of all the samples presented so far, the sum of the intensities of the fragment ions relative to the intensity of the quasi-parent ion in the low pressure mass spectrum, far exceeds that in the high pressure mass spectrum and it is unlikely that this is due solely to the mass discrimination of the Quistor.

No association ions were observed in the low pressure mass spectrum but ions at m/e's 213 and 215 in the high pressure mass spectrum probably correspond to the species $(M+39)^+$ and $(M+41)^+$ respectively. These arise as the result of addition reactions between the sample molecules and $C_3H_3^+$ and $C_3H_5^+$ species from the isobutane plasma.

Another feature of the high pressure mass spectrum, which was not observed in any low pressure CI mass spectra, was the presence of metastable ions at m/e's 79.1 and 95.1 corresponding to the decomposition processes indicated by asterisks in the scheme shown in Figure 6.7. Metastable peaks occur in high pressure CI mass spectra as a result of the unimolecular decomposition of excited ions, having half lives of the order of 10^{-6}s, in the ion source, or as a result of collisional dissociation owing to the relatively high pressures present in the field-free regions of a mass spectrometer operated in the high pressure CI mode[168]. Since all ions are trapped in the Quistor for *ca.* 10^{-2}s and it is operated at low pressures compared to the high pressure ion source no metastable

peaks would be expected in low pressure CI mass spectra. However, the Quistor in combination with the quadrupole mass filter has been employed to study very long-lived metastable species[122].

6.3.1.2(e) Alcohols

The low and high pressure isobutane-CI mass spectra of n-hexanol, n-heptanol and n-octanol are shown in Figures 6.8, 6.9 and 6.10 respectively. The relative intensities of the $(M+57)^+$ species in the high pressure CI mass spectra of n-hexanol and n-heptanol are very large compared to those in the mass spectra published in an extensive study of the isobutane-CI mass spectra of alcohols by Field[148]. However, this apparent discrepancy may be due to the fact that the ion source temperature employed in Field's study was 180°C and that for this study was 110°C since such a temperature dependence for the $(M+57)^+$ ion in the isobutane-CI mass spectra of secondary alcohols has already been reported[169]. The relative intensity of the $(2M+1)^+$ species in the high pressure mass spectrum of n-octanol is so large in this case that it is indicative of an excessively high sample partial pressure.

The $(M-1)^+$ and $(M+1 - H_2O)^+$ species are present in both the low and high pressure CI mass spectra of all three of the alcohols studied. The former ion is formed by hydride abstraction, most probably from the α carbon atom of the alcohol[169]:

$$t - C_4H_9^+ + R' - CH_2 - OH \longrightarrow R' - \overset{+}{C}H - OH + C_4H_{10}$$

$$R' - CH = \overset{+}{O}H \longleftarrow R' - \overset{+}{C}H - OH$$

There are two possible mechanisms for the formation of the $(M+1 - H_2O)^+$ ion in alcohols, as has already been mentioned in Section 6.3.1.2(a)[148]:

$$\left.\begin{aligned} t - C_4H_9^+ + R - OH &\rightarrow R - OH_2^+ + C_4H_8 \\ R - OH_2^+ &\rightarrow R^+ + H_2O \end{aligned}\right\} \quad I$$

Figure 6.8 (a) Low and (b) High Pressure Isobutane-CI Mass Spectra of n-Hexanol

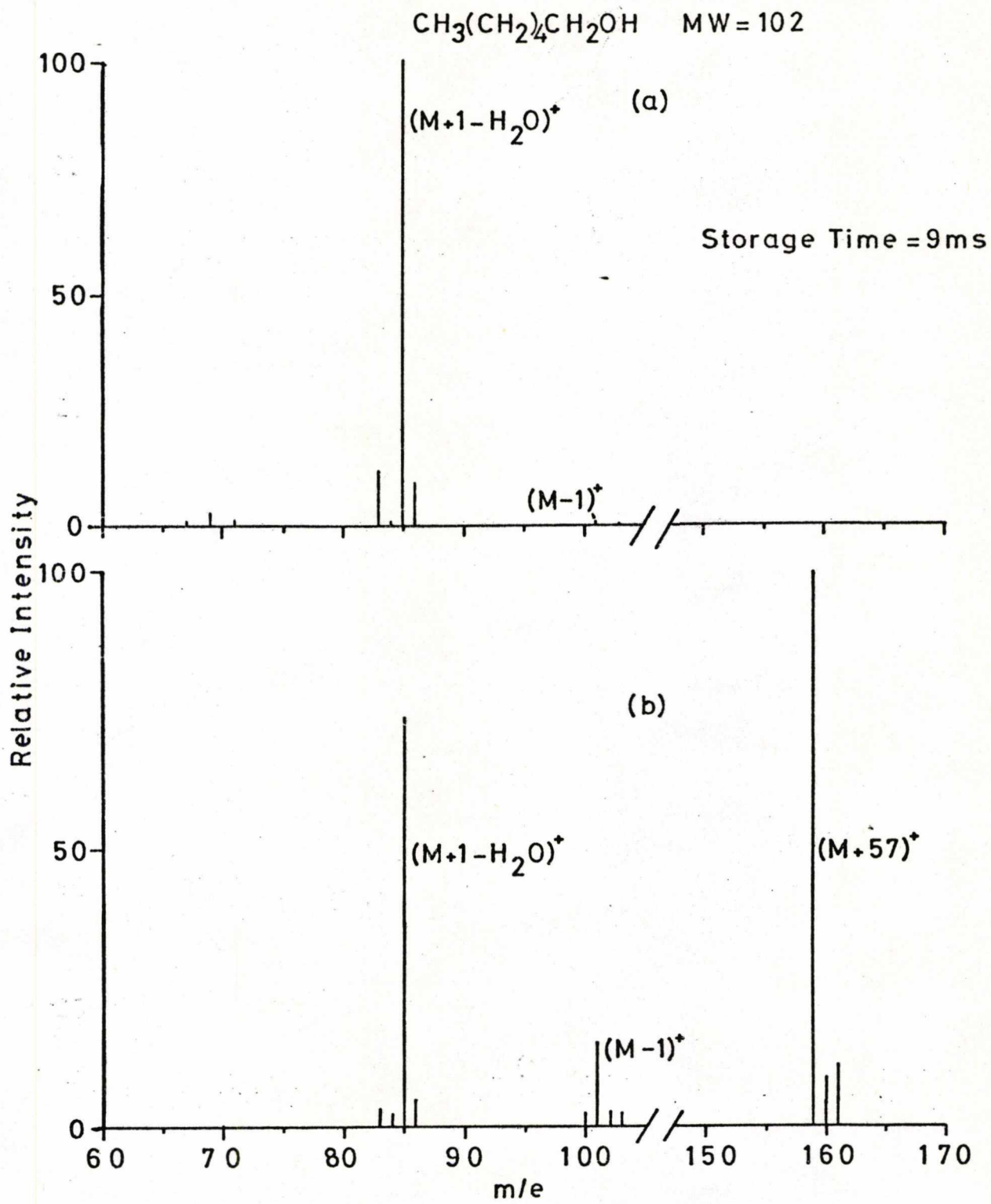

Figure 6.9 (a) Low and (b) High Pressure Isobutane-CI Mass Spectra of n-Heptanol

$CH_3(CH_2)_5CH_2OH$ MW = 116

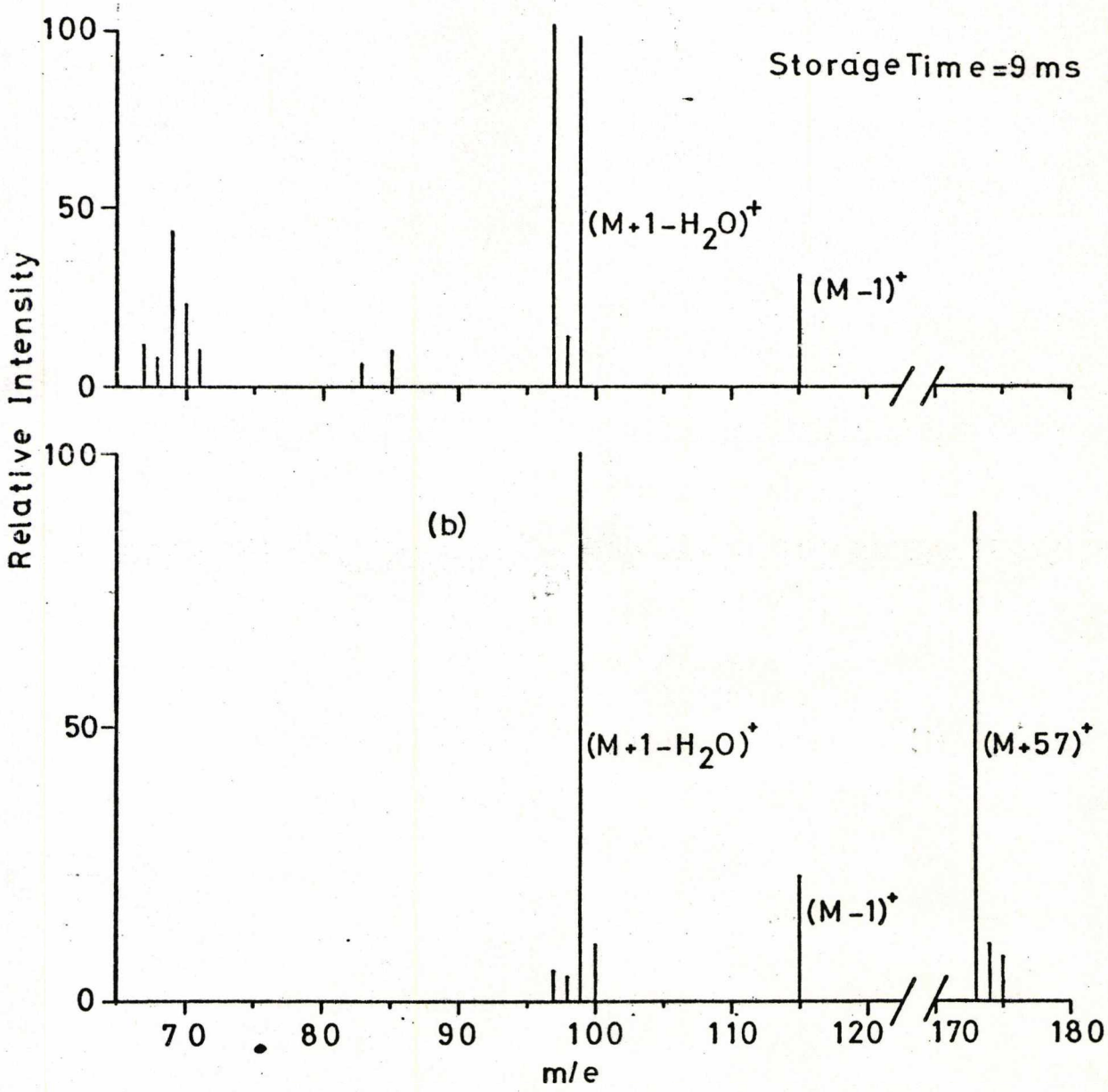

Figure 6.10 (a)Low and (b)High Pressure Isobutane-CI Mass Spectra of n-Octanol

$CH_3(CH_2)_6CH_2OH$ MW = 130

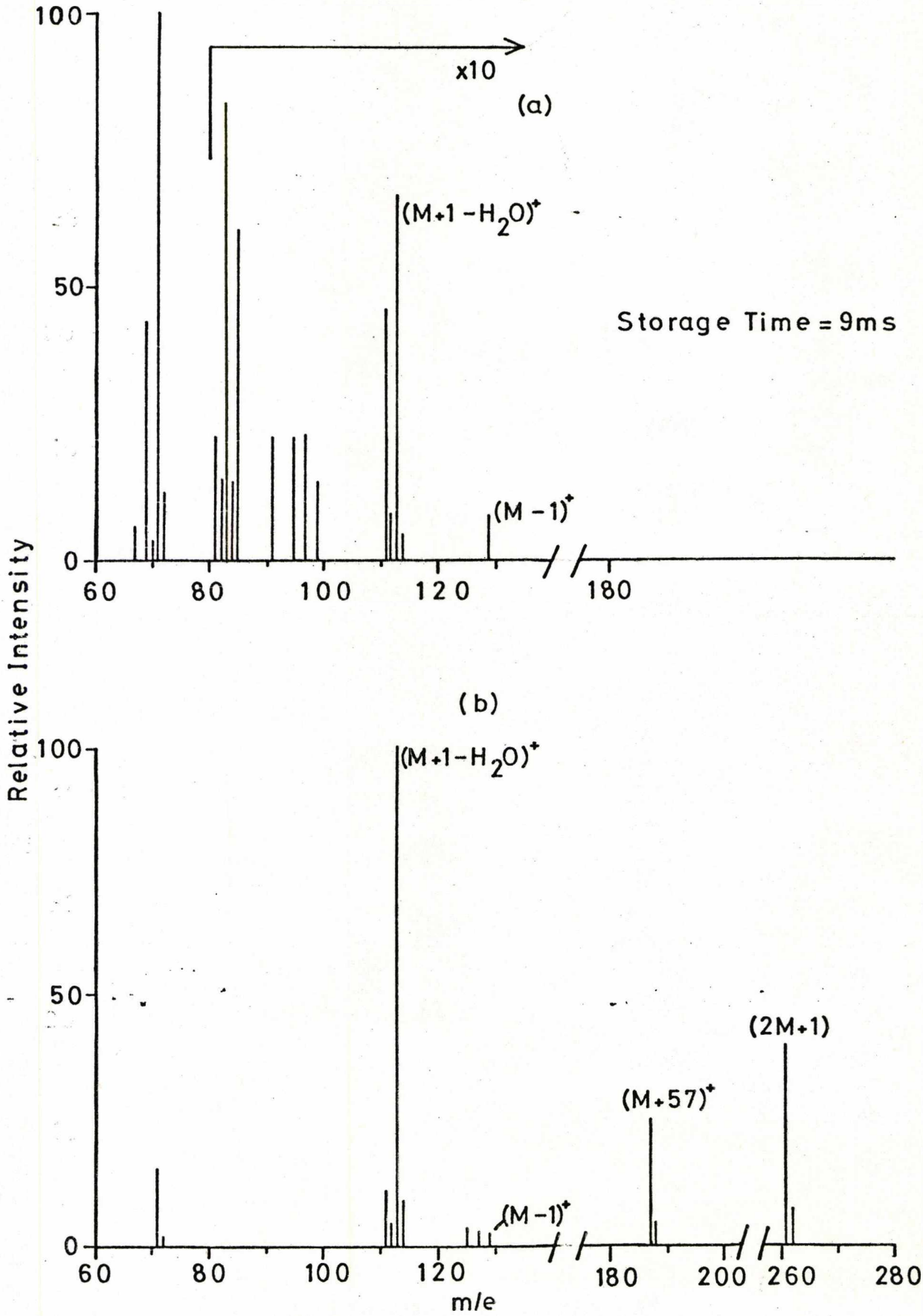

or

$$t - C_4H_9^+ + R - OH \rightarrow R^+ + t - C_4H_9 - OH \qquad II$$

where $R^+ \equiv (M+1 - H_2O)^+$.

Jelus *et al*[169] have shown that the $(M+1 - H_2O)^+$ ion in the isobutane-CI mass spectra of secondary alcohols is formed by both of the above pathways, and that the latter mechanism proceeds via the long-lived $(M+57)^+$ ion. The relative intensity of the $(M+1)^+$ ion is very small in both the low and the high pressure CI mass spectra of n-hexanol and does not occur in the mass spectra of n-heptanol or n-octanol. This suggests that if the $(M+1 - H_2O)^+$ species is formed by mechanism I then the second step of this mechanism is very fast.

In the low pressure CI mass spectrum of n-octanol there are many other fragment ions in addition to the $(M+1 - H_2O)^+$ species, these are comprised mainly of the two series of ions $C_nH^+_{2n-1}$ and $C_nH^+_{2n+1}$. Munson and Field[6] reported the occurrence of a similar set of fragment ions in the high pressure methane-CI mass spectrum of n-decanol and postulated that both series were formed as a result of the fragmentation of the $(M+1 - H_2O)^+$ ion. By applying the same reasoning to the case of n-octanol where the $(M+1 - H_2O)^+$ ion corresponds to the $C_8H^+_{17}$ species at m/e 113 the fragmentation pathways for the production of the alkyl series of ions $(C_nH^+_{2n+1})$ are:

$$C_8H^+_{17} \longrightarrow C_6H^+_{13} \text{ (m/e 85)} + C_2H_4$$

$$\longrightarrow C_5H^+_{11} \text{ (m/e 71)} + C_3H_6$$

$$\vdots$$

and for the alkenyl series $(C_nH^+_{2n-1})$

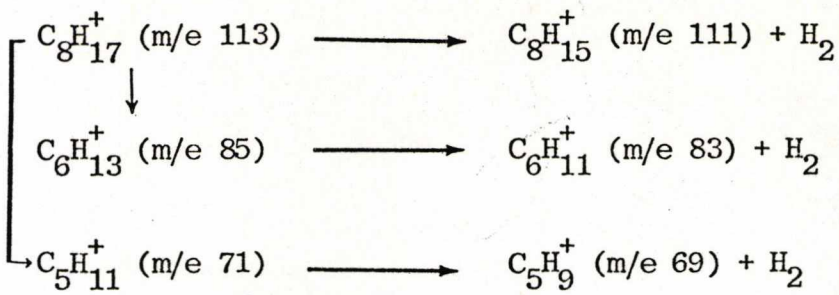

The large relative intensities of the above fragment ions in the low pressure CI mass spectrum of n-octanol compared to that in the high pressure CI mass spectrum (Figure 6.10) suggests that the $C_8H_{17}^+$ ion (i.e. $(M+1 - H_2O^+)$) is formed in the Quistor with a considerably larger internal excitation energy than when it is formed in the high pressure ion source. This is consistent with factors discussed in Section 6.2. The $(M+1 - H_2O)^+$ species in the low pressure CI mass spectra of n-hexanol and n-heptanol (i.e. $C_6H_{13}^+$ and $C_7H_{15}^+$ respectively) would be expected to fragment in the same way as that for octanol. However, it was not possible to determine with certainty whether this was in fact the case since many of the possible fragmentation pathways of $C_6H_{13}^+$ and $C_7H_{15}^+$ lead to the production of fragment ions with the same m/e values as the major primary and reagent ions present in the isobutane plasma.

6.3.1.2(f) Di-n-Butyl Phthalate

One of the initial problems encountered when operating the Quistor as a low pressure CI ion source arose due to the limited mass (strictly m/e) storage range of the device. In an effort to discover the upper limit, in terms of the sample molecular weight, for which isobutane could be employed as a reagent gas (i.e. such that $t - C_4H_9^+$ and $(M+1)^+$ are stored simultaneously) di-n-butyl phthalate was introduced into the Quistor system. The low pressure CI mass spectrum shown in Figure 6.11(a) demonstrates that it was possible to store the $(M+1)^+$ ion from di-n-butyl phthalate which is at m/e 279. This mass spectrum contains the same fragment ions as are present in the high pressure CI mass spectrum shown

Figure 6.11 (a) Low and (b) High Pressure Isobutane-CI Mass Spectra of Di-n-Butyl Phthalate

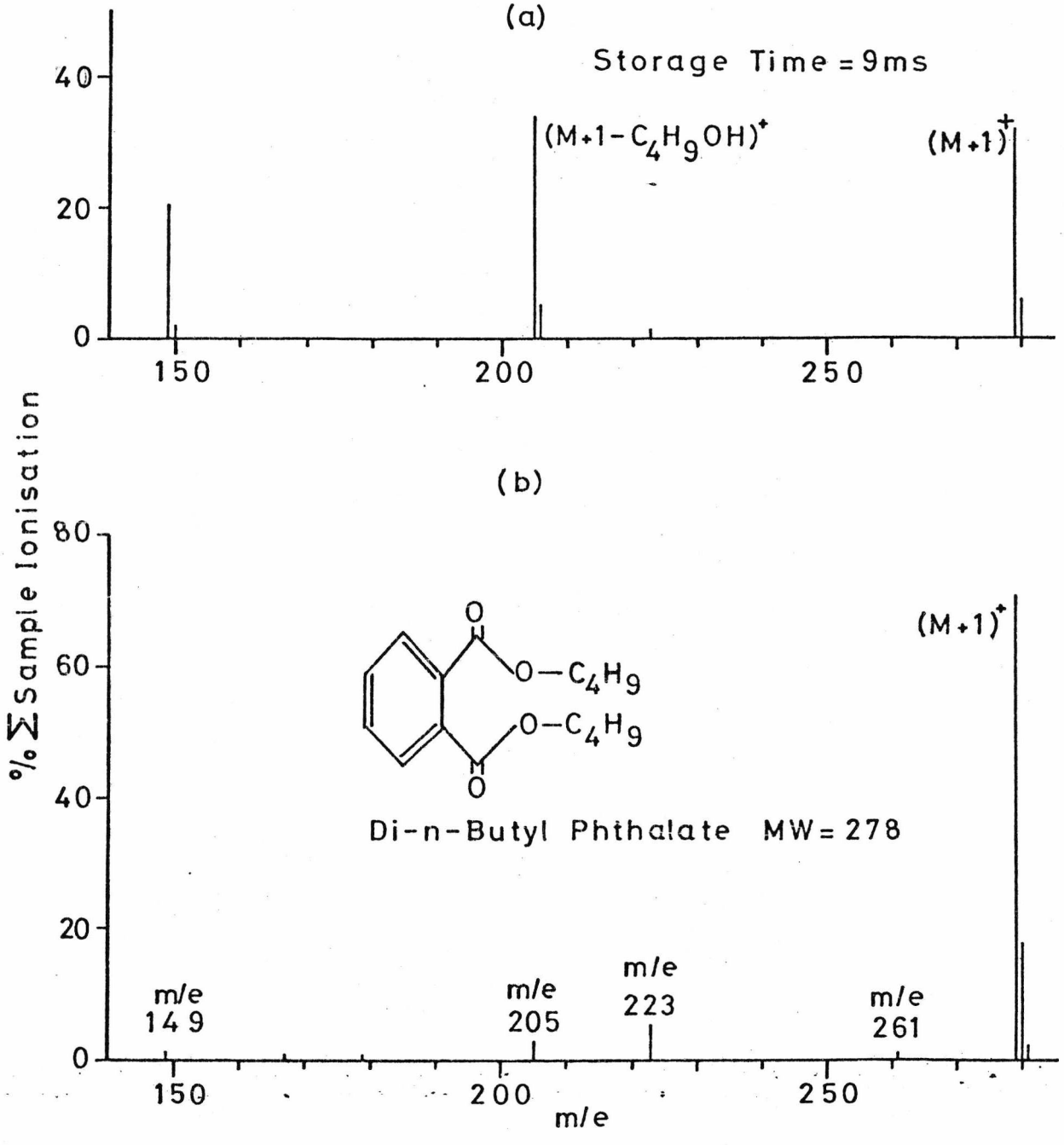

Figure 6.11(c) Fragmentation Scheme for Ions in the High Pressure Isobutane-CI Mass Spectrum of Di-n-Butyl Phthalate

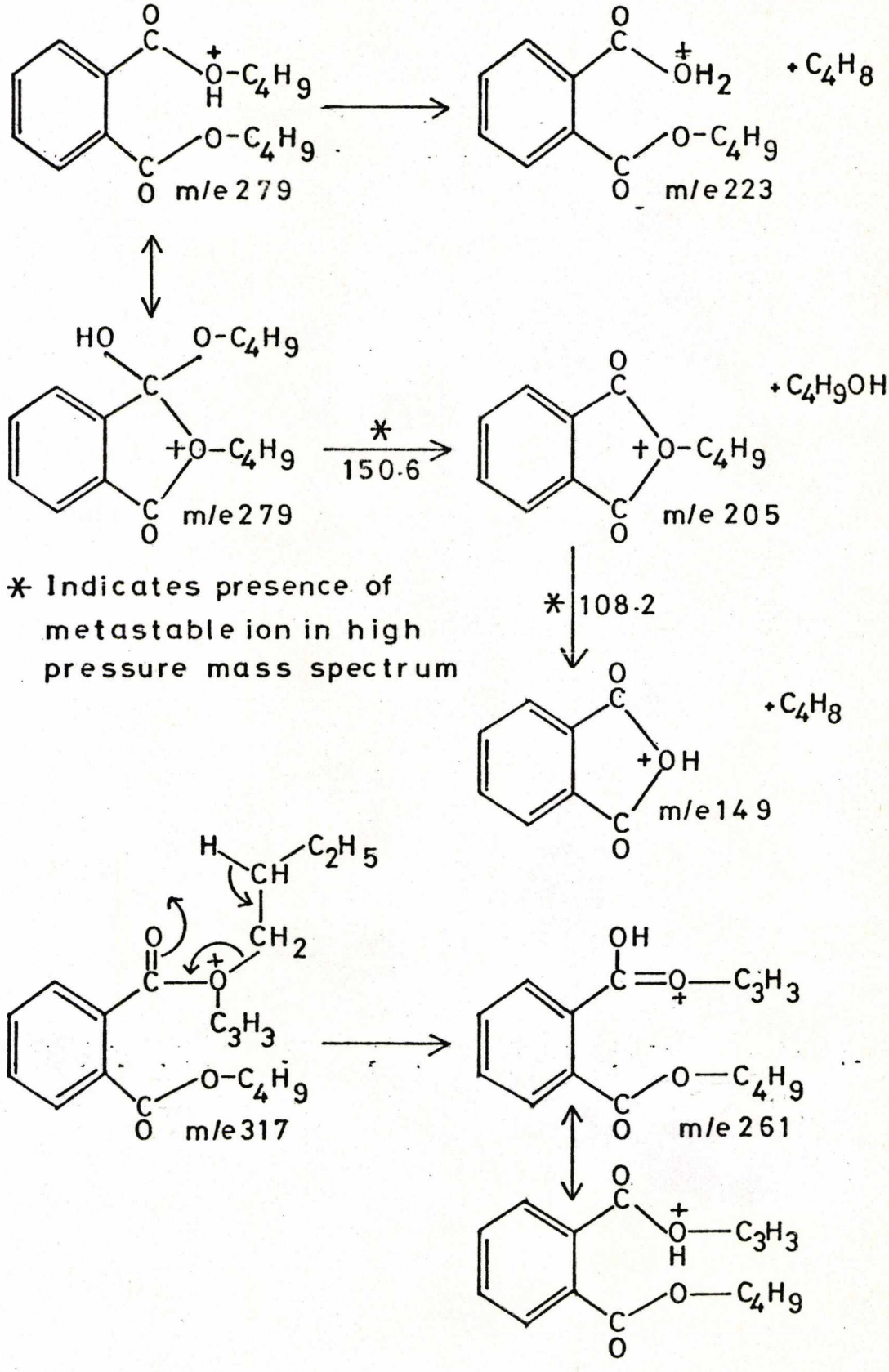

* Indicates presence of metastable ion in high pressure mass spectrum

in Figure 6.11(b) but the sum of the percentage total fragment ion intensities is higher in the low pressure mass spectrum. Most of the fragment ions arise as a result of the fragmentation of the $(M+1)^+$ species according to the scheme given in Figure 6.11(c). However, the fragment ion at m/e 261 is more likely to have been produced as a result of alkyl group exchange in the $(M+39)^+$ species which is also present in the high pressure mass spectrum (% Σ sample ionisation = 1.1%).

The fact that the Quistor ion source could not be heated prevented any further investigation into the possibility of storing ions of m/e values greater than 279 since high molecular weight samples tend to be of relatively low volatility and the introduction of such samples into the Quistor/MS9 system resulted in their condensation on the Quistor electrodes which rendered the device incapable of storing ions.

6.3.1.3 Conclusions Regarding the Use of Isobutane as a Reagent Gas

In summary, the salient points regarding the use of isobutane as a reagent gas to obtain low pressure CI mass spectra using the Quistor/MS9 system are:

(i) the low pressure CI mass spectra of the samples investigated, with the possible exception of that for octanol, were in general remarkably similar to the high pressure CI mass spectra;

(ii) quasi-parent ions, either $(M+1)^+$ or $(M-1)^+$, were present in the low pressure CI mass spectra of all the samples investigated;

(iii) the quasi-parent ions appeared to fragment in the same way in both ion sources, but the degree of fragmentation, in terms of the sum of the fragment ion intensities, was greater in the low pressure CI mass spectra;

(iv) no association ions were observed in the low pressure CI mass spectra;

(v) isobutane is suitable as a reagent gas for the Quistor/MS9 system for samples up to a molecular weight of at least 280.

6.3.2 The Use of Hexane as a Reagent Gas

Since reagent gases such as n-hexane and n-octane have been successfully employed in high pressure CIMS[170] it was decided to investigate the use of normal paraffins as reagent gases for low pressure CIMS.

6.3.2.1 The Low and High Pressure Mass Spectra of n-Hexane

As can be seen from Figures 6.12(a) and 6.12(b) the mass spectra of n-hexane recorded at an indicated pressure of 1.0×10^{-5} Torr change dramatically in going from zero to 9 ms storage time. The Quistor operating conditions employed to record these spectra were identical to those used to record the isobutane-CI mass spectra. The major product ion after a storage time of 9 ms is at m/e 85 which corresponds to the species $(C_6H_{13})^+$. Similarly, m/e 85 is the base peak in the high pressure mass spectrum of n-hexane shown in Figure 6.12(c), recorded at a pressure of *ca.* 0.1 Torr. The hexane pressure was estimated by direct comparison of relative ion intensity data with the results of Yu and Field[170] who have studied the variation in the relative intensities of ions in the mass spectrum of n-hexane as a function of pressure. According to Yu and Field[170] most of the odd-mass ions in the mass spectrum of n-hexane undergo exothermic ion-molecule reactions with hexane molecules to produce the $(C_6H_{13})^+$ ion by hydride abstraction. Other ions in the high pressure mass spectrum at *ca.* 0.1 Torr include: $(C_6H_{12})^+$, $(C_4H_9)^+$ $(C_4H_8)^+$ and $(C_3H_7)^+$.

6.3.2.2 Mass Spectra Obtained with n-Hexane as the Reagent Gas

The operating conditions employed to obtain the mass spectra presented in this section were identical to those used to obtain the isobutane CI mass spectra, for both the Quistor and the high pressure system, except for the pressure of n-hexane in the high pressure ion

Figure 6.12 Mass Spectra of n-Hexane Recorded at (a) zero (b) 9ms Storage Time and (c) at High Pressure.

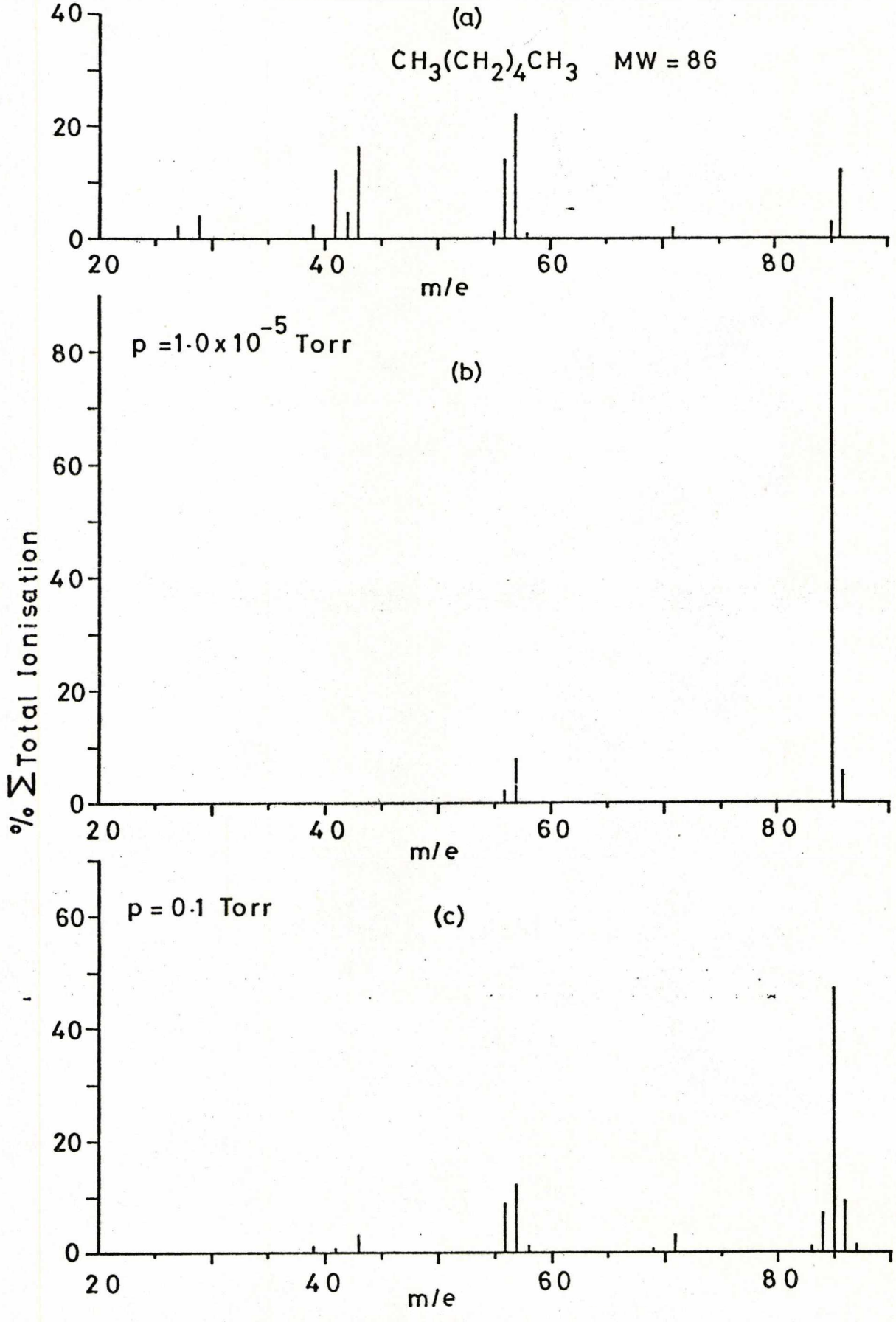

source which was maintained at *ca.* 0.1 Torr. In this way it was possible to make direct comparisons between low and high pressure CI mass spectra obtained using different reagent gases.

6.3.2.2(a) Benzaldehyde

The low and high pressure n-hexane CI mass spectra of benzaldehyde are shown in Figures 6.13(a) and 6.13(b) respectively. Except for the presence of association ions in the latter spectrum, there is a greater degree of similarity between the low and high pressure n-hexane CI mass spectra of benzaldehyde than there is between the corresponding isobutane-CI mass spectra (Figures 6.6(c) and 6.6(d)). This is because the $(C_6H_7)^+$ species of m/e 79 is not present in the low pressure n-hexane-CI mass spectrum. One possible explanation for this is as follows: the average ion kinetic energy of the $(C_6H_{13})^+$ species trapped in the Quistor is *ca.* 4eV (calculated using the pseudo-potential model), which is 2eV lower than that for the $(C_4H_9)^+$ ion stored under the same conditions, this value could be below the kinetic energy threshold for the fragmentation of the $(M+1)^+$ species to form the $(C_6H_7)^+$ ion.

6.3.2.2(b) Methyl Benzoate

As was the case with benzaldehyde the low and high pressure n-hexane CI mass spectra of methyl benzoate, shown in Figures 6.14(a) and 6.14(b) respectively, are more alike than the corresponding isobutane-CI mass spectra (Figure 6.6). Both the low and the high pressure n-hexane mass spectra contain only two major ions: $(M+1)^+$ and $(M+1 - CH_3OH)^+$.

6.3.2.2(c) Diethyl Succinate

The low and high pressure n-hexane CI mass spectra of diethyl succinate are shown in Figure 6.15. In this case there is a marked similarity between these spectra and the corresponding isobutane-CI mass spectra.

Figure 6.13 (a)Low and (b) High Pressure Hexane - CI Mass Spectra of Benzaldehyde

C_6H_5CHO MW = 106

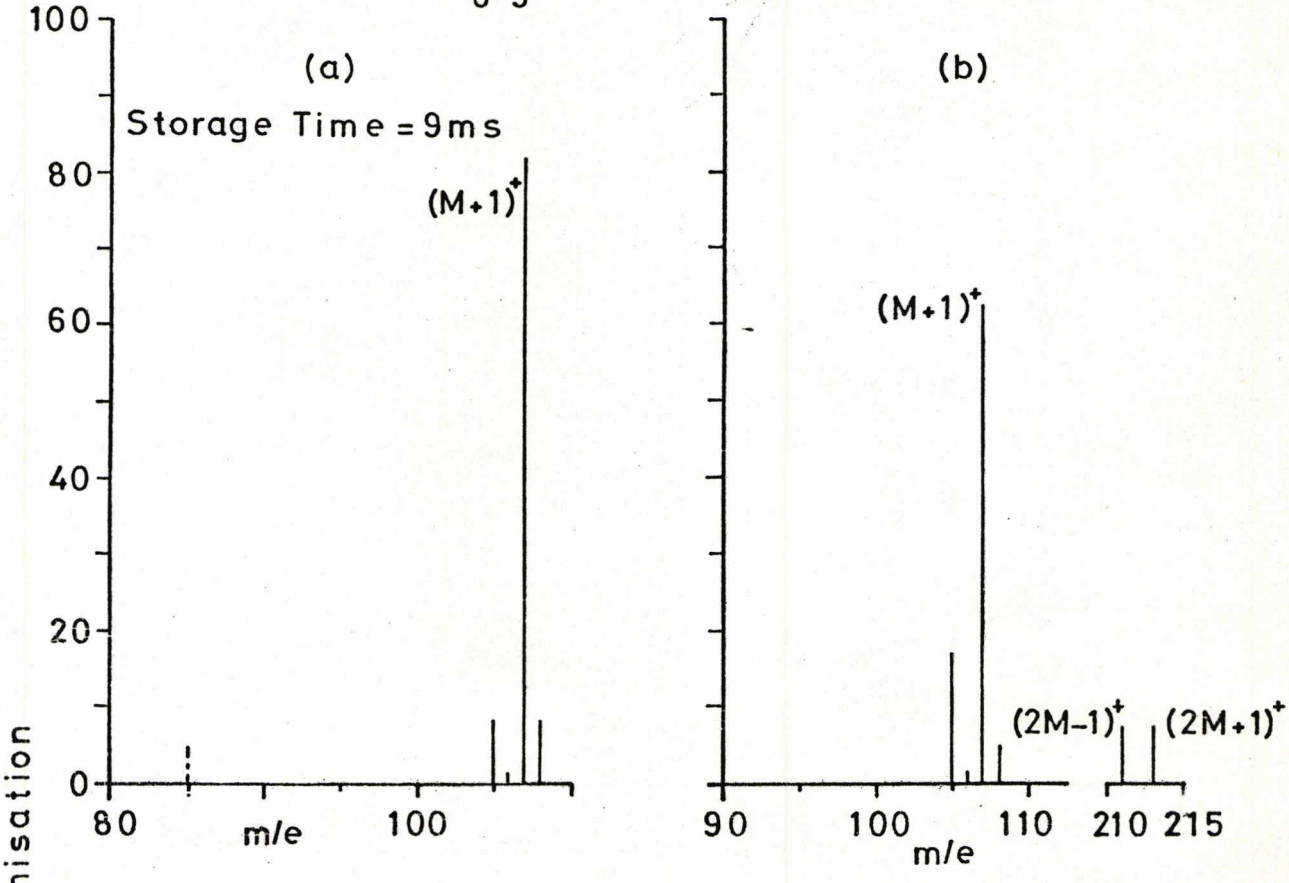

Figure 6.14 (a) Low and (b) High Pressure n-Hexane CI Mass Spectra of Methyl Benzoate

$C_6H_5COOCH_3$ MW = 136

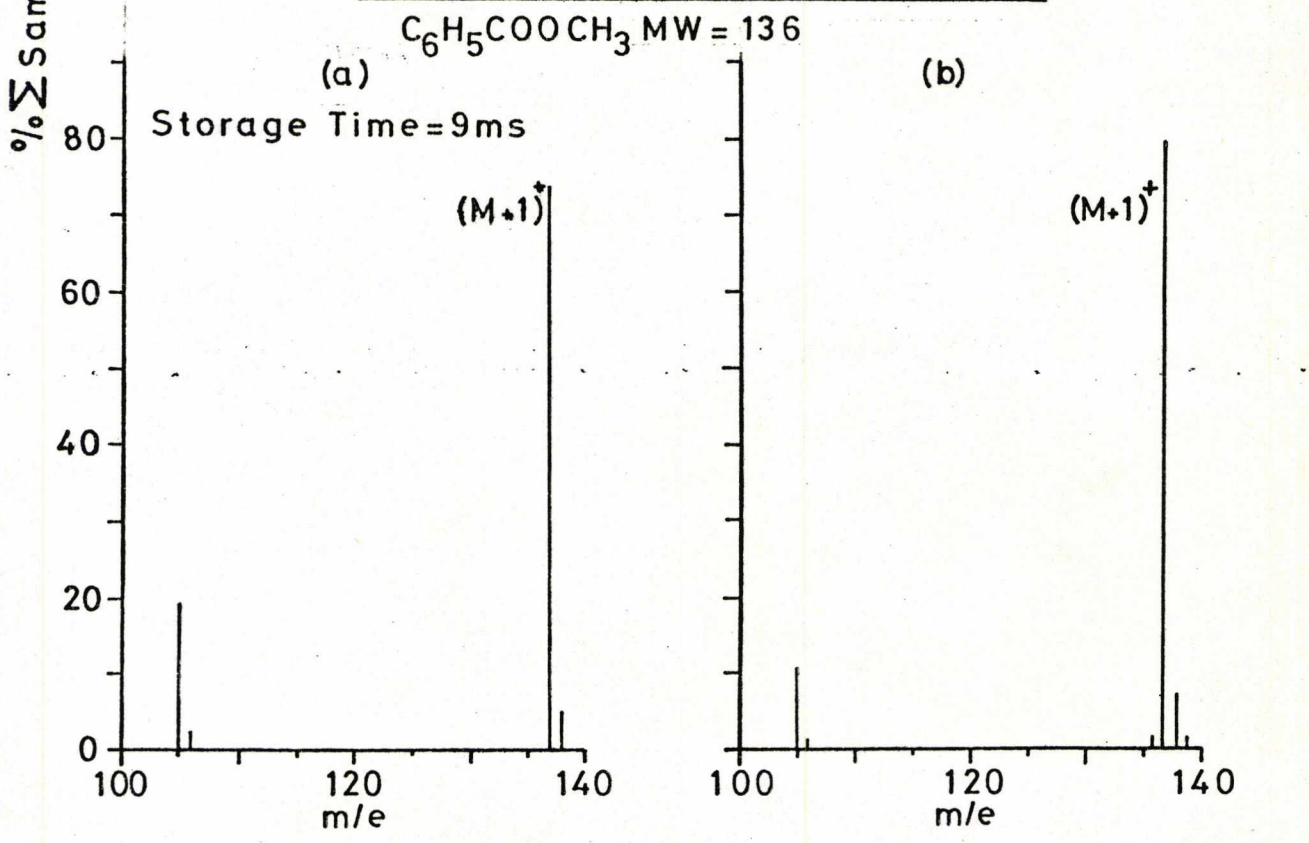

Figure 6.15 (a) Low and (b) High Pressure n-Hexane CI Mass Spectra of Diethyl Succinate

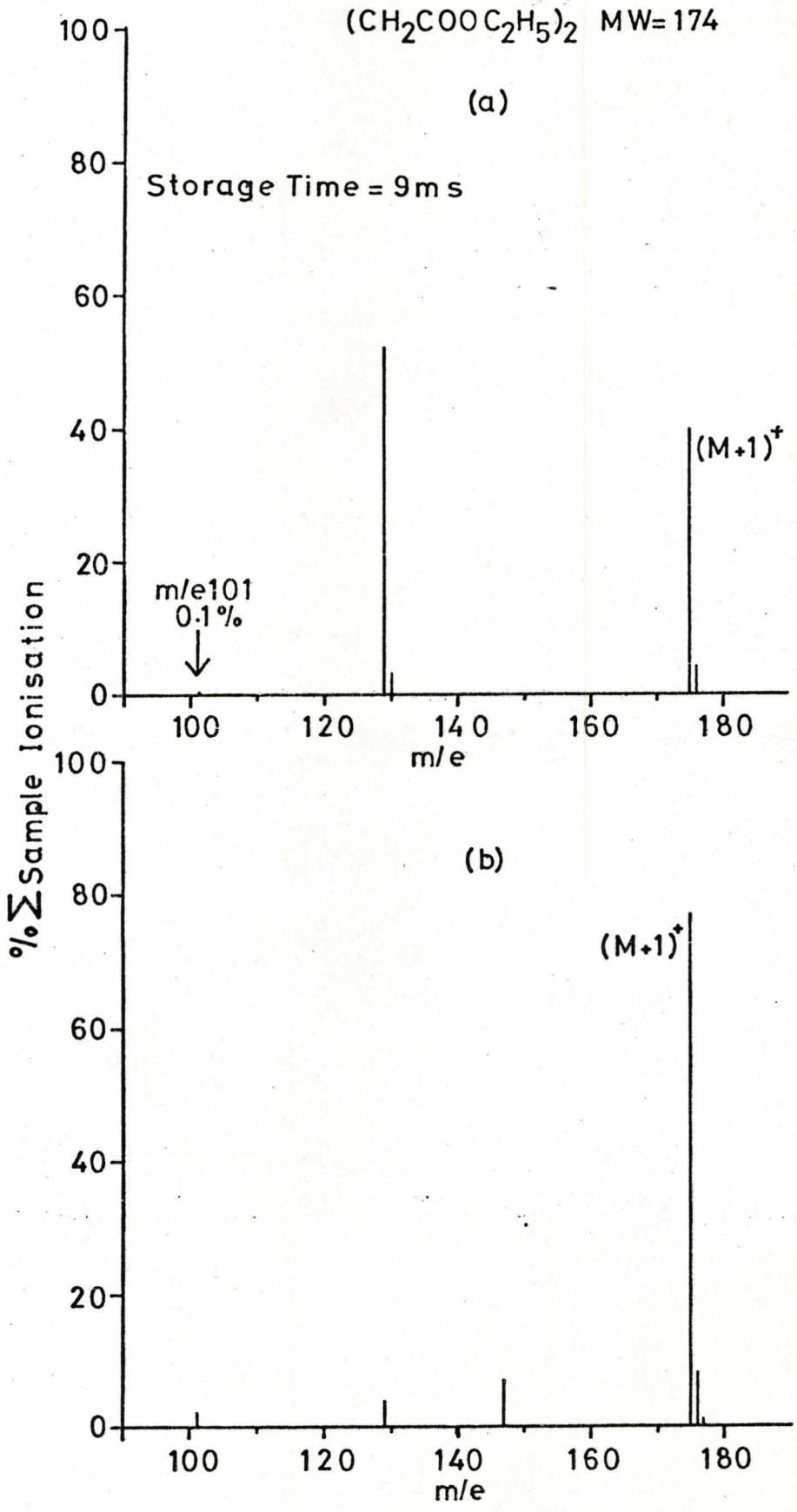

6.3.2.2(d) Di-n-Butylamine

In the low and high pressure n-hexane CI mass spectra of di-n-butylamine shown in Figure 6.16, the intensity of the $(M+1)^+$ species amounts to over 80% of the total ionisation in both cases. There are no ions in either spectrum with m/e values lower than that of the $(M-1)^+$ species.

6.3.2.2(e) Cyclohexanone

The low and high pressure n-hexane CI mass spectra of cyclohexanone shown in Figure 6.17 contain the major features which are characteristic of the differences between low and high pressure CI mass spectra in general. These are: the higher relative intensity of ions arising due to the fragmentation of the quasi-parent ions in the low pressure CI mass spectra, and the presence of association ions, in this case $(2M+1)^+$, in the high pressure CI mass spectra which are not generally observed in low pressure CI mass spectra.

6.3.2.3 Conclusions Regarding the Use of n-Hexane as a Reagent Gas

In general both the high and the low pressure n-hexane CI mass spectra of the samples investigated were very similar to those obtained using isobutane as a reagent gas.

Yu and Field[170] postulated that since the degree of fragmentation in the high pressure CI mass spectra obtained with isobutane and n-hexane as reagent gases is so similar, then the $C_6H_{13}^+$ reagent ion from n-hexane probably has a tertiary structure. This postulate is supported by the following thermodynamic considerations. The degree of fragmentation of a particular quasi-parent ion MH^+, formed by a proton transfer reaction, is in some way proportional to the difference between the proton affinities of M and the conjugate base of the reagent ion; in the case of the t - $C_4H_9^+$ species from isobutane the conjugate base is isobutene which has a proton affinity (PA) of 194[171] K.cal.mol^{-1}.

Figure 6.16 (a)Low and (b)High Pressure n-Hexane CI Mass Spectra of Di-n Butylamine

$(C_4H_9)_2NH$ MW = 129

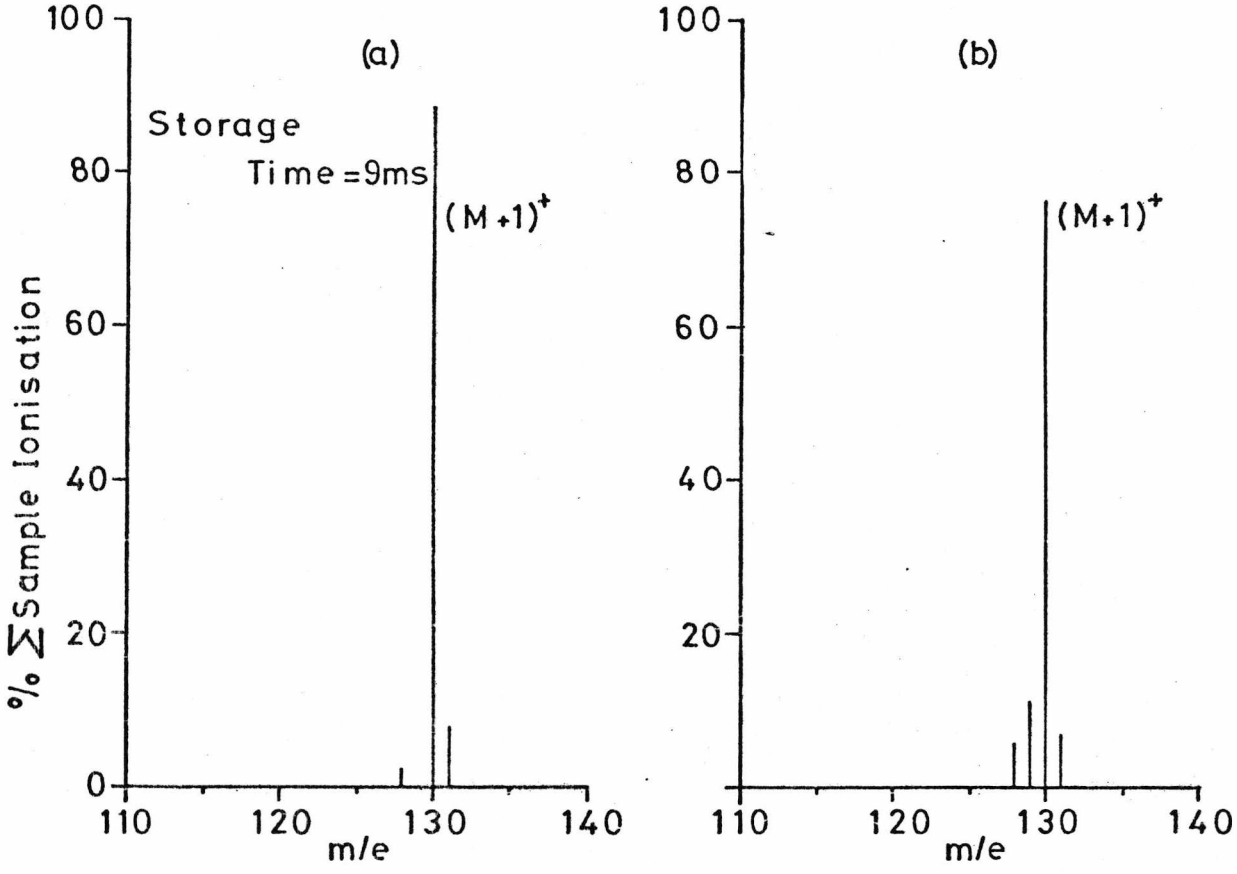

Figure 6.17 (a)Low and (b)High Pressure n-Hexane CI Mass Spectra of Cyclohexanone

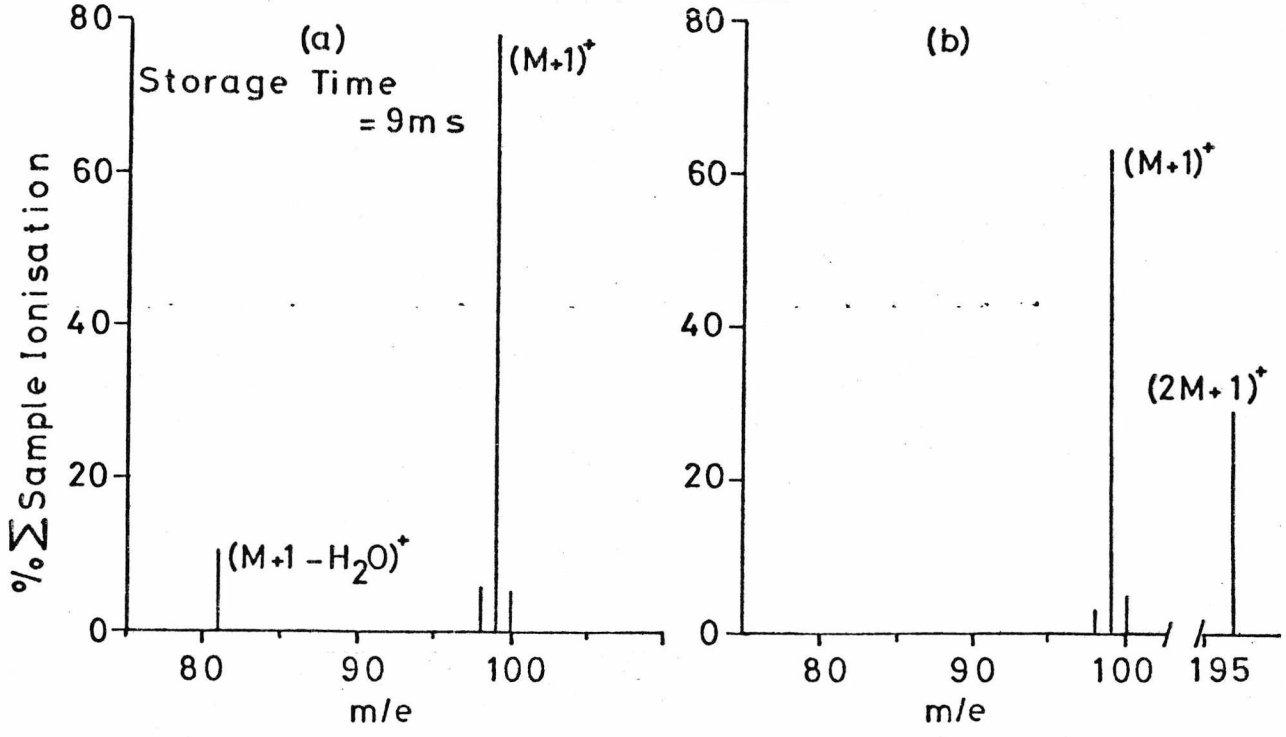

$$t - C_4H_9^+ + M \longrightarrow MH^+ + CH_2 = C(CH_3)_2$$

$$PA = 194 \text{ K.cal.mol}^{-1}$$

The two most likely structures for a tertiary $C_6H_{13}^+$ ion from n-hexane are:

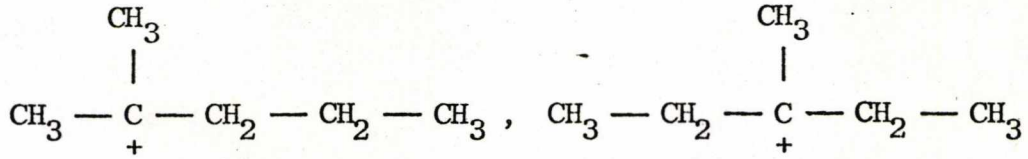

If these ions underwent proton transfer reactions with M then the conjugate bases formed would be:

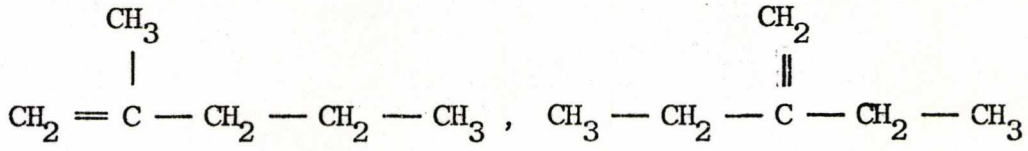

or

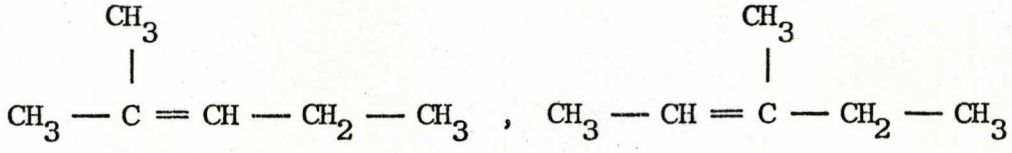

The proton affinities of these molecules are all within 1 K.cal. of 198[171] K.cal.mol^{-1} and since this is very close to the value of the proton affinity for isobutene, a similar degree of fragmentation would be expected in isobutane and n-hexane CI mass spectra of a particular sample if the major reagent ions were $t - C_4H_9^+$ and $t - C_6H_{13}^+$ respectively.

6.3.3 The Possibility of Using n-Heptane as a Reagent Gas

One of the major processes which occurs when n-heptane is subjected to either electron impact[172] or chemical ionisation[173] is the formation of the $C_7H_{15}^+$ species and its subsequent fragmentation:

$$C_7H_{15}^+ \longrightarrow C_4H_9^+ + C_3H_6$$

Parisod and Gaumann[173] have shown that the $C_4H_9^+$ species formed in this way has a tertiary structure irrespective of whether its precursor ion was formed under CI or EI conditions. It is therefore reasonable to assume that, the ion at m/e 57, which is the base peak in both the low and the high pressure mass spectra of n-heptane shown in Figure 6.18, corresponds to the t - $C_4H_9^+$ species. By comparing these spectra with the zero storage mass spectrum shown in Figure 6.18(a) it appears that the $C_7H_{15}^+$ ions are formed by hydride abstraction reactions between some of the n-heptane primary ions and n-heptane molecules, in an analogous fashion to the formation of the $C_6H_{13}^+$ species in n-hexane.

Clearly if n-heptane were employed as a reagent gas then the major reagent ion would be identical to that formed in isobutane, that is the t - $C_4H_9^+$ species, and consequently the CI mass spectra produced using these two reagent gases should be very similar. This was confirmed by obtaining the high pressure n-heptane CI mass spectrum of diethyl succinate and comparing it with the high pressure isobutane mass spectrum which was shown in Figure 6.7(b). From the data presented in Table 6.3 it is apparent that the two mass spectra were indeed quite similar.

No further studies were performed on the use of n-heptane as a reagent gas since it appeared to have no particular advantage over isobutane with respect to the nature of the CI mass spectra obtained and more importantly, since it is a liquid up to *ca.* 100°C and the reagent gas inlet systems could not be conveniently heated, it was very difficult to maintain a constant pressure of n-heptane in either the high pressure ion source or the Quistor system.

Figure 6.18 Ion Storage and High Pressure Mass Spectra of n-Heptane

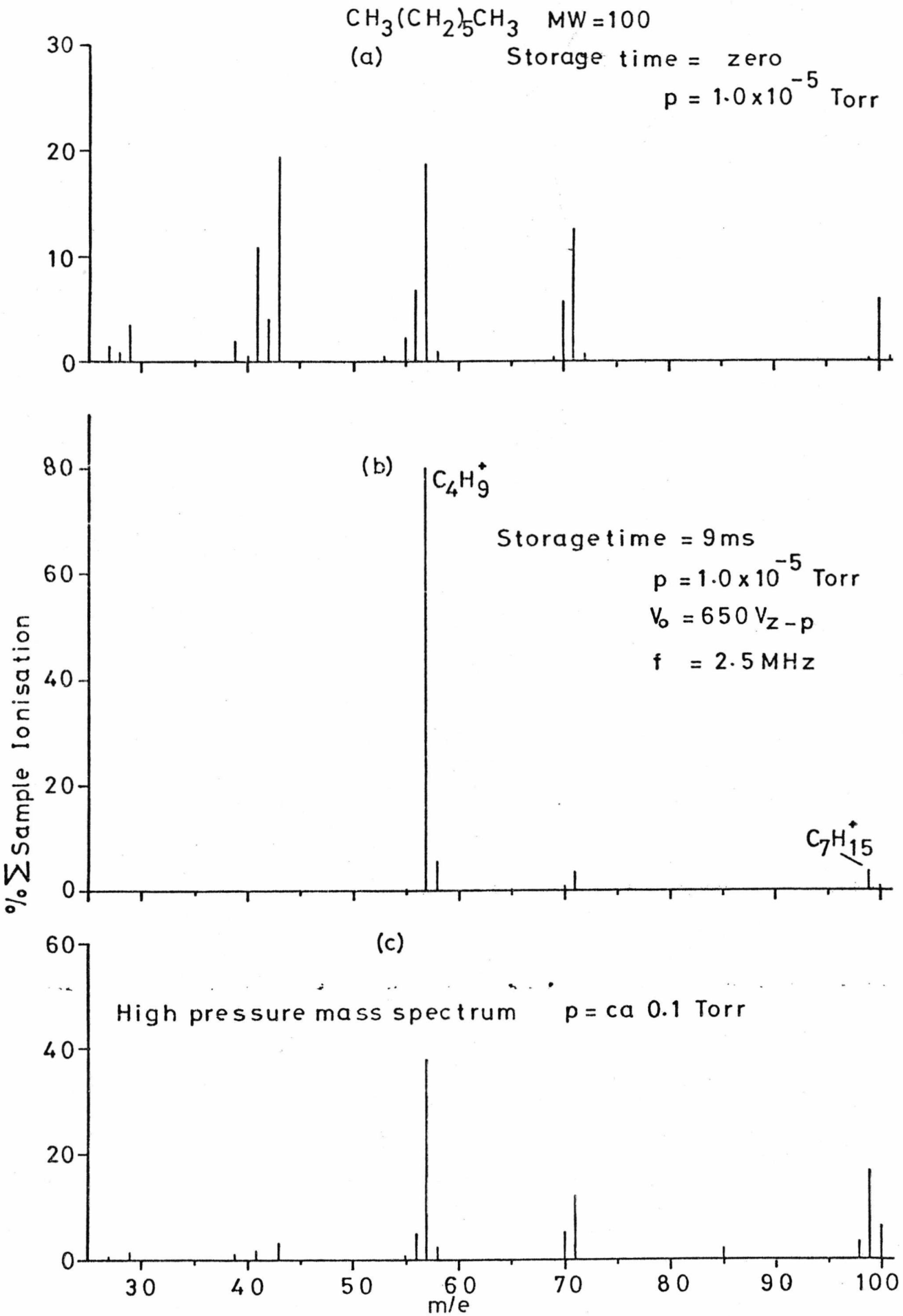

Table 6.3 Comparison of the High Pressure n-Heptane and Isobutane-CI Mass Spectra of Diethyl Succinate

m/e	Percentage Total Sample Ionisation	
	Isobutane	n-Heptane
101	0.2	0.3
129	13.2	12.8
130	1.1	0.8
175	72.7	78.9
176	8.3	6.0
213	1.9	-
215	1.4	-

6.4 Self-Chemical Ionisation in the Quistor

During the course of this work it was noticed that, for certain compounds chemical ionisation processes occur in the Quistor without a reagent gas being present. For example the mass spectrum of cyclohexanone recorded at 2 ms storage time, which is shown in Figure 6.19, consists essentially of the same ions which are present in the EI mass spectrum of cyclohexanone[166] with the addition of ions at m/e 81 and m/e 99 which correspond to the $(M+1 - H_2O)^+$ and $(M+1)^+$ species respectively. Similarly, in the mass spectrum of benzaldehyde recorded at 2 ms storage time, which is shown in Figure 6.20, the major ions, at m/e 77, 105 and 106 are also found in the EI mass spectrum of benzaldehyde[166]. In addition to these there are ions at m/e 79 and 107 which were observed in the isobutane-CI mass spectrum of benzaldehyde.

The occurrence of CI-type ions under these conditions is not surprising since most of the fragment ions formed by the initial electron

Figure 6.19 Mass Spectrum of Cyclohexanone Recorded at 2ms Storage Time

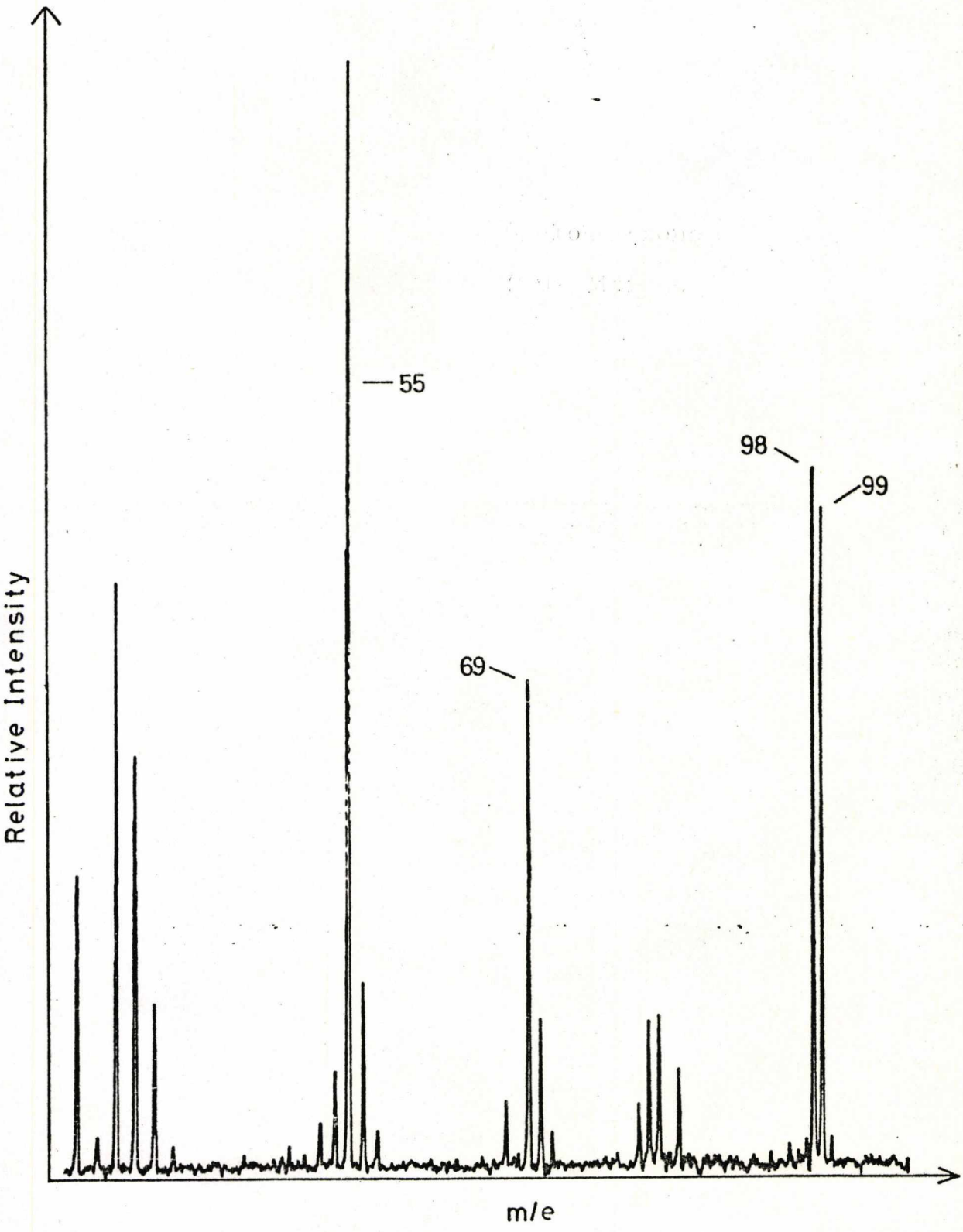

Figure 6.20 Mass Spectrum of Benzaldehyde Recorded at 2ms Storage Time

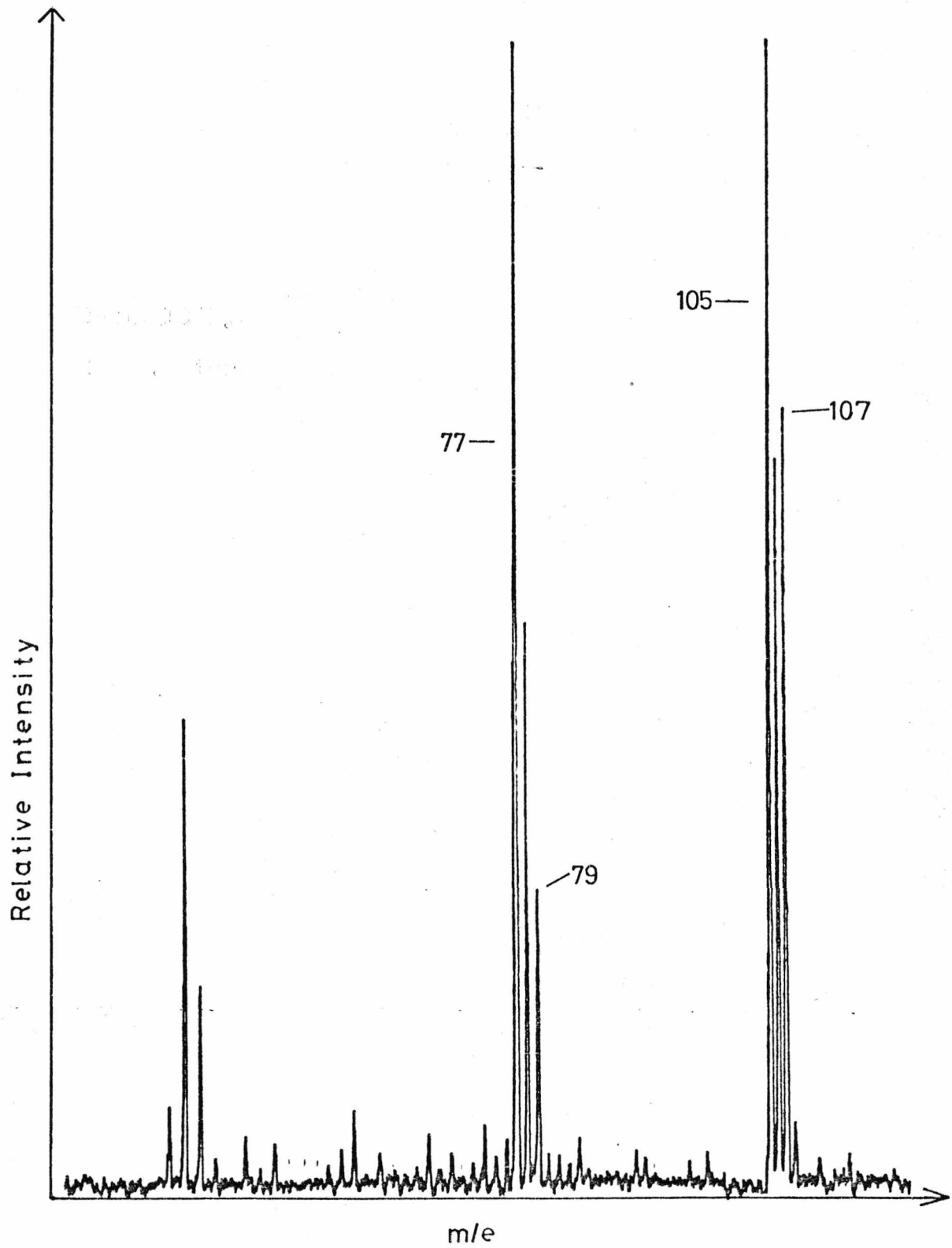

impact ionisation of the sample have stable trajectories in the device and will thus have the opportunity to react with sample molecules. Mass spectra such as those shown in Figures 6.19 and 6.20, which are in effect combined EI-CI mass spectra, may be particularly useful in the analysis of samples which produce molecular ions of very low relative intensity under electron impact conditions. For such samples a combined EI-CI mass spectrum would provide structural information from the EI fragment ions and also an indication of the molecular weight of the sample from the CI quasi-parent ion. The occurrence of 'self-chemical ionisation' in the Quistor is of course wholly dependent on the production of suitable reagent ions by the initial electron impact ionisation of the sample. Combined EI-CI mass spectra are also obtained when reagent gas mixtures such as argon-water and nitrogen-water are employed in high pressure CIMS[112].

6.5 Comparison of the Performance of the MS9 when Operated with the Quistor and the High Pressure Ion Source

The high resolution capability of the MS9 was severely impaired when operated with the Quistor ion source, in direct contrast to the situation when the high pressure ion source was employed as has already been mentioned in Chapter 5. When the MS9 was tuned to m/e 29 a resolution of 20,000 (10% valley definition), as measured using the peak switching system, was easily attainable when the high pressure ion source was installed; but when operated with the Quistor the maximum resolution was 2500 (10% valley definition). The reason for this is related to the fact that the Quistor is a pulsed ion source, in that, as the resolution is increased the scan time per mass unit decreases and when this time becomes less than the length of the Quistor duty cycle the probability of an ion pulse arriving in a particular 'mass window' is less than unity. In practice this results in an intermittent ion signal and consequently, under these conditions it is impossible to obtain reproducible mass

spectra. The value of 2500 for the maximum resolution was obtained while operating the Quistor at a duty cycle of 10 ms. It was possible to increase the resolution by shortening the duty cycle, however, for low pressure CI studies it is essential to have as long a storage time as possible and since a decrease in the length of the duty cycle necessarily means a decrease in the maximum available storage time, the determination of resolution at shorter duty cycles was not relevant to the present application.

In comparing the performance of two ion sources it is important to have a knowledge of their relative sensitivities. One of the most meaningful definitions of sensitivity is the total charge produced from a known quantity of a particular sample introduced into the ion source. This may be determined in the case of a double focussing magnetic mass spectrometer, such as the MS9, by slowly evaporating a known quantity of sample from the end of the direct insertion probe into the ion source, and measuring the current collected on a total ion collector, which is mounted between the electrostatic analyser and the magnet, as a function of time. Unfortunately, this method is not applicable to the determination of sensitivities of CI-type ion sources because it is impossible to distinguish between the ion current produced from the sample and the relatively large ion currents which arise through the presence of the reagent ions. This problem may be avoided by employing a method, suitable for determining relative sensitivities, which involves recording a series of mass spectra which are integrated and digitised using a data system[15]. By scanning the mass spectrometer over a mass range which does not include the reagent ions, the total ion current collected is then, that which arises from the sample alone.

A number of problems were encountered in attempting to find a method of determining the relative sensitivities of the Quistor and the high pressure ion source. Firstly, any method which involves repetitive recording of mass spectra could not be employed because of the very slow

maximum scan rate available with the Quistor system. Secondly, in order to determine the relative sensitivities of any two ion sources, the means of sample introduction must be such that, either the exact amount of the sample introduced into each ion source is known or, that the relative amounts (or relative mass flow rates) are known. The All Glass Heated Inlet System (AGHIS) was unsuitable for this purpose because it could not be used to introduce samples into the high pressure ion source and also because it could not be used for the introduction of known amounts of sample. The only available alternative sample inlet systems were the reagent gas/sample introduction probe for the high pressure ion source and the AEI direct insertion probe for the Quistor. However, it was discovered that when a sample was introduced into the Quistor using the probe, the total sample ion current produced was a factor of two or three orders of magnitude lower than when the same sample was introduced using the AGHIS even though the indicated sample partial pressure was the same in both cases. One possible explanation for this effect is that when samples are introduced by way of the AGHIS they enter the ion source through the same inlet port as, and mixed with, the reagent gas, whereas when introduced on the probe they enter through the port exactly opposite that through which the reagent gas is introduced. This arrangement may have resulted in unfavourable conditions for the flow of sample from the probe into the ion source. Consequently, the use of the direct insertion probe would have given an unrepresentative measure of the sensitivity of the Quistor and.since no other suitable means of sample introduction was available it was not possible to make a meaningful determination of the relative sensitivities of the two ion sources.

In an effort to gain some insight into factors related to the sensitivity of the two ion sources, the following approximate calculations were performed for typical operating conditions. One factor which deserves consideration is the sample consumption rate (R) which may be estimated for the case of the Quistor using the following expression

$$R = 5.9\times10^{-5}\ [S] \cdot Q \quad \text{moles s}^{-1} \quad (\text{at } 298^{o}\text{K})$$

where S is the sample pressure in Torr and Q the pumping speed in $l\ s^{-1}$ of the vacuum system. For the studies described in this chapter the Quistor was mounted on the instrument with the high capacity pumping system, therefore $Q \simeq 125\ l\ s^{-1}$ and since S is typically 10^{-7} Torr, then the sample consumption rate for the Quistor is *ca.* 7×10^{-10} moles s^{-1}. In Chapter 5 it was calculated that at an internal pressure of 1 Torr the rate of effusion from the high pressure ion source is $\simeq 3.7\times10^{-2}$ Torr $l\ s^{-1}$. It is reasonable to assume for this approximate calculation that for a typical sample partial pressure of 10^{-3} Torr, the rate of effusion of the sample will be *ca.* 3.7×10^{-5} Torr $l\ s^{-1}$. Therefore the sample consumption rate for the high pressure system is $3.7\times10^{-5} \times 5.9\times10^{-5} \simeq 2\times10^{-9}$ moles s^{-1}. Although it appears from these calculations that the sample consumption rates are very similar for the two systems the Quistor does not of course require such a large pumping speed. If instead the Quistor were installed in an instrument with a standard pumping system (Q = *ca.* 25 l/s) then the sample consumption rate would be an order of magnitude lower than that estimated for the high pressure ion source.

Chemical ionisation of samples occurs mainly by fast proton transfer reactions between the reagent ions and sample molecules. These reactions are known to have zero or negative activation energies[146] and may be assumed to proceed at almost every collision. It is therefore possible to estimate the average number of sample ions produced per reagent ion using the following expression which was also employed in Section 6.2.2

$$z_c = k_c \cdot N \cdot \tau$$

k_c (the collision rate constant) may be assumed to have a value of 1×10^{-9} $cm^3\ mol^{-1}\ s^{-1}$. For the high pressure ion source the sample pressure

is typically 10^{-3} Torr, which is equivalent to a number density, N of *ca.* 3×10^{13} mol.cm^{-3} and since the ion residence time (τ) is of the order of 10^{-5}s then the average number of sample ions produced per reagent ion calculated using the above expression is *ca.* 0.3. A similar calculation for the Quistor assuming a sample partial pressure of 10^{-7} Torr ($\equiv 3\times10^{9}$ mol. cm^{-3}) and a residence time of 10^{-2}s gives a value of *ca.* 0.03 for the average number of sample ions produced per reagent ion in the Quistor, which is a factor of 10 lower than that calculated for the high pressure ion source. Although the above calculation is probably only accurate to plus or minus an order of magnitude it does show that for typical operating conditions there is no great difference between the "efficiency" of sample ionisation in the two ion sources.

6.6 Conclusion

The relative merits of the use of the Quistor as a CI ion source will be discussed in detail in Chapter 7. In summary, the results presented in this chapter have demonstrated that :-

(i) the Quistor may be employed to produce both EI and CI mass spectra of a particular sample;

(ii) the low pressure CI mass spectra of the samples investigated were, in general, remarkably similar to the high pressure CI mass spectra;

(iii) the quasi-parent ions appeared to fragment in the same way in both ion sources, but the degree of fragmentation in terms of the sum of the fragment ion intensities, was greater in the low pressure CI mass spectra;

(iv) isobutane, n-hexane and n-heptane are suitable low pressure CI reagent gases.

(v) no cluster ions or association ions were observed in any low pressure CI mass spectra.

CHAPTER 7

CONCLUSION AND DISCUSSION

7.1 Summary of this Work

The experimental work described in the previous chapters was all directly related to the development and evaluation of the Quistor as a chemical ionisation ion source. In the first part of this study a number of physical characteristics of the device were investigated using the original Quistor/quadrupole mass filter combination. These included:

(i) a study of the limits of ion stability in the Quistor from which it was shown that there was a definite limit to the mass range of ions which could be simultaneously stored in the device, and also that it possesses an inherent mass discrimination, due to the variation of storage efficiency with q_z;

(ii) an investigation into ion loss processes in the Quistor in which values for the ion loss rate constants were determined for various different values of the pressure and q_z;

(iii) a study of the ion ejection process in which it was shown how the value of the ejection pulse amplitude required to eject all of the ions from the Quistor was dependent on the depth of the pseudo-potential well ($\bar{D}_z$), in which these ions may be considered to oscillate.

The results of this study were of value in establishing the optimum conditions for the operation of the Quistor in the chemical ionisation mode.

The next part of this work involved the design, construction and characterisation of a Quistor ion source for an AEI MS9 mass spectrometer. This device was found to have similar ion storage characteristics to the original Quistor. In addition to the Quistor ion source a conventional high pressure CI ion source and the inlet systems necessary for its

operation were also constructed for the MS9. The high pressure system was found to produce CI mass spectra which were very similar to those obtained by other workers.

Finally, the two ion sources were compared by obtaining the low and high pressure CI mass spectra of a variety of different compounds. There was, in general, a remarkable degree of similarity between the CI mass spectra of a particular sample produced using the two different ion sources.

7.2 Conclusions Regarding the Use of the Quistor as a CI Ion Source

The first aspect to be considered, as regards the suitability of the Quistor as a CI ion source, is whether the low pressure CI mass spectra obtained, provide the same, or a similar, amount of information as the high pressure CI mass spectra. As was originally stated in Chapter 1, the principal characteristic features of the latter type of CI mass spectra are: high relative intensities of ions at m/e values corresponding to the quasi-parent ions $(M+1)^+$ or $(M-1)^+$, and fragment ions which usually arise as the result of the loss of small molecules such as H_2O or CH_3OH from the $(M+1)^+$ species, the degree of fragmentation being small compared to that in EI mass spectra. In almost all of the low pressure CI mass spectra presented in Section 6.3 the quasi-parent ions are prominent species and if any fragment ions are present they occur at the same m/e values as they do in the high pressure CI mass spectra. The alcohols were exceptional in that the relative intensities of the $(M+1 - H_2O)^+$ species were greater than those of the quasi-parent ions in the low pressure CI mass spectra and this was also found to be the case in the high pressure CI mass spectra. As has already been discussed in Section 6.3 the major differences between the low and high pressure CI mass spectra were that, in the former, no cluster ions or association ions were found to occur and also that the total fragment ion intensity relative to the intensity of the quasi-parent ions was greater than in the latter. Field[40] has argued that the presence

of association ions in CI mass spectra may serve to determine the molecular weight of the sample with greater certainty since they will occur at a known number of m/e units above the $(M+1)^+$ ion, the actual m/e value at which they occur will of course depend on the reagent gas employed. However, the relative intensities of these ions vary widely depending on the nature of the sample and it is possible that one of these ions could be mistaken for the quasi-parent ion. Since association ions were not found to occur in low pressure CI mass spectra, the ion of highest m/e value will correspond to either the $(M+1)^+$ or $(M-1)^+$ species so no such confusion can occur. In qualitative terms the fact that the total fragment ion intensity was greater in the low pressure CI mass spectra is of no great importance since structural information may be derived from the presence of fragment ions irrespective of their intensities. From the previous discussion it is reasonable to conclude that information on the molecular weight of a sample, from the quasi-parent ion, and on the type of functional groups present in the sample molecule, from the fragment ions, may be obtained with equal facility from either low or high pressure CI mass spectra.

In order to complete the assessment of the Quistor as a CI ion source it is necessary to consider a number of instrumental factors. In Chapter 1 it was proposed that as regards instrumentation, the Quistor may have an advantage over a high pressure ion source in that its operation in the CI mode does not require a mass spectrometer with a high capacity source pumping system. However, as has already been mentioned in Chapter 2, demands for CI facilities have reached the stage that CI, and therefore high capacity pumping systems, are standard features on many commercial instruments, and so this does not represent a real advantage. In terms of instrumental requirements the Quistor - low pressure CI system has two distinct disadvantages. Firstly, it requires the construction of a special ion source, each electrode of which has to be machined to within tolerances of $\pm 10^{-3}$ cm, and secondly additional electronic equipment is required, some

of which is highly specialised and therefore very expensive.

In addition to the above factors there are a number of other limitations to the operation of the Quistor as a CI ion source which do not apply to the high pressure system:-

(i) The maximum resolution at which the MS9 could be operated with the Quistor as the ion source was 1000 (10% valley definition).

(ii) The maximum rate at which the mass spectra could be scanned was 5 minutes/decade, this posed serious problems in keeping the reagent gas and sample pressure constant while the mass spectrum was recorded.

(iii) Since the Quistor could not be directly heated the introduction of relatively involatile samples often resulted in their condensation on the Quistor electrodes with the result that the device was rendered incapable of ion storage.

(iv) Although the problems associated with the limited mass storage range of the Quistor were solved by using different reagent gases, this meant that it was impossible to compare directly the low pressure CI mass spectra of all samples since different reagent gases produce mass spectra with varying amounts of fragmentation.

(v) Owing to the inherent mass discrimination of the Quistor it is impossible to draw any positive conclusions about CI processes from the relative intensities of ions in low pressure CI mass spectra.

Finally, one possible advantage of the Quistor is that it is possible to obtain an EI mass spectrum or a CI mass spectrum simply by changing the storage time, whereas, the high pressure ion source developed for this study could not be employed to produce EI mass spectra. However, the Quistor system has so many disadvantages that it cannot be considered

as a serious rival to the well tried and proven high pressure CI systems.

7.3 Suggestions for Further Work

This work has been mainly concerned with the use of the newly-developed Quistor/MS9 system to produce low pressure CI mass spectra. However, it would be of interest to investigate the potential of this system in fields where the Quistor/quadrupole mass filter combination has been used, such as the study of ion-molecule reactions[68]. In this particular application it may have an advantage over the latter system in that the high resolution available will allow the separation of product ions which are of different identity but occur at the same nominal mass. It must be remembered, however, that the use of the Quistor in this particular application is rather limited due to the uncertainty that exists about the energy of stored ions. The MS9 mass spectrometer which was employed in this study could be operated in either the positive or negative mode, and since it has recently been shown that the Quistor may be used as a source of either positive or negative ions[175], it would be of interest to investigate the potential of the Quistor/MS9 system in the negative ion mode.

The possibility of employing the Quistor as a novel type of ion source for a time-of-flight mass spectrometer is currently under investigation in this Laboratory.

Of the many applications of the Quistor which were mentioned in Chapter 3, one of the most promising is its operation in the mass spectrometric mode. During the course of this work an investigation was performed on the characterisation of the Quistor as a mass spectrometer[176]. A block diagram of the experimental system employed for this study is shown in Figure 7.1. This is basically the same as the Quistor/quadrupole mass filter system with the exceptions that the quadrupole rods and power supplies are not used and that an Extranuclear Laboratories Inc. quadrupole power supply has been installed to provide the potentials necessary for the

Figure 7.1 Experimental System for the Operation of the Quistor as a Mass Spectrometer

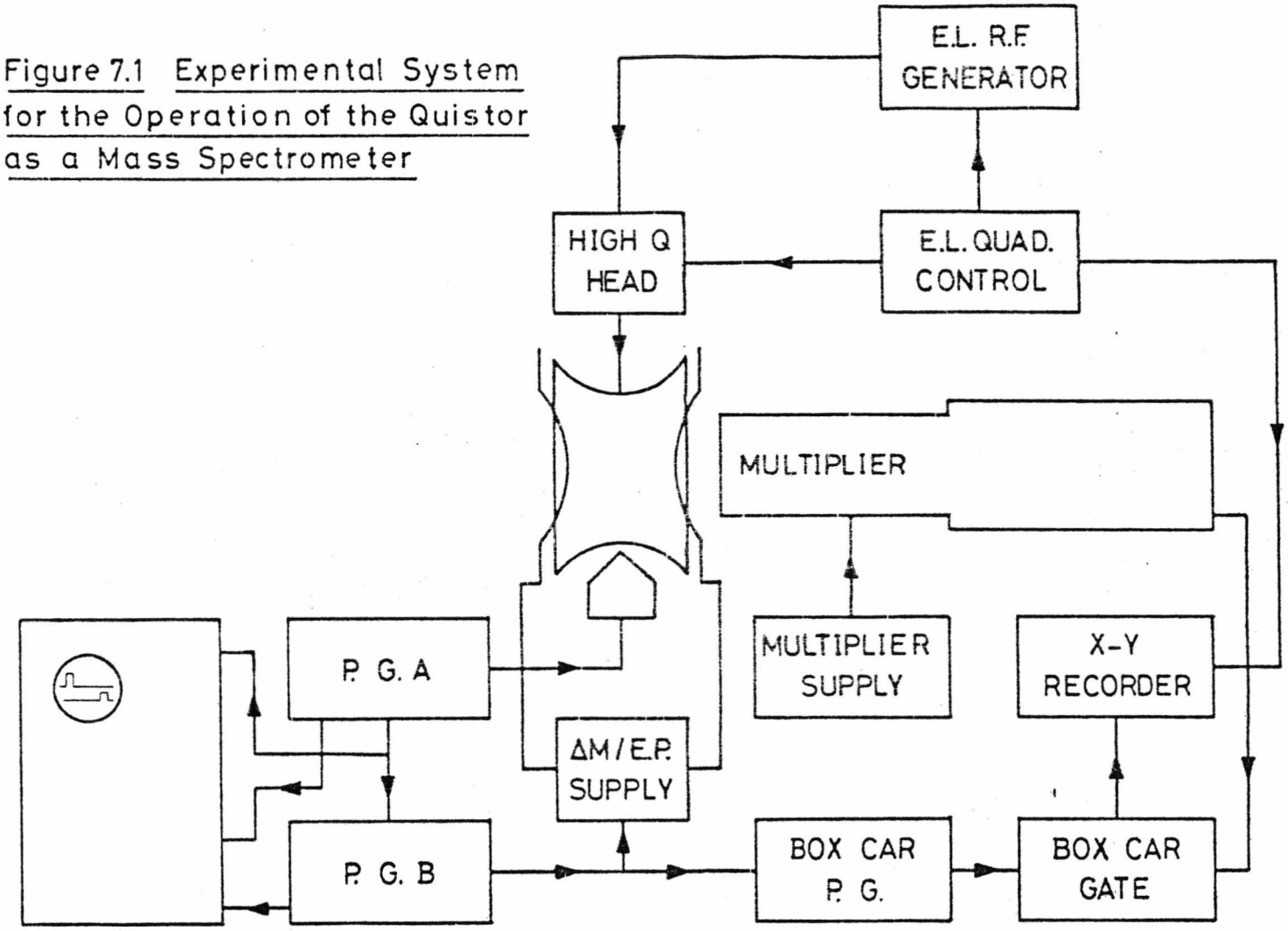

Figure 7.2 Stability Diagram for the Quistor

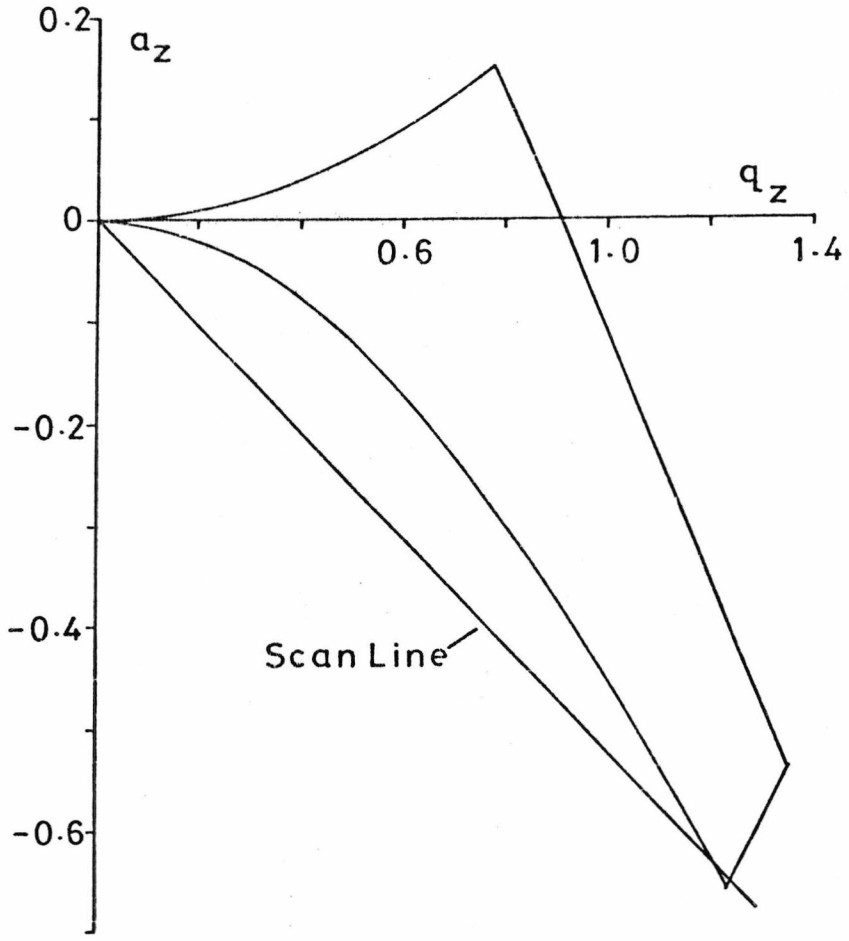

operation of the Quistor as a mass spectrometer. The pulse timing sequence for this system is similar to that shown in Figure 3.13. For operation as a mass spectrometer the values of the potentials applied to the Quistor ring electrode must be chosen to yield pairs of a,q values close to the lower apex of the stability diagram shown in Figure 7.2 (this is identical to that shown in Figure 3.5 but is reproduced here for convenience); in this way the storage conditions are such that only ions of one mass are stable. As in the quadrupole mass filter a mass spectrum is generated by varying U and V_o at a constant ratio of U/V_o such that for each mass the a,q coordinates move along the locus labelled 'scan line' in Figure 7.2. Ions are created inside the Quistor by a pulse of electrons from the electron gun and then the ions remaining after a storage time of 500μs are pulsed out directly onto the first dynode of an electron multiplier. If the values of the applied potentials are set to store only ions of mass m then after a storage time of 500μs ions of other masses will have been lost from the trap and consequently the mass peak arising from the ions pulsed out into the multiplier will comprise exclusively ions of mass m. A complete mass spectrum can be obtained in this way by ramping the values of U and V_o (at a constant ratio) slowly with respect to the duty cycle of the pulse sequence. A mass spectrum of an air/n-heptane mixture recorded using this system is shown in Figure 7.3, in which the resolution at m/e 43 is 215 (FWHM). This is good performance on quadrupole standards and considering that the complete Quistor and multiplier assembly would fit into a cylinder 5 cm in diameter and 15 cm long, it is excellent for such a small device. Therefore, one worthwhile area of further study using the Quistor may be its development as a miniature, and perhaps portable mass spectrometer. This would necessarily involve the design and construction of a special vacuum system and also the customisation and miniaturisation of the necessary electronic supplies.

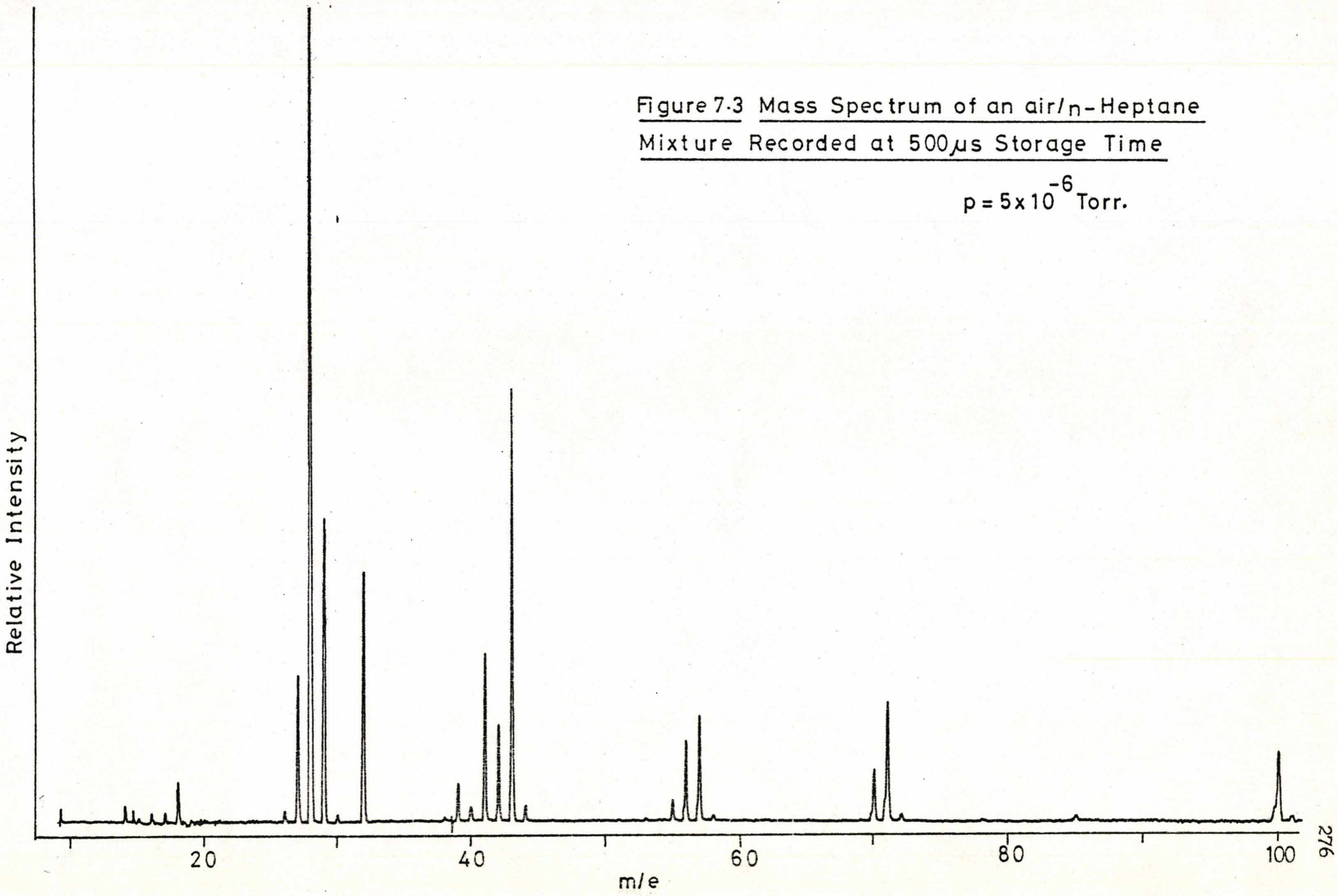

Figure 7.3 Mass Spectrum of an air/n-Heptane Mixture Recorded at 500μs Storage Time

$p = 5 \times 10^{-6}$ Torr.

BIBLIOGRAPHY

1. C.E. Melton and P.S. Rudolph, J. Chem. Phys. 30, 847 (1959). 'Mass Spectrum of Acetylene Produced by 5.1 MeV Alpha Particles'.

2. S. Wexler and N. Jesse, J. Amer. Chem. Soc. 84, 3425 (1962). 'Consecutive Ion-Molecule Reactions in Methane'.

3. F.H. Field and M.S.B. Munson, J. Amer. Chem. Soc. 87, 3289 (1965). 'Reactions of Gaseous Ions XIV. Mass Spectrometer Studies of Methane at Pressures of 2 Torr'.

4. P. Kebarle and A.M. Hogg, J. Chem. Phys. 42, 668 (1965). 'Mass Spectrometer Study of Ions at Near Atmospheric Pressures I. The Ionic Polymerisation of Ethylene'.

5. M.S.B. Munson and F.H. Field, United States Patent No. 3,555,272, (1971). 'Process for Chemical Ionisation for Intended use in Mass Spectrometry and the Like'.

6. M.S.B. Munson and F.H. Field, J. Amer. Chem. Soc. 88, 2621 (1966). 'Chemical Ionisation Mass Spectrometry. I. General Introduction'.

7. F.H. Field, Accounts Chem. Res. 1 42 (1968). 'Chemical Ionisation Mass Spectrometry'.

8. M.S.B. Munson and F.H. Field, J. Amer. Chem. Soc. 87, 3294 (1965). 'Reactions of Gaseous Ions XV. Methane + 1% Ethane and Methane + 1% Propane'.

9. M.S.B. Munson and F.H. Field, J. Amer. Chem. Soc. 87, 4242 (1965). 'Reactions of Gaseous Ions XVI. Effect of Additives on Ionic Reactions of Methane'.

10. F.H. Field, M.S.B. Munson and D.A. Becker, Advances in Chemistry Series No. 58 167 (1966). 'Chemical Ionisation Mass Spectrometry III. Paraffin Hydrocarbons'.

11. M.L. Vestal, T.A. Elwood, L.H. Wojcik and J.H. Futrell, Procs. of the 20th Annual Conference on Mass Spectrometry and Allied Topics, Dallas, Texas, U.S.A. p. 328 (1972). 'A New Chemical Ionisation Mass Spectrometer'.

12. J.H. Futrell and L.H. Wojcik, Rev. Sci. Instrum. 42, 244 (1971). 'Modification of High Resolution Mass Spectrometer for Chemical Ionisation Studies'.

13. J. Michnowicz and M.S.B. Munson, Org. Mass Spectrom. 4, 481 (1970). 'Studies in Chemical Ionisation Mass Spectrometry'.

14. A.K. Bhattacharya, W.R. Powell and J.H. Futrell, Procs. 20th Annual Conference on Mass Spectrometry and Allied Topics, Dallas, Texas, U.S.A. p. 322 (1972). 'Studies in Chemical Ionisation Mass Spectrometry. I. Ketones'.

15. D.P. Beggs, M.L. Vestal, H.M. Fales and G.W.A. Milne, Rev. Sci. Inst. 42, 1578 (1971). 'A Chemical Ionisation Mass Spectrometer Source'.

16. R.S. Ampulski, Chem. Intrum. 7, 1 (1976). 'Modification of a Varian Atlas CH-4B Mass Spectrometer to Permit Chemical Ionisation'.

17. A.M. Hogg, Anal. Chem. 44, 227 (1972). 'Modification of an AEI MS12 Mass Spectrometer for Chemical Ionisation'.

18. J. Yinon and H.G. Boettger, Chem. Instrum. 4, 103 (1972). 'Modification of an AEI/GEC MS9 High-Resolution Mass Spectrometer for Electron Impact/Chemical Ionisation Studies'.

19. S.P. Markey, R.C. Murphy and D.A. Wenger, Procs. 20th Annual Conference on Mass Spectrometry and Allied Topics, Dallas, Texas, U.S.A. p. 318 (1972). 'Chemical Ionisation Mass Spectrometry of Ceramides and Gangliosides'.

20. W.A. Garland, R.J. Weinkam and W.F. Trager, Chem. Instrum. 5, 271 (1974). 'Relatively Simple Modification of an AEI MS-902 High Resolution Mass Spectrometer to Permit Chemical Ionisation Studies'.

21. G.P. Arsenault, J.J. Dolhun and K. Biemann, Anal. Chem. 43, 1720 (1971). 'Alternate or Simultaneous Electron Impact - Chemical Ionisation Mass Spectrometry of Gas Chromatographic Effluent'.

22. A.M. Hogg, Advances in Mass Spec. Vol. 6 p. 391 (1973). 'The Use of a Tandem Electron Impact - Chemical Ionisation Source on AEI MS9 and MS12 Mass Spectrometers.

23. M.A. Baldwin and F.W. McLafferty, Org. Mass Spectrom. 7, 1353 (1973). 'Direct Chemical Ionisation of Relatively Involatile Samples. Application to Underivatised Oligopeptides'.

24. J.B. Knight and S.B. Matin, Anal. Letts 7, 529 (1974). 'The Use of a Solid Sampler in Chemical Ionisation Mass Spectrometry for the Determination of Compounds Unstable under Gas-Liquid Chromatographic Conditions'.

25. D.F. Hunt, J. Shabanowitz, F.K. Botz and D.A. Brent, Anal. Chem. 49, 1160 (1977). 'Chemical Ionisation Mass Spectrometry of Salts and Thermally Labile Organics with Field Desorption Emitters as Solid Probes'.

26. S.E. Buttrill and A.F. Findeis, Anal. Chem. 48, 627 (1976). 'Generation of Reagent Gas for Chemical Ionisation Mass Spectrometry within the Solid Sample Probe. Increased Sensitivity for Relatively Involatile Compounds'.

27. C. Chang, G.J. Sroka and G.G. Meisels, Int. J. Mass Spectrom. Ion Phys. 11, 367 (1973). 'Arrival Time Distributions in High-Pressure Mass Spectrometry III. Effects of Ion Source Geometry on Arrival Times and their Distributions'.

28. J. Yinon, Vacuum 24, 73 (1974). 'Instrumentation and Vacuum Aspects of Chemical Ionisation Mass Spectrometry'.

29. M.S. Story, J.R. Reeher and R.B. Squires, Procs. 22nd Annual Conference on Mass Spectrometry and Allied Topics, Philadelphia, Pennsylvania, U.S.A. p. 521 (1974). 'Improvements in CI Ion Sources'.

30. G.P. Arsenault, United States Patent No. 3,984,692, (1976). 'Ionisation Apparatus and Method for Mass Spectrometry'.

31. G.P. Arsenault, United States Patent No. 4,005,291, (1977). 'Ionisation Method for Mass Spectrometry'.

32. Scientific Research Instruments Inc., British Patent No. 1,338,213, (1973). 'Dual Mode Chemical or Electron Impact Ionisation Source for Mass Spectrometer'.

33. Hewlett-Packard Ltd., British Patent No. 1,450,320, (1976). 'Multi-configuration Ionisation Source'.

34. R. Ryhage, Anal. Chem., 48, 1829 (1976). 'Gas Chromatograph - Mass Spectrometer with Dual Electron Impact/High Pressure Ion Source'.

35. H.H. Gierlich, A. Heindrichs and H.D. Beckey, Rev. Sci. Instrum. 45, 1208 (1974). 'A Combined Electron Impact, Chemical Ionisation, Field Ionisation and Field Desorption Mass Spectrometer Source'.

36. W.A. Wolstenholme and R.M. Elliott, Internat. Lab. May/June 55 (1976). 'Double-Beam Mass Spectrometry'.

37. F.D. Hileman, T.A. Elwood, M.L. Vestal and J.H. Futrell, Procs. 22nd Annual Conference on Mass Spectrometry and Allied Topics, Philadelphia, Pennsylvania p. 511 (1974). 'Dual Beam Electron Impact/Chemical Ionisation Mass Spectrometry'.

38. I. Dzidic, D.M. Desiderio, M.S. Wilson, P.F. Crain and J.A. McClaskey, Anal. Chem. 43, 1877 (1971). 'Mass Standards for Chemical Ionisation Mass Spectrometry'.

39. D.V. Bowen and F.H. Field, Anal. Chem. 47, 2289 (1975). 'Chemical Mass Markers in Chemical Ionisation Mass Spectrometry'.

40. F.H. Field, in 'Mass Spectrometry' A. Maccall editor, M.T.P. International Review of Science, Series 1, Vol. 5, Butterworths, London. p. 133 (1972). 'Chemical Ionisation Mass Spectrometry'.

41. M.S.B. Munson, in Interactions Between Ions and Molecules, P. Ausloos editor, Plenum London. p. 505 (1975). 'Chemical Ionisation Mass Spectrometry: Analytical Applications of Ion Molecule Reactions'.

42. B. Hoegger and P. Bommer, Int. J. Mass Spectrom. Ion Phys. 13, 35 (1974). 'Mass Spectrometric Study of Chemical Ionisation in High Frequency Flow Discharges'.

43. H. Kambara and I. Kanomata, Int. J. Mass Spectrom. Ion Phys. 24, 453 (1977). 'Chemical Ionisation by a Needle Electron Source'.

44. D.F. Hunt, C.N. McEwen and T.M. Harvey, Anal. Chem. 47, 1730 (1975). 'Positive and Negative Chemical Ionisation Mass Spectrometry Using a Townsend Discharge Ion Source'.

45. M.S.B. Munson and F.H. Field, J. Amer. Chem. Soc. 88, 4337 (1966). 'Chemical Ionisation Mass Spectrometry II. Esters'.

46. M.S.B. Munson, Anal. Chem. 43, 28A (1971). 'Chemical Ionisation Mass Spectrometry'.

47. P.C. Price, H.S. Swofford and S.E. Buttrill, Anal. Chem. 49, 1497 (1977). 'New Drift Tube Source for Use in Chemical Ionisation Mass Spectrometry'.

48. R.V. Hodges and J.L. Beauchamp, Anal. Chem. 48, 825 (1976). 'Application of Alkali Ions in Chemical Ionisation Mass Spectrometry'.

49. E.C. Horning, M.G. Horning, D.I. Carroll, I. Dzidic and R.N. Stillwell, Anal. Chem. 45, 936 (1973). 'New Picogram Detection System Based on a Mass Spectrometer with an External Ionisation Source at Atmospheric Pressure'.

50. D.I. Carroll, I. Dzidic, R.N. Stillwell, M.G. Horning and E.C. Horning, Anal. Chem. 46, 706 (1974). 'Subpicogram Detection System for Gas Phase Analysis Based on Atmospheric Pressure Ionisation Mass Spectrometry'.

51. F.W. Karasek, Anal. Chem. 46, 710A (1974). 'Plasma Chromatography'.

52. F.W. Karasek, D.W. Denney and E.H. De Decker, Anal. Chem. 46, 970 (1974). 'Plasma Chromatography of Normal Alkanes and its Relationship to Chemical Ionisation Mass Spectrometry'.

53. F.W. Karasek, H.H. Hill and S.H. Kim, J. Chromatogr. 117, 327 (1976). 'Plasma Chromatography of Heroin and Cocaine with Mass Identified Mobility Spectra'.

54. D.M. Schoengold and M.S.B. Munson, Anal. Chem. 42, 1811 (1970). 'Combination of Gas Chromatography and Chemical Ionisation Mass Spectrometry'.

55. T.L. Kruger, J.F. Litton, R.W. Kondrat and R.G. Cooks, Anal. Chem. 48, 2113 (1976). 'Mixture Analysis by Mass-Analysed Ion Kinetic Energy Spectrometry'.

56. J.H. Futrell and C.D. Miller, Rev. Sci. Inst. 37, 1521 (1966). 'Tandem Mass Spectrometer for Study of Ion-Molecule Reactions'.

57. J. Sunner and I. Szabo, 7th International Mass Spectrometry Conference, Florence, Italy. Paper 44-S/1 (1976). 'The Analytical Usage of Chemical Ionisation in a Tandem Mass Spectrometer'.

58. F.A. Baker and J.B. Hasted, Phil. Trans. Roy. Soc. London. A261, 33 (1966). 'Electron Collision Studies with Trapped Positive Ions'.

59. A.J. Bourne and C.J. Danby, J. Sci. Instrum. 1, 155 (1968). 'A Technique for Ion Trapping in Pulsed-Source Mass Spectrometry'.

60. A.A. Herod and A.G. Harrison, Int. J. Mass Spectrom. Ion Phys. 4, 415 (1970). 'Bimolecular Reactions of Ions Trapped in an Electron Space Charge'.

61. K.R. Ryan and I.G. Graham, J. Chem. Phys. 59, 4260 (1973). 'Ion Collision Processes in Mixtures of Hydrogen and Rare Gases'.

62. A.S. Blair and A.G. Harrison, Can. J. Chem. 51, 1645 (1973). 'Bimolecular Reactions of Trapped Ions. VI. Ion-Molecule Reactions Involving CH_5^+ and $C_2H_5^+$'.

63. W. Paul, O. Osberghaus and E. Fischer, Forschungsber. Wirtsh. Verkehrministriums Nordheim Westfalen No. 415 (1958). 'Das Ionenkäfig'.

64. E. Fischer, Z. Physik 156, 26 (1959). 'Die Dreidimensionale Stabiliserung von Ladungsträgern in einem Vierpolfeld'.

65. G. Rettinghaus, Z. Angew Phys. 22, 321 (1967). 'Nachweis Niedriger Partialdrucke mit dem Ionenkäfig'.

66. P.H. Dawson, J.W. Hedman and N.R. Whetten, Rev. Sci. Instrum. 40, 1444 (1969). 'A Simple Mass Spectrometer'.

67. G. Lawson, R.F. Bonner and J.F.J. Todd, J. Phys. E. 6, 357 (1973). 'The Quadrupole Ion Store (QUISTOR) as a Novel Source for a Mass Spectrometer'.

68. G. Lawson, R.F. Bonner, R.E. Mather, J.F.J. Todd and R.E. March, J. Chem. Soc. Faraday I 72, 545 (1976). 'Quadrupole Ion Store (QUISTOR) Part I Ion-Molecule Reactions in Methane, Water and Ammonia'.

69. R.F. Bonner, G. Lawson and J.F.J. Todd, J. Chem. Soc. Chem. Comm. 1179 (1972). 'A Low Pressure Chemical Ionisation Source : An Application of a Novel Type of Mass Spectrometer'.

70. J.A. Hipple, H. Sommer and H.A. Thomas, Phys. Rev. 76, 1877 (1949). 'A Precise Method for Determining the Faraday by Magnetic Resonance'.

71. H. Sommer, H.A. Thomas and J.A. Hipple, Phys. Rev. 82, 697 (1951). 'The Measurement of e/m by Cyclotron Resonance'.

72. L.R. Anders, J.L. Beauchamp, R.C. Dunbar and J.D. Baldeschwieler, J. Chem. Phys. 45, 1062 (1966). 'Ion Cyclotron Double Resonance'.

73. J.L. Beauchamp and J.T. Armstrong, Rev. Sci. Instrum. 40, 123 (1969). 'An Ion Ejection Technique for the Study of Ion-Molecule Reaction Rates with Ion Cyclotron Resonance Spectrometry'.

74. R.T. McIver, Rev. Sci. Instrum. 41, 555 (1970). 'A Trapped Ion Analyser Cell for Ion Cyclotron Resonance Spectrometry'.

75. R.T. McIver and A.D. Baranyi, Int. J. Mass Spectrom. Ion Phys. 14, 449 (1974). 'High Resolution Ion Cyclotron Resonance Spectrometry'.

76. R.T. McIver, E.B. Ledford and J.S. Miller, Anal. Chem. 47, 692 (1975). 'Proposed Method for Mass Spectrometric Analysis for Ultra-Low Vapour Pressure Compounds'.

77. C.V. Pesheck and S.E. Buttrill, J. Amer. Chem. Soc. 96, 6027 (1974). 'Ion Cyclotron Resonance Studies of the Chemical Ionisation of Esters'.

78. M.M. Bursey, T.A. Elwood, M.K. Hoffman, A. Lehman and J.M. Tesarek, Anal. Chem. 42, 1370 (1970). 'Analytical Ion Cyclotron Resonance Spectrometry'.

79. R.P. Clow and J.H. Futrell, J. Amer. Chem. Soc. 94, 3748 (1972). 'Ion Cyclotron Resonance Study of the Mechanism of Chemical Ionisation. Mass Spectroscopy of Selected Hydrocarbons Using Methane Reagent Gas'.

80. E.W. McDaniel, Collision Phenomena in Ionised Gases, Wiley, London (1964). Chapter 9.

81. F.H. Field, J. Amer. Chem. Soc. 91, 2827 (1969). 'Chemical Ionisation Mass Spectrometry IX. Temperature and Pressure Studies with Benzyl Acetate and t-Amyl Acetate'.

82. S. Vredenberg, L. Wojcik and J.H. Futrell, J. Phys. Chem. 75, 590 (1971). 'Kinetics of Chemical Ionisation. I. Reactions of tert-$C_4H_9^+$ with Benzyl Acetate'.

83. G. Sroka, C. Chang and G.G. Meisels, J. Amer. Chem. Soc. 94, 1052 (1972). 'Arrival Time Distributions in High Pressure Mass Spectrometry. I. Residence Times of Reactant Ions in Chemical Ionisation and the Measurement of Reaction Rate Constants'.

84. R.C. Dougherty and C.R. Weisenberger, J. Amer. Chem. Soc. 90, 6570 (1968). 'Negative Ion Mass Spectra of Benzene, Naphthalene and Anthracene. A New Technique for Obtaining Relatively Intense and Reproducible Negative Ion Mass Spectra'.

85. C.E. Melton, Principles of Mass Spectrometry and Negative Ions, Marcel Dekker, New York (1970).

86. M. von Ardenne, K. Steinfelder and R. Tümmler, Z. Chem. (Leipzig) 5, 287 (1965). 'Beitrag zur Molekül-Massenspektrographie von Naturstoffen'.

87. R. Tümmler and K. Steinfelder, Z. Chem (Leipzig) 7, 1 (1967). 'Über einige Bildungsprozesse Negativer Ionen Organischer Moleküle bei der Elektronen - anlagerungo - Massenspektrographie'.

88. M. von Ardenne, K. Steinfelder and R. Tümmler, Z. Phys. Chem. (Leipzig) 221, 240 (1963). 'Erweiterung der EA-Massenspektrographischen Methode durch den Mechanisms der Anlagerung Negativer Ionen an Moleküle'.

89. M. von Ardenne, Kernenergie 1, 1029 (1958). 'Der Dresdner Molekülspektrograph, ein Neuartiger Präsisions - Massenspektrograph für Negative Hochmolekulare Ionen'.

90. M. von Ardenne and K. Steinfelder, Kernenergie 3, 717 (1960). 'Über eine Elecktronenanlagerungs - Ionenquelle mit Fernhaltung des Testdampfes von der Entladungskatode'.

91. R.C. Dougherty, J. Dalton and F.J. Biros, Org. Mass Spectrom. 6, 1171 (1972). 'Negative Chemical Ionisation Mass Spectra of Polycyclic Chlorinated Insecticides'.

92. R.C. Dougherty, J.D. Roberts and F.J. Biros, Anal. Chem. 47, 54 (1975). 'Positive and Negative Chemical Ionisation Mass Spectra of some Aromatic Chlorinated Pesticides'.

93. H.P. Tannenbaum, J.D. Roberts and R.C. Dougherty, Anal. Chem. 47, 49 (1975). 'Negative Chemical Ionisation Mass Spectrometry - Chloride Attachment Spectra'.

94. T.W. Carr, Anal. Chem. 49, 828 (1977). 'Negative Ions in Plasma Chromatography - Mass Spectrometry'.

95. D.F. Hunt, G.C. Stafford, F.W. Crow and J.W. Russell, Anal. Chem. 48, 2098 (1976). 'Pulsed Positive Negative Ion Chemical Ionisation Mass Spectrometry'.

96. D.F. Hunt, G.C. Stafford, J. Shabanowitz and F.W. Crow, Anal. Chem. 49, 1884 (1977). 'Determination of Molecular Composition on a Quadrupole Mass Spectrometer by Pulsed Positive Negative Chemical Ionisation Mass Spectrometry'.

97. W.H. McFadden, Techniques of Combined Gas Chromatography/Mass Spectrometry, Wiley, London (1973).

98. W. Henderson and G. Steel, Anal. Chem. 44, 2302 (1972). 'Total-Effluent Gas Chromatography - Mass Spectrometry'.

99. R.L. Foltz, Procs. 19th Annual Conference on Mass Spectrometry and Allied Topics, Atlanta, Georgia, U.S.A., p. 142 (1971). 'Applications of Chemical Ionisation Mass Spectrometry'.

100. G.P. Arsenault, J.J. Dolhun and K. Biemann, J. Chem. Soc. Chem. Comm. 1542 (1970). 'Gas Chromatography - Chemical Ionisation Mass Spectrometry'.

101. E.O. Oswald, L. Fishbein, B.C. Corbett and M.P. Walker, J. Chromatogr. 73, 43 (1972). 'Metabolism of Naturally Occurring Propenylbenzene Derivatives. II. Separation and Identification of Tertiary Amino-propiophenones by Combined Gas-Liquid Chromatography and Chemical Ionisation Mass Spectrometry'.

102. F. Hatch and M.S.B. Munson, Anal. Chem. 49, 169 (1977). 'Techniques in Gas Chromatography/Chemical Ionisation Mass Spectrometry'.

103. U. Mathiesen, B. Kump and W. Staib, Chromatographia, 10, 303 (1977). 'Über die Kopplung eines Kapillargas - Chromatographen an ein

Massenspektrometer mit Einrichtung für Chemische Ionisation und die Registrierung der Gas Chromatogramme mit einem Spektrenintegrator'.

104. W. Blum and W.J. Richter, Tet. Letts. 835 (1973). 'Analysis of Alkene Mixtures by Combined Capillary Gas Chromatography - Chemical Ionisation Mass Spectrometry'.

105. F. Hatch and M.S.B. Munson, Anal. Chem. 49, 731 (1977). 'Reagent Ion Monitoring for Selective Detection in Gas Chromatography/Chemical Ionisation Mass Spectrometry'.

106. V.L. Tal'rose, V.D. Grishin, V.E. Skurat and G.D. Tantsyrev, Recent Developments in Mass Spectrometry, K. Ogata and T. Hayakawa editors, University Park Press Baltimore U.S.A. p. 1218 (1970). 'New Techniques in Chromato-Mass Spectrometry'.

107. M.A. Baldwin and F.W. McLafferty, Org. Mass Spectrom. 7, 1111 (1973). 'Liquid Chromatography - Mass Spectrometry Interface I. The Direct Introduction of Liquid Solutions into a Chemical Ionisation Mass Spectrometer'.

108. P.J. Arpino, B.G. Dawkins and F.W. McLafferty, J. Chromatogr. Sci. 12, 574 (1974). 'A Liquid Chromatography/Mass Spectrometry System Providing Continuous Monitoring with Nanogram Sensitivity'.

109. P.J. Arpino, M.A. Baldwin and F.W. McLafferty, Biomed. Mass Spectrom. 1, 80 (1974). 'Liquid Chromatography - Mass Spectrometry. II. Continuous Monitoring'.

110. D.F. Hunt, Prog. Anal. Chem. 6, 359 (1973). 'Selective Reagents for Chemical Ionisation Mass Spectrometry'.

111. N. Einolf and M.S.B. Munson, Int. J. Mass Spectrom. Ion Phys. 9, 141 (1972). 'High Pressure Charge Exchange Mass Spectrometry'.

112. D.F. Hunt, Adv. Mass Spectrom. 6, 517 (1974). 'Reagent Gases for Chemical Ionisation Mass Spectrometry'.

113. F.H. Field, in Ion Molecule Reactions, Vol. 1, J.L. Franklin, editor, Butterworths (1972). Chapter 6. 'Chemical Ionisation Mass Spectrometry'.

114. M.S.B. Munson, Anal. Chem. 49, 772A (1977). 'Chemical Ionisation Mass Spectrometry : Ten Years Later'.

115. J.M. Wilson, in Mass Spectrometry, Vol. 3, R.A.W. Johnstone, editor, The Chemical Society, London, p. 96 (1975).

116. J.M. Wilson, in Mass Spectrometry, Vol. 4, R.A.W. Johnstone, editor, The Chemical Society, London, p. 102 (1977).

117. K.R. Jennings, in Mass Spectrometry, Vol. 4, R.A.W. Johnstone, editor, The Chemical Society, London, p. 203 (1977).

118. I. Jardine and C. Fenselau, J. Amer. Chem. Soc. 98, 5086 (1976). 'Proton Localisation in Chemical Ionisation Fragmentation'.

119. D.F. Hunt and C.N. McEwen, Org. Mass Spectrom. 7, 441 (1973). 'Chemical Ionisation Mass Spectrometry Studies - VIII Deuterium Labeled Decanes'.

120. G. Lawson and J.F.J. Todd, Anal. Chem. 49, 1619 (1977). 'Weak Peak Enhancement by Selective Ion Trapping in a Quadrupole Ion Storage Source'.

121. G. Lawson, J.F.J. Todd and R.F. Bonner, in Dynamic Mass Spectrometry, Vol. 4, D. Price and J.F.J. Todd, editors, Heyden, London, p. 39 (1975).

122. J.F.J. Todd, in Quadrupole Mass Spectrometry and its Applications, P.H. Dawson, editor, Elsevier, Amsterdam, p. 241 (1976).

123. J.F.J. Todd, G. Lawson and R.F. Bonner, in Quadrupole Mass Spectrometry and its Applications, P.H. Dawson, editor, Elsevier, Amsterdam, p. 181 (1976).

124. P.H. Dawson, in Quadrupole Mass Spectrometry and its Applications, P.H. Dawson, editor, Elsevier, Amsterdam, p. 9 (1976).

125. J.F.J. Todd and G. Lawson, in International Review of Science, Physical Chemistry, Series 2, Vol. 5, Mass Spectrometry, A. Macoll, editor, Butterworths, London, p. 289 (1975).

126. G. Lawson, Ph.D Thesis, University of Kent (1972).

127. R.F. Bonner, Ph.D Thesis, University of Kent (1974).

128. P.H. Dawson, in Quadrupole Mass Spectrometry and its Applications, P.H. Dawson, editor, Elsevier, Amsterdam, p. 79 (1976).

129. R.M. Waldren and J.F.J. Todd, in Dynamic Mass Spectrometry, Vol. 5, D. Price and J.F.J. Todd, editors, Heyden, London, p. 14 (1978).

130. R.F. Wuerker, M. Shelton and R.V. Langmuir, J. Appl. Phys. 30, 342 (1959). 'Electrodynamic Confinement of Charged Particles'.

131. H.G. Dehmelt, Atom. Mol. Phys., 3, 53 (1967). 'R.F. Spectroscopy of Stored Ions. I. Storage'.

132. M. Baril and A. Septier, Rev. Phys. Appl. 9, 525 (1974). 'Piegeage des Ions dans un Champ Quadrupolaire Tridimensional a Haute Fréquence'.

133. P.H. Dawson and N.R. Whetten, J. Vac. Sci. Technol. 5, 11 (1968). 'Ion Storage in Three Dimensional, Rotationally Symmetric, Quadrupole Fields. II. A Sensitive Mass Spectrometer'.

134. N.R. Whetten and P.H. Dawson, J. Vac. Sci. Technol. 6, 100 (1968).

'Some Causes of Poor Peak Shapes in Quadrupole Field Mass Analysers'.

135. F. von Busch and W. Paul, Z. Physik 164, 588 (1961). 'Uber Nicht-lineare Resonanzen im Elecktrischen Massenfilter als Folge von Feldfehlern'.

136. W.J. Sternberg and T.L. Smith, in The Theory of Potential and Spherical Harmonics, University of Toronto Press (1961).

137. P.H. Dawson and N.R. Whetten, Int. J. Mass Spectrom. Ion Phys. 2, 45 (1969). 'Non-Linear Resonances in Quadrupole Mass Spectrometers due to Imperfect Fields. I. The Quadrupole Ion Trap'.

138. P.H. Dawson, in Quadrupole Mass Spectrometry and its Applications, P.H. Dawson, editor, Elsevier, Amsterdam, p. 95 (1976).

139. C.S. Harden and P.E. Wagner, EATR 4545, Edgewood Arsenal, Maryland, U.S.A. (1971). 'A Three Dimensional Quadrupole Mass Analyser. II. Operational Characteristics'.

140. E.W. McDaniel, V. Cermak, A. Dalgarno, E.E. Ferguson and L. Friedman, in Ion Molecule Reactions, Wiley-Interscience (1970).

141. J.F.J. Todd, R.M. Waldren, R.E. Mather and G. Lawson, Int. J. Mass Spectrom. Ion Phys., Accepted for Publication. 'On the Relative Efficiency of Confinement of Ar^+ and Ar^{2+} Ions in a Quadrupole Ion Storage Trap (Quistor)'.

142. P.H. Dawson, Int. J. Mass Spectrom. Ion Phys. 24, 447 (1977). 'The Effect of Collisions on Ion Motion in Quadrupole Fields'.

143. J. André, J. Phys. 37, 719 (1976). 'Etude Théorique de L'influence des Collisions Elastiques sur un Gaz Dilué de Particules Chargées, Confinées par un Champ de Radio-Fréquence a Symetrie Quadrupolaire'.

144. F.G. Major and H.G. Dehmelt, Phys. Rev. 170, 91 (1968). 'Exchange -

Collision Technique for the r.f. Spectroscopy of Stored Ions'.

145. J.R. Pierce, in The Theory and Design of Electron Beams, Van Nostrand, Princeton, N.J., U.S.A. (1954).

146. M. Henchman, in Ion Molecule Reactions, Vol. 1, J.L. Franklin, editor, Butterworths, London, p. 101 (1972).

147. Catalog of Mass Spectral Data, American Petroleum Research Project 44, Spectrum No. 368.

148. F.H. Field, J. Amer. Chem. Soc. 92, 2672 (1970). 'Chemical Ionisation Mass Spectrometry. XII. Alcohols'.

149. M.S.B. Munson, J.L. Franklin and F.H. Field, J. Phys. Chem. 68, 3098 (1964) 'High Pressure Mass Spectrometric Study of Alkanes'.

150. B.H. Solka, A.Y-K. Lau and A.G. Harrison, Can. J. Chem. 52, 1798 (1974).'Bimolecular Reactions of Trapped Ions. VIII. Reactions in Propane and Propane-Methane Mixtures'.

151. J. Michnowicz and B. Munson, Org. Mass Spectrom. 6, 283 (1972) 'Studies in Chemical Ionisation Mass Spectrometry : Aryl Ketones'.

152. J. Michnowicz and B. Munson, Org. Mass Spectrom. 6, 765 (1972) 'Studies in Chemical Ionisation Mass Spectrometry : 17-Hydroxy Steroids'.

153. J. Michnowicz and B. Munson, Org. Mass Spectrom. 8, 49 (1974) 'Studies in Chemical Ionisation Mass Spectrometry: Steroidal Ketones'.

154. P.H. Dawson, Int. J. Mass Spectrom. Ion Phys. 20, 237 (1976) 'Energetics of Ions in Quadrupole Fields'.

155. R.M. Waldren and J.F.J. Todd, Int. J. Mass Spectrom. Ion Phys. Accepted for Publication.

156. C. Lambert, M. Sc. Thesis, Laval University, Quebec, Canada, (1974).

157. P.H. Dawson and N.R. Whetten, Naturwissenschaften, 56, 109 (1969) 'The Quadrupole Ion Trap'.

158. R.F. Bonner, R.E. March and J. Durup, Int. J. Mass Spectrom. Ion Phys. 22, 17 (1976) 'The Effects of Charge Exchange Reactions on the Motion of Ions in Three-Dimensional Quadrupole Electric Fields'.

159. R.F. Bonner and R.E. March, Int. J. Mass Spectrom. Ion Phys. 25, 411 (1977).'The Effects of Charge Exchange Collisions on the Motion of Ions in Three Dimensional Quadrupole Electric Fields. Part II Program Improvements and Fundamental Results'.

160. D.P. Beggs and F.H. Field, J. Amer. Chem. Soc. 93, 1567 (1971). 'Reversible Reactions of Gaseous Ions I Methane-Water System'.

161. D.P. Beggs and F.H. Field, J. Amer. Chem. Soc. 93, 1576 (1971). 'Reversible Reactions of Gaseous Ions II. Propane-Water System'.

162. C. Chang, G.G. Meisels and J.A. Taylor, Int. J. Mass Spectrom. Ion Phys. 12, 411 (1973). 'High Pressure Mass Spectrometry: Ion Energies and their Distributions in Chemical Ionisation Sources'.

163. G.H. Wannier, Bell Systems Tech. J. 32, 170 (1953)

164. G.G. Meisels, A.J. Illies, R.S. Stradling and K.R.Jennings, J. Chem. Phys. 68, 866 (1978).'Time Resolved Measurement in High Pressure Mass Spectrometry: An Analysis of Assumptions'.

165. M.S.B. Munson, J.L. Franklin and F.H. Field, J. Phys. Chem. 68, 3098 (1964).'High Pressure Mass Spectrometric Study of Alkanes'.

166. H. Budzikiewicz, C. Djerassi and D.H. Williams, in Mass Spectrometry of Organic Compounds, Holden-Day (1967)

167. H.M. Fales, G.W.A. Milne and R.S. Nicholson, Anal. Chem. 43, 1785

(1971).'Chemical Ionisation Mass Spectrometry of Complex Molecules -Esters of Di- and Tricarboxylic Acids'.

168. W.T. Huntress, D.K. Sen-Sharma , K.R. Jennings and M.T. Bowers, Int. J. Mass Spectrom Ion Phys. 24, 25 (1977).'Metastable Peaks in Chemical Ionisation Mass Spectrometry: Unimolecular Decompositions of Protonated Methanol Ions'.

169. B.L. Jelus, R.K. Murry and B. Munson, J. Amer. Chem. Soc. 97, 2362 (1975).'Studies in Chemical Ionisation Mass Spectrometry. Secondary Alcohols with Isobutane'.

170. T.Y. Yu and F.H. Field, Org. Mass Spectrom. 8, 267 (1974).'Chemical Ionisation Mass Spectrometry XIX n-Hexane and n-Octane as Reactants'.

171. A. Goren and B. Munson, J. Phys. Chem. 80, 2848 (1976) 'Thermochemistry of Alkyl Ions'.

172. D. Stahl and T. Gaumann, in Advances in Mass Spectrometry Vol. 7B, N.R. Daly, editor, Heyden, London. p.1190 (1978).

173. G. Parisod and T. Gaumann, in Advances in Mass Spectrometry Vol. 7B, N.R. Daly, editor, Heyden, London. p. 1402 (1978).

174. J.E. Fulford, J.W. Dupuis and R.E. March, Can. J. Chem. 56, 2324 (1978)'Gas Phase Ion Molecule Reactions of Dimethylsulphoxide'.

175. R.E. Mather and J.F.J. Todd, Submitted for Publication.

176. R.E. Mather, R.M. Waldren and J.F.J. Todd, in Dynamic Mass Spectrometry Vol. 5, D.Price and J.F.J. Todd, editors, Heyden, London. p.71 (1978).'The Characterisation of a Quadrupole Ion Storage Mass Spectrometer'.

APPENDIX

Papers Published as a Result of this Work

R.E. Mather, G. Lawson, J.F.J. Todd and J.M.B. Bakker, Int. J. Mass Spectrom. Ion Phys. 28, 347 (1978).'The Quadrupole Ion Storage Trap (QUISTOR) as a Low Pressure Chemical Ionisation Source for a Magnetic Sector Mass Spectrometer'.

R.E. Mather and J.F.J. Todd, Int J. Mass Spectrom. Ion Phys. Accepted for Publication. 'Chemical Ionisation Mass Spectrometry: A Survey of Instrument Technology'.

R.E. Mather and J.F.J. Todd, Int. J. Mass Spectrom. Ion Phys. Accepted for Publication.'The Quadrupole Ion Store(QUISTOR) Part IV. A Simple Model for the Ion Ejection Process'.

KENT LIBRARY UNIVERSITY